Paleozoic and Mesozoic tectono-thermal history of central Dronning Maud Land, East Antarctica - evidence from fission-track thermochronology

Paläozoische und mesozoische tektono-thermale Geschichte des centralen Dronning Maud Land, Ostantarktis, basierend auf Spaltspur-Untersuchungen

---

Stefanie Meier

Ber. Polarforsch. 337 (1999)
ISSN 0176 - 5027

Stefanie Meier

Geologie der Polargebiete
Fachbereich Geowissenschaften
Universität Bremen
Postfach 330440
28334 Bremen

Die vorliegende Arbeit ist die inhaltlich unveränderte Fassung der Dissertation, die 1999 dem Fachbereich Geowissenschaften der Universität Bremen unter gleichem Titel vorgelegt wurde.

Contents

Abstract

Titanite, zircon and apatite fission-track thermochronology on 123 basement samples from central Dronning Maud Land (CDML) records a complex mid-Paleozoic to Late Cretaceous cooling and denudation history. New constraints were placed on the evolution of the passive margin of CDML during the Early Jurassic breakup of the Gondwana supercontinent.

Fission-track analyses on titanites and zircons gave ages ranging from 531±51 Ma to 293±28 Ma and from 364±47 Ma to 237±31 Ma, respectively. The apatite fission-track ages (FTA) range from 315±18 Ma to 83±3 Ma with the oldest FTA being confined to the farthest south of CDML and the youngest ages occurring in close vicinity to the coastline. The mean track lengths point towards different degrees of track annealing. In addition to the basement samples, fission-track dating was performed on six dropstone samples from the offshore region of CDML, giving apatite FTA between 170±9 Ma and 78±4 Ma. The FTA basically confirm that the dropstones represent the products of glacial erosion of the basement of CDML.

After the Pan-African event (~600-500 Ma), the basement of CDML was subjected to post-orogenic cooling during which the central part being affected by post-tectonic intrusions has cooled more deliberately than the surrounding metamorphic basement. In the late Paleozoic the basement has attained a stable cratonic temperature distribution. It is suggested that CDML served in the Permo-Triassic as a region, where crustal material was removed and deposited elsewhere, probably in the Transantarctic basin along the proto-Pacific margin of East Antarctica. The successive denudation by this time was accompanied by faulting and exhumation of crustal blocks in the continental interior of CDML. During the Early Jurassic a major cooling step affected the basement which is interpreted to reflect a period of mantle plume - related exhumation and denudation preceding the separation of East and West Gondwana by continental rifting. Though the continental margin of CDML has formed during the Early Jurassic, the full morphological development of the passive margin occurred in the mid-Cretaceous when the basement experienced a further step of accelerated cooling. The mechanism accounting for the middle Cretaceous cooling is considered being purely isostatic and resulted from the establishment of a new erosional base level due to major plate reorganisations and enhanced seafloor spreading during the fragmentation of Gondwana. As a reaction to the newly created base level, differential denudation across the CDML passive margin was initiated while leading to a flexural isostatic upward movement of the lithosphere.

The total thickness of crustal material that has been denuded since the early stage of the Pan-African until present-day was approximately 31-45 km.

Zusammenfassung

Die Titanit-, Zirkon- und Apatit-Thermochronologie an 123 Grundgebirgsproben aus dem centralen Dronning Maud Land (CDML) ergab eine komplexe mittelpaläozoische bis spätkretazische Abkühlungs- und Denudationsgeschichte. Es wurden neue Ergebnisse bezüglich der Entwicklung des passiven Kontinentalrandes des CDML während der frühjurassischen Gondwana-Fragmentierung erzielt.

Die Spaltspuruntersuchungen an Titaniten und Zirkonen ergaben jeweils Alter zwischen 531±51 Ma und 293±28 Ma sowie zwischen 364±47 Ma und 237±31 Ma. Die Apatitspaltspuralter reichen von 315±18 Ma bis 83±3 Ma, wobei die ältesten Spaltspuralter im äußersten Süden des CDML vorkommen und die jüngsten Alter in nächster Nähe zur Küstenlinie auftreten. Die mittleren Spurenlängen deuten auf eine unterschiedlich intensive Spurenausheilung hin. Zusätzlich zu den Grundgebirgsproben wurden Spaltspurdatierungen an sechs *dropstone*-Proben aus der küstennahen Region vor dem CDML durchgeführt, welche Apatitspaltspuralter zwischen 170±9 Ma und 78±4 Ma ergaben. Grundsätzlich bestätigen diese Spaltspuralter, daß die *dropstones* Produkte der glazialen Erosion des Grundgebirges des CDML repräsentieren.

Nach dem Panafrikanischen Ereignis (~600-500 Ma) unterlief das Grundgebirge des CDML einer postorogenen Abkühlung, währenddessen der zentrale Teil, der durch posttektonische Intrusionen beeinflußt wurde, langsamer abkühlte als das umgebende metamorphe Grundgebirge. Im späten Paläozoikum hatte das Grundgebirge eine stabile kratonale Temperaturverteilung erreicht. Es wird angenommen, daß das CDML während der Permotrias als eine Region diente, in der Krustenmaterial entfernt und anderswo abgelagert wurde, möglicherweise im Transantarktischen Becken entlang des Protopazifischen Randes der Ostantarktis. Die sukzessive Denudation in dieser Zeit wurde von Zerblockung und der Heraushebung von Krustenblöcken im kontinentalen Inneren des CDML begleitet. Während des frühen Juras erfuhr das Grundgebirge eine wichtige Abkühlungsphase, die als das Resultat einer Mantelplume-bezogenen tektonischen Heraushebung und Denudation interpretiert wird, die der Trennung von Ost- und Westgondwana durch kontinentales Rifting vorausging. Obwohl

der Kontinentalrand des CDML während des frühen Juras gebildet wurde, erfolgte die vollständige Entwicklung des passiven Kontinentalrandes in der mittleren Kreide, als das Grundgebirge einen weiteren Schritt beschleunigter Abkühlung erfuhr. Der Mechanismus, der für die mittelkretazische Abkühlung in Frage kommt, war wahrscheinlich ausschließlich isostatischer Natur und resultierte aus der Bildung einer neuen Erosionsbasis durch einschneidende Plattenreorganisationen und beschleunigte Meeresbodenspreizung während des Gondwana-Zerfalls. Als Reaktion auf die niedrigere Erosionsbasis setzte die differentielle Denudation des passiven Kontinentalrandes des CDML ein und führte zu einer flexurellen isostatischen Aufwärtsbewegung der Lithosphäre.
Die Mächtigkeit des denudierten Krustenmaterials seit dem frühen Stadium des Panafrikanischen Ereignisses bis heute beläuft sich auf ca. 31-45 km.

1. Introduction

1.1 Discovery and exploration of central Dronning Maud Land

Dronning Maud Land occupies approximately one sixth of the perimeter of the Antarctic continent encompassing the region between 20°W and 45°E (Fig. 1.1). Originally, the name Dronning Maud Land was given to a smaller area between 37°E and 50°E to honour the Norwegian Queen Maud (1869-1938) (cf. Fritzsche and Bormann, 1995). When in 1937, Norway claimed its sector on the Antarctic continent to secure its whaling activities, the whole claim was named after her.
From 1773 until the 1920s the ice shelf edges and the coastal regions of Dronning Maud Land were first sighted from expedition ships that approached the Antarctic continent. In the 1930s, Dronning Maud Land was systematically mapped using aircraft and aerophotogrammetry of Norwegian and German expeditions. Tens of years later the exploration of Dronning Maud Land was followed by the establishment of logistic bases on the ice shelves and the continent.

The area of study, located in the central part of Dronning Maud Land (8°-14°E), was mapped in detail for the first time in 1958/59 during a Norwegian Antarctic Expedition. The resulting maps, created from oblique aerial photometry, were published by the *Norsk Polarinstitutt Oslo* at a scale of 1:250 000. They provide the basis for the geographical maps used in this study.
In 1959, Russian scientists visited central Dronning Maud Land (CDML) during the 4th Soviet Antarctic Expedition in order to set up a permanent base for later ongoing geographical and geological observations. This led to the establishment of the Lazarev station (69°58'S, 12°55'E) at the edge of the Lazarev Ice Shelf. Due to the limited lifetime of ice based stations, two years later the Russians set up a new station at the Schirmacheroase named Novolazarevskaya (70°46'S, 11°49'E). In 1976, an East German laboratory base was also erected at the Schirmacheroase for ionospheric observations. This base was expanded during later expeditions, and in 1987 it was named the Georg Forster Station.
India started research activities in CDML in 1981 focussing on meteorological and geological surveys. Two new stations were built on the Novolazarevskaya Ice Shelf and at the Schirmacheroase. Up to 1992 eleven Indian expeditions were undertaken to CDML.

During the last German visit, the GeoMaud Expedition of 1995/96, a party of international scientists carried out detailed onshore and offshore geophysical and geological investigations across CDML. One year later an Indian-German party was sent to CDML for further mainly geophysical surveys.

A summary of all expeditions until 1992 as well as references of published reports and results have been compiled by Fritzsche and Bormann (1995).

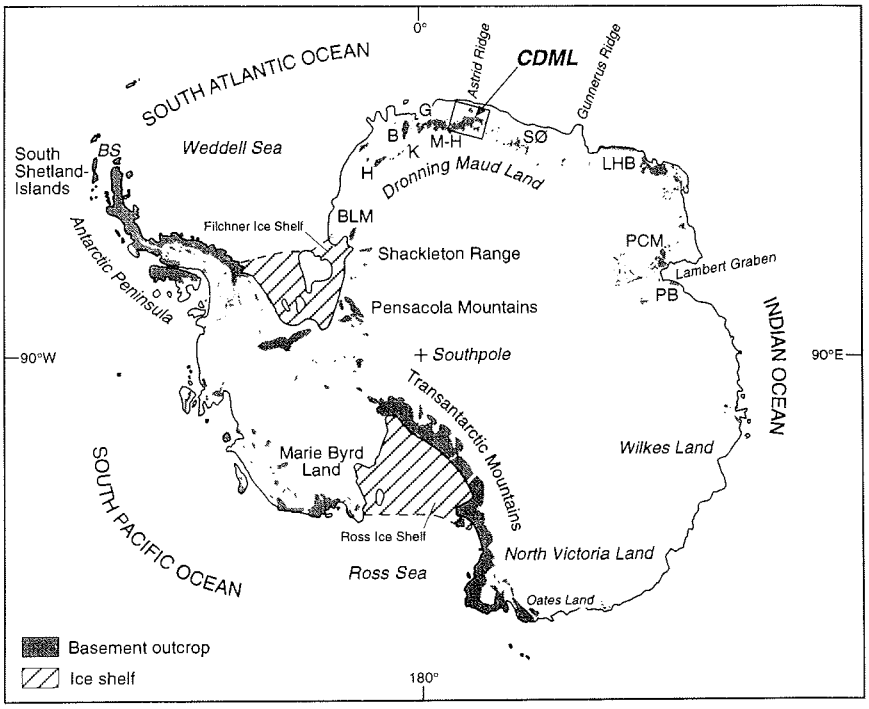

Fig. 1.1 Map of the Antarctic continent.Abbreviations: BS - Bransfield Passage; BLM - Bertrab, Littlewood and Moltke Nunataks; H - Heimefrontfjella; K - Kirwanveggen; B - Borgmassivet; G - Gjelsvikfjella; M-H - Mühlig-Hofmann-Gebirge; SØ - Sør Rondane Moutains; LHB - Lützow-Holm-Bay; PCM - Prince Charles Mountains; PB - Prydz Bay.

1.2 Geographic overview

The study area of CDML is located between 8°E and 14°E, and forms part of an E-W trending mountain chain extending subparallel to the coastline of East Antarctica. The coastal section along the central part of Dronning Maud Land is termed the Princess Astrid Coast (5-20°E). In a N-S direction, the investigated area stretches from 70°40'S (Schirmacheroase) to 72°S (Weyprechtberge).

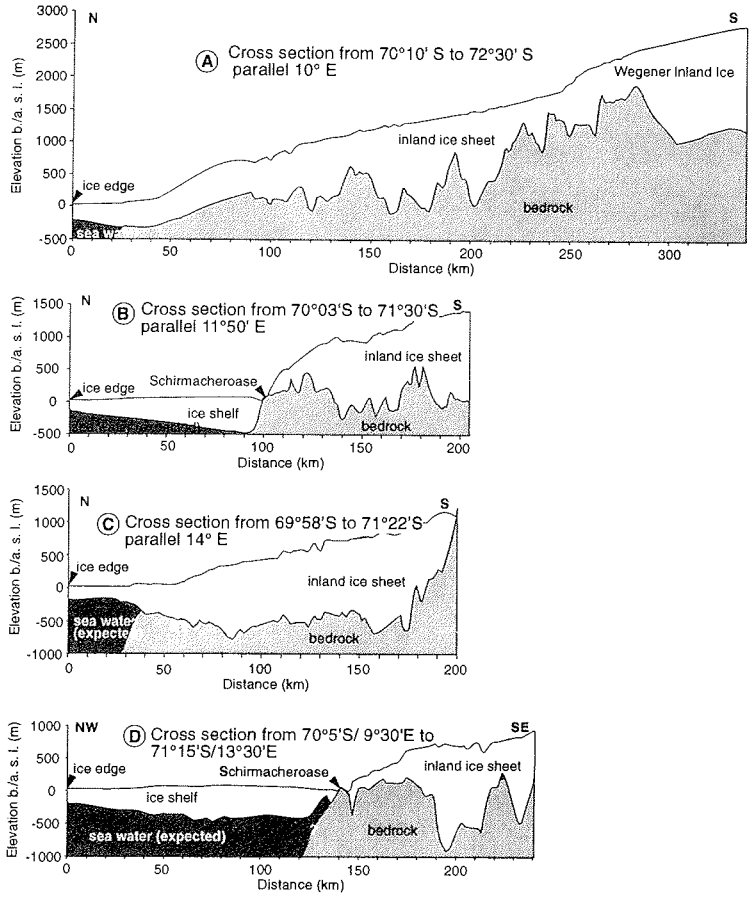

Fig. 1.2 Radar-based subice topographic profiles from CDML showing a highly dissected morphology, locally overdeepened to ~1000 m b.s.l. (from Damm and Eisenburger, 1999). The sites of the profiles are displayed in Fig. 1.5.

To the west CDML is bordered by the mountain ranges of the Mühlig-Hofmann-Gebirge and continues to the east into the Sør Rondane Mountains (see Fig. 1.1). The continental boundary to the approximately 80 km wide Nivlisen (Novolazarevskaya) and Lazarev ice shelves is formed by the Schirmacheroase which is the northernmost ice-free spot in CDML. To the south of CDML, the polar plateau is constituted by the Wegener-Inland Ice and defines the southern limit of the investigated area.
The interior of CDML is dominated by the prominent N-NE trending mountain chains of the Orvinfjella (Drygalskiberge, Holtedahlfjella, Conradgebirge, Dallmannberge, Gjeruldsenhøgda) and further to the east by the Wohlthatmassiv (A.-v.-Humboldt-Gebirge, Zwieselhöhe, Petermannketten, Schneidegebirge, O.-v.-Gruber-Gebirge, Untersee). To the north, the area between the Orvinfjella/Wohlthatmassiv and the Schirmacheroase is largely ice-covered with only a few nunataks protruding the ice sheet.

Fig. 1.3 Sharply incised relief and needle-shaped summit regions of the Petermannketten, Wohlthatmassiv.

Generally the morphology of CDML is characterised by a strongly accentuated relief which reaches maximum values of ~4000 m (Fig. 1.2). From the subice topographic profiles it is evident that the topographic elevations are highest in the central mountain chains where the morphology is characterised by an alpine, sharply incised relief with steep slopes and needle-shaped summits. Here, elevations reach more than 3200 m (Fig.

1.3). Towards the north, elevations decrease with the highly dissected topography locally overdeepened to ~1000 m below sea level. In contrast to the hinterland, the Schirmacheroase region has smooth relief with low elevations ranging between ~0-200 m and a strong imprint of glacial erosion (Fig. 1.4).

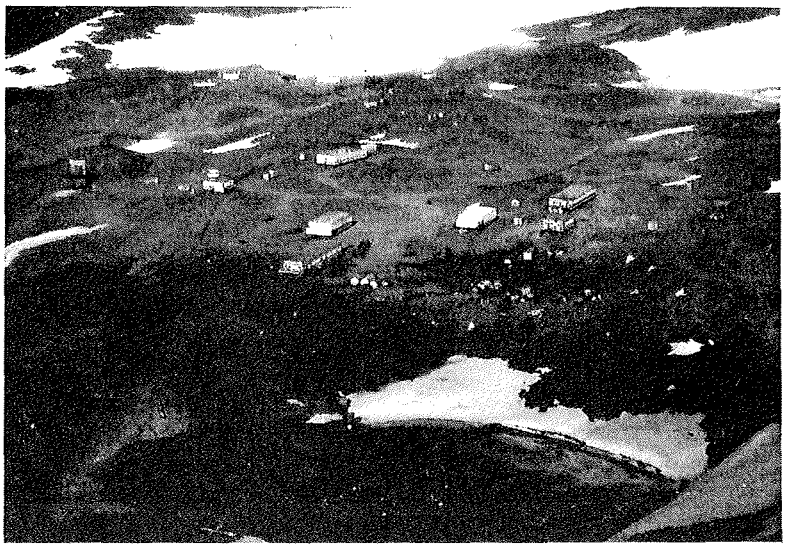

Fig. 1.4 Glacially eroded subdued morphology of the Schirmacheroase. Also shown is the Georg-Forster-Station.

The thickness of the ice sheet in CDML gradually increases from north to south. Behind the Schirmacheroase, an ice ramp is developed with an elevation increasing from ~100 m to ~1000 m further to the south. In the Orvinfjella and Wohlthatmassiv the valleys between the mountain ranges are drained by roughly south to north running glacial streams. These flow into a larger approximately E-W trending glacier discharging into the sea east of the Schirmacheroase. Further south, behind the mountain ranges of the Orvinfjella and the Wohlthatmassiv, the Wegener Inland Ice covers the bedrock totally where it has a thickness between ~2000-2700 m.

1.3 Regional geology

1.3.1 Basement lithology

The outcropping bedrock of CDML is exclusively comprised of crystalline basement rocks which are dominated by interlayered sequences of metasedimentary and metavolcanic units that have undergone polyphase deformation and metamorphism (Fig. 1.5). Plutonic intrusions and laccolites as well as magmatic dykes with a wide range of compositions occur throughout CDML and crosscut the metamorphic basement. Their individual tectono-thermal histories are manifested in the varying degrees of deformation (cf. Bauer et al., 1996; Jacobs et al., 1998).

The lithological assemblage of the metavolcanic sequences has a bimodal character. This is reflected in alternating layers of fine-grained felsic gneisses and amphibolites. Within the metasedimentary units garnet-biotite-paragneisses, sillimanite-cordierite-bearing metapelites as well as forsterite-phlogopite-spinel-marbles and calcsilicates occur. Prekinematically emplaced granites have been locally metamorphosed to garnet-bearing migmatic orthogneisses. The interlayered sequences of metavolcanic and metasedimentary rocks as well as orthogneisses are mainly exposed in the Kurzegebirge, the Conradgebirge, the Dallmannberge and in Småskeidrista, whilst the A.-v.-Humboldt-Gebirge and the western Petermannketten are dominated by metasedimentary units. Within the basement complex garnet-bearing leucogranites are also found (Jacobs et al., 1998). The northeastern part of the Wohlthatmassiv (O.-v.-Gruber-Gebirge) and the In der Schüssel is largely intruded by an anorthosite massiv with subordinate norites and ferrodiorites showing in part syn-magmatic deformation (Kämpf and Stackebrandt, 1985; Bauer et al., 1996). The latest deformational and metamorphic event is postdated by the emplacement of voluminous A-type granites that range in composition from syenitic to monzodioritic and charnockitic. This magmatic suite occupies about 50% of the crystalline basement and constitutes major parts of the Drygalskiberge, the Holtedahlfjella, Gjeruldsenhøgda, the southern and eastern Petermannketten as well as some nunataks which are distributed throughout CDML. Additionally, a variety of post-tectonic lamprophyric and basaltic dykes occurs across CDML (Kaiser and Wand, 1985; D'Souza et al., 1994).

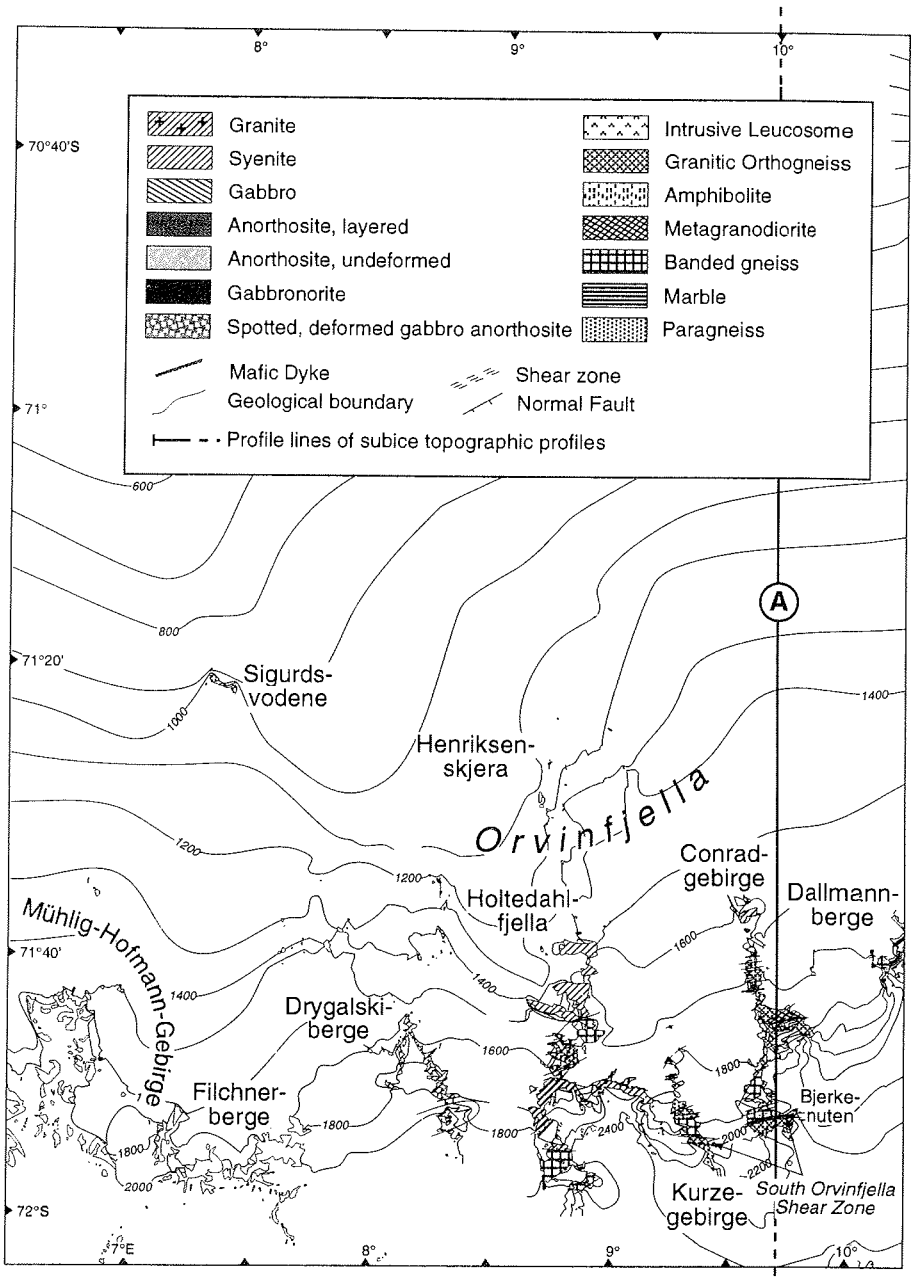

Fig. 1.5 Geological map of CDML.

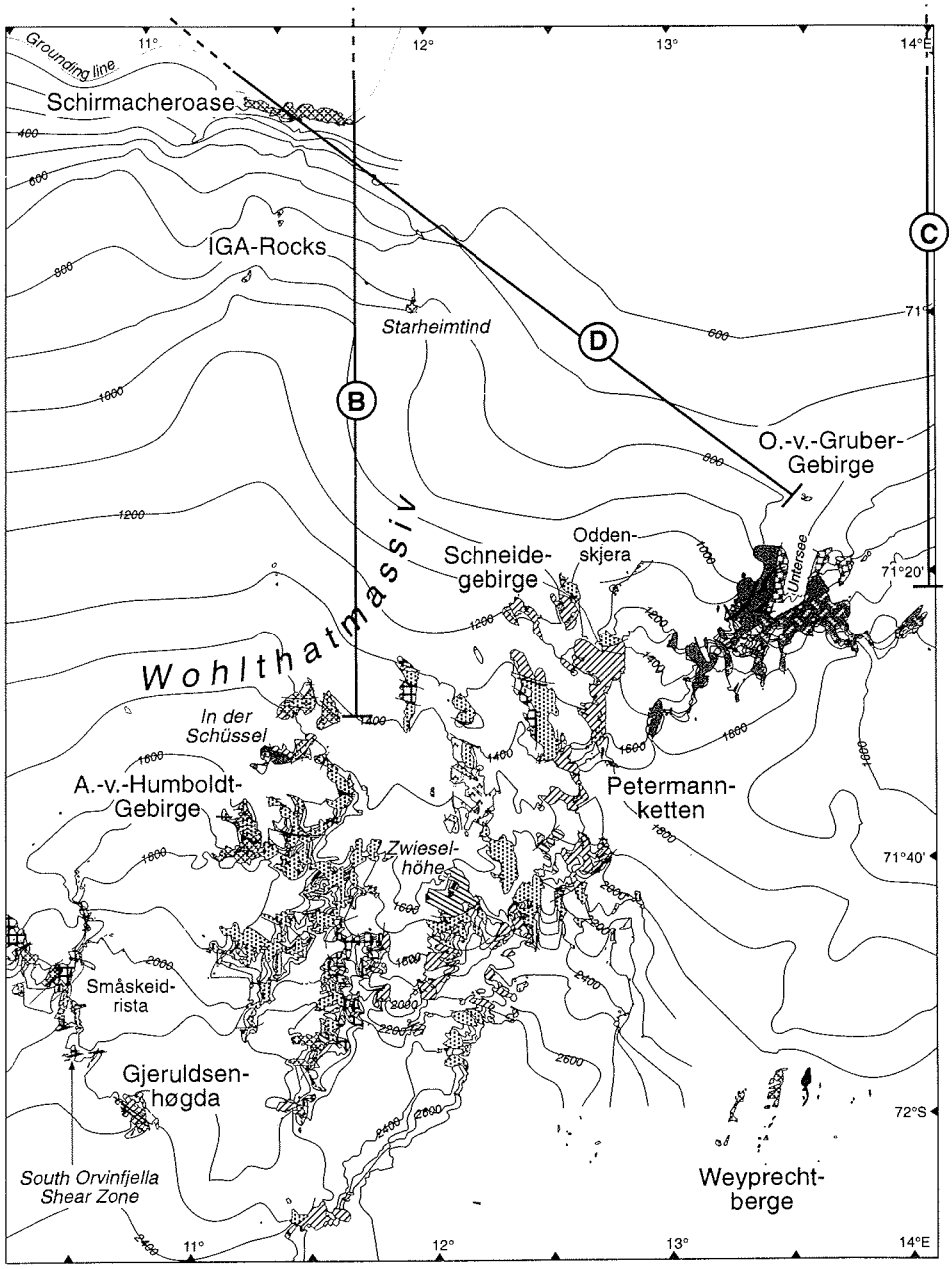

Fig. 1.5 Geological map of CDML (continuation).

1.3.2 Structural basement evolution

The tectono-metamorphic evolution of CDML was controlled by four deformation stages, most of them reaching regional granulite- and amphibolite-facies conditions (cf. Sengupta, 1991; Bauer et al., 1999). From its structural expression the basement can be subdivided into a western (Orvinfjella) and an eastern main structural trends being E-W to NE-SW and N-S, respectively. The E-W-trend can be traced from the Orvinfjella further to the west across the Mühlig-Hofmann-Gebirge to the Gjelsvikfjella, whereas the Wohlthatmassiv structurally resembles the more easterly located Sør Rondane Mountains (Van Autenboer and Loy, 1972; Otha et al., 1990; Shiraishi et al., 1991). In both complexes the earliest stage of deformation (D_1) is preserved only as residual isoclinal folding in gneisses and metavolcanic sequences with the original orientation not restorable (Bauer et al., 1999). The second period of deformation (D_2) superimposed the most extensive structural imprint on the basement rocks of CDML. In the Orvinfjella this major deformational phase led to the development of an E to NE trending foliation and N-vergent folds, also affecting the pre- and synkinematically intruded plutonites. In the central part of the O.-v.-Gruber-Gebirge an anorthositic intrusion retains an E-W trending foliation with the strike gradually developing into a N-S-direction towards the western part of the massiv. The D_2 deformation, accompanied by granulite-facies metamorphism, is also apparent in the Schirmacheroase and the IGA (Institute Geologii Arktiki) Rocks. It has been suggested that an episode of transpressive sinistral shearing (D_3) postdates D_2 deformation (Bauer et al., 1999). In the Orvinfjella intense shearing has led to the development of an E-W-striking proto- to ultramylonitic foliation which can be traced from the Kurzegebirge to the southern part of the Conradgebirge (Bjerkenuten) and the southern Dallmannberge (South Orvinfjella Shear Zone) (see Fig. 1.5). The D_3 deformation is also apparent in the ferrodiorites of the O.-v.-Gruber-Gebirge but here exhibits a NW-directed shear component associated with a granulite-facies metamorphic overprint. Due to the lack of evidence for an E-W-directed compressional regime, the N-S structures in the westerly located parts of the Wohlthatmassiv are interpreted as being related to the rotation of D_2-structures (Bauer et al., 1999). In the Schirmacheroase and the IGA Rocks NW-striking shear zones are also developed. The youngest phase of deformation (D_4) has been recognised throughout CDML to varying intensity. D_4 led to the formation of discrete mylonite shear zones which mainly strike NW-SE in the Orvinfjella and NE-SW in the Wohlthatmassiv. This was accompanied by amphibolite-facies metamorphism (Bauer et al., 1999). A study on metamorphic phase assemblages revealed that the basement of CDML was subjected to at least two metamorphic events with the first one occurring during the Neoproterozoic (Jacobs et al., 1998; Piazolo and Markl, 1998; Colombo and Talarico, 1999). As suggested by Colombo and Talarico (1999) upper

amphibolite conditions prevailed at ~570 Ma (Jacobs et al., 1998) (see below) associated with enhanced migmatisation. This was followed by high-pressure granulite facies metamorphism that possibly occurred between ~530-515 Ma (Jacobs et al., 1998; Colombo and Talarico, 1999).

1.8 Previous geochronological work

Recently published results of zircon U-Pb SHRIMP analyses on samples from CDML have placed new constraints upon its Precambrian and early Paleozoic evolution. With the new data it has been possible to trace back the history of CDML until Mesoproterozoic times (Fig. 1.6). The oldest ages of ~1130 Ma correspond to a time of felsic volcanism which was followed by granulite facies metamorphism and the intrusion of granites between ~1085 Ma and ~1075 Ma. In the anorthosites the oldest U/Pb zircon ages scatter around ~600 Ma, and are interpreted as recording their emplacement. The widespread occurrence of magmatic and metamorphic U/Pb zircon ages between ~570 Ma and ~515 Ma signifies that during the Pan-African event, CDML was affected by at least two stages (570 Ma and 530-515 Ma) of amphibolite- to granulite-facies metamorphic overprinting. According to Jacobs et al. (1998) the last stage was accompanied by the intrusion and granulite-facies metamorphic overprinting of the metagranodiorite and the leucogranites. The last metamorphic event is postdated by the intrusion of a syenite suite at ~512 Ma (Mikhalsky et al., 1997).

The post-Pan African Paleozoic history of CDML is only poorly constrained despite the existence of various radiometric ages obtained mainly by Russian and East German scientist. This includes weak evidence from a Rb-Sr age (biotite) for an unspecified post-Pan African thermal event at ~460 Ma (Mikhalsky et al., 1997). Ravich and Solov'ev (1966) carried out K-Ar whole rock analyses on pegmatite veins from the Wohlthat-masssiv, and obtained ages of ~450 Ma. Similar ages (Rb-Sr on phlogopite, feldspar, amphibole and whole rock) of 458±6 Ma and 455±12 Ma have also been determined by Dayal and Hussain (1997) on lamprophyre dykes from the Schirmacheroase. Their results were interpreted as manifesting post-orogenic igneous activity linked to the Ross Orogeny in the Transantarctic Mountains. K-Ar and Rb-Sr biotite ages on charnockites from the eastern Mühlig-Hofmanngebirge indicate cooling to 300°C at ~450 Ma (Henjes-Kunst and Markl, 1998). Additionally, K-Ar analyses on amphiboles and biotites from lamprophyric dykes of the Schirmacheroase yielded ages of 535-495 Ma (Henjes-Kunst and Markl, 1998). The K-Ar whole rock analyses by Kaiser and Wand (1984) on a basaltic and a

gabbroic sample from the Schirmacheroase gave ages of 383±10 Ma and 154±13 Ma, respectively. In a later study Wand et al. (1988) presented K-Ar whole rock ages on basaltic and doleritic dykes from the Schirmacheroase which range from 330 Ma to 108 Ma with peak distributions at 310±10 Ma and 170±10 Ma. They support a coherence between the Jurassic emplacement of the Karoo igneous province and the basaltic dykes in CDML during the dispersal of East and West Gondwana.

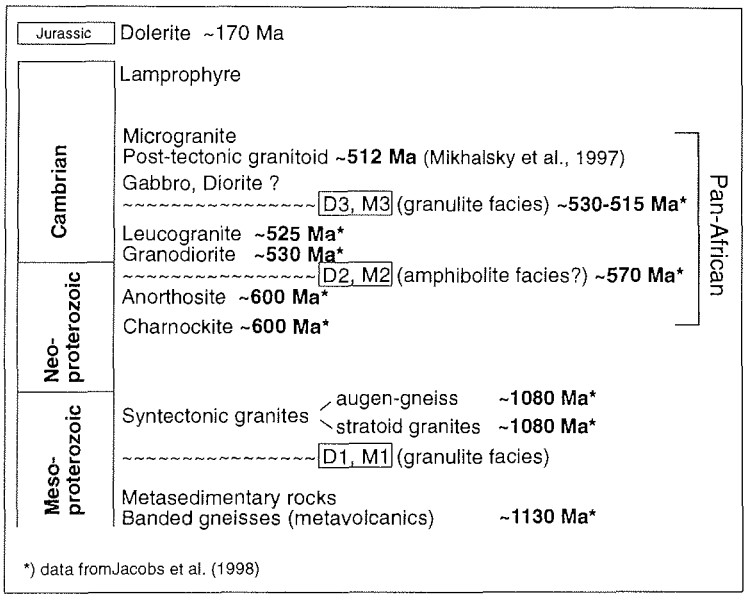

Fig. 1.6 Magmatic and metamorphic basement evolution of CDML as indicated by U-Pb SHRIMP zircon analyses (modified from Jacobs et al., 1998).

1.5 CDML during the assembly of Gondwana

During the Pan-African cycle in Neoproterozoic/early Paleozoic times when East and West Gondwana became amalgamated, CDML was located next to the eastern rim of southern Africa (Fig. 1.7). By this time, the roughly N-S striking Mozambique Belt has formed as a collisional orogen through the closure of the Mozambique Ocean (e.g. Grunow et al., 1996; Dalziel, 1997).

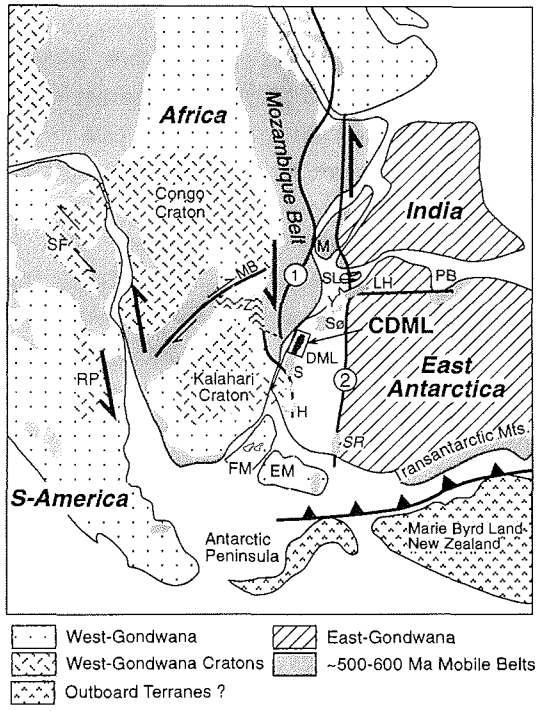

Fig. 1.7 Position of CDML within the late Precambrian/early Paleozoic Gondwana supercontinent (based on Lawver and Scotese, 1987). Geological contours are adopted from Porada (1989), Grunow et al. (1996) and Wilson et al. (1997). Hypothetical continuations of suture zones (1) and (2) between East and West Gondwana, as suggested by Shackleton (1996) as well as Grunow et al. (1996) and Wilson et al. (1997), respectively. Abbreviations: DML - Dronning Maud Land; S - Sverdrupfjella; H - Heimefrontfjella; SR - Shackleton Range; EM - Ellsworth Mountains; FM - Falkland microplate; RP - Rio de la Plata craton; SF - São Franzisco craton; MB - Mwembeshi shear zone; Z - Zambezi belt; M - Madagascar; SL - Sri Lanka; LH - Lützow-Holm Complex; PB - Prydz Bay; Y - Yamato-Belgica Complex; Sø - Sør Rondane Mountains (from Jacobs et al., 1998).

It has been shown by several authors that fundamental similarities exist between the tectono-metamorphic and petrological features of Dronning Maud Land and Mozambique (cf. Pinna et al., 1993; Kröner, 1997; Jacobs et al., 1998). They conclude that the Mozambique Belt finds its southern continuation in Dronning Maud Land. Despite the similarities between the two, there is an ongoing debate about the location of the suture zone in East Antarctica and Africa along which the continental amalgamation occurred. However, the whole assembly trending from western to eastern Dronning Maud Land and farther east has been termed the East Antarctic mobile belt of which CDML is proposed to have formed the central part (e.g. Dirks and Wilson, 1995; Jacobs et al., 1998). There is also evidence that the East Antarctic mobile belt continued to the east, projecting into Sri Lanka and southern India, although the exact position of the eastern extension of the mobile belt is not well defined (Piazolo and Markl, 1998 and references therein). Several studies have demonstrated that striking petrographical and petrological similarities exist between CDML, Madagascar and the Kerala Khondalite Belt in southern India that point towards an analogous metamorphic evolution during the Pan-African event (e.g. Stackebrandt, 1990; Rosen and Raith, 1995; Pradeepkumar et al., 1996; Piazolo and Markl, 1998; Colombo and Talarico, 1999).
In CDML, the Pan-African event possibly terminated with an orogenic collapse that was caused by underthrusting and doubling of the thickness of the continental crust (Bauer et al., 1999; Colombo and Talarico, 1999).

1.6 CDML during the fragmentation of Gondwana

During the dispersal of the supercontinent Gondwana, the continental margins around Antarctica developed progressively into passive margins in a clockwise manner. While Antarctica separated from Africa during the Jurassic, India/Madagascar became disconnected from Antarctica during the Cretaceous. The palaeoposition of East Antarctica before and during the breakup is illustrated in Fig. 1.8 – 1.12.
In the Permo-Carboniferous, extension and active rifting were initiated in a triple junction centred on the Kenyan coast and contemporaneously, the deposition of the Karoo sequence along the southeastern African margin begun (Reeves et al., 1987; Lawver et al., 1991; Salman and Abdula, 1995). The rifting zone along the Kenyan coast possibly extended as far south as southern Africa and led to the formation of broad platform depressions (Mozambique Plateau) which were successively filled with the terrigenous and carbonate sediments of the Karoo Group (Reeves et al., 1987; Salman and Abdula,

1995). It is probable that the rifting between East and West Gondwana occurred at the suture zone along which the two continents were amalgamated during the Pan-African event.

In the Jurassic, widespread intracontinental magmatic activity in southern Africa and Antarctica which marked the increasing extensional forces, led to the eruption of large continental flood basalt provinces known as the Karoo (southern Africa) and Ferrar (East Antarctica) provinces (e.g. Kyle et al., 1981; Eales et al., 1984; Cox, 1988; Brewer et al., 1992). According to Duncan et al. (1997), Karoo and Ferrar magmatism took place between 184 Ma and 179 Ma. At the same time, thick sequences of volcanic rocks were erupted offshore along the Explora Escarpment (Hinz, 1981; Hinz and Krause, 1982). White and McKenzie (1989) suggest that the basaltic volcanism was associated with a thermal anomaly that developed as a mantle plume beneath the lithosphere of Gondwana. Generally, the separation of East and West Gondwana was preceded by a period of strike-slip movements between continental fragments along transform faults and the subsequent development of ocean basins. In the Weddell Sea region, the early extension was followed by transtension and transpression leading to the shearing of the margin of Dronning Maud Land which is represented by the Explora Escarpment (Hinz, 1981; Hinz and Krause, 1982; Kristoffersen and Haugland, 1986; Lawver et al., 1991).

Southward movement of the Antarctic/Indian/Australian plate relative to South Africa/South America took place along the Davie Fracture zone and a system of associated transform faults (see Fig. 1.8 - 1.12) (Martin and Hartnady, 1986; Roeser et al., 1996).

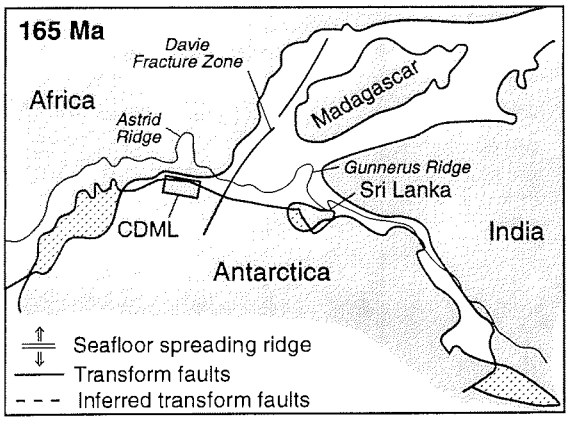

Fig. 1.8 – 1.12 Reconstructions do not include the Falkland Plateau and South America because their movements do not provide significant constraints on the reconstruction shown in this figure. The reconstruction of Roeser et al. (1996) is based on their own data. For clarity reasons the 2000-m-depth contour is shown only for East Antarctica. Abbreviations: eRLS, wRLS = eastern, western Riiser-Larsen Sea; MB = Mozambique Basin; SB = Somali Basin.

Fig. 1.8 Plate reconstruction of Roeser et al. (1996) for the region of the Riiser-Larsen Sea before the onset of seafloor spreading at 165 Ma.

It is suggested that by this time the Astrid Ridge, offshore CDML, was connected to the Mozambique Ridge by a system of transform faults (Bergh, 1987; Sandwell, 1992; Roeser et al., 1996). The Astrid Ridge is separated by the Astrid transform fault into a northern fragment which is most probably oceanic in nature while the southern part consists of continental crust and subordinately volcanic complexes (Bergh, 1987; Roeser et al., 1996; Hinz et al., 1998).

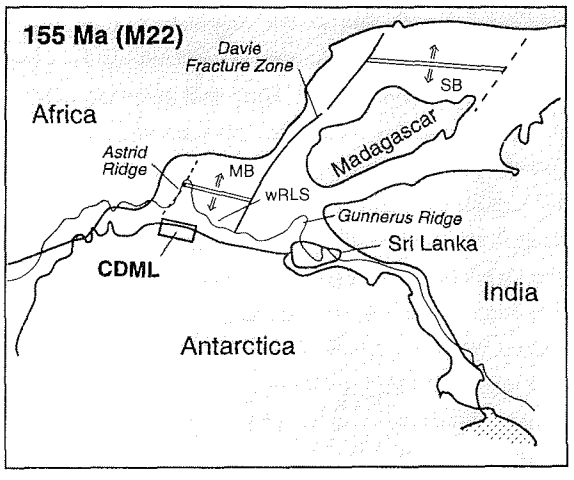

Fig. 1.9 Plate reconstruction for chron M22 (155 Ma). The western Riiser-Larsen Sea and the Somali Basin have opened by about 550 km (modified from Roeser et al., 1996).

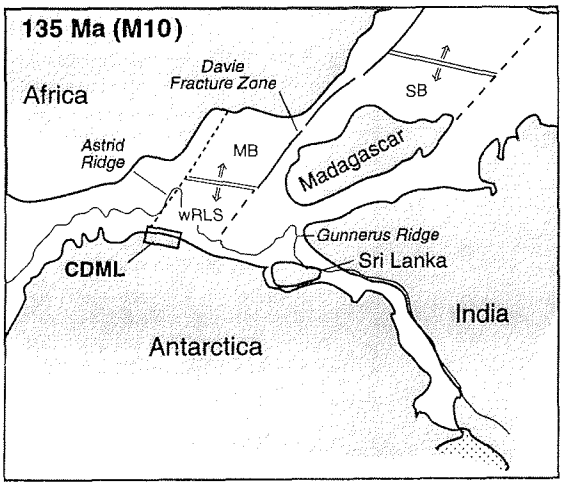

Fig. 1.10 Plate reconstruction for chron M10 (135 Ma). Relative southward movement of East Antarctica by 750 km (modified from Roeser et al., 1996).

Southward movement of the Antarctic/Indian/Australian plate relative to South Africa/South America took place along the Davie Fracture zone and a system of associated transform faults (see Fig. 1.8 - 1.12) (Martin and Hartnady, 1986; Roeser et al., 1996). It is suggested that by this time the Astrid Ridge, offshore CDML, was connected to the Mozambique Ridge by a system of transform faults (Bergh, 1987; Sandwell, 1992; Roeser et al., 1996). The Astrid Ridge is separated by the Astrid transform fault into a northern fragment which is most probably oceanic in nature while the southern part consists of continental crust and subordinately volcanic complexes (Bergh, 1987; Roeser et al., 1996; Hinz et al., 1998).

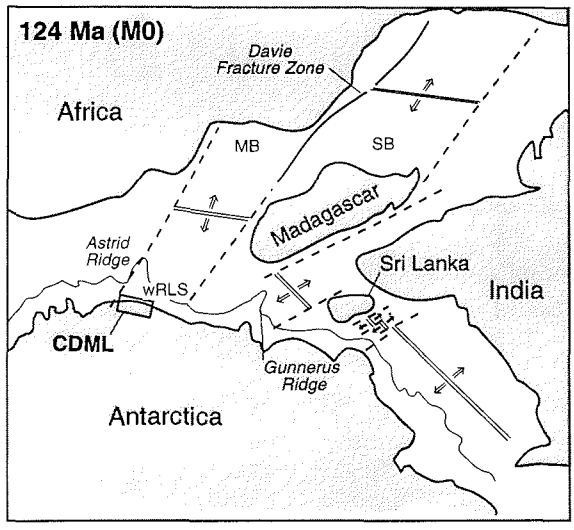

Fig. 1.11 Plate reconstruction for chron M0 (124 Ma). A closed basin opened between East Antarctica, Madagascar, India and Sri Lanka. Strike-slip northward movement of India relative to Madagascar caused the westward propgation of the spreading axis between India and East Antarctica to cut through the Gunnerus Ridge (modified from Roeser et al., 1996).

As a reaction to the strike-slip movements along the transform fault system, major ocean basins as e.g. the Somali Basin, Mozambique Basin and the western Riiser-Larsen Sea have opened (e.g. Ségoufin, 1978; Simpson et al., 1979; Rabinowitz et al., 1983; Cochran, 1988; Roeser et al., 1996) (Fig. 1.8 - 1.11). The onset of oceanfloor production was recognised from the earliest magnetic anomalies in the Mozambique Basin and in the western Somali Basin, dated at ~152 Ma (magnetic anomaly M22) (e.g. Ségoufin, 1978; Simpson et al., 1979; Rabinowitz et al., 1983; Storey, 1995). Hinz et al. (1998) suggest that seafloor spreading has started in the western Riiser-Larsen Sea ~160 Ma ago. The eastern Riiser-Larsen Sea has opened later, between 135-124 Ma (Fig. 1.12).

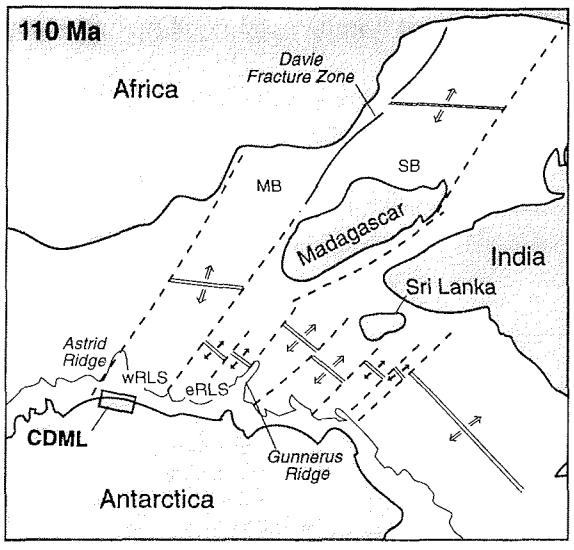

Fig. 1.12 Plate reconstruction for 110 Ma with the opening of the eastern Riiser-Larsen Sea (modified from Roeser et al., 1996).

Since India started its rapid northward drift away from Antarctica from ~96 Ma on (Powell et al., 1988), the South Atlantic-faced continental margin of East Antarctica has attained a more isolated position.

1.7 Scope of the thesis

The primary aim of the thesis is to resolve the tectono-thermal history of a rifted continental margin. Fission-track thermochronology was was chosen as an appropriate tool to reach this aim. The combination of the titanite, zircon and apatite fission-track results on rocks from CDML allows to establish a cooling history for a temperature range of ~320-60°C and, furthermore, to discriminate between continuous and stepwise cooling phases. The passive margin of CDML in East Antarctica is highly suitable for a fission-track based passive margin study, because it is structurally less complex than that of western Dronning Maud Land, where shearing, rifting and the development of a failed rift complicated the margin evolution.

The continental separation in CDML during the initial breakup of Gondwana is discussed in context with a mantle plume that significantly influenced the cooling history of western Dronning Maud Land. The fission-track analyses on rocks from CDML provide important

information about the involvement of a mantle plume into continental separation, because field evidence for mantle plume-related extensive basaltic volcanism in CDML is less apparent than in western Dronning Maud Land with remnants of basaltic lava piles cropping out.

To constrain the post-rift evolution of the passive margin of CDML a geomorphic approach and the contributions of endogenic factors are presented. This topic is closely related to the redistribution of masses in a continental margin setting, with denudation in the continental interior and subsequent sedimentation on the continental shelf. An approach is made to quantify inland denudation and offshore sedimentation deduced from apatite fission-track data and reflection seismic results (cf. Hinz and Krause, 1982). Six dropstone fission-track samples from offshore CDML can provide additional information about the inland denudation and shelf sedimentation.

The fission-track data from CDML are discussed in correlation with the geological and tectonic structures on a local and regional scale. Furthermore, the amount denudation since cooling to below ~320°C is calculated from the fission-track data. Possible relationships between the fission-track results and the sample lithology and/or the mineral composition are also considered.

1.8 Previous fission-track studies on Antarctica

Most of the fission-track investigations available on Antarctica concern the Pacific rim of East Antarctica. The majority of fission-track studies focus on the uplift and denudation history of the Transantarctic Mountains (see Fig. 1.1) (e.g. Gleadow et al., 1984; Fitzgerald, 1986; Gleadow and Fitzgerald, 1987; Gleadow and Fitzgerald, 1988; Wagner et al., 1989; Fitzgerald and Stump, 1997). The fission-track studies of Gleadow et al. (1984) (Dry valleys area), as well as Fitzgerald (1992) manifest the cooling and denudation history of the Transantarctic Mountains in southern Victoria Land, while Balestrieri et al. (1993) (Granite Harbour Intrusives), Fitzgerald and Gleadow (1988), Gleadow and Fitzgerald (1988), Lisker (1996) (Granite Harbour Intrusives and Admiralty Intrusives) and Schäfer (1998) (Oates Land) have deduced the tectono-thermal evolution of the extension of the Transantarctic Mountains in northern Victoria Land. The investigations of Schäfer (1998) also comprised a fission-track analysis of samples from the Shackleton Range. Arne et al. (1993) have carried out a fission-track reconnaissance study on the East Antarctic shield with samples from the Prince Charles Mountains and Wilkes Land and fission-track analysis on the northern Prince Charles Mountains was

performed by Arne (1994). Western Dronning Maud Land was the subject of the fission-track studies of Jacobs (1991) and Jacobs et al. (1992, 1996). The first fission-track apatite and zircon results from CDML were published by Meier et al. (1999).
Fission-track thermochronological studies on West Antarctica (Storey et al., 1989, 1996) are available for Marie Byrd Land (e.g. Adams et al., 1995; Lisker and Olesch, 1997, 1998; Richard et al., 1994). Furthermore, Fitzgerald and Stump (1991, 1992) carried out fission-track investigations on the Ellsworth Mountains in West Antarctica.

1.9 Terminology of vertical crustal movements

In the present study, the term surface uplift is employed for the displacement of the earths surface with respect to the geoid and has an areal extend of at least 10^3-10^4 km^2. Uplift of rocks describes the displacement of rocks relative to the geoid. For rocks being displaced with regard to the surface, the term exhumation is applied (England and Molnar, 1990). Dynamic uplift assesses the contributions of convective flow in the asthenosphere (Buck, 1986; Buck et al., 1988).
The term erosion is used for the simple removal of crustal material, whereas denudation comprises erosional processes as well as the successive isostatic readjustment. The crustal stripping due to exhumation is referred to as tectonic denudation (Summerfield and Brown, 1998)

2. Evolution of passive continental margins

2.1 Introduction

It has long been known that marginal upwarps are common features of rifted continental margins. However, thermal and/or tectonic models have so far been incapable of accounting for marginal upwarps persisting for more than 100 Ma after continental rupture (e.g. Royden and Keen, 1980; Weissel and Karner, 1989; White and McKenzie, 1989; Gilchrist and Summerfield, 1990, 1994; Keen and Beaumont, 1990). With respect to the long-term landscape development of a passive margin, it is crucial to review the thermal, tectonic and geomorphic factors controlling the rifting event itself, as well as the post-rifting evolution of the rifted continental margin (cf. Gilchrist and Summerfield, 1994).

From their morphological expression mature passive margins (>~60 Ma) can broadly be subdivided into two phenotypes. High-elevation passive margins are characterised by a narrow continental shelf and a low-lying coastal region of significant relief, but the most prominent feature is a steeply inclining escarpment or a series of escarpments further inland (Gilchrist and Summerfield, 1990). Behind the escarpment front which is most elevated in this type of passive margin, the morphology develops towards an elevated (>500 m) interior plateau (Gilchrist and Summerfield, 1990, 1994; Gallagher and Brown, 1997). If the marginal upwarp is located in close vicinity to the rift, it is termed a rift flank uplift, but in most cases it is situated more than 100 km from the rift hinge and thus represents the subsequent erosional escarpment retreat (Ollier, 1985). During the Mesozoic fragmentation of Gondwana a variety of such high-elevation-type margins with prominent escarpments were created including SW-Africa (Great Escarpment) (e.g. De Swardt and Bennett, 1974; Summerfield, 1985; Partridge and Maud, 1987, 1988; Rust and Summerfield, 1990), E-Brazil and eastern Australia (e.g. Gilchrist and Summerfield, 1990, 1994; Gallagher et al., 1994).

In contrast, low-elevation-type margins have a more subdued morphology with a broad continental shelf gradually rising towards a low-lying interior. Such margins can be found, for instance, along the coast of southern Australia and eastern Argentina (Gilchrist and Summerfield, 1990). A clear distinction between the two phenotypes is, however, not al-

ways possible. It is likely that a wide range of transitional morphologies exists between these two endmember types (Summerfield, 1991).

2.2 Rift tectonics

During the initial breakup of Gondwana many new continental margins were created around the Atlantic and Indian Oceans. Their formation was initiated by continental rifting - a mechanism which can be either active or passive (e.g. Sengör and Burke, 1978; Beaumont et al., 1982; Keen, 1985; Buck et al., 1988; Bott, 1995). The terms "active" and "passive" refer to the role of the asthenosphere with respect to the lithosphere. Active rifting involves interactions between the mantle and the lithosphere and is basically a process of heat transference, whereas passive rifting is confined to the lithosphere and is considered being the result of differential stresses therein (Sengör and Burke, 1978). In active rifting processes, the development of a rift zone may be related to thermal anomalies that evolve, for example, from mantle anomalies located deep within the asthenosphere (>400 km) which migrate as a mantle plume through the mantle to the base of the lithosphere (Sengör and Burke, 1978; White and McKenzie, 1989; Bott, 1995) (Fig. 2.1). The development of an asthenospheric thermal anomaly promotes a density deficiency within the upper mantle by remelting and removing lithospheric material. This leads to lithospheric thinning and a broadly coincident domal uplift of the area located above the anomaly. Due to subsequent heating from below, the lithosphere becomes thinned and the increasing tension therein can trigger stretching and faulting (Bott, 1995).

Passive rifting, in contrast, is preceded by an episode of large deviatoric tension which mainly concentrates on the rift-external region (Bott, 1995) (Fig. 2.2). If tension is sufficiently large, the lithosphere within the rift-region becomes thinned. As a result of crustal thinning and upwelling asthenospheric material, stretching and faulting can be initiated (McKenzie, 1978).

Volcanism is often an accomplishing feature of both modes of rifting. However, the mechanisms for magma generation can be different in each case. In an active setting, decompression melting will occur in the upper part of the upwelling diapir, but for a passive setting, the decompression melting of rising asthenospheric material will be related directly to lithospheric thinning (Bott, 1995).

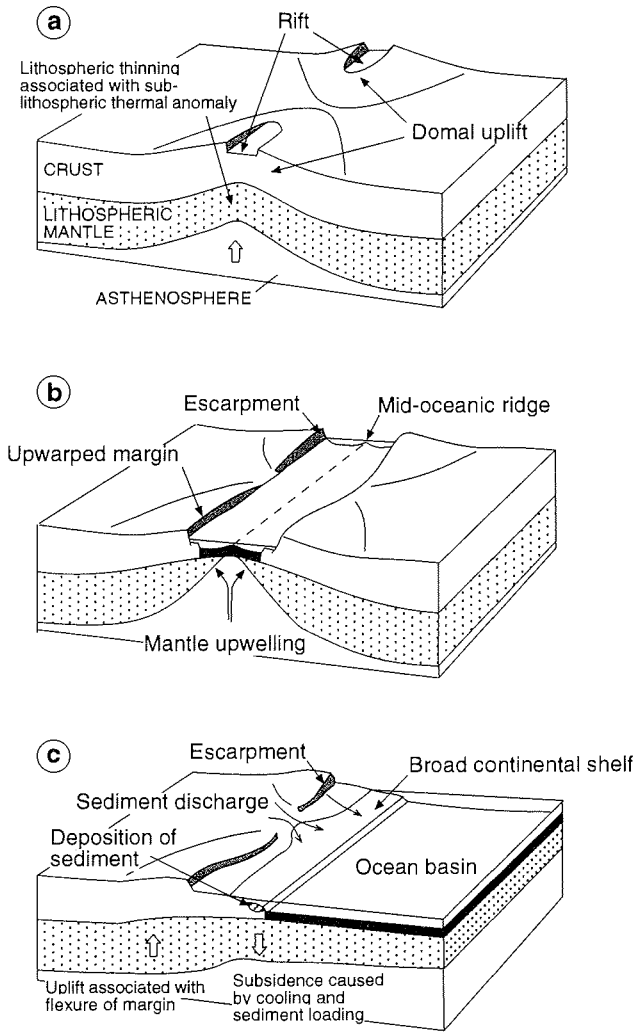

Fig. 2.1 Schematically illustrated process of active rifting and the evolution of a passive continental margin. (a) Onset of rifting and initial updoming. (b) Beginning of seafloor spreading and development of a nascent passive margin. (c) In this case the mature passive margin corresponds to a low-elevation type margin (modified after Summerfield, 1991).

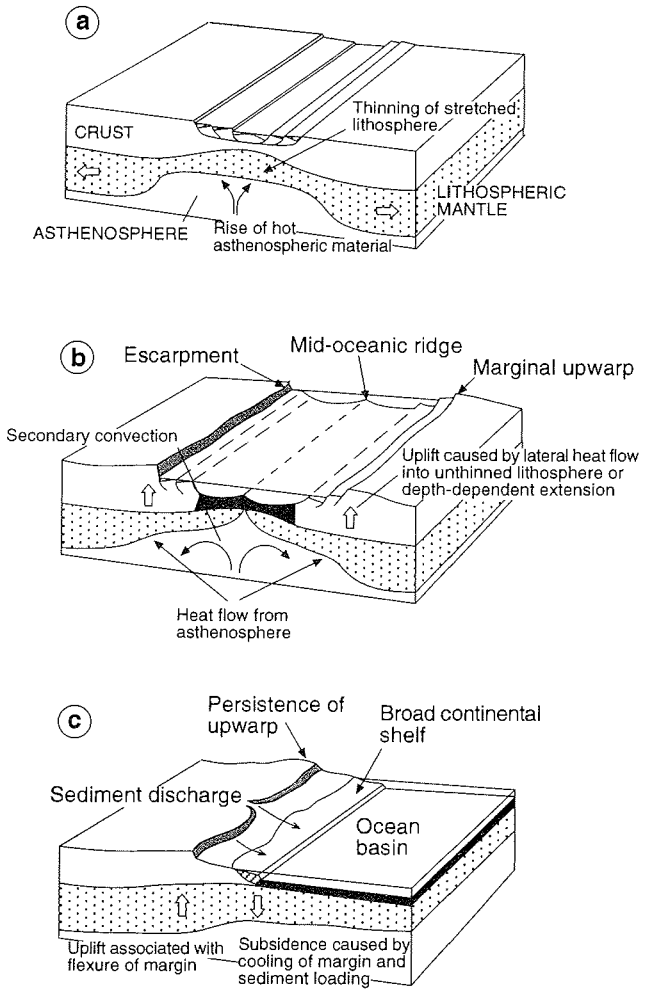

Fig. 2.2 Schematically illustrated process of symmetric passive rifting and the evolution of a passive continental margin. (a) Onset of rifting. (b) Beginning of seafloor spreading and development of a nascent passive margin. Marginal upwarp caused by secondary convection, non-uniform extension and lateral heat flow. (c) In this case the mature passive margin corresponds to a low-elevation type margin (modified after Summerfield, 1991).

Generally, the distinction between the two endmembers refers only to the method of rift initiation. While the rift development progresses, the modes will be rather transitional than clearly distinguishable (cf. Bott, 1995). Nevertheless, the initial mode strongly influences the future geomorphic development of the rift and the rift flanks. For many palaeorifts it is not possible to trace back the mechanism that has been responsible for the initial rift formation but the present-day geomorpholgy of the ancient rift environments can contribute information about the kinematics of rift flank uplift and the post-rifting evolution.

2.3 Mechanisms of rift flank uplift

Young rift zones are characterised by distinct marginal upwarps which are attributed to the thermal and dynamic effects of the rifting event itself. During active rifting the surface uplift is attributed to thinning of the lithosphere from below by convection and to the subsequent removal of material. Hence, the denser lithospheric mantle becomes replaced by hot asthenosphere, and isostatic reequilibration due to the lithospheric density deficiency is attained by surface uplift. The amount of surface uplift can be on the order of several kilometers (Keen and Beaumont, 1990). Because this mechanism can create extensive surface uplift only in slowly moving plates, penetrative magmatism has been proposed to account for increasing uplift in fast moving plates that also show signs of dome-shaped surface uplift (Crough, 1983; Fleitout et al., 1986; Gilchrist and Summerfield, 1994).

In a passive rift setting with a uniformly stretched lithosphere, the vertical movement will be subsidence rather than uplift (McKenzie, 1978). According to Royden and Keen (1980) surface uplift of 1.5 km can be generated by differential extension of the lithosphere. In contrast to the uniform stretching model of McKenzie (1978), differential extension requires a decoupling of the crustal lithosphere from the lithospheric mantle, with the crust being thinned out proportionally less than the sub-crustal lithosphere, while extensional forces operate (Royden and Keen, 1980; Lister et al., 1986; White and McKenzie, 1988). Consequently, by replacing lithospheric mantle with asthenospheric material, surface uplift can occur. Another mechanism for inducing surface uplift in a passive rifting setting is small-scale convection which can be established by lateral temperature gradients in the mantle beneath the rift. Heat advection into the rift shoulders can lead to uplift of more than 1000 m (Keen, 1985; Buck, 1986).

The mechanisms attributed to thermal effects and the dynamic effects of convection are only capable of creating transient uplift that will decay after a period of time. As proposed by McKenzie (1984) thermal effects which are generally time-dependent, are expected to decay within ~60 Ma, and thus thermally and dynamically supported rift flanks can remain uplifted solely as long as extension prevails (e.g. Buck, 1986; Buck et al., 1988).

Permanent uplift of rift flanks can be generated by subsequent isostatic adjustment in response to lithospheric deformation (Gilchrist and Summerfield, 1994). An approach to explain permanent surface uplift was made by Karner (1985) who proposed that thermally induced surface uplift can be maintained while the rigidity of an oceanic lithosphere increases during cooling, and therefore can lock the pre-existing surface uplift. Weissel and Karner (1989) developed a model that relates permanent rift flank uplift to a flexural isostatic compensation caused by mechanical unloading of the lithosphere during asymmetric rifting and detachment faulting. Although the amount of uplift can be several kilometers, sediment loading in the rift basin will reduce the amplitude of uplift substantially. Nevertheless, permanent uplift as a consequence of isostatic rebound is confined to the area adjacent to the rift and it cannot account for upwarps located more than 100 km inland.

A viable explanation could be that magmatic underplating and thickening of the crust from below occurs. White and McKenzie (1989) inferred an areal extension of the domal uplift associated with underplating on the order of 1000-2000 km in diameter. Underplating can take place by decompression melting of asthenospheric material due to lithospheric extension and by addition of anomalous hot asthenosphere to the crust. Depending on the temperature, and hence the density of the anomalous hot mantle, permanent uplift in the range of 1000-2000 m is expected (White and McKenzie, 1989). The continental flood basalts that have been observed in a couple of palaeorift environments, for instance the Ferrar (Antarctica) or the Karoo (southern Africa) and Deccan Trapps (India) magmatic provinces are considered as having been generated by the effusion of crust-penetrating magma from such asthenospheric thermal anomalies (see White and McKenzie, 1989; Baksi, 1994; Duncan et al., 1997). However, such domal uplifts do not explain marginal upwarps with a riftparallel extension that commonly have a shorter wavelength topography than would be the case for a domal uplift triggered by magmatic underplating.

From the above discussion it can be concluded that none of the models described can account adequately for the features observed at mature passive margins. Thermally induced uplift will decay after ~60 Ma and the high heat flow will be confined to the vicinity of the rift, and thus

cannot be responsible for uplifts >100 km inland. Magmatic underplating is unable to create riftparallel upwarps and the dynamic and mechanical models are not capable creating uplift located more than 100 km away from the rift hinge (cf. Royden and Keen, 1980; Buck, 1986; Weissel and Karner, 1989; White and McKenzie, 1989).
So far, denudational processes have not been included into the models of passive margin evolution. But the thicknesses of offshore sediments that were deposited adjacent to rifted continental margins, e.g. in the Cape Basin clearly imply that significant erosion must have occurred after rifting (Rust and Summerfield, 1990). Depending on the lithospheric rigidity, the post-rifting denudation can invoke a flexural isostatic rebound of the lithosphere rather than an Airy isostatic compensation, and potentially it can result in surface uplift. The geomorphic expression of high-elevation type passive margins is thought to reflect the interaction of differential denudation across the continental margin and the subsequent flexural isostatic compensation by the unloaded lithosphere (Gilchrist and Summerfield, 1990, 1994).

2.4 Differential denudation and flexural isostasy

It is crucial to the geomorphological evolution of a mature passive margin to make assumptions about its pre-rifting topography. Although significant rift flank uplift can be generated during rifting, the pre-breakup regional elevation within a supercontinent, such as Gondwana and Laurasia might have initially been high. According to Gilchrist and Summerfield (1990, 1994) the landscape development of highly elevated regions within a supercontinent would have been characterised by low channel gradients and thus low denudation rates due to the larger distances between the source and the mouth of riversystems. Furthermore, any relief modification could have been lowered by arid climatic conditions. Climate models for Gondwana and Laurasia during the Permo-Triassic suggested that the climate would have been dominated by extreme continentality and low denudation rates for latitudes <40° (Kutzbach and Gallimore, 1989). However, any residual elevation may have been modified by rifting-related surface uplifts as described in the previous chapter.
As soon as continental breakup occurs, the evolution of a dual denudational system across the developing passive margin is initiated in response to the lowering of the erosional base level. Along the rift flanks an oceanward directed drainage system will evolve separated by an escarpment or a series of escarpments from internally draining rivers (Fig. 2.3). The high

relief of the newly formed continental margin will lead to enhanced denudation of the coastal catchment whereas beyond the escarpment erosion will be less aggressive due to the inherited subdued relief (Gilchrist and Summerfield, 1990). As a consequence of progressive denudation along the escarpment front, the escarpment will retreat further inland. The best studied example of passive margin evolution by escarpment retreat is given by the Great Escarpment (southern Africa) (e.g. Ollier and Marker, 1985; Summerfield, 1985; Partridge and Maud, 1987, 1988; Rust and Summerfield, 1990) but similar features have been observed at the continental margins of eastern Australia (e.g. Moore et al., 1986; Dumitru et al., 1991) and the Red Sea (e.g. Bohannon et al., 1989; Omar and Steckler, 1995; Menzies et al., 1997). Nonetheless, discontinuous denudation across a passive margin is not solely confined to mature passive margins, but is also a phenomenon of young margins such as the Red Sea. This led Gilchrist and Summerfield (1994) to conclude that the differential in denudation must be maintained from the onset of the post-rift evolution until the mature stage.

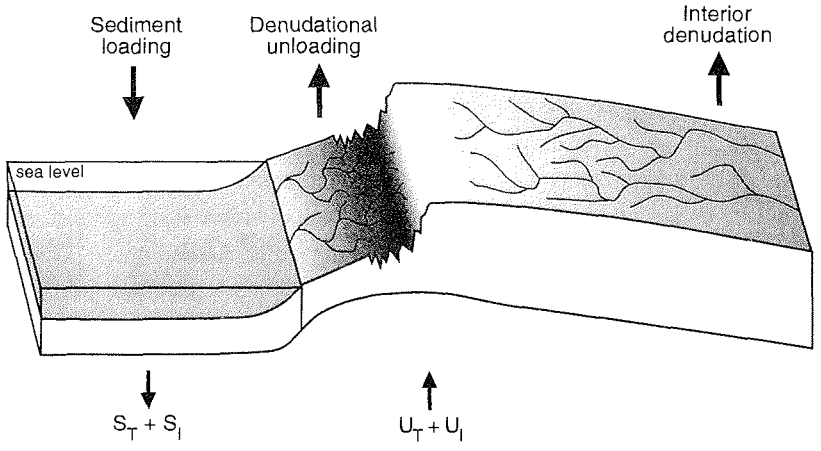

Fig. 2.3 Schematic cross-section of an idealised passive margin with an escarpment crest separating two oppositely directed drainage systems (modified from Tucker and Slingerland, 1994). S_T, U_T = thermally induced subsidence/uplift; S_I, U_I = isostatically induced subsidence/uplift. The denudational-flexural coupling reflects enhanced denudation along the coastal region and subsequent upward movement of the escarpment. In addition, the offshore shelf subsides due to sediment loading.

The permanent uplift observed at mature passive margins is considered to reflect the flexural isostatic upward compensation as a reaction to the differential denudation across the margin.

In contrast to an (local) Airy isostatic compensation which is confined to the immediate area where material has been removed, a flexural readjustment will extend over an area larger than that altered by erosion. The amount of flexural upwarp/downwarp along the passive margin is mainly controlled by the lithospheric rigidity D which is given by

$$D = \frac{E \times T_e^3}{12 \times (1 - \upsilon)}$$

with E = Young modulus, T_e = effective elastic thickness and υ = Poisson's ratio (cf. Gilchrist and Summerfield, 1994). This equation forms the base of the models discussed below.

Normally, hot lithosphere has a low rigidity whereas older and cooler lithosphere becomes increasingly rigid. During the initial stage of the post-rift evolution, subsidence mainly occurs because of thermal contraction and the resulting increase in density of the cooling lithosphere. When the lithosphere has cooled sufficiently, flexural bending starts to overcome the thermal relaxation. As soon as the rigidity of the lithosphere is high enough, denudational unloading along the continental rupture can create an isostatic flexural upwarp which can be anticipated by sediment loading on the seaward side of the margin and an isostatic flexural downward compensation. With increasing lithospheric rigidity the bulge of maximum flexural uplift retreats further inland (Summerfield, 1985).

Gilchrist and Summerfield (1994) have modelled the topographic evolution of the Namibian Atlantic margin through time by employing different elastic thicknesses of the lithosphere (Fig. 2.4).

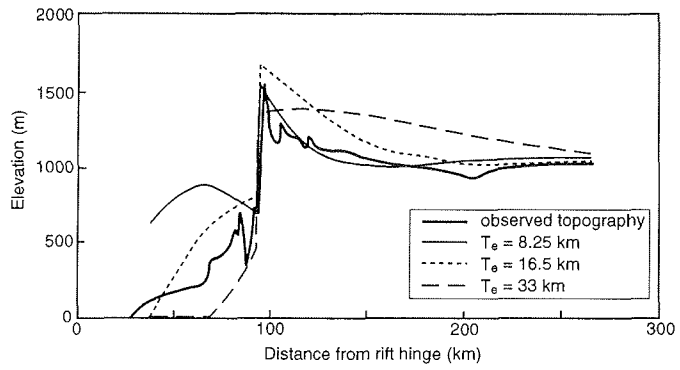

Fig. 2.4 Models of the denudational-flexural behaviour of the western margin of southern Africa (Great Escarpment) (from Gilchrist and Summerfield, 1994)."Rift hinge" = axis defining the transition from unstretched to stretched lithosphere. Comparison between the observed and modelled topography across the passive margin for a denudational-flexural coupling. The results are shown for different elastic thicknesses T_e.

The models show that the elastic thickness does not have a significant effect on the amplitude of marginal upwarp but has a substantial influence on the wavelength of the topography. The longest wavelengths would be thus expected for the largest values of the elastic lithospheric thickness. Fig. 2.5 illustrates the distribution of the accumulative denudation across the margin since the onset of rifting.

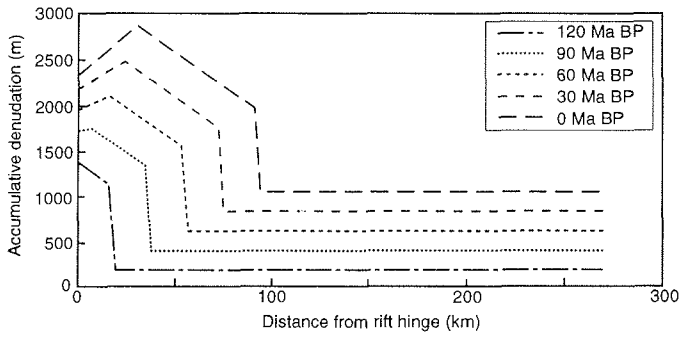

Fig. 2.5 Evolution of the denudational pattern through time for T_e = 16.5 km.

Throughout the post-rifting evolution of the margin the amount of denudation is highest in the coastal region, whereas behind the escarpment denudation significantly decreases towards a constant value. As displayed in Fig. 2.6 the flexural uplift along the passive margin develops progressively with time. Synchronously the axis of the maximum upwarp retreats further inland (Fig. 2.7).

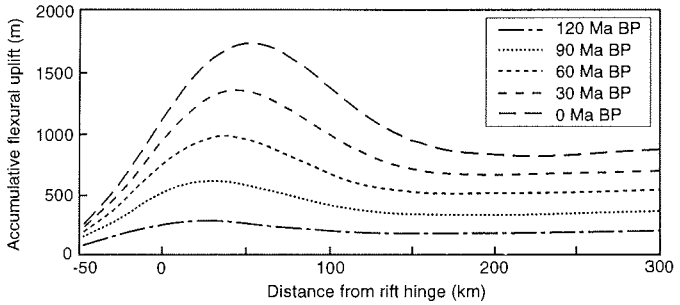

Fig. 2.6 Increasing flexural uplift through time (T_e = 16.5 km).

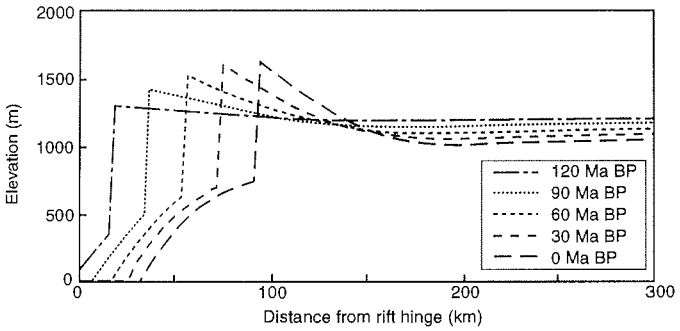

Fig. 2.7 Inland migration of the axis of maximum flexural uplift and retreat of the escarpment (T_e = 16.5 km).

The continental margin evolution has also been modelled for an Airy-isostatic case which is based on a zero-value elastic lithospheric thickness and for a lithosphere of infinite rigidity (Fig. 2.8 and 2.9). Both models are not capable of producing the amount of marginal uplift

that has been observed at the Namibian Atlantic margin. From this Gilchrist and Summerfield (1994) concluded that the flexural isostatic response must play an important role in the generation of the denudational pattern observed at mature passive margins.

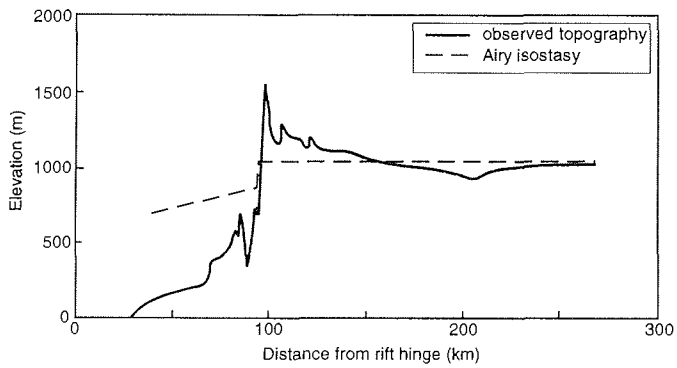

Fig. 2.8 Airy-isostatic case for a zero-value lithospheric rigidity.

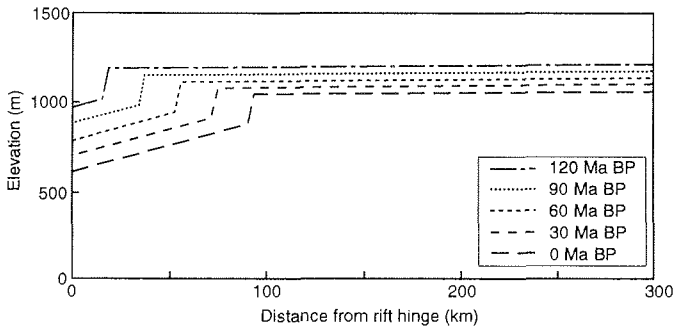

Fig. 2.9 Airy-isostatic case for an infinite rigidity through time. No uplift is created by this mechanism operating alone.

It should be noted that Gilchrist and Summerfield (1994) based their models involving a flexural response of the lithosphere on an effective elastic thickness of 16.5 km which is relatively low in comparison with other studies. So far, no adequate models are available for eleastic thicknesses of >40 km and thus the models of Gilchrist and Summerfield (1994)

approximate a potential passive margin evolution. For instance, Ten Brink and Stern (1992) assumed an elastic thickness of ~90 - 110 km for the Transantarctic Mountains and Stephenson and Lambeck (1985) employed a value of 22 km for southeastern Australia. Van der Beek (1995) concludes that the elastic thickness of the lithosphere should be on the order of >40 km in the onshore region and decrease towards ~20 km in adjacent offshore basins.

In order to assess quantitatively the isostatic readjustment in the offshore and onshore regions two concepts have been developed; one is based on the "backstripping" of sediments from the rift-basin, the second concerned with the "backstacking" of eroded material onto the pre-existing topography (Steckler and Watts, 1978; Brown, 1991). The "backstripping" procedure of Steckler and Watts (1978) serves to estimate the amount of isostatically driven subsidence and additionally to differentiate between the isostatic and tectonic effects on a subsiding rift-basin. By removing the sediment load from the offshore margin, the amplitude of an Airy and a flexural isostatic downward compensation that is attributable to the deposition of sediments alone, can be calculated. The amount of subsidence U_T can be determined by applying the transformation

$$U_T = w + s\frac{(\rho_s - \rho_a)}{(\rho_w - \rho_a)}$$

with w = present-day water depth, s = sediment thickness and ρ_s, ρ_a, ρ_w = density of sediment, asthenosphere and seawater, respectively (modified by Van der Beek, 1995).
Complementary to the "backstripping" concept is the "backstacking" technique of Brown (1991). This allows the erosional and local isostatic rebound component to be resolved from fission-track-based uplift profiles. The amount of upward movement U_T is given by

$$U_T = (H_0 + \Delta E) - \left(\frac{\Delta E \times \rho_c}{\rho_a}\right) - H_i - \Delta H_{SI}$$

with H_0, H_i = present-day and initial elevation, ΔE = mean thickness of erosion, ρ_c, ρ_a = crustal and asthenospheric densities and ΔH_{SI} = change from initial to present-day sea level. By knowing the present-day and palaeo-sea level as well as the palaeo-elevation it is therefore

possible to analyse the contributions of erosion, isostatic upward compensation and true tectonic uplift to highly elevated rifted margins.

2.5 Surface processes and landscape evolution of passive margins

When resolving the post-rift evolution of a passive margin surface processes governing the denudation pattern must also be taken into account. A series of studies have been published which are mainly concerned with the modelling of various surface parameters controlling long-term escarpment retreat (e.g. Gilchrist et al., 1994; Kooi and Beaumont, 1994; Tucker and Slingerland, 1994). One of the exogenic factors influencing the lateral escarpment retreat is the steepness of bedrock channels. Their power to incise the underlying bedrock increases with the size of the drainage area. Additionally, low sedimentation rates and a high elevation of the area as well as flexural isostatic upward movement help to maintain the escarpment morphology through time. The models of Kooi and Beaumont (1994) use a different approach which relates the denudational and morphological features observed in an escarpment environment to the effects of hillslope and fluvial transport. In their models they have shown that the escarpment can retreat if its front coincides with the drainage divide and if the reaction time for fluvial mass transport is long. Flexural isostatic compensation along the escarpment front helps to keep the crest as a drainage divide, and for low flexural lithospheric rigidities the velocity of escarpment retreat will be reduced. For an arid climate with low weathering rates the escarpment will have a sharp-topped shape with straight contours, whereas in a humid and temperate climate the escarpment will develop towards a convex upper slope and a concave lower slope morphology. Furthermore, resistant caprocks, as for instance the Karoo basaltic sequence, exert a major control on the long-term evolution of an escarpment while preventing erosion of the underlying and possibly less resistant rocks (Kooi and Beaumont, 1994). The model results of Kooi and Beaumont (1994) have been applied by Gilchrist et al. (1994) to the development of the Great Escarpment along the Namibian Atlantic margin. By combining the erosion-relevant parameters, the various morphological features of the Great Escarpment could be resolved.

2.6 Passive margin evolution constrained by apatite fission-track analysis

Fission-tracks studies on the evolution of passive margins have mainly focused on the timing and the tectonic post-rifting development of the newly formed continental margin (cf. Gallagher and Brown, 1997). Most of these studies deal with the passive margins that formed during the Mesozoic breakup of Gondwana, e. g. in southeastern Australia (Moore et al., 1986; Dumitru et al., 1991), southeastern Brazil (Gallagher et al., 1994), Red Sea/Gulf of Aden (e.g. Bohannon et al., 1987; Menzies et al., 1997) and southeastern Africa (Brown et al., 1990; Brown, 1992). The majority of these studies show a distinct pattern of increasing apatite fission-track ages (FTA) with increasing distance from the continental margin as well as a pronounced positive correlation of the FTA with the topographic elevation. The appearance of the youngest apatite fission-track ages is commonly associated with the lowest elevations in vicinity to the coastline whilst the oldest apatite fission-track ages are expected to occur further inland, somewhere in the more elevated interior. The amounts of denudation that have been deduced from fission-track analysis are typically higher than those calculated from numerical models for a simple morphological escarpment evolution (see above). By successive adjustment of the numerical modelling parameters for individual passive margins, a good agreement between the fission-track based estimates and the model results can indeed be obtained (cf. Gilchrist et al., 1994; Gallagher and Brown, 1997).

In addition to the quantitative information on denudation, fission-track analyses can be employed to date tectono-thermal events, using the assumption that the FTA directly reflect tectonic events, i. e. tectonically related denudation. Although initial rifting-related periods of accelerated denudation have been observed in a wide range of continental margin studies, morphologically-driven mechanisms for enhanced denudation have been neglected in the interpretation of fission-track data. For instance, it is crucial to the mode of landscape development to know, how fast any new drainage system becomes established. If river systems of the coastal catchment captured those draining landward shortly after breakup, then crustal cooling and denudation will occur over a large area extending far into the interior. In contrast, for a retarded breaching of the marginal upwarp the period of enhanced denudation and crustal cooling will be confined to a narrow zone adjacent to the coast, with the interior region recording a later phase of cooling (Summerfield and Brown, 1998). The importance of local morphological effects can be seen in the Lesotho Highlands of southern Africa. Here the results of an apatite fission-track study (Brown, 1992) imply the removal of less than 1 km of

crustal material in the last 130 Ma. The extremely low denudation rate required over this time is in marked contrast to the high elevation (>2000 m) and the present strongly accentuated local relief of the Lesotho Highlands as well as their proximity to the Indian Ocean (Brown, 1992; Summerfield and Brown, 1998). The present local relief of the Lesotho Highlands implies a currently prevailing high denudation rate of >100 m/Ma (Summerfield, 1991a). Summerfield and Brown (1998) attribute the recent accelerated denudation in the Lesotho Highlands to the erosional power of the Orange River headwaters that have cut through the resistant Karoo basalts into the softer, underlying sediments. Such denudational events can also be recorded in the fission-track data and they are not related to any tectonic upward movement.

3. Fission-track thermochronology

3.1 Introduction

Fission tracks are nuclear damage trails in solids. They are produced either by spontaneous fission of naturally abundant radioactive elements, such as uranium and thorium, or by induced fission through irradiation of elements, for example with neutrons, protons or γ-rays. The fission reaction of a single nucleus produces two heavily positive charged nuclides that travel away from their source with high velocity while leaving behind a linear track in the insulating solid (Fleischer et al., 1975; Wagner and Van den haute, 1992).

The exploitation of fission reactions for geochronological applications takes advantage of the natural abundance of ^{238}U in certain minerals. To be suitable for fission-track dating, a mineral must contain substantial amounts of ^{238}U due to the very slow fission decay of ^{238}U (half life 8.2 x 10^{15} a; Holden, 1989). Additionally, the minerals should occur in relative abundance among the rock-forming minerals. Routinely employed are apatite, zircon and titanite, with apatite being the best studied mineral. In analogy to conventional radiometric dating methods where parent/daughter isotopic concentrations are measured, fission-track dating is based on the determination of spontaneous and induced track densities by counting the fission tracks. Induced fission tracks are generated by irradiation with thermal neutrons which cause the fission of ^{235}U. Due to a constant $^{235}U/^{238}U$ ratio and a constant nuclear fission rate in natural minerals, the apparent (see below) fission-track age (FTA) of a mineral grain can be determined from the ratio between the spontaneous and induced tracks. When a sample containing fission tracks is heated through a certain temperature range, the fission tracks will become progressively erased. This erasure or annealing begins at a mineral-specific temperature with the degree of annealing increasing towards higher temperatures. This temperature range is known as the partial annealing zone (PAZ). As soon as a distinct temperature threshold is reached, the fission tracks become totally annealed. The temperature range of the PAZ is best investigated for apatite. Due to its low temperature range, the apatite PAZ (APAZ) can be observed *in situ* in deep borehole samples (Naeser and Forbes, 1976; Naeser, 1979; Gleadow and Duddy, 1981). Based on drillcore fission-track results, an APAZ from ~60°C to ~110°C has been established (e.g. Gleadow and Duddy, 1981; Fitzgerald et al., 1988; O'Sullivan et al., 1996; O'Sullivan and Currie, 1996). In addition to

the *in-situ* observation, the well investigated crystallographical properties of apatite render this mineral highly suitable for fission-track analysis. The annealing behaviour for zircon and titanite is less well constrained because their partial annealing zones occur at higher temperatures and hence at deeper crustal levels, where natural track fading cannot be studied *in situ*. From laboratory annealing experiments, Yamada et al. (1995) suggest a zircon PAZ (ZPAZ) ranging from ~210°C to ~320°C for a heating duration of 10^7 years. The titanite PAZ (TPAZ) is inferred to range from 265 - 310°C (Coyle and Wagner, 1998). Coyle and Wagner (1998) also revealed that no *in situ* annealing occurred in titanites recovered from ultra-deep drillcores to at least depth of ~9 km. If palaeotemperature information of a fission-track sample plus the FTA are known, then estimates about the minimum amount of denudation to bring the sample to surface conditions since the time dated by the FTA can be made. Additional information about the thermal history of a sample can be drawn from measuring the lengths of fission tracks. When a sample is heated through the PAZ the lengths of fission tracks are subjected to progressive shortening. Hence, the lengths of confined fission tracks (true lengths of horizontal tracks) serve as an indicator for the degree of annealing a sample has experienced. This is routinely applied to apatite fission-track analysis, but is also increasingly employed for titanite (e.g. Gleadow et al., 1986ab; Gleadow and Fitzgerald, 1987; Coyle and Wagner, 1998). Currently, efforts are made to extend the applicability of track length measuring to zircon samples (Yamada, 1998).

Generally, FTA are apparent ages and do not record a samples age or a distinct cooling event, but reflect the time a sample has spent within the PAZ. The more rapid a sample has cooled through the PAZ, the closer the FTA will match the time of the cooling event. For a sample cooling slowly or having a polyphase cooling history, the FTA record any moment within the PAZ. In the present study, the term FTA is used throughout, but it should be kept in mind that these FTA are apparent ages.

3.2 Principles of fission-track analysis

During the spontaneous fission decay of natural ^{238}U the two positively charged fragments traverse the crystal at high speed creating a linear track within the host-mineral lattice. To render these fission tracks visible, they can be enlarged by chemical etching. Appropriate

etching conditions can be basically controlled by the concentration of the etchant and the etching time (Wagner and Van den haute, 1992).
The fission decay of ^{235}U in a crystal is induced by irradiation with thermal neutrons. During the irradiation process the sample is bombarded with thermal (slow), epithermal (partially slowed) and fast neutrons with thermal neutrons triggering the desired fission of ^{235}U. However, epithermal neutrons are also capable of inducing fission of ^{235}U whereas fast neutrons trigger the fission of ^{238}U. Both effects can lead to an underestimation of the FTA if the reactor facility is not well thermalised (Wagner and Van den haute, 1992). A good thermalisation of the reactor is therefore of great importance for irradiation (Wagner and Van den haute, 1992) because tracks whether induced by the fission of ^{235}U or ^{238}U are microscopically indistinguishable.
When the external detector method is applied for fission-track analysis, usually U-poor muscovite planar crystals are attached to the surface of the sample before irradiation. During irradiation new tracks that also shoot into the mica are formed in the mineral grains. After irradiation, the induced tracks in the mica can be revealed by appropriate etching. For the fission-track analysis, the induced tracks are counted in the external detector. The newly formed tracks are also present in the sample itself, though they remain invisible, because the sample is not etched again. The external detector method allows counting of spontaneous and induced tracks separately for individual grains. This therefore permits the calculation of individual ages within a rock sample.
The neutron fluence and gradient of the sample suite is monitored by using precisely calibrated U-doped glass monitors.

3.3 Annealing kinetics and interpretation of fission-track data

Radiation damage generated by nuclides through fission decay indicates an energetically unstable state of the crystal lattice within the host. With increased temperature this damage becomes restored by progressive diffusion and the fission tracks anneal, causing the spatial and areal density of fission tracks within each grain to be reduced (Laslett et al., 1987; Wagner and Van den haute, 1992). This means that the probability of tracks intersecting a mineral surface decreases during annealing, and the FTA of the analysed sample will become younger (Wagner, 1981; Green, 1988). In addition to the FTA, the lengths of the horizontal

tracks will be subsequently reduced within the PAZ (Gleadow and Duddy, 1981; Gleadow et al., 1986a; Green et al., 1986). For titanite, annealing kinetics analogous with those of apatite are assumed but have been studied to a far lesser extent (Coyle and Wagner, 1998). Partial annealing of fission tracks is a non-linear process (Fig. 3.1).

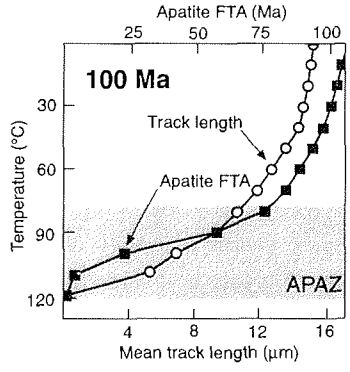

Fig. 3.1 Variation in apatite fission-track age and mean track length with temperature based on the annealing model of Laslett et al. (1987) for the Durango apatite. The model illustrates the annealing process for 100 Ma-stable thermal regime at a geothermal gradient of 30°C/km. The curvature of the slopes results from the sharply increasing reduction of fission-track ages and mean track length within the PAZ (from Laslett et al., 1987).

The annealing kinetics are not only governed by temperature but also by the heating duration (e.g. Gleadow and Duddy, 1981; Naeser, 1981; Green et al., 1986), the annealing anisotropy (Green and Durrani, 1977; Green et al., 1986; Donelick, 1991) and the chemical composition (Green et al., 1986; O'Sullivan and Parrish, 1995). In particular the F/Cl ratio in apatites can have a significant influence on the annealing behaviour. This has been demonstrated for instance by Green et al. (1986) from a fission-track and microprobe study on sandstones from the Otway Basin (Victoria, Australia). Green et al. (1986) draw the conclusion that chlorine-rich apatites are more resistant to track annealing than fluorine-rich ones causing a significant scatter of FTA among detrital apatites.

The FTA with the addition of mean track length data can be used to deduce the thermal history of an apatite sample (Wagner, 1979; Gleadow et al., 1986a,b; Wagner, 1988) (Fig. 3.2). If a sample has cooled rapidly through the PAZ, the FTA will be close to the age of formation and a relatively long mean track length (14.5-15 μm) with a small standard deviation (~1 μm) and nearly symmetric track length distribution are expected (Fig. 3.2a). This applies for example to volcanic rocks which have not been thermally influenced since their time of extrusion. For a slow and continuous cooling path, the mean track lengths will be shorter (~12-13 μm) with increased standard deviations (~1.2-2 μm) (Fig. 3.2b). The track length distributions broaden with a negatively skewed shape. This is typical for

crystalline basement rocks of the Precambrian cratons that have cooled slowly through the PAZ to ambient surface temperatures.

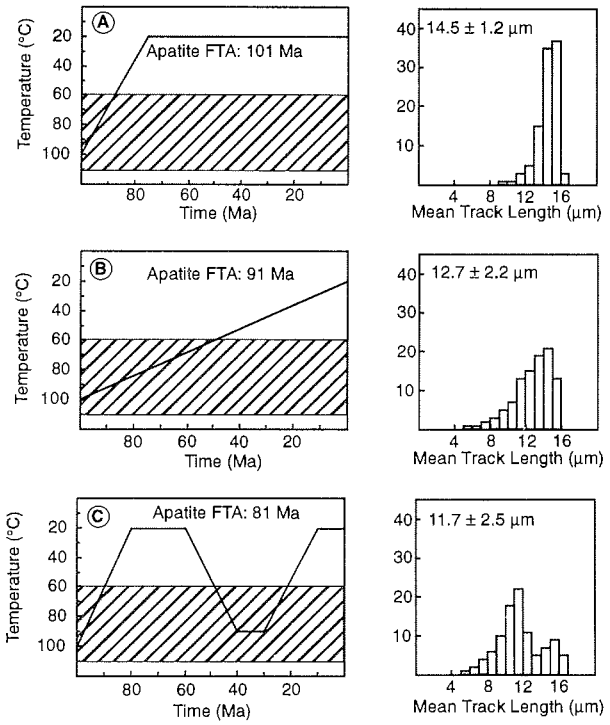

Fig. 3.2 Time-temperature paths and mean track length distributions for three different model thermal histories. Additionally, the fission-track ages and the mean track length (± 1 Standard Deviation) are quoted. Hatched boxes represent the APAZ. **(A)** Rapid cooling. **(B)** Continuous slow cooling. **(C)** Reheating (from Van Der Beek, 1995).

For a sample that has been reheated after cooling below 60°C, the fission tracks are either totally erased or undergo partial annealing (Fig. 3.2c). Reheating can be caused for instance by the intrusion of hot magmatic material into the crust. In case of total erasure, the thermal history prior to reheating is removed completely, whereas partial overprinting leads to the preservation of a two step cooling history. This would be reflected in a usually bimodal track length distribution with strongly annealed tracks having formed prior to heating, and new

long tracks being generated after thermal overprinting. Furthermore, the FTA of the sample is decreased. For samples with a complex thermal history, the track length distributions will represent a series of transitional rather than bimodal distributions. Such track length distributions are often broad and contain a significant portion of strongly annealed short tracks (cf. Gleadow et al., 1986a).

3.4 Qualitative information and estimation of denudation rates

Apatite fission-track results from deep borehole studies revealed that the apatite FTA rapidly approach a zero age towards the base of the PAZ, i.e. its high-temperature limit (cf. Fig. 3.1).

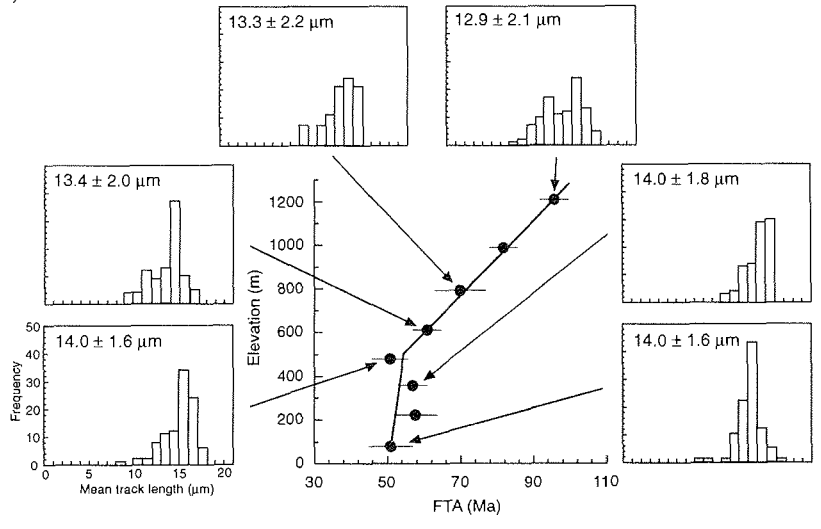

Fig. 3.3 Age-elevation plot from the Transantarctic Mountains (from Fitzgerald, 1992). Error bars represent the 1σ-error on the apatite FTA. The histograms illustrate the development of track lengths and their distributions above and below the break. Histograms are normalised to 100 tracks. The samples from above the break in slope have larger standard deviations and contain a significant portion of strongly shortened tracks suggesting some degree of annealing prior to denudation. For the younger samples below the break, the confined tracks are comparatively long and have small standard deviations. They reflect only minor annealing.

If such a suite of samples has cooled rapidly to surface temperatures after being exposed to temperatures between 110-60°C for considerable time, this pattern can be retained in the vertical sample profile. This profile will exhibit a marked change in the apatite FTA gradient (Fig. 3.3) with a shallow gradient above the break-in-slope and a steep gradient below it (e.g. Naeser, 1979; Gleadow et al., 1984; Gleadow and Fitzgerald, 1987; Green, 1989; Brown et al., 1990). A break-in-slope is interpreted to reflect the base of an exhumed fossil PAZ and its FTA marks the approximate onset of rapid cooling (Gleadow and Fitzgerald, 1987).The samples from above the break-in-slope are characterised by strongly decreasing ages and mean track lengths with decreasing elevation, while those from below the break-in-slope have long mean track lengths with narrow standard deviations. The FTA of the break-in-slope underestimates to some degree the onset of rapid cooling due to partial annealing during the rapid cooling (Fitzgerald et al., 1995). From the present-day topographic elevation of the break-in-slope, the amount of denudation since the onset of rapid cooling can be calculated, if the palaeogeothermal gradient is known (Gleadow and Fitzgerald, 1987).

Thermal histories of rocks can also be deduced from the relationship between the FTA and the mean track length (Fig. 3.4). This approach was introduced by Green (1986) and since that time has found application in a variety of studies (e.g. Moore et al., 1986; Omar et al., 1989; Gallagher et al., 1994). By relating the FTA to the mean track lengths of a suite of samples from different elevations, a boomerang-shaped trend often becomes apparent. The longest mean track lengths are confined to the youngest samples whereas the oldest samples have track lengths indicating some degree of annealing prior to denudation. The shortest mean track lengths are attributed to those samples with intermediate ages. Green (1986) interpreted the concave shape as the mixing of two cooling components producing the track length distributions shown in Fig. 3.4. Between the two end points of the boomerang there exists a series of transitional bimodal track length distributions where the abundance of inherited annealed tracks becomes reduced in favour of newly formed long tracks while the FTA of the samples decrease.

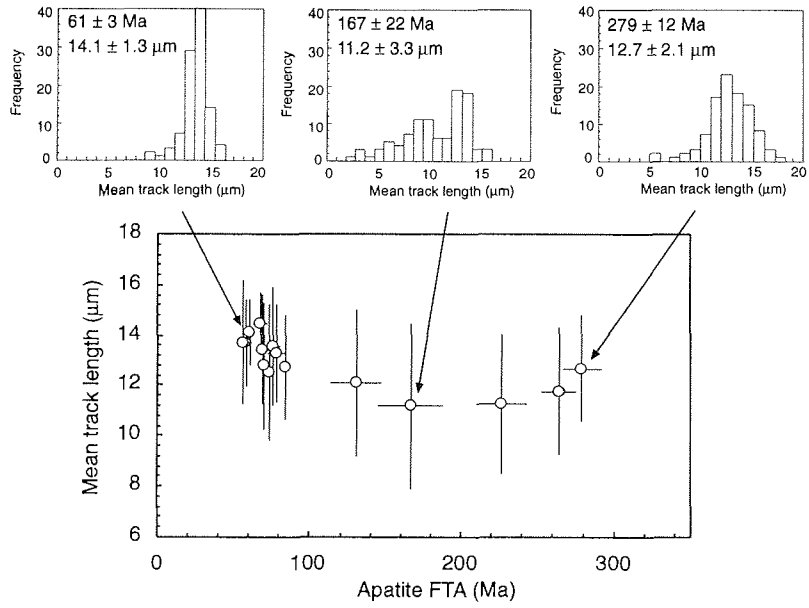

Fig. 3.4 Relationship between the fission-track age and the mean track length in samples from Northern England. Error bars on the age are quoted $\pm 1\sigma$, the mean track lengths are reported ± 1 Standard Deviation. The concave shape of the plot indicates a partial to complete thermal overprint, where in the samples older than ~100 Ma pre-existing tracks have become substantially annealed while in the youngest samples inherited tracks have been totally erased (from Green, 1986).

Fission-track age and/or mean track length profiles can provide quantitative information about vertical movements that have occurred since the samples have cooled through the PAZ. If the palaeo-geothermal gradient is known, then the amount of crustal material that has been removed since the cooling recorded in the fission-track data, can be calculated (e.g. Gleadow and Fitzgerald, 1987).

In thermochronological studies denudation rates are determined either from isotopic and/or fission-track systems with differing closure temperatures or from the slopes of cooling ages in an age-elevation plot. Parrish (1983) implies a horizontal orientation of the critical isotherms and a constant depth of the isotherms with respect to the surface to make an appropriate calculation of the denudation rate. Additionally, the rate of uplift must equal the

rate of denudation, so that no change in surface elevation takes place. Such criteria are difficult to meet, in particular the maintaining of the position and shape of isotherms (e.g. Brown, 1991; Stüwe et al., 1994; Mancktelow and Grasemann, 1997). According to Mancktelow and Grasemann (1997) it is crucial to consider that the geothermal gradient can change due to heat advection during denudation. Other than for surface uplift, where during uplift an overall cooling of the surface occurs, tectonic exhumation leads to the displacement of points within the crust from higher to ambient surface temperatures, and thus causes advection of heat. When the denudation rate is calculated using different closure temperatures, the rate estimation is strongly dependent on the geothermal gradient which is usually assumed to be constant and steady (Fig. 3.5a). For a dynamic approach that involves a change of the geothermal gradient by advection, the calculated denudation rate will be increased, and the rate quoted for a constant geothermal gradient will therefore be an underestimate of the true denudation rate (Fig. 3.5b). From fission-track profiles the apparent denudation rate can be calculated without knowing the geothermal gradient, if the critical isotherms were located at the same depth (Fig. 3.6a and 3.6b). Denudation rates derived from vertical fission-track profiles are apparent rates because they include the time lag between cooling and the onset of exhumation (Mancktelow and Grasemann, 1997).

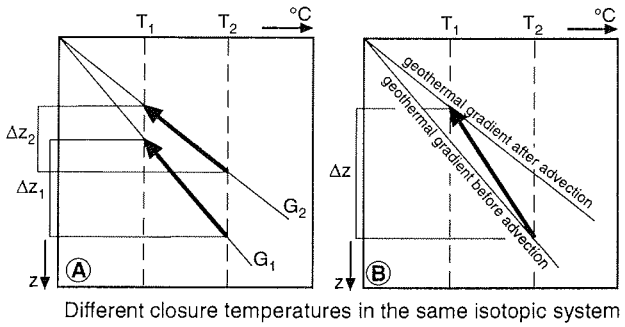

Fig. 3.5 Influence of the geothermal gradient on the determination of denudation rates. T_1 and T_2 refer to two different closure temperatures; T_{FT} represent a fission-track closure temperature. G_1 and G_2 are two different geothermal gradients, Δz is the estimated amount of denudation. **(A)** Steady-state geothermal gradients and the resulting denudation for two isotopic systems with different closure temperatures. The highest denudation rate is obtained for G_1 with a decreasing denudation rate for lower geothermal gradients. **(B)** Increasing geothermal gradient due to heat advection. The true denudation will be larger than for a constant geotherm which is illustrated in Fig. 3.5a (from Mancktelow and Grasemann, 1997).

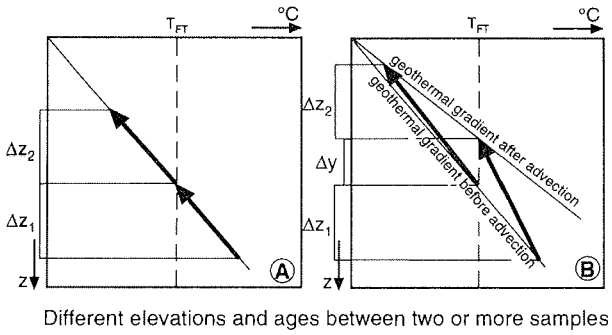

Fig. 3.6 Δz is the estimated amount of denudation. **(A)** Both samples from different elevations record the same amount of denudation independent of the prevailing gradient. **(B)** In case of heat advection, the denudation will be the same for both samples, but an additional distance Δy results from crossing the critical isotherms at different depths (from Mancktelow and Grasemann, 1997).

Brown (1991) and Stüwe et al. (1994) have demonstrated that the topography can bear significant influence on the depth and the shape of isotherms within the crust (Fig. 3.7 and 3.8).

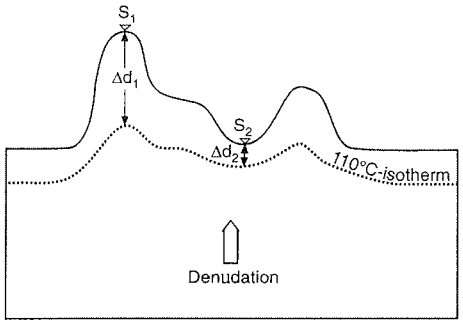

Fig. 3.7 Effects of topography on the position and shape of the 110°C-isotherm. (a) S_1 and S_2 represent two sample localities on a ridge crest and in a valley, Δd_1 and Δd_2 are the distances between the critical isotherm and the sample elevation. The sample from S_1 will record a younger FTA than S_2 (from Stüwe et al., 1994).

As shown in Fig. 3.7 the 110°C-isotherm is comparatively far apart from the surface underneath ridges and more closely-spaced beneath valleys. The FTA of sample from the valley thus records an older FTA than the sample from the mountain crest, though originating from higher topographic elevation. The perturbation of isotherms due to topographic effects is relevant for denudation rates of >400-500 m/Ma and is negligible for lower rates of denudation (Stüwe et al., 1994). For the zircon and titanite fission-track systems with closure

temperatures of ~240°C and ~300°C, respectively, topographical effects have a fading influence on isotherms at temperatures >200°C (Mancktelow and Grasemann, 1997).

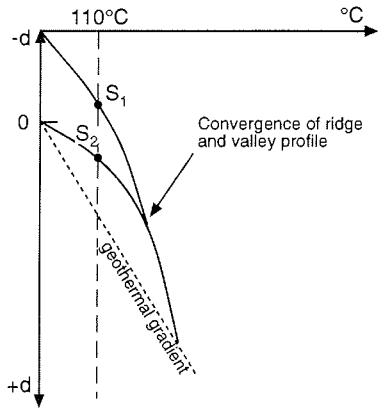

Fig. 3.8 Temperature-depth plot for S_1 and S_2. S_1 and S_2 will record different FTA because they cross the critical isotherm at different distances from the surface (from Stüwe et al., 1994).

The effects of topography on the denudation rate are counteracted by the influence of heat advection which causes an apparent decrease in the denudation rate (Mancktelow and Grasemann, 1997).

3.5 Fission-track data analysis

The FTA equation is based on the law of radioactive decay that provides also the basis to other conventional isotopic dating methods. The standard age equation is modified for fission-track analysis to account for the fission-track specific recruitments (see below). The derivations and transformations are explicitly reported by Fleischer et al. (1975) and by Wagner and Van den haute (1992).
The age equation is developed upon the basic equation that describes the process of radioactive decay:

$N_D = N_P \times (e^{\lambda t} - 1)$ with

$$t = \frac{1}{\lambda} \ln\left(\frac{N_D}{N_P} + 1\right)$$

where
t = time
N_D = number of daughter atoms (per unit of volume)
N_P = number of parent atoms (per unit of volume)
λ_t = decay-constant.

Instead of measuring the concentrations of parent and daughter isotopes, the fission-track method is based on counting spontaneous and induced tracks. To account for this, the standard age equation is modified by involving the fission decay constant, the spontaneous and induced track densities, a geometry factor, the $^{235}U/^{238}U$ ratio and the neutron fluence (see Dumitru, 1996):

$$t = \left(\frac{1}{\lambda_t}\right) \times \left\{ \ln \times \left[1 + \left(\frac{\lambda_t}{\lambda_f}\right) \times \left(\frac{g \times \rho_s}{\rho_i}\right) \times I \times a \times \Phi \right] \right\}$$

with
λ_t = 1.551 x 10^{-10} yr^{-1} (total (alpha and fission) decay constant of ^{238}U)
λ_f = ~ 8.46 x 10^{-17} yr^{-1} (spontaneous fission decay constant of ^{238}U)
g = 0.5 (geometry factor for external detector method; see Wagner and Van den haute (1992) for explanation)
ρ_s = measured spontaneous fission-track density (number of tracks cm^{-2})
ρ_i = measured induced fission-track density (number of tracks cm^{-2})
I = 7.2527 x 10^{-3} ($^{235}U/^{238}U$ ratio)
a = 584.25 x 10^{-24} cm^2 $neutron^{-1}$ (thermal neutron capture cross section as an indicator of how likely a thermal neutron induces fission of a ^{235}U nucleus)
ϕ = thermal neutron dose (neutrons cm^{-2}).

Because the fission decay constant λ_f of ^{238}U and the neutron dose ϕ are difficult to determine precisely, Hurford and Green (1983) developed the zeta calibration approach to avoid

imposing these uncertainties on the FTA. The zeta factor ζ substitutes λ_f, ϕ and the $^{235}U/^{238}U$ ratio I by a calibration with standards of isotopically determined age:

$$\zeta = \left(\frac{1}{\lambda_t}\right) \times \left[e^{(t_{std} \times \lambda_t)} - 1\right] \times \left[\frac{\rho_i}{g \times \rho_s}\right] \times \left(\frac{1}{\rho_d}\right)$$

with
t_{std} = age of standard sample
ρ_d = measured fission-track density in glass monitor (number of tracks cm^{-2}).

Hence, by modifying the basic fission-track age equation (see above), the FTA can be obtained from the following age equation:

$$t = \left(\frac{1}{\lambda_t}\right) \times \left\{\ln \times \left[1 + \left(\frac{g \times \rho_s}{\rho_i}\right) \times \lambda_t \times \zeta \times \rho_d\right]\right\}$$

Fission decay of uranium is a randomly governed process. The areal and spatial distributions of fission tracks per unit volume thus follow Poissonian statistics. For calculating the error of the FTA, the "conventional analysis" (Green, 1981) was applied:

$$\sigma(t) = t \times \sqrt{\left\{\frac{1}{N_s} + \frac{1}{N_i} + \frac{1}{N_d} + \left[\frac{\sigma(\zeta)}{\zeta}\right]^2\right\}}$$

where
$\sigma(t) = \pm 1\sigma$ uncertainty on the FTA
N_s, N_i = number of spontaneous and induced tracks
N_d = number of tracks counted in glass monitor
$\sigma(\zeta) = \pm 1\sigma$ uncertainty on the zeta factor.

Several experimental factors exist that introduce non-Poissonian distributions to the fission-track counting. These experimental factors include the identification of track-like defects as

fission tracks, an insufficient contact between the samples surface and the mica detector, etching anisotropy, natural contamination of samples (e.g. in sedimentary and volcanic rocks), misalignment of the counting area, vertical uranium inhomogeneities and variations in the neutron fluence (Green, 1981). This can lead to variations in ρ_s and ρ_i, and therefore in the FTA. In order to assess non-Poissonian fluctuations in the FTA, Galbraith (1981) has developed the χ^2-test where measured track densities are compared with those expected from a Poissonian distribution:

$$\chi^2 = \sum_{j=1}^{n} \frac{\left(N_{sj}+\hat{N}_{sj}\right)^2}{\hat{N}_{sj}} + \sum_{j=1}^{n} \frac{\left(N_{ij}+\hat{N}_{ij}\right)^2}{\hat{N}_{ij}}$$

with

$$\hat{N}_{sj} = \frac{N_s}{N_s + N_i} \times \left(N_{sj} + N_{ij}\right); \qquad \hat{N}_{ij} = \frac{N_i}{N_s + N_i} \times \left(N_{sj} + N_{ij}\right)$$

n = number of countable grains
N_s, N_i = sum of measured spontaneous and induced tracks
N_{sj}, N_{ij} = number of spontaneous and induced tracks in the jth grain
$\hat{N}_{sj}$, $\hat{N}_{ij}$ = number of expected counts of spontaneous and induced tracks in the jth grain.

The FTA of a sample can simply be calculated by determining the arithmetic mean of all single grain ages (mean age). However, the mean age does not take into account the precisions of the single grain ages. This is particularly important for samples that fail the χ^2-test (<5%), which are characterised by a considerable scatter in single grain ages. This is assessed by reporting the population geometric mean age (central age) instead of the mean age for χ^2-values less than 5% (cf. Galbraith, 1981; Green, 1981; Galbraith and Laslett, 1993). If the relative error of the central age decreases towards zero, a median age (pooled age) is approached. The pooled age is quoted in case where a sample passes the χ^2-test. In the present study the pooled age is quoted for samples having χ^2-values >5%, otherwise the central ages are given.

3.6 Sample preparation

123 samples of kilogram-size from various metamorphic and magmatic rocks have been prepared for fission-track analysis.

The first step was to fragment the samples with a jawcrusher to <cm-size. From the crushed material the fraction <315 µm was sieved for further treatment. The grains <315 µm were run over a Wilfley table in order to concentrate the denser minerals in two fractions and also to remove any dust particles. After drying, the two fractions which contain the heavy minerals, including apatite, zircon and titanite, were run through a Frantz isodynamic magnetic separator to remove the ferro-magnetic minerals from the non-magnetic apatites and zircons as well as from the diamagnetic titanites. The best results were obtained by using a forward slope of 15° and a side slope of 25° at a direct current of 0.6 A.

From the non-magnetic fraction the apatites, zircons and titanites were concentrated by heavy liquid separation. First, the fission-track relevant minerals were separated with tetrabromoethane (2.93 g/cm^3) from the lighter fraction mainly containing quartz and feldspar. For the separation of the lighter apatite grains from the heavier zircons and titanites methylene iodide (3.32 g/cm^3) was used. When the apatite fraction still contained a portion of heavier minerals like zircons, impurities were removed by isodynamic separation at 1.2 A with 15° forward slope and 25° side slope. The same adjustments were employed for the isolation of the titanites from the zircon fraction after heavy liquid separation.

The apatite and titanite grains were mounted in epoxy resin, ground with ~20 µm grinding powder and polished with 0.05 µm aluminiumoxide powder to attain even and smooth mineral surfaces. Apatites were etched with 5% HNO_3 at 23°C for ~60 seconds in order to reveal the spontaneous fission tracks. Etching of the titanites was carried out with a mixed liquid of HF, HNO_3, HCl and H_2O (1:2:3:6) for 17-22 minutes at 21°C (Naeser and McKee, 1970). The zircon grains were mounted in PFA Teflon®, ground with ~20 µm grinding powder and polished with 0.05 µm aluminiumoxide to an optical finish. Thereafter, they were etched in an eutectic NaOH-KOH melt at 215 ± 1°C (Gleadow et al., 1976). To obtain a high quality etch, each sample required an individual etching period ranging from 12-28 hours.

After the etching procedure, U-poor muscovite detectors were attached tightly onto the samples surfaces, and the samples were placed in a polyethylene tube together with at least one age standard and two U-doped glass monitors at each end of the tube. For monitoring the neutron fluence, CN5 monitors (Corning Glass Inc.) with a U-content of 12.5 ppm were

used for irradiation of apatite, whereas for titanite and zircon the CN2 detector with a higher natural uranium concentrations (~38 ppm U) was chosen. The age standards used for zeta calibration in the present study are listed below (Tab. 3.1).

Table 3.1 Age standards employed for ζ-calibration.

Age standard → / Mineral ↓	Fish Canyon Tuff (27.8 ± 0.2 Ma)[1]	Durango (31.4 ± 0.6 Ma)[2]	Tardree Rhyolite (58.7 ± 1.1 Ma)[3]	Mount Dromedary (98.8 ± 0.6 Ma)[4]
Apatite	×	×	—	×
Zircon	—	—	×	—
Titanite	—	—	—	×

[1] $^{40}Ar/^{39}Ar$ (biotite); Hurford and Hammerschmidt (1985)

[2] K-Ar; McDowell and Keizer (1977)

[3] K-Ar, $^{40}Ar/^{39}Ar$ (sanidine); Hurford et al. (unpubl.); see Wagner and Van den haute (1992)

[4] Rb-Sr (biotite); Williams et al. (1982).

Irradiation of the samples was carried out in the well-thermalised graphite reflector facility R3 at Risø (Denmark). The significance of a good thermalisation of the reactor during irradiation has been pointed out in section 3.2. After irradiation, the mica detectors were etched for 15 minutes in 40% HF in order to render the induced fission tracks visible. Finally, the samples and the mica detectors were prepared for microscopic investigations by mounting them mirror-imaged on glass slides.

3.7 Data acquisition - technical equipment, track counting and measuring of confined track lengths

The basic technical equipment employed for fission-track analysis was a ZEISS Axioplan microscope connected to an Apple Macintosh™ computer and a high-resolution CalComp™ Drawing Board II with a 16-button cursor. The fission-track slides were positioned on an automated Kinetek™ scanning stage which was operated with a joystick. With the scanning stage it was possible to move between the counting areas in grains and the mica with high precision (±2 μm). Additionally, the microscope was equipped with a drawing tube for track

length measurements. The fission-track stage was operated using the "FT-stage" software provided by Dumitru (1993a,b). This was used for calibrating the fission-track slide, for marking the countable grains as well as for confined track length measurements.
In practice, the counting of fission tracks was carried out in transmitted light with a rotatable counting grid of known areal extent. Track counting in apatite was done with an air objective and a total magnification of 1000x. Confined tracks were measured with a total magnification of 2000x. This magnification was also used for track counting in titanite and zircon due to their higher track densities. For zircon an oil objective was employed. The practice of track counting and confined track length measuring was accomplished according to the recommendations outlined by Gleadow (1984), Gleadow et al. (1986a) and Wagner and Van den haute (1992). In apatite specimen generally ~20-30 grains were dated, whereas in titanite and zircon samples commonly only ~10-20 grains were datable. In most of the apatite samples between 40-100 confined track length measurements were made, although in some samples less than 40 horizontal tracks were measured due to low track densities.

4. Results and interpretation

4.1 Introduction

Fission-track analyses have been performed on 123 rock samples from which 114 apatite, 19 titanite and 14 zircon fission-track ages were obtained.
The majority of samples are constituted by *in-situ* basement rocks from the onshore region of CDML. The altitude of the sample locations were determined barometrically, and were then corrected to fixed GPS reference points, using a correction factor of -4.7% (cf. Reitmayr, 1996). The samples cover an area of ~35000 km^2 and span a range in topographic elevation from near sea level to 3100 m with sample elevations increasing from the grounding line towards the mountain chains of the Orvinfjella and the Wohlthatmassiv. Most of the *in-situ* samples were collected from the latter two localities. Additional samples from the easternmost Mühlig-Hofmann-Gebirge, the Weyprechtberge as well as from the nunataks of Sigurdsvodene, Henriksenskjera and Starheimtind were included for fission-track analyses. The northernmost rock samples were obtained from the Schirmacheroase located adjacent to the grounding line. The areal distribution of apatite and titanite fission-track data over CDML is well balanced, whereas zircon fission-track ages (FTA) are available from the Conradgebirge and Schneidegebirge.
In addition to the *in-situ* basement samples, six dropstone apatite samples from the offshore region of CDML have been dated. The dropstones were kindly provided by the "Alfred-Wegener-Institut für Polar- und Meeresforschung" (Bremerhaven) and were collected with a large box corer (GKG) or an Agassiz trawl (AGT) during the Polarstern cruise ANT-IX/3 (Bathmann et al., 1992). Their sample locations are situated between 6-12°E and 69°57'-69°59'S (Fig. 4.1).
Lithologically, the *in-situ* as well as the dropstone samples from CDML comprise a broad petrographical range of metamorphic and magmatic basement rocks (Tab. I.I – I.III, Appendix).

The sample data (latitude/longitude, locality, lithology and elevation) as well as the fission-track data and the counting parameters are presented in Tab. I.I – I.III (Appendix). In addition, for each sample the distributions of single grain ages and mean track lengths are illustrated as radialplots and frequency histograms (Fig. IA-C, Appendix). The fission-track ages (FTA) are quoted with $\pm 1\sigma$-error throughout and the mean track lengths are given $\pm$ their standard deviation, unless otherwise stated.

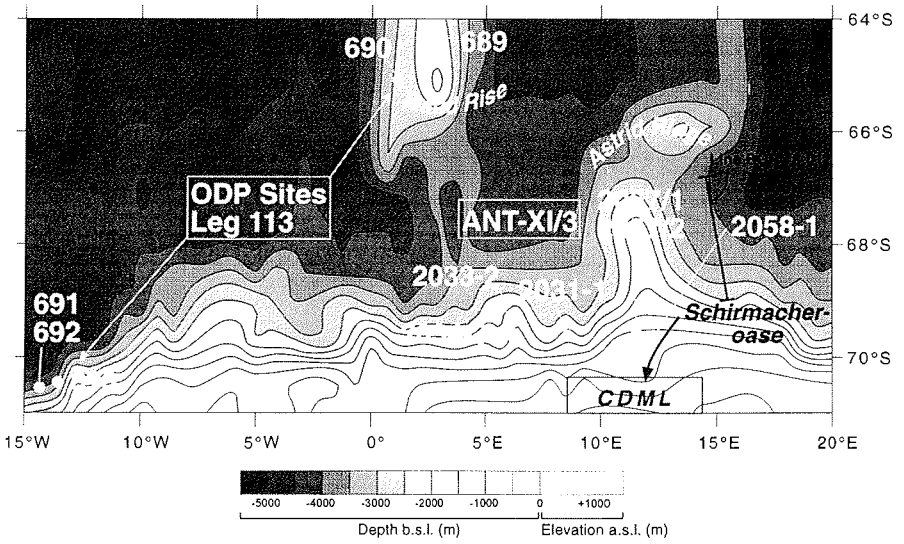

Fig. 4.1 Contour map of continental margin of Dronning Maud Land. Positive isopleths represent topographic elevation above sea level, negative isopleths represent depth below sea level. Map was created from the ETOPO-5 database. Thick black line corresponds to seismic line of profile BGR 78-012 for the seismostratigraphic sequence of Fig. 5.6.

Analyses on *in-situ* basement titanites gave the oldest apparent FTA from CDML. They vary between 894±171 Ma and 293±28 Ma with χ^2-values of 0-100%. From zircon fission-track analysis FTA between 364±47 Ma and 237±31 Ma with χ^2-probabilities from 20% to 99% were obtained. The apatite FTA of the *in-situ* basement samples from CDML range from 344±20 Ma to 83±3 Ma and the χ^2-probabilities of which range from 0% to 92%. Measurements (40-100 confined tracks measurable) of the mean confined track lengths in the apatite samples gave values between 12.0 µm and 14.1 µm with standard deviations ranging from 0.8 µm to 2.3 µm. Fission-track dating of the dropstone samples yielded apatite FTA between 170±9 Ma and 78±4 Ma with χ^2-probabilities of 0% to 68%. Due to the low apatite uranium-content, no apatite confined track length measurements were possible on the dropstone samples.

The sample numbers and their FTA are compiled in Fig. 4.2 and Fig. 4.3, respectively. More detailed illustrations together with the age-elevation plots are given with the presentation of the results (Fig. 4.8 – 4.14).

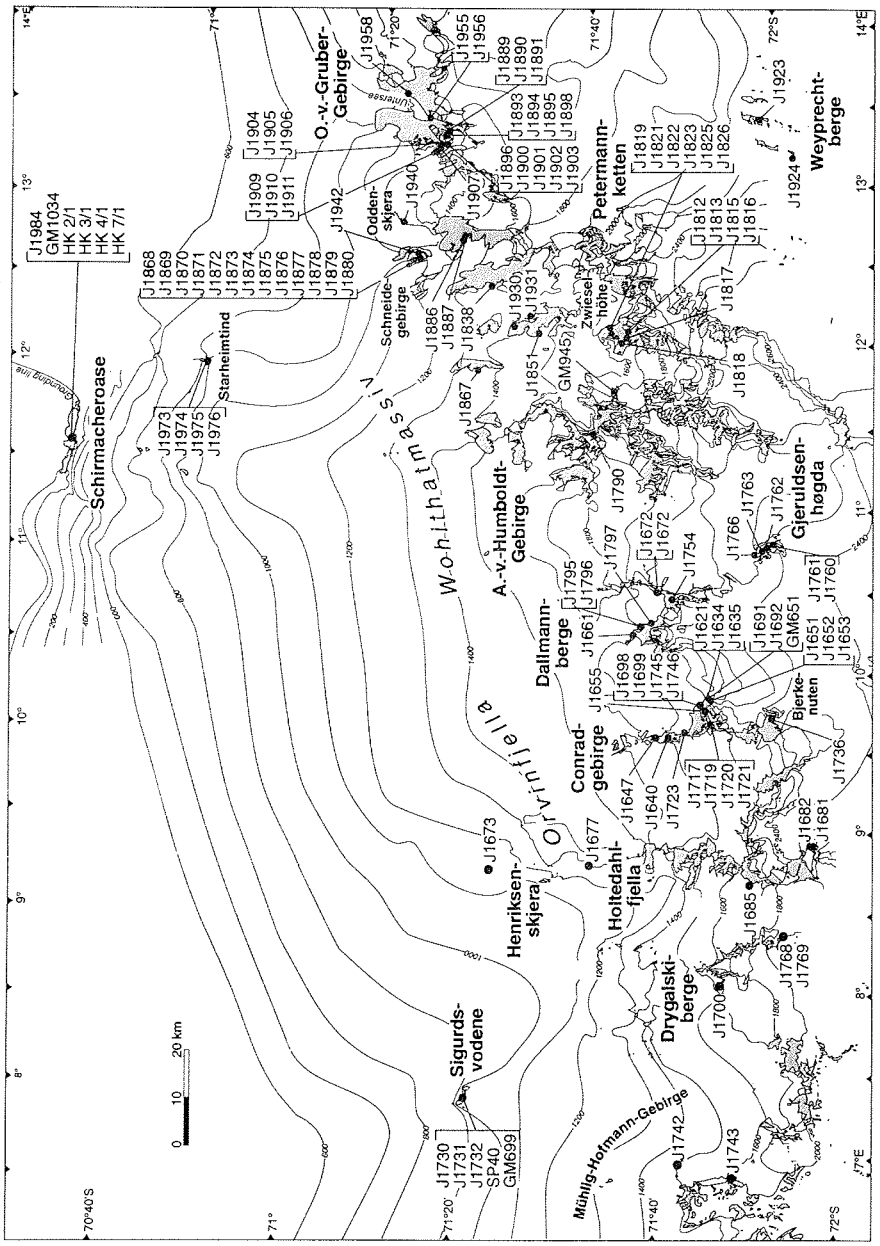

Fig. 4.2 Overview map of CDML with sample localities and sample numbers.

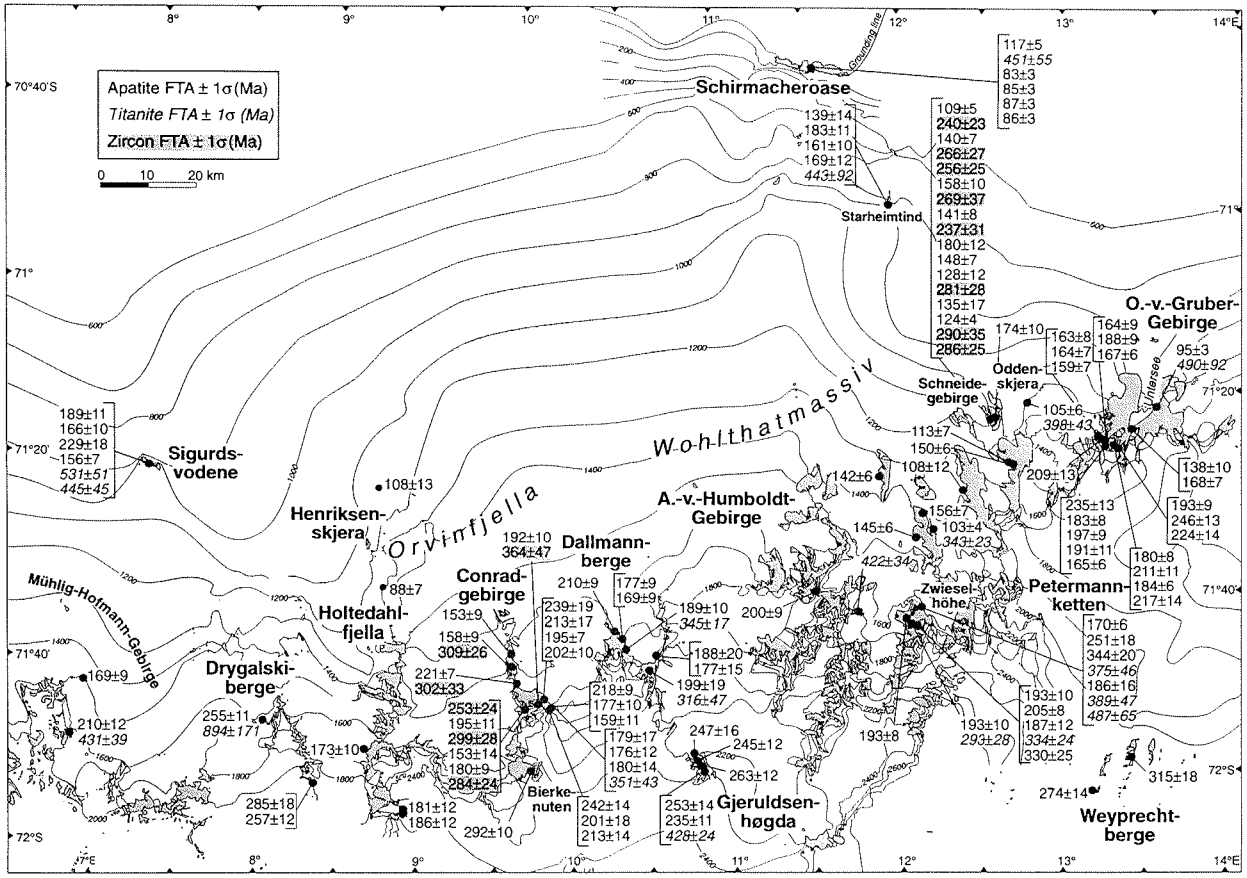

Fig. 4.3 Overview map of CDML with FTA reported ±1σ.

4.2 Titanite fission-track analysis

The titanite fission-track analysis yield FTA from 894±171 Ma to 293±28 Ma with χ^2-values between 0-100%. In spite of the broad scatter in ages, most of the samples fall in the range between ~450 Ma and ~300 Ma. Sample J1700 with an extremely old age of 894±171 Ma was excluded from further discussion, because of the low statistical relevance of the number of tracks counted in the detector. Due to the very small titanite grains of this sample, too few tracks per grain could be counted in the external detector.
The relationship between the titanite FTA and the topographic elevation is only weakly developed, although it appears that the ages do decrease towards higher elevations (Fig. 4.4).

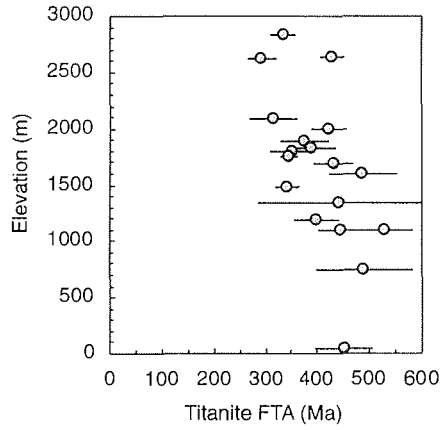

Fig. 4.4 Age-elevation plot of titanite FTA. Error bars represent the 1σ-error on the FTA.

As illustrated in Fig. 4.5 the older titanite FTA seem to be confined to the peripheral part of CDML whilst the youngest ages occur in the central part of the Orvinfjella and the Wohlthatmassiv. Due to the fact that the sampling sites of the titanites are widely dispersed over CDML, it is likely that local variations in the positions of isotherms have influenced the individual annealing properties of the fission tracks. A fluctuating geothermal gradient during the time of titanite fission-track accumulation could also account for the differential annealing recorded by the scatter in FTA, in particular with respect to the post-Pan-African cooling (see section 5.2 for discussion).

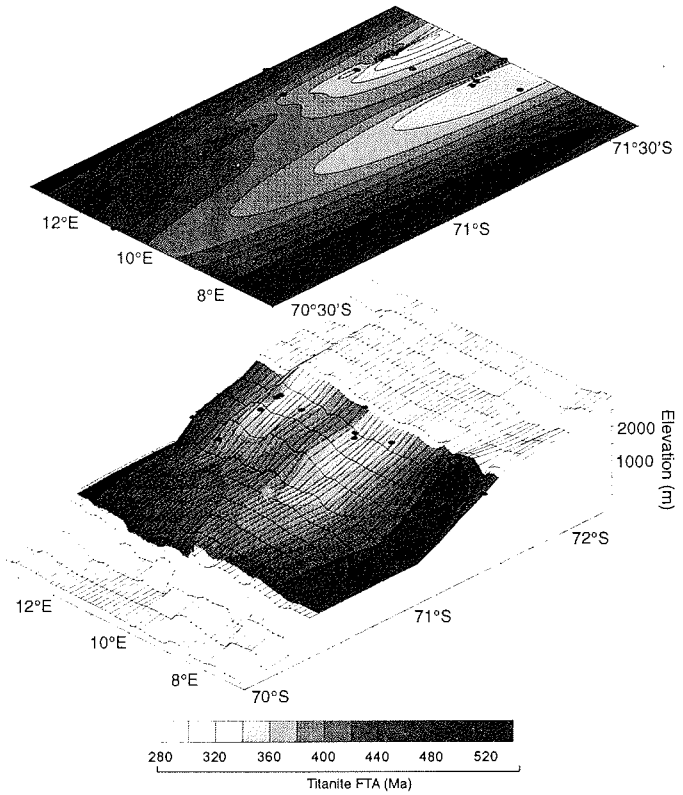

Fig. 4.5 Three dimensional surface and contour plot of titanite FTA from CDML. Black dots depict the titanite sample locations (samples positions are estimated from the Norwegian topographic maps). Both maps show an accumulation of relatively young titanite FTA in central parts of the Orvinfjella and the Wohlthatmassiv. Towards the north, the titanite FTA subsequently decrease. The plots are stretched by 50% in E-W direction. The data for the topographic grid were compiled from the ETOPO-5 database.

Though, the titanite fission-track system is not as well constrained as the apatite system, and compositional effects on the annealing properties in titanite are still unknown, it is probable that such factors contribute to a differential track retention behaviour (cf. Coyle and Wagner, 1998). The broad range in single grain ages and the mainly high χ^2-values suggest that the titanite FTA have a common origin and reflect a continuous slow cooling process through the TPAZ from middle to early late Paleozoic times.

4.3 Zircon fission-track analysis

Zircon FTA range from 364±47 Ma to 237±31 Ma with most of them falling in the range between 310 Ma and 240 Ma. In the Conradgebirge and Schneidegebirge the zircon FTA are substantially older than the apatite FTA. The relatively old age of 364±47 Ma was obtained from sample J1655 which was of poor quality and where only seven grains were datable. All samples passed the χ^2-test with values of 20-99% inferring that all ages comprise single age populations. The correlation between increasing zircon FTA and the topographic elevation is well developed and is characterised by a steep slope (Fig. 4.6).

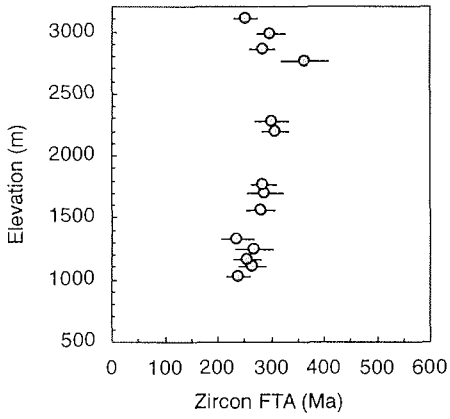

Fig. 4.6 Age-elevation plot of zircon FTA. Error bars represent the 1σ-error on the FTA.

The zircon FTA from the Schneidegebirge are slightly younger than those of the Conradgebirge. On the basis of their high χ^2-probabilities and broad distributions of single grain ages, steady cooling through the ZPAZ from the late Paleozoic until the early Mesozoic is inferred. Compared to the scattered titanite FTA, the zircon fission-track data show much less variation in their ages, although this is probably because they were obtained from spatially limited areas, in contrast to the widely distributed titanite fission-track samples. The well developed zircon FTA-elevation relationship in comparison to that for the titanite FTA, implies that the isotherms had most probably attained a stable position within the upper crust by this time.

4.4 Apatite fission-track analysis

For a more detailed presentation and interpretation, the apatite fission-track data of the *in-situ* basement samples that constitute the major part of this study, are treated in more detail and subdivided according to their localities. It was necessary to make this differentiation in order to account for local variance in the fission-track data, and to emphasise regional differences. The results of the dropstones apatite fission-track analyses are presented separately at the end of this chapter.

Generally, in most of the vertical profiles (Fig. 4.8 - 4.14) a distinctive relationship between the mean track length and the topographic elevation is not observable, though it appears that the fraction of shortened tracks commonly decreases in favour of long tracks towards lower elevations.

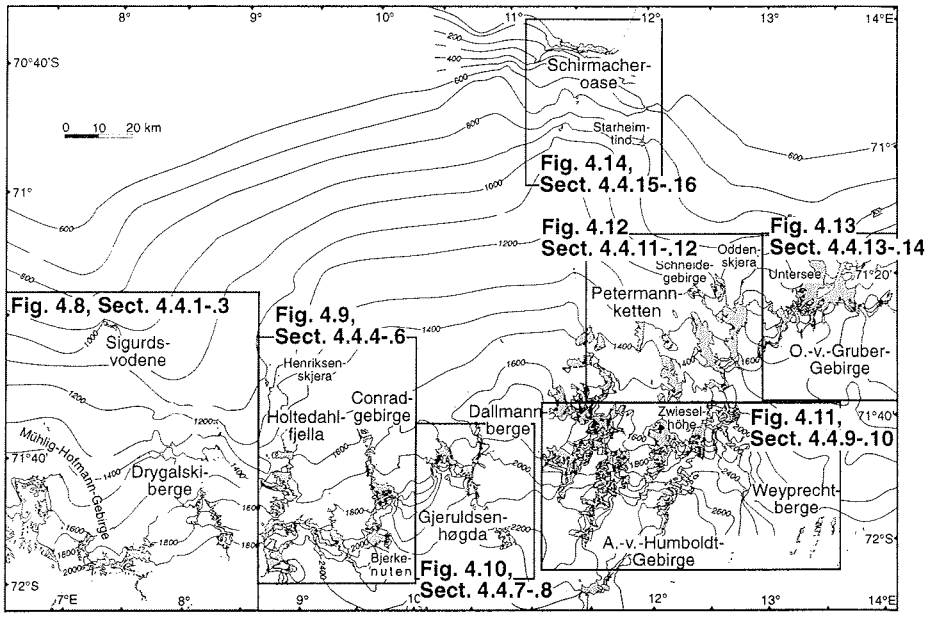

Fig. 4.7 Overview map of CDML. Boxes represent frames of detail maps from Fig. 4.8 – 4.14.

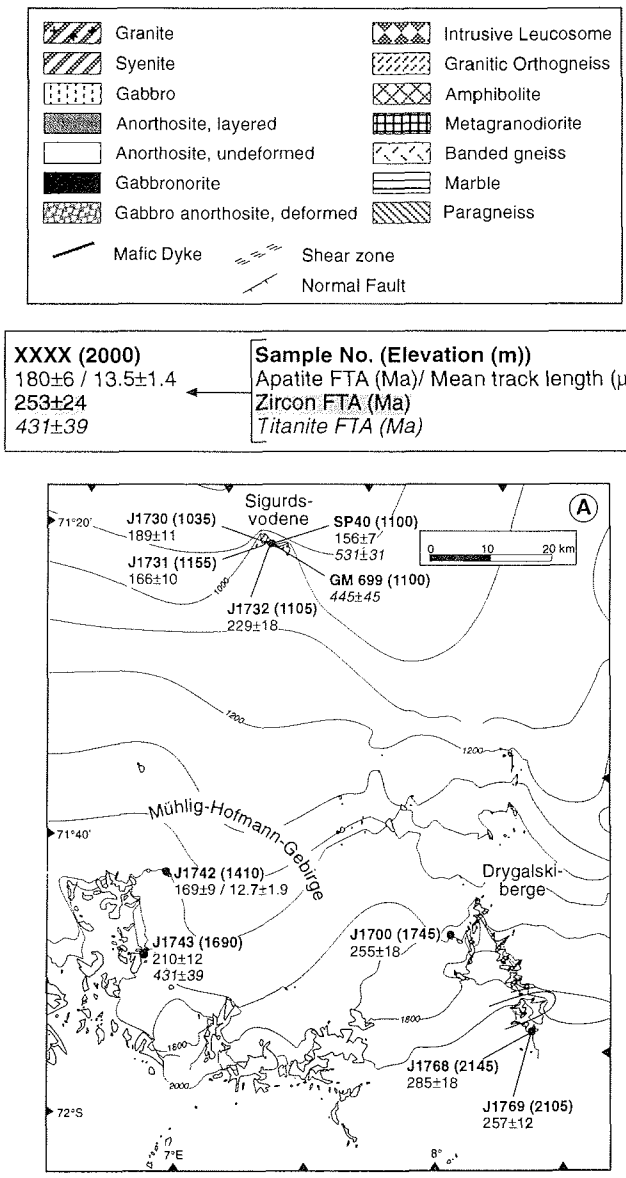

Fig. 4.8 Legend for Fig. 4.8 - 4.14. **(A)** Geological map with sample locations, FTA (±1σ) and mean track lengths (± 1 Std. Dev.) of the eastern Mühlig-Hofmann-Gebirge and the western Orvinfjella.

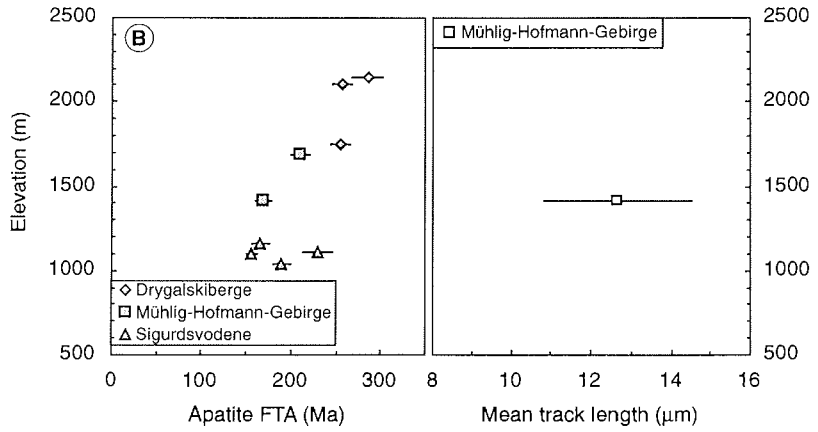

Fig. 4.8 (B) Apatite age-elevation plot and mean track length-elevation plot. Error bars represent the 1σ-error on the FTA and the standard deviation on the mean track length.

4.4.1 Mühlig-Hofmann-Gebirge

Samples J1742 and J1743 from the Mühlig-Hofmann-Gebirge were collected from a granitic gneiss unit and from a syenite intrusion (Fig. 4.8). The two samples have apatite FTA of 169±9 Ma and 210±12 Ma, both of them are characterised by zero χ^2-probabilities suggesting a mixed age population. The younger FTA is confined to the less elevated sample J1742 (~1400 m), whereas the older FTA belongs to the more southerly located and higher elevated sample J1743 (~1700 m) (Fig. 4.8b). Both samples have single grain age components >300 Ma, but it should be noted that the 1σ-error on these ages is relatively large and that compositional effects could have influenced the annealing behaviour of these grains (see section 4.5.2 for discussion). The mean track lengths of 12.7±1.9 µm and 12.4±1.9 µm as well as their frequency distributions imply significant shortening of confined tracks, although for sample J1743 only 23 track length measurements were possible.

The shortened mean track lengths as well as the broad frequency distributions of the single grain ages imply that the samples from the Mühlig-Hofmann-Gebirge spent considerable time within the APAZ. This is supported by the single grain age distributions comprising ages between ~100 Ma and ~350 Ma. This is interpreted to reflect a prolonged cooling time within the APAZ. The youngest single grain ages indicate cooling of these grains below 110°C in the Early Jurassic with the samples remaining within the APAZ until the mid-Cretaceous.

4.4.2 Sigurdsvodene

For the fission-track dating of apatites from Sigurdsvodene, felsic gneisses (J1730, SP40), a hornblende-bearing gneiss (J1731) and an amphibolite (J1732) were sampled from elevations between 1035 m and 1155 m (Fig. 4.8).

The apatite fission-track analyses gave apparent ages ranging from 156±7 Ma to 229±18 Ma with χ^2-probabilities of 0-39%. Most of the Sigurdsvodene samples exhibit a significant spread in single grain age distributions with ages between 140-200 Ma being most frequent. Particularly sample J1732 contains a large fraction of ages >200 Ma, but the 1σ-errors on these ages are extremely large. Sample SP40 is characterised by a narrow single grain age distribution with a comparatively high χ^2-probability. Most probably this sample is representative of the cooling history of Sigurdsvodene. Due to the very low track densities in the apatite grains no confined track length measurements were possible. There is no observable correlation between the apatite FTA and the elevation (Fig. 4.8b).

From the apatite FTA of sample SP40 and the abundance of Early and Middle Jurassic single grain ages, the samples from Sigurdsvodene resemble those of the Mühlig-Hofmann-Gebirge, and might have experienced a similar cooling history.

4.4.3 Drygalskiberge

The three samples of the Drygalskiberge are syenitic, pegmatitic and amphibolitic in nature and were collected from elevations between 1745-2145 m (Fig. 4.8).

They yield apparent apatite FTA between 255±11 Ma and 285±18 Ma. Their single-grain age distributions are characterised by low χ^2-values (3% and 7%) with the exception of sample J1769 which passed the χ^2-test with a value of 70%. The youngest apatite FTA belongs to the sample (J1700) from the lowest elevation in the northern part of the Drygalskiberge (Fig. 4.8b). For the higher elevated samples from the southern tip of the Drygalskiberge older FTA were obtained. The Drygalskiberge samples are substantially older than the apatite FTA from the Mühlig-Hofmann-Gebirge and Sigurdsvodene, the FTA of. From their youngest single grain ages it is apparent that the samples most probably cooled below 60°C at ~180 Ma. The most abundant single grain ages occur between 260-240 Ma. Every sample from the Drygalskiberge contained fewer than 40 measurable confined track lengths due to their low track densities. The mean track lengths with 10.4±1.6 µm to 12.1±1.1 µm are relatively short. The small standard deviations could be attributed to the low number of track length measurements. It can be inferred from these mean track length distributions that significant track annealing occurred while samples cooled through the APAZ.

4.4.4 Holtedahlfjella

The syenitic sample J1685 from the central Holtedahlfjella (1710 m) has an apatite FTA of 173±10 Ma and a χ^2-value of 17% (Fig. 4.9). The migmatic and gneissic samples J1681 and J1682 that were collected from elevations of 2765 m and 2680 m in the southern Holtedahlfjella have apatite FTA of 181±12 Ma and 186±12 Ma. Sample J1681 failed the χ^2-test while J1682 passed it with 49% (Fig. 4.9b).

Although the single grain age distributions do not display a distinct peak, it is probable that the samples were cooled below 60°C sometime during the Cretaceous. The mean track lengths vary between 12.8 μm and 13.5 μm while the standard deviations range from 1.3 μm to 1.6 μm. Their distributions contain a large fraction of shortened confined tracks. Because of the Jurassic FTA and the shortened mean track lengths of the Holtedahlfjella samples, it is thought that this area was exposed to APAZ temperatures for a long time and was affected by a potential cooling step around 180-160 Ma.

4.4.5 Henriksenskjera

From the nunataks of Henriksenskjera a leucogranite and a gneissic unit were sampled (J1673 and J1677) (Fig. 4.9). The oldest apatite FTA (108±13 Ma) belongs to sample J1673 that was collected at a topographic elevation of 1200 m from the northernmost nunatak (Fig. 4.9b). Sample J1677 (1315 m) from the southern part of Henriksenskjera has a younger apatite FTA of 88±7 Ma. Both ages failed the χ^2-test and have relatively large 1σ-errors. The mean track length measurements gave a value of 12.4±1.6 μm for sample J1673 and of 13.0±1.7 μm for J1677.

The apatite FTA of the samples from Henriksenskjera are distinctively younger than at the previous localities, with single grain ages <140 Ma being most abundant. Though the mean track lengths indicate track annealing prior to cooling below 60°C, a comparatively large fraction of confined tracks >14 μm is retained in the frequency distributions. As inferred by the apatite FTA and the single grain ages, cooling of the Henriksenskjera samples must have occurred during the Cretaceous.

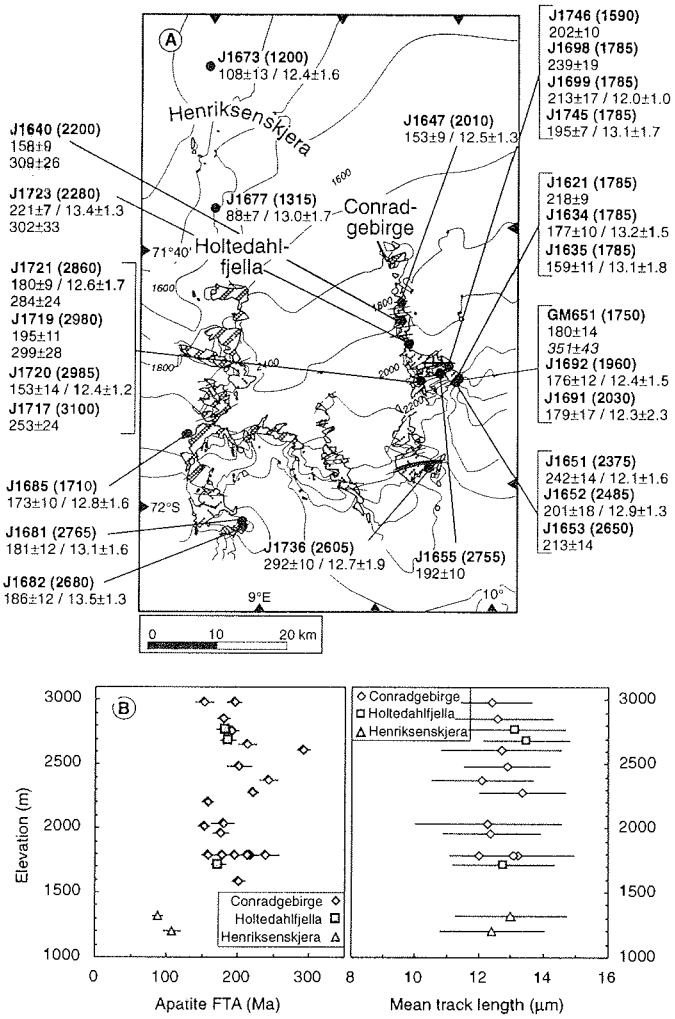

Fig. 4.9 **(A)** Geological map with sample locations, FTA (±1σ) and mean track lengths (± 1 Std. Dev.) of the Holtedahlfjella, Henriksenskjera and the Conradgebirge. **(B)** Apatite age-elevation plot and mean track length-elevation plot. Error bars represent the 1σ-error on the FTA and the standard deviation on the mean track length.

4.4.6 Conradgebirge

Twenty samples from the Conradgebirge were collected over a N-S distance of ~25 km and vertically from elevations between 1590 m and 3100 m. Their rock types are heterogeneous and range in composition from leucogranites to amphibolites (Fig. 4.9).

Samples J1640 (2200 m) and J1647 (2010 m) were collected from the northern part of the Conradgebirge and have the youngest FTA among all samples. They gave apatite FTA of 158±9 Ma and 153±9 Ma and χ^2-probabilities of 12% and 16%. Both of them have abundant Jurassic and Cretaceous single grain ages with a distribution peak at 120-140 Ma and no single grain ages younger than ~100 Ma. For sample J1640 an extremely short mean track length of 10.4±1.4 µm was obtained, but the statistical relevance of this value is negligible, because only 24 track lengths measurements were possible. Sample J1720 from the summit region of the Conradgebirge (2985 m) has a similar young FTA of 153±14 Ma, but the 1σ-error on this age is comparatively large.

In the central part of the Conradgebirge, most of the samples have Early Jurassic apatite FTA showing an indistinct correlation with the topographic elevation. In this part of the Conradgebirge, the χ^2-values range from 0-75%, but most of the samples have values less than 20%. Though the samples single grain age frequency distributions scatter, nearly all of them have a peak at ~180-200 Ma developed. Towards lower elevations, it seems that the old age components are reduced in favour of younger ones. The comparatively old apatite FTA of sample J1698 (1785 m) could be related to the very low track density of the apatite grains and the mica, introducing substantial errors on the single grain ages. In sample J1651 with a FTA of 242±14 Ma, the track densities vary significantly among the apatite grains. In this part of the Conradgebirge, the mean track lengths range from 12.0-13.4 µm with standard deviations between 1.0-2.3 µm. The shortened mean track lengths suggest that track annealing took place to differing degrees, before the samples have cooled below 60°C. With exception of sample J1723, it appears that the longest mean track lengths (>13 µm) are confined to samples from lower elevations (J1634, J1635, J1745).

Sample J1736 has a distinctively older FTA (292±10 Ma) than the other Conradgebirge samples. It passed the χ^2-test with 57% and has a mean track length of 12.7±1.9 µm. This sample was collected from an elevation of 2605 m and belongs to the southernmost tip of the Conradgebirge (Bjerkenuten). Its FTA comprises abundant single grain ages of 300-320 Ma. No single grain ages younger than 220 Ma are preserved.

From the spatial distribution of apatite FTA in the Conradgebirge, it appears that the samples have cooled through the APAZ from south to north with the oldest southernmost sample cooling first below 60°C. The samples from the northern Conradgebirge experienced cooling below 60°C most probably later.

With respect to the scatter in data, particularly in the central part of the Conradgebirge, it should be kept in mind that the samples were not collected from a strictly vertical profile but instead are spread across the whole mountain range. Additionally, the samples are lithologically heterogeneous and hence the apatites might bear variations in their chemical composition. Such effects may have influenced the annealing behaviour and be a cause of the scattering of the fission-track data. This problem is discussed in more detail in section 4.5.2.

4.4.7 Dallmannberge

Seven samples were analysed from the Dallmannberge. Lithologically, most of these are metavolcanic rocks with exception of samples J1754 and J1797 being granitic orthogneisses. Sample J1661 was collected from a granitic dyke (Fig. 4.10). The samples topographic elevations range from 1640 m to 2080 m.

The apatite FTA of the Dallmannberge samples fall in a range between 169±9 Ma and 210±9 Ma. Generally, the χ^2-probabilities for the Dallmannberge samples are very low (<8%), only sample J1797 passed the χ^2-test with a probability of 47%. The single grain age distributions show a peak at ~180-200 Ma though the abundance of a Jurassic age component is reduced in the younger FTA, where single grain ages younger than 100 Ma predominate. The mean track lengths are relatively short and range from 12.0 µm to 13.4 µm with standard deviations between 1.4-1.9 µm. Their distributions contain a number of shortened tracks indicating confined track length reductions.

To the samples of the Conradgebirge and Holtedahlfjella as well as Sigurdsvodene and the Mühlig-Hofmann-Gebirge, the Dallmannberge samples show similar fission-track characteristics.

4.4.8 Gjeruldsenhøgda

At Gjeruldsenhøgda two samples were collected from a syenite body, whereas two additional samples were obtained from amphibolite xenoliths within the syenite. Sample J1763 was taken from a diorite sill (Fig. 4.10). The vertical profile of Gjeruldsenhøgda covers a range in elevation between 2100 m and 2660 m.

The apatite FTA are distinctively older than those of the nearby Dallmannberge samples and do not change significantly with the topographic elevation (Fig. 4.10b). They range from 245±12 Ma to 263±12 Ma and have χ^2-probabilities between 0-35%. Single grain ages between 220-280 Ma are most frequent with the youngest ages implying cooling to temperatures <60°C during the Jurassic. The samples mean track lengths vary between

12.6 µm and 13.4 µm with standard deviations of 1.6 µm to 1.7 µm. The track length distributions are relatively broad and contain a portion of tracks <11 µm.

On the basis of their fission-track data, the samples from Gjeruldsenhøgda resemble the samples from the Drygalskiberge as well as the southernmost sample from the Conradgebirge (J1736). From the appearance of the youngest single grain ages (~140-160 Ma) the samples from Gjeruldsenhøgda could have cooled below 60°C by that time.

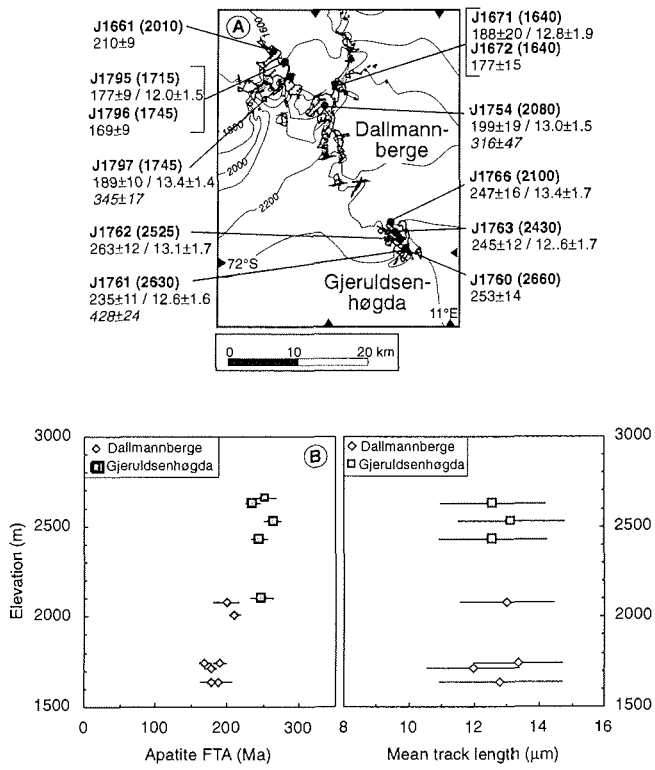

Fig. 4.10 **(A)** Geological map with sample locations, FTA (±1σ) and mean track lengths (± 1 Std. Dev.) of the Dallmannberge and Gjeruldsenhøgda. **(B)** Apatite age-elevation plot and mean track length-elevation plot. Error bars represent the 1σ-error on the FTA and the standard deviation on the mean track length.

4.4.9 A.-v.-Humboldt-Gebirge and Zwieselhöhe

Sample J1790 from the A.-v.-Humboldt-Gebirge has an amphibolitic composition and was collected from an elevation of 2110 m (Fig. 4.11). Eight of the samples from the Zwieselhöhe are gabbroic rocks with exception of the charnockitic and gneissic samples J1821 and J1823. The Zwieselhöhe samples belong to a vertical profile ranging from 1670 m to 2965 m.

The A.-v.-Humboldt-Gebirge sample has an apatite FTA of 200±9 Ma and a χ^2-probability of 21%. In the Zwieselhöhe, the apatite FTA range from 170±6 Ma to 344±20 Ma and have χ^2-values between 0% and 92%.

For three of the Zwieselhöhe samples (J1816, J1821, J1822) extremely old apatite FTA were obtained. Within these samples, the apatite grain sizes were very small and additionally track densities were relatively low. These FTA were considered not to be representative, because of the low statistical relevance of the small number of tracks countable in the external detector. They were therefore excluded from further discussion.

Related to the topographic elevation, the apatite FTA of the A.-v.-Humboldt-Gebirge sample and the Zwieselhöhe samples do not change substantially, but the distribution peaks of the single grain ages indicate a successive shift towards younger age components with decreasing elevation. No single grain ages younger than 100 Ma are retained pointing towards cooling below 60°C by that time.

The mean track lengths of the Zwieselhöhe samples fall in the range between 12.0 µm and 13.2 µm and consist of a significant portion of highly annealed tracks. The standard deviations remain almost constant (1.5-1.6 µm). In the A.-v.-Humboldt-Gebirge sample no confined track length measurements were possible due to low track densities.

4.4.10 Weyprechtberge

The felsic gneiss samples J1923 (2365 m) and J1924 (2685 m) from the Weyprechtberge yield relatively old apatite FTA of 315±18 Ma and 274±14 Ma, respectively (Fig. 4.11). Both passed the χ^2-test with probabilities of 58% and 15%. On the basis of their single grain age components it is inferred that both samples were cooled below 60°C at ~200-220 Ma. The mean track length measurements give values of 14.0±1.4 µm for J1923 and of 13.0±1.8 µm for sample J1924. This therefore points towards a more rapid cooling of sample J1923. Compared to the localities described previously, the samples from the Weyprechtberge appear to be similar to the samples from the Drygalskiberge, Bjerkenuten and Gjeruldsenhøgda with regard to their fission-track data.

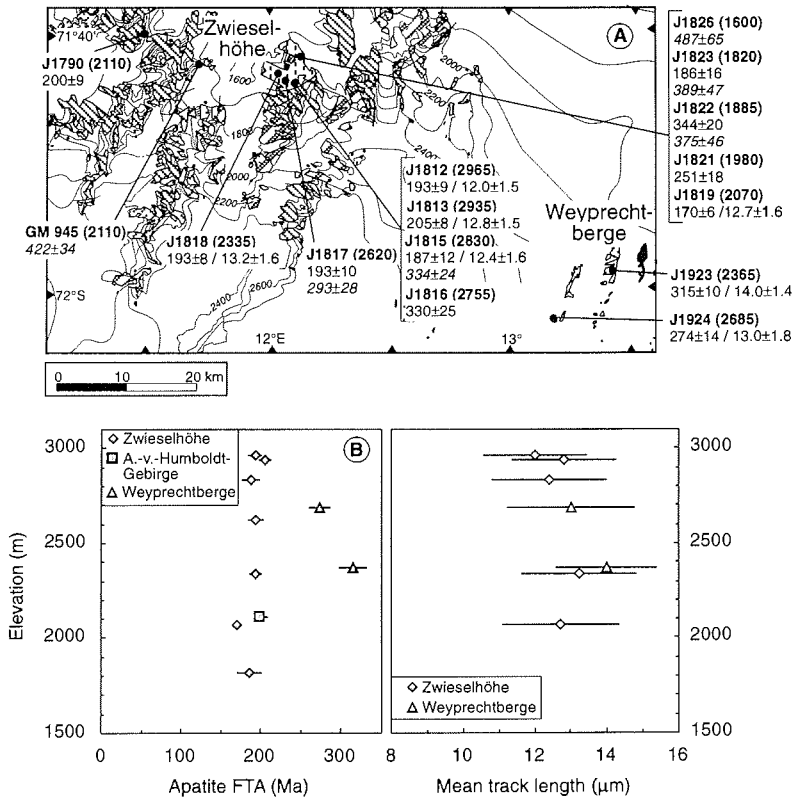

Fig. 4.11 **(A)** Geological map with sample locations, FTA (±1σ) and mean track lengths (± 1 Std. Dev.) of the A.-v.-Humboldt-Gebirge, Zwieselhöhe and Weyprechtberge. **(B)** Apatite age-elevation plot and mean track length-elevation plot. Error bars represent the 1σ-error on the FTA and the standard deviation on the mean track length.

4.4.11 Petermannketten

The seven samples from the Petermannketten are felsic in nature but range petrographically from diorite dykes to leucosomes (Fig. 4.12). They were taken from an area of ~30 x 30 km and from elevations between 1125 m and 1600 m with the elevations of the samples decreasing from south to north.

The apatite FTA of the samples from the Petermannketten range from 156±7 Ma to 103±4 Ma. Their χ^2-values are relatively low and vary between 0% and 32%. Compared to the apatite FTA of the localities described previously the FTA of the Petermannketten samples

are distinctively younger and are confined to lower elevations. Because of the low track densities in all samples, mean track length measurements were possible in only four samples. Indeed in three of them fewer than 15 confined tracks were measurable. They range from 12.4±0.9 μm to 13.6±1.9 μm. Due to the low statistical significance of so few measurements only the mean track length data from J1887 are considered worthy for interpretation.

The apatite FTA are only weakly related to the topographic elevation and show considerable scatter, but the frequency distributions of single grain ages show a successive decrease of age components >200 Ma in S-N direction. Additionally, the abundance of single grain ages <100 Ma increases further north. The moderate correlation between the apatite FTA and the elevation could be attributed to fact that the samples do not belong to a strictly vertical profile, and thus they could have experienced differential cooling histories. Furthermore, the broad range of lithologies samples could have influenced the annealing behaviour to some degree (see section 4.5.2).

4.4.12 Schneidegebirge and Oddenskjera

Nine samples from the Schneidegebirge were collected from a syenite body, although sample J1942 was taken from a mafic xenolith within the syenite. The Oddenskjera sample is a fluorite-bearing biotite-granite. The samples elevations range from 1020 m to 1980 m.

The apatite FTA of the Schneidegebirge and Oddenskjera vary between 105±6 Ma and 180±12 Ma. Nearly all samples failed the χ^2-test, except of samples J1875 and J1942 which have high χ^2-values >70%. The mean track lengths range from 13.3±1.6 μm to 13.7±1.3 μm, but because of low track densities, length measurements could be carried out on only three samples.

The apatite FTA are positively correlated with the elevation while defining a steep slope. In the single grain age distributions of the upper samples a peak at 200-180 Ma is developed, whilst towards the less elevated samples the peaks are shifted towards younger single grain ages. From the appearance of single grain ages no younger than 40-60 Ma in the less elevated samples, it is inferred that cooling below 60°C took place by that time.

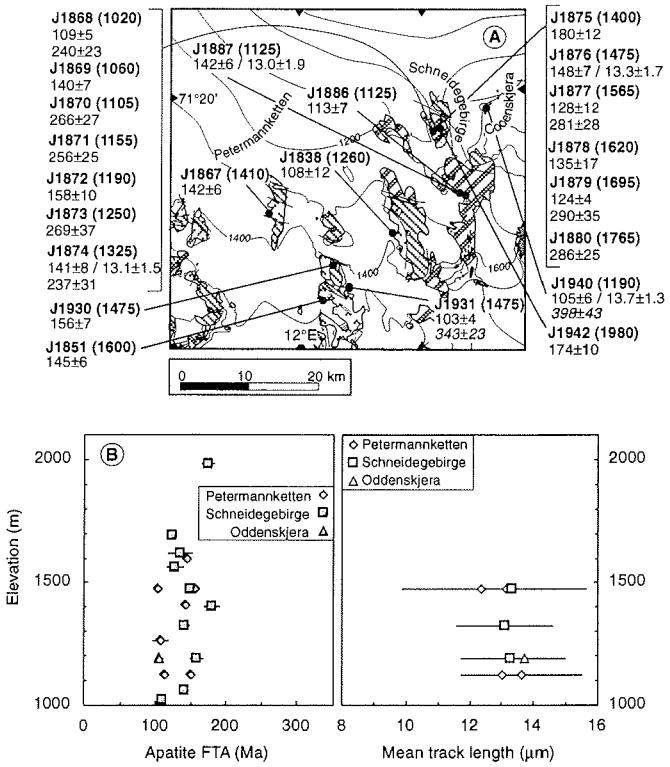

Fig. 4.12 **(A)** Geological map with sample locations, FTA (±1σ) and mean track lengths (± 1 Std. Dev.) of the Petermannketten, Schneidegebirge and Oddenskjera. **(B)** Apatite age-elevation plot and mean track length-elevation plot. Error bars represent the 1σ-error on the FTA and the standard deviation on the mean track length.

4.4.13 O.-v.-Gruber-Gebirge

In the O.-v.-Gruber-Gebirge the twenty samples analysed almost entirely have an anorthositic composition. Samples J1902 and J1907 are gabbronorites. Vertically the profile comprises samples from elevations of 1285-2840 m (Fig. 4.13).

The apatite FTA vary between 159±7 Ma and 246±13 Ma. Their χ^2-probabilities fall in the range from 0% to 70%. There is a clearly positive correlation between the apatite FTA and the elevation developed, although a few samples do not quite fit the main trend. With respect to the samples single grain age histograms, it is evident that the distributions are broadest for the samples from elevations >~2400 m and more narrow towards the less

elevated samples. This is coincident with low χ^2-values for the upper part of the profile, whereas nearly all samples from the lower section have passed the χ^2-test. Peak distributions of ~180-200 Ma were obtained for those samples with broad distributions. Towards lower elevations the peaks are subsequently shifted to younger ages with the youngest peak of ~100 Ma being confined to the lowermost sample. Furthermore, the youngest single grain ages of the samples from elevations >~2400 m range from ~140-160 Ma suggesting cooling below 60°C by this time. In the samples from elevations <~2400 m the youngest single grain ages are shifted towards younger ages, but cooling out of the APAZ most probably occurred no later than ~100 Ma.

The mean track lengths of the O.-v.-Gruber-Gebirge samples range from 12.5 µm to 14.0 µm with most of them being >13 µm. Their standard deviations vary from 0.7 µm to 2.0 µm. There is only a small number of tracks <10 µm retained in the frequency distributions suggesting that cooling progressed more rapidly than at other localities with similar FTA such as in the Conradgebirge.

4.4.14 Untersee

The three samples from the Untersee oasis are also anorthositic species and were collected from an elevation of 745 m (Fig. 4.13).

Though the samples were collected from the same elevation, they show substantial scatter in their FTA. The oldest apatite FTA of 168±7 Ma (J1956) and 138±10 Ma (J1955) resemble the FTA of the O.-v.-Gruber-Gebirge samples. The FTA of samples J1955 and J1956 are characterised by high χ^2-values of 60-84%, but sample J1955 has a broader single grain age distribution. In both samples single grain ages of ~140-160 Ma are most abundant, despite the apatite FTA of sample J1956 does not contain age components younger than ~140 Ma. The mean track length of sample J1956 is with 13.6±1.6 µm relatively long.

In contrast, sample J1958 (95±3 Ma) does not contain single grain age components older than ~150 Ma but has a pronounced frequency peak at 90±10 Ma developed. Its single grain age distribution is characterised by a high χ^2-value of 82%. Its mean track length with 13.3±0.9 µm suggest more intense annealing than for sample J1956.

Similar single grain ages in samples J1955 and J1956 and in the samples from the O.-v.-Gruber-Gebirge, indicate that the samples J1955 and J1956 were subjected to a similar cooling history until cooling below 60°C. Thereafter, sample J1955 could have experienced renewed partial track annealing being recorded in the youngest age components. In sample J1958 which has a distinctively younger FTA, reheating to temperatures higher 60°C could have been far more intense and led to the partial annealing

of older ages. A mechanism that could have been responsible for such a reheating will be discussed in section 5.7.4.

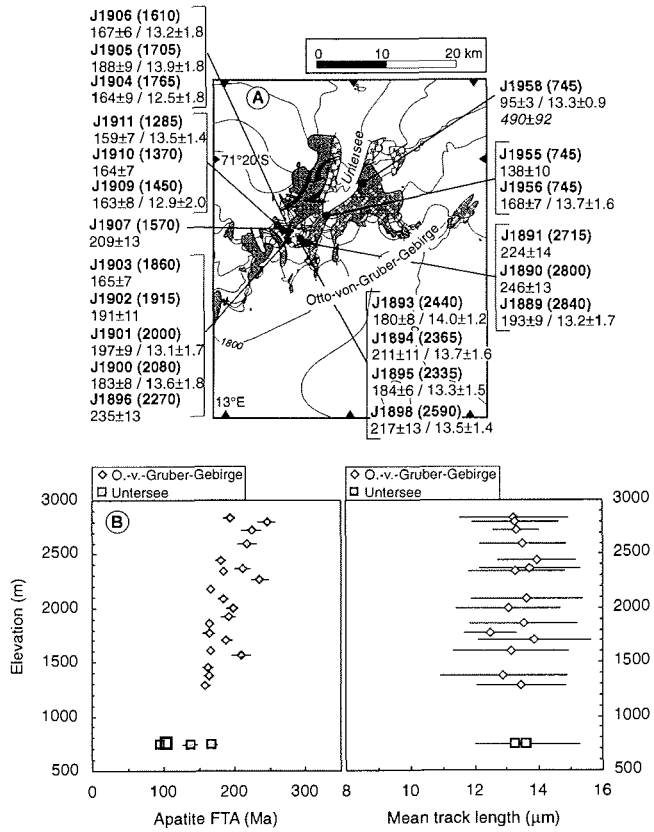

Fig. 4.13 **(A)** Geological map with sample locations, FTA (±1σ) and mean track lengths (± 1 Std. Dev.) of the O.-v.-Gruber-Gebirge and the Untersee oasis. **(B)** Apatite age-elevation plot and mean track length-elevation plot. Error bars represent the 1σ-error on the FTA and the standard deviation on the mean track length.

4.4.15 Starheimtind

In Starheimtind, the apatite FTA of the dioritic samples vary between 139±14 Ma and 183±11 Ma (Fig. 4.14). Their single grain age distributions are characterised by χ^2-probabilities between 14% and 83%. The single grain age data of the individual samples show no clear pattern, but instead a broad spread in single grain ages with no distinctive

age peaks. In particular, sample J1973 displays an extremely broad range in single grain ages that scatter between ~600-40 Ma. This sample has extremely low track densities and in some grains only very few tracks (<3) could be counted, though the grains are relatively large. The very old single grain ages are attributed to the grains with the low track densities. Thus, the associated error on the old single grain ages is extremely large. However, the youngest single grain ages infer cooling <60°C at ~60-100 Ma.
No confined track length determinations were possible for the samples because of their small grain size and the low track densities within the grains.
No distinctive relationship between the FTA and the elevation (1075-1345 m) is developed. Although the majority of samples reveal a positive coherence with the elevation, the oldest FTA is confined to the lowermost sample.
From the characteristics of their FTA, it seems probable that the samples from Starheimtind were subjected to a cooling history similar to e.g. the O.-v.-Gruber-Gebirge samples. The samples from Starheimtind have distinctively older apatite FTA than, for instance, those from the Petermannketten and Schneidegebirge occurring at the same topographic elevation.

4.4.16 Schirmacheroase

The five samples from the Schirmacheroase are gneissic in nature and were collected from an elevation of approximately 50 m (Fig. 4.14).
For the apatite samples FTA between 83±3 Ma and 117±5 Ma with high χ^2-values from 19% to 86% were obtained. Their mean track lengths are long and range from 13.8 µm to 14.1 µm with standard deviations between 1.1-1.3 µm. The mean track length distributions are dominated by tracks longer than 14 µm while no tracks <10 µm are retained.
Because of the long mean track lengths and the narrow distributions of mean track lengths and single grain ages, the Schirmacheroase samples are considered to reflect a rapid cooling through the APAZ. This is also supported by the high χ^2-values which are indicative of all single grain ages belonging to one single age population.

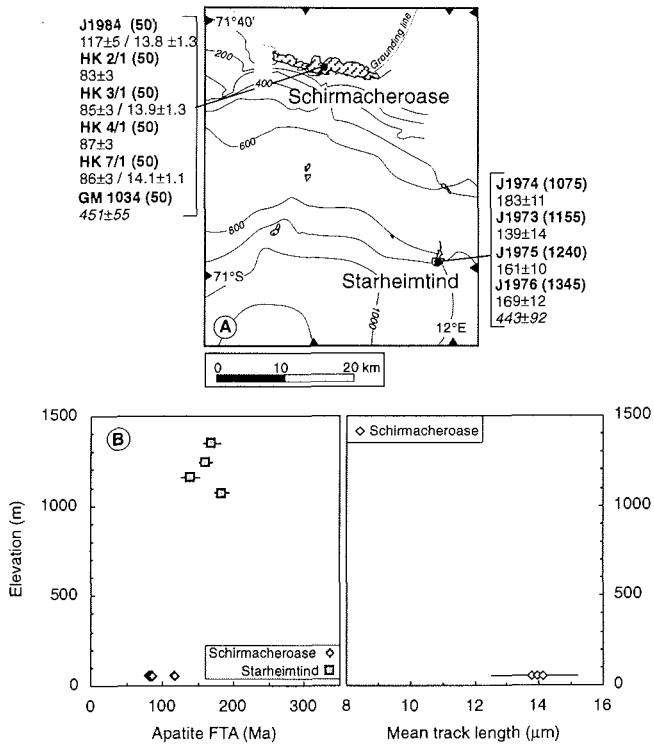

Fig. 4.14 **(A)** Geological map with sample locations, FTA (±1σ) and mean track lengths (± 1 Std. Dev.) of Starheimtind and the Schirmacheroase. **(B)** Apatite age-elevation plot and mean track length-elevation plot. Error bars represent the 1σ-error on the FTA and the standard deviation on the mean track length.

4.4.17 Dropstones

The six dropstones samples comprise a variety of rock types but most of them are granitic in nature. Samples 2057/1 and 2057/2 have an anorthositic composition. Their sample localities are presented in Fig. 4.1. The samples were collected from waterdepths between 155 m and 905 m along the Fimbulisen and Nivlisen.

The range in apatite FTA is very broad varying between 170±9 Ma and 78±4 Ma with χ^2-probabilities of 0-62%. Their single grain ages also cover a broad range with single grain ages of ~120-160 Ma being most frequent. Only sample 2033-2 with an apatite FTA of

78±4 Ma shows a distinctive peak in its single grain ages frequency at 70±10 Ma. The youngest single grain ages of the dropstone samples infer that the samples cooled below 60°C not before ~100 Ma and no later than ~40 Ma.
No mean track length measurements were possible in the dropstone samples because of the low track densities within the apatite grains.
There is neither a systematic pattern in the local distribution of the apatite FTA evident nor is a coherence between the FTA and the water depth observable.

4.5 Interpretation of apatite fission-track results of *in-situ* basement rocks

In summary the apatite fission-track data from the analysed *in-situ* basement samples yield apparent FTA from 315±18 Ma to 83±3 Ma with Early to Middle Jurassic ages being most abundant. They have χ^2-probabilities between 0-92%, with the majority falling below 50% and approximately half of the samples failing the χ^2-test (<5%). Due to the generally low χ^2-values of the fission-track samples from CDML it is proposed that the majority of samples contain mixed age populations probably as a consequence of a polyphase tectono-thermal evolution. This is supported by the predominantly broad single grain age distributions with single grain ages of ~180±20 Ma being most frequent in the Jurassic-aged samples, whereas ages of ~100-80 Ma are most abundant in samples of Cretaceous FTA.
The track length measurements give mean values ranging from 10.4 µm to 14.1 µm with most of them being shorter than 13.5 µm. The corresponding standard deviations yielded values between 0.7-2.3 µm. Most of the samples have broad mean track length distributions indicative of considerable track annealing at temperatures between 110-60°C. The samples from the Schirmacheroase (~120-85 Ma) differ from this pattern, and show long mean track lengths with narrow distributions and well defined single grain age populations. Such results reflect rapid cooling through the APAZ, in contrast to most of the other samples which can be interpreted as mixed ages and therefore represent a more complex thermal evolution (cf. Wagner, 1979; Wagner, 1988; Gleadow et al., 1986a, b).

4.5.1 Topographic relationship

Generally, the apatite FTA of the *in-situ* basement samples show a positive correlation with the topographic elevation, although the relationship is often distorted by scattering

FTA, as for instance in the Conradgebirge or the Petermannketten. As most of the FTA from CDML are mixed ages, the slopes should not be directly converted into exhumation/denudation rates. Indeed, the age-elevation correlation provides only limited information about the thermal history of the analysed samples. Nonetheless, the common occurrence of mixed ages in CDML indicates that the samples spent a prolonged time within the APAZ, although modest differences in the mean track lengths between the localities also infer some regional variation in the tectono-thermal evolution. For instance, the mean track lengths of the O.-v.-Gruber-Gebirge profile are slightly longer than those of the Conradgebirge samples and thus are interpreted as having cooled more rapidly below 110°C. In order to explain such variations between the localities, block tectonics and differential movements of crustal blocks along faults across CDML must be considered. The amount of vertical offsets between the crustal blocks is estimated to be on the order of a few hundreds of meters.

4.5.2 Possible compositional effects on apatite fission-track results

As it has been shown in section 4.4 a linear correlation between the apatite fission-track data and the topographic elevation in CDML is often obscured by scattered FTA and an indistinct pattern of mean track lengths. This is especially true for Sigurdsvodene, Conradgebirge, Dallmannberge and Starheimtind. Other profiles such as from Gjeruldsenhøgda, the O.-v.-Gruber-Gebirge, the Zwieselhöhe and the Schneidegebirge display a more obvious relationship between the FTA and the elevation. As summarised earlier many of the sampling sites within each mountain range were spatially distributed over a large area and do not comprise ideal true vertical profiles. In addition, the fission-track data of the majority of samples point towards a protracted cooling history, and therefore different annealing properties might have influenced variably the retention of single grain ages as well as a differential reduction in mean track lengths (cf. Gleadow and Duddy, 1981; Green et al., 1985, 1986). Another important point is that the sampled rock types are very heterogeneous and cover a broad petrographical and compositional range.

It is widely accepted that the fluorine/chlorine ratio in apatites bears significant influence on the annealing behaviour of fission tracks in apatite (e.g. Gleadow and Duddy, 1981; Green et al., 1985, 1986; O'Sullivan and Parrish, 1995; Van der Beek, 1995). According to these studies apatite grains with a high chlorine content are more resistant to annealing than apatites rich in fluorine. If a sample is cooled below 110°C or reheated to APAZ temperatures, then the chlorine-rich grains will retain older ages while those grains

enriched in fluorine are expected to have younger FTA. This can lead to a substantial spread in single grain ages within a single sample, although such variance in the apatite chemical composition may not necessarily be related to the lithology of the sample.
Apart from potentially varying fluorine/chlorine ratios in the apatite grains, Carpéna (1998) emphasised the significance of substitution reactions at the cation sites in apatite, with actinides, REE and metals acting as substitutes within the apatite crystal lattice. Furthermore, it was proposed by Carpéna (1998) that the number of substitutions on the cation and anion sites are inversely correlated and that this may imply that the number of cation substitutions is responsible for varying thermal stabilities in apatite crystals and not in fact the fluorine/chlorine ratio. The conclusion drawn was that the degree of substitution could bear strong influence on the annealing behaviour of fission tracks in apatites. In mafic rocks (e.g. gabbro, diorite) which are generally depleted in heavy elements, the apatites are expected to be more resistant to track annealing. Consequently, felsic and alkaline rocks (e.g. granites, pegmatites), usually enriched in heavy elements, should anneal more readily. Though the true chemical composition of the various sampled lithologies from CDML is not known, it has been observed that a positive FTA-elevation correlation is better developed in the profiles which are lithologically homogeneous. For instance, the O.-v.-Gruber-Gebirge and Zwieselhöhe profiles are composed almost entirely of anorthosites and gabbros, respectively, both show a well defined, steep slope in the FTA-elevation plot. In contrast, the Conradgebirge and Dallmannberge profiles, which comprise a broad compositional range of rocks, are characterised by distinctive scatter of apatite fission-track data. Carpéna et al. (1988) also suggest that the U-Th content of the apatites and consequently the radiation damage in the crystal lattice can increase the sensitivity of fission tracks to thermal events. However, apart from the fluorine/chlorine content the effects of the chemical composition on the annealing properties in apatite are still quantitatively poorly constrained and are the subject of ongoing research.

4.5.3 Regional distribution of apatite FTA across CDML

One of the most striking features of the apatite fission-track data from CDML is the continuous increase of apatite FTA with increasing distance from the continental margin (Fig. 4.15, Fig. 4.16). This pattern is also evident from the single grain age frequencies of the samples from the Conradgebirge and Petermannketten, where the distribution peaks are successively shifted towards younger ages with decreasing distance to the continental margin. The 70°S-latitude is chosen to approximate the position of the continental margin because continental rupture in CDML occurred almost parallel to the present-day coastline

(Bormann et al., 1986). This implies that the youngest FTA are confined to the northernmost locality (Schirmacheroase), whereas the oldest apatite fission-track datings were obtained for those samples from the southernmost part of CDML.

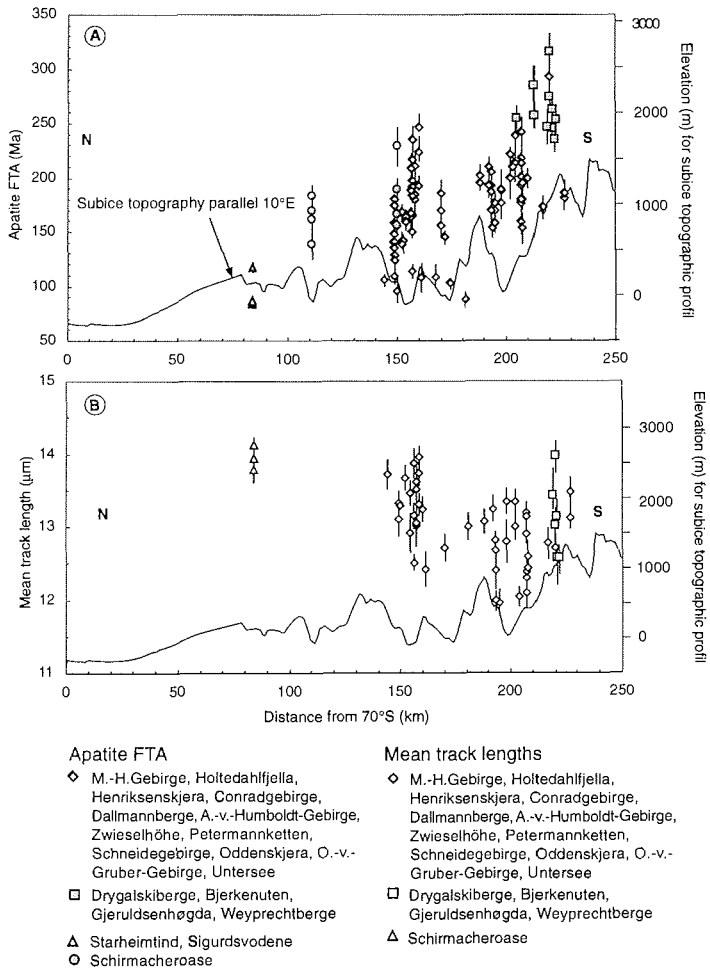

Fig. 4.15 **(A)** Apatite FTA against distance from 70°S. **(B)** Mean track lengths against distance from 70°S. Error bars represent the 1σ-error on the FTA and the standard deviation on the mean track length. Grey line and right axis correspond to a subice topographic profile from 70°10'S to 72°30'S/parallel 10°E) (from Damm and Eisenburger, 1999). The scatter in apatite fission-track data could be related to the fact that the data are projected onto a common surface, irrespective of the samples topographic elevation as well as local and individual tectono-thermal influences.

The longest mean track lengths occur in close vicinity to the continental margin and also furthest from it (Fig 4.15b). Those samples in between reveal a broad range in apatite FTA and to some degree shortened mean track lengths.

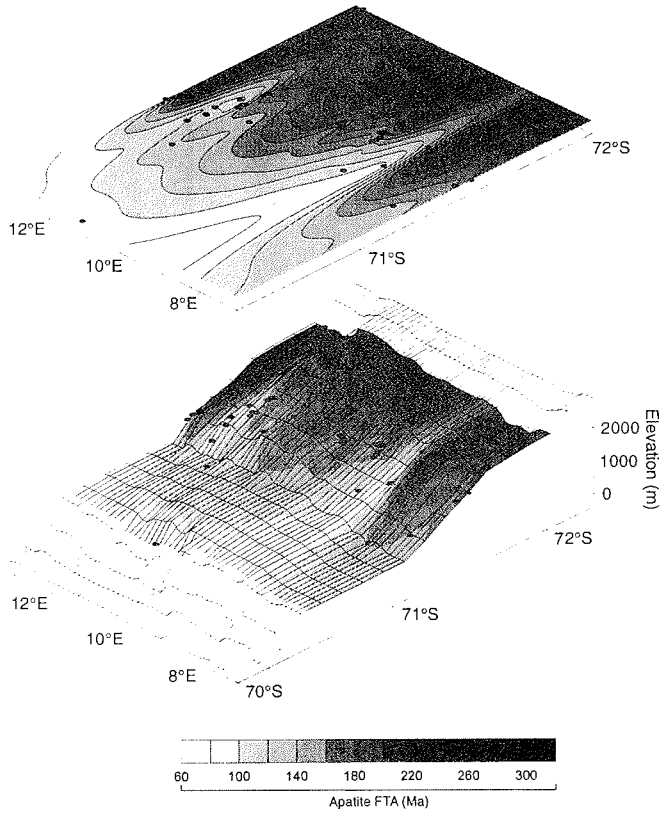

Fig. 4.16 Three dimensional surface plot with apatite FTA from CDML and contour plot of apatite FTA illustrating the increasing apatite FTA with increasing distance from the continental margin and with increasing topographicelevation. Black dots represent sampled localities (sample positions are estimated from the Norwegian topographic maps). The plots are stretched by 50% in E-W direction. The topographic data for the surface and contour plots were obtained from the ETOPO-5 database.

This pattern is typical for passive margin settings and usually is interpreted as being attributed to the syn- and post-rift evolution of continental margins (cf. Moore et al., 1986; Brown et al., 1990; Gallagher et al., 1994; Gallagher and Brown, 1997). In addition to increasing FTA further inland, at most passive margins the FTA are coherently

related to the topography, i.e. the oldest FTA are confined to the highest elevations which in turn generally occur most remote from the continental margin. Because of the occurrence of significantly older apatite FTA at the same elevations as Jurassic FTA, the trend is disrupted in the southernmost part of CDML (see below). The importance of this trend will be discussed in detail in section 5.7.

The regional distribution of the apatite FTA in CDML reveals a complex pattern, although several distinct apatite FTA groups can be discriminated across the study area (Fig. 4.17). In the easternmost part of the Mühlig-Hofmann-Gebirge, in the Orvinfjella, the A.-v.-Humboldt-Gebirge, Zwieselhöhe and O.-v.-Gruber-Gebirge the samples with apparent apatite FTA between ~210-150 Ma are confined to elevations of ~1000-3000 m, and indicate cooling to below 60°C between the Early Jurassic and Early Cretaceous.
The samples from the Petermannketten, Schneidegebirge and Oddenskjera have distinctively younger apatite FTA of ~170-100 Ma and belong to elevations between ~1000-2000 m. Similarly, the samples from Henriksenskjera (northern Orvinfjella) come from an elevation of ~1250 m and have apatite FTA of ~90 Ma and ~110 Ma. It is suggested that the Cretaceous-aged samples cooled to below 60°C during and after the Late Cretaceous.
In the Orvinfjella the abundance of mainly Jurassic apatite FTA is interrupted by the occurrence of FTA >255±11 Ma in the Drygalskiberge and the southernmost Conradgebirge (Bjerkenuten). Similar apparent apatite FTA were obtained from samples from Gjeruldsenhøgda and the Weyprechtberge, both localities representing the southernmost part of CDML. The single grain age distributions of these samples indicate cooling below the APAZ during the Late Triassic/Early Jurassic, when the other samples were still at temperatures of ≥60°C. The markedly older samples were also collected from elevations of ~1750-2700 m and they were not obtained from elevations any higher than the other samples from the central mountain chains.
The regular pattern of increasing FTA landwards from the continental margin is also distorted by the apatite FTA of Sigurdsvodene and Starheimtind which are relatively old with respect to their proximity to the continental margin and their topographic elevation. Cooling in these areas to <60°C is also proposed to have occurred during the Late Jurassic/Early Cretaceous.
The young apatite FTA, the long mean track lengths and the low elevation of the Schirmacheroase occupies a unique position within CDML, and reflect a period of accelerated cooling through the APAZ in the late Early to Late Cretaceous.

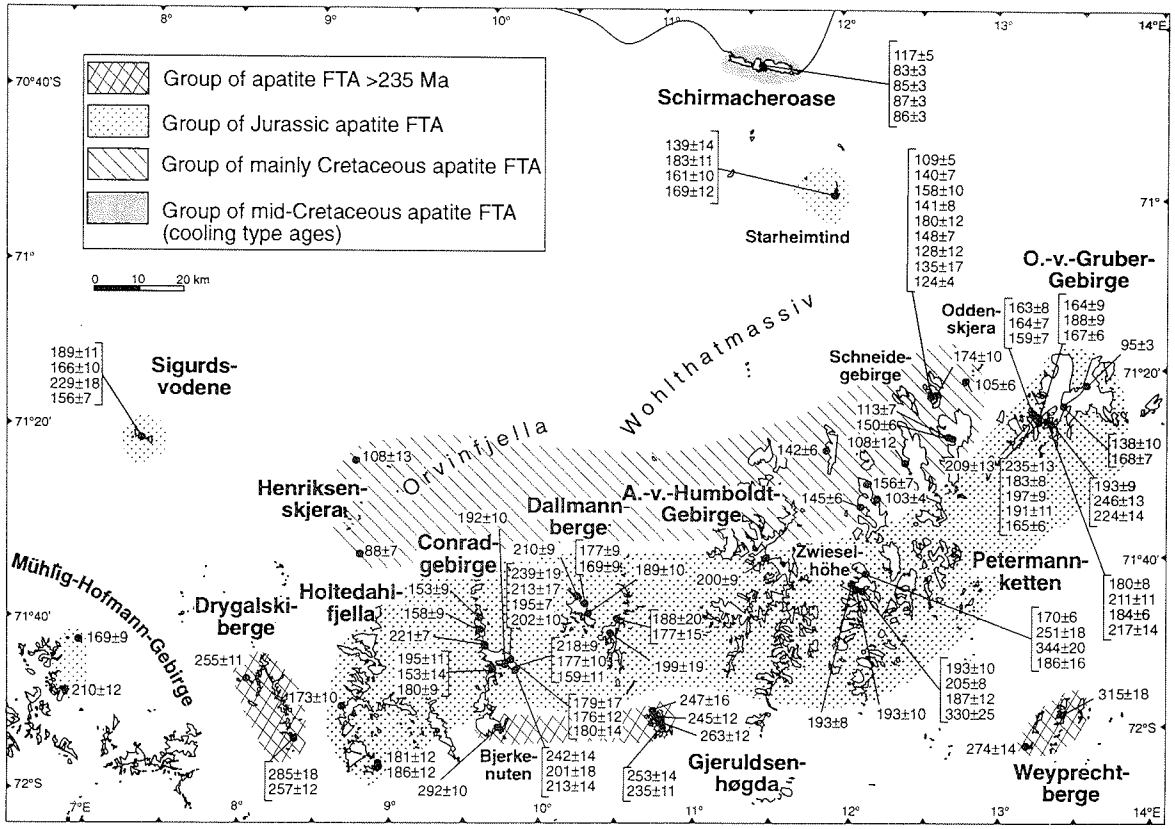

Fig. 4.17 Overview map of CDML showing the sample apatite FTA and the different apatite FTA groups.

Irrespective of any spatial coherences, the thermal evolution of CDML can largely be constrained by the relationship between the apparent apatite FTA and the mean track length (Fig. 4.18).

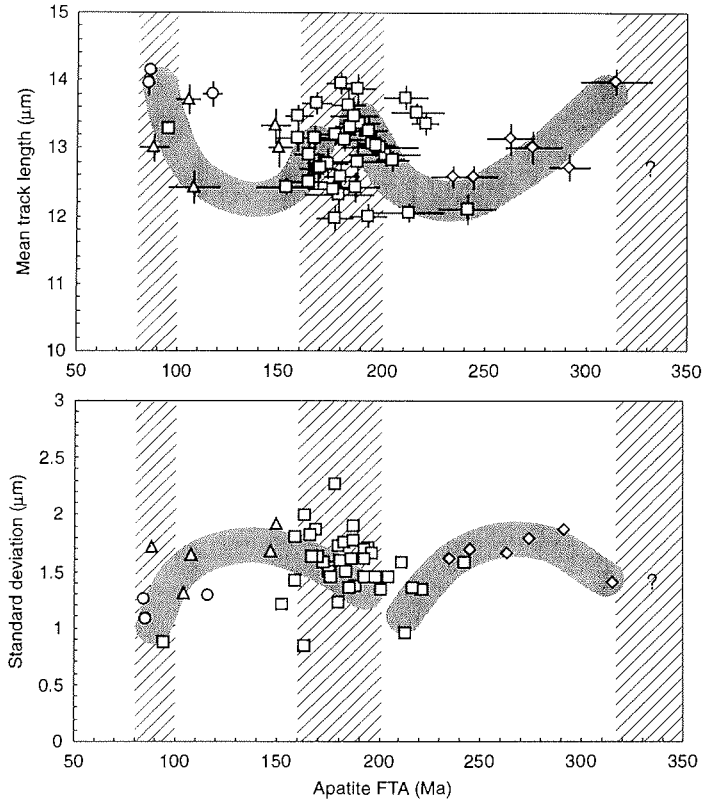

Fig. 4.18 **(A)** Apatite FTA-mean track length relationship. Error bars correspond to the 1σ-error on the FTA and the mean track length. **(B)** Coherence between the apatite FTA and the standard deviation of the mean track lengths. The error bars are omitted for clearity reasons. The grey lines emphasize the trend of increasing/decreasing mean track lengths/standard deviations towards younger FTA. The hatched rectangles mark times of enhanced cooling.

A three- or at least two-staged thermal history can be proposed for CDML with a significant increase in mean track lengths at ~180 Ma and a second one at ~90 Ma. Furthermore, the oldest apatite FTA from CDML has a mean confined track length of 14.0 µm and possibly reflects a very old cooling step at ~315 Ma. The lowest standard deviations also occur at ~315 Ma, 180 Ma and at ~90 Ma and support enhanced cooling at these times.

4.6 Interpretation of apatite fission-track results for dropstones

A provenance study (Kuhn et al., 1993) on clasts in glaciomarine sediments from the Lazarev Sea, offshore CDML, yields hat the deposition of such clasts occured predominantly from the nearest land-ice source. According to Kuhn et al. (1993), mixing with exotic clasts from far-travelled icebergs is negligible in this region. Hence, it is concluded that the dropstones were transported from the continental region of CDML apatite FTA of the dropstones represent fragments of the tectono-thermal history of the adjacent landmass. Samples 2057/1 and 2057/2 for instance, both give Jurassic ages and originate from anorthosites. By comparing the two samples with the *in-situ* anorthosite samples, the dropstone samples FTA would fit well in the data sets of the O.-v.-Gruber-Gebirge and the Untersee profile. Assuming that the two dropstones originated from the large anorthosite intrusion in the O.-v.-Gruber-Gebirge or possibly from the In der Schüssel area, the likely glacial transport of the clasts was accomplished within the large NE-ward flowing glacier draining onto the ice shelf east of the Schirmacheroase. Samples 2058-1 and 2031-1, located adjacent to the ice shelf and the grounding line, give Jurassic apatite FTA similar to the FTA obtained from CDML. However, it is difficult to assign them to a specific locality in CDML because of their less prominent lithology. Sample 2034-3 may also originate from CDML, although its sampling site is situated furthest from the ice shelf and ~2° west of the western border of the area of study (~8°E). Sample 2033-2 was also collected from an ice-shelf-edge remote site and has the youngest apatite FTA of all samples dated from CDML. Due to the fact that the youngest apparent FTA are confined to the Schirmacheroase which bounds the investigated area of CDML to the north, ages younger than 83±3 Ma would be expected at elevations <50 m. Subsequently, the sample may either have been transported by glacier to the west, although this seems to be inhibited by a rather NE-ward directed glacial flow or the sample may have originated

from the Mühlig-Hofmann-Gebirge, and represent a part of the continental margin evolution of the neighbouring mountain ranges of CDML.

4.7 Note on modelling thermal histories

Some authors (e.g. Clift et al., 1997; Gallagher et al., 1994) apply modelling programs (e. g. MONTE TRAX; Gallagher, 1995) for specifying thermal histories of apatite fission-track samples. Based on the apatite single grain ages and the track lengths of a sample as well as individual time-temperature frames, the program approaches an optimal fit between the observed data and the data predicted for a specific thermal history. The program allows to chose between different annealing models and runs either in the random Monte Carlo simulation or in the genetic algorithm mode. A good model fit is attained for apatite samples of known chemical composition which apparently experienced a relatively simple thermal evolution.

In the present study, thermal modelling was not carried out for a variety of reasons. Generally, the apatite fission-track data of the samples from CDML scatter substantially, and the majority of FTA refers to mixed ages and mostly are characterised by low χ^2-values (<20%) or even failed the χ^2-test (<5%). As pointed out in the previous interpretation of the results, it cannot be determined precisely when the samples have individually cooled <110°C, and later on <60°C. In addition, a samples specific position during its stay within the APAZ cannot be constrained exactly from the fission-track data, if no break-in-slope is retained in the vertical profiles. Though discussed in detail in the next chapter, the data are interpreted to reflect a principally common thermal history of the basement, but local differences also could have contributed to the observed distribution of the fission-track data. Furthermore, the apatite fission-track data from CDML record a smooth cooling history rather than a sequence of drastic cooling steps. The smooth thermal development is further complicated by the local variations in the apatite fission-track data.

The resolution of the MONTE TRAX program is considered not to be high enough to constrain the complex apatite fission-track data from CDML and appears to be incapable to account for such small-scale variations as observed in the data from studied area. The modelling was performed attemptively on some samples, but a consistent cooling path in agreement with the fission-track data of the other samples and with the field evidence could not be obtained. Furthermore, the annealing models available for running the

modelling procedure could be inappropriate for apatites of possibly varying chemical composition (see section 4.5.2).

5. Discussion

5.1 Pan-African cooling constrained from metamorphic P-T conditions

It is known that the basement of CDML was metamorphically overprinted in two major periods during Pan-African times. The first metamorphic imprint at ~570 Ma reached temperatures of 810-850°C at a depth of 20-25 km (Piazolo and Markl, 1998). A later metamorphic Pan-African imprint in CDML occurred between ~530 Ma and 500 Ma, when the presently outcropping basement was located at temperatures of ~650°C in a depth of ~15 km. For both periods of metamorphism elevated geothermal gradients are suggested (Piazolo and Markl, 1998). Piazolo and Markl (1998) also propose that the implied highly elevated heat flow for the duration of 50-100 Ma could have been caused by magmatic underplating and the melting and intrusion of syenitic magma into a crust that was already heated at this time.

From the position of the isotherms during the Pan-African metamorphism, the amount of cooling of the basement rocks from CDML between ~570 Ma and ~530-500 Ma can be estimated as about 160-200°C (Fig.5.1). Using the calculated depth of the 650°C- and 810-850°C-isotherms, this corresponds to a total denudation of crustal rocks on the order of 4-11 km at a rate of 60-275 m/Ma. It is not known, however, if the high geothermal gradients affected the crust throughout the Pan-African event or if the crust cooled down between the metamorphic episodes to a normal cratonic temperature distribution. If a normal geotherm became stabilised between the two metamorphic episodes, this would even have increased the calculated amount of denudation during the Pan-African event.

The metamorphic PT-estimations of Piazolo and Markl (1998) differ greatly from the estimates of Jacobs et al. (1998) and Colombo and Talarico (1999) who assigned upper amphibolite facies to the metamorphic imprint at ~570 Ma and granulite facies conditions for the time between ~530-515 Ma. The amount and rate of denudation derived from the calculations of Piazolo and Markl (1998) for the Pan-African event might therefore overestimate the true amounts.

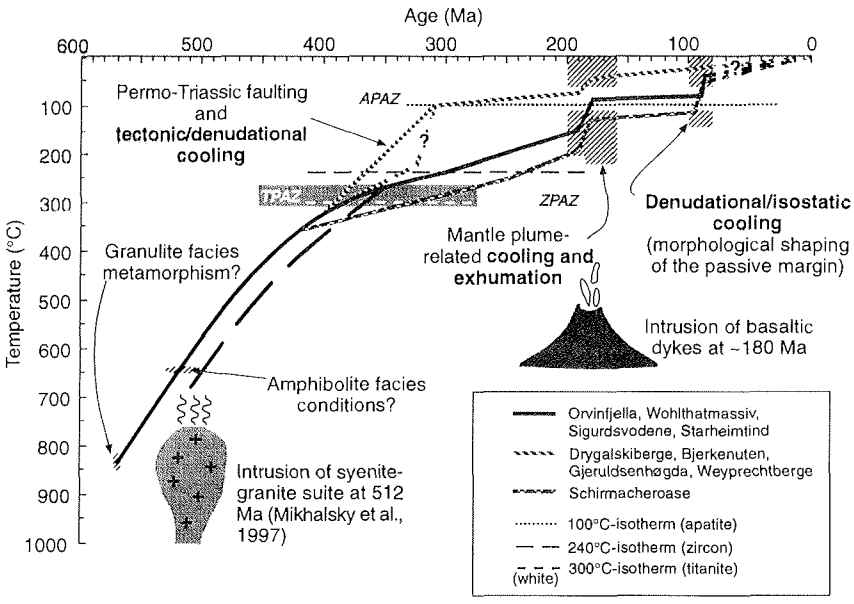

Fig. 5.1 Generalized time-temperature path for the basement of CDML through the last 600 Ma. The thick solid black line represents the cooling path of the central mountain ranges, the thick broken line corresponds to the samples with younger titanite FTA, being affected by the 512 Ma-syenite intrusion. For the oldest apatite fission-track samples (cross hatched line) an alternative cooling path for the Permo-Triassic is depicted (cross hatched broken line).

In the late Precambrian/early Paleozoic CDML formed part of an extensive collisional orogen that was created by the closure of the Mozambique Ocean during the amalgamation of East and West Gondwana. CDML therefore probably represents the southern continuation of the Mozambique Belt to the south (see Fig. 1.7) (Jacobs et al., 1998). Compared to young collisional orogens, such as the Alps (e.g. Hurford et al., 1989), the Andes (Kohn et al., 1984) or the Southern Alps of New Zealand (e.g. Kamp et al., 1989), where denudation rates on the order of 500 m/Ma to 1000 m/Ma are reported, the rates in CDML during Pan-African times are relatively low. However, any enhanced crustal uplift and denudation in CDML, combined with an elevated heat flow, could have been attributed to magmatic underplating that affected large parts of the Gondwana supercontinent during the Pan-African event (Unrug et al., 1994; Veevers, 1995; Piazolo and Markl, 1998). Veevers (1995) suggested that the Pan-African cycle (950-450 Ma) ended at ~500 Ma with rapid uplift and cooling/denudation in Gondwana. The widespread buoyancy of the supercontinent was attributable to thermal rejuvenation, shear zone

activation and anorogenic magmatism which also incorporated magmatic underplating of the lower crust during the Pan-African cycle.

5.2 Post-Pan African to mid-Paleozoic cooling history of CDML

The early to mid-Paleozoic cooling history of CDML is largely constrained by the titanite FTA which range from ~450-300 Ma. Sample SP40 (Sigurdsvodene), whose titanite FTA of 531±51 Ma overlaps with the latest stage of metamorphic overprinting in CDML, is interpreted to postdate the Pan-African event within its 1σ-error.

It seems that the oldest titanite FTA (≥430 Ma) (Mühlig-Hofmann-Gebirge, Sigurdsvodene, Untersee, Starheimtind and Schirmacheroase) from CDML are distributed around the Orvinfjella and Wohlthatmassiv (cf. Fig. 4.5). Most of the samples from the peripheral zone of CDML experienced the last metamorphic overprint no later than ~530 Ma. The youngest titanite FTA are roughly confined to the central parts of the Orvinfjella and the Wohlthatmassiv where at ~510 Ma the voluminous post-tectonic syenite-granite suite intruded the metamorphosed basement (Mikhalsky et al., 1997). This affected in particular the central mountain chains of the Wohlthatmassiv, but also areas of the western Orvinfjella as well as Gjeruldsenhøgda (cf. Fig. 1.5). The central part of the Conradgebirge was affected at ~530 Ma by the intrusion of a granodiorite and syn-magmatic high grade metamorphic overprinting (Jacobs et al., 1998).

It is concluded that the titanite FTA from CDML most probably record a differential post-orogenic cooling. The basement surrounding the Orvinfjella and the Wohlthatmassiv potentially could have cooled from temperatures of no less than 650°C after the last metamorphic overprinting at ~530 Ma (cf. Jacobs et al., 1998; Piazolo and Markl, 1998; Colombo and Talarico, 1999). The titanite FTA of sample J1743 is in good agreement with the K-Ar and Rb-Sr biotite ages of ~450 Ma for the eastern Mühlig-Hofmann-Gebirge indicating cooling to 300°C by that time (cf. Henjes-Kunst and Markl, 1998).

While the surrounding basement samples record a progressive post-Pan-African cooling, the samples from Oddenskjera and the Zwieselhöhe were emplaced with the intrusion of the syenite-granite suite at ~510 Ma (cf. Mikhalsky et al., 1997). Their younger titanite FTA therefore reflect a slower and/or later cooling of the intrusive bodies through the TPAZ in a thermal environment characterised by condensed isotherms and high heat flow. The sample from the syenite intrusion of Gjeruldsenhøgda has a comparatively old titanite FTA of 428 Ma and perhaps traces a more rapid post-magmatic cooling and/or a

tectonically different evolution. The young titanite FTA of sample GM651 (351±43 Ma) is interpreted to record the delayed and/or slow cooling of the granodiorite intrusion in the Conradgebirge. In the Petermannketten, the A.-v.-Humboldt-Gebirge and Dallmannberge, the titanite FTA are also younger than ~430 Ma. It is possible that magmatic intrusions were emplaced in this area at a lower crustal level, although igneous activity in these areas during the late Pan-African has not been recognised. However, it seems that the titanite samples from this area were influenced by the high heat flow predominating in the Orvinfjella and the Wohlthatmassiv. The scatter in titanite FTA in the Orvinfjella and the Wohlthatmassiv could reflect local variations in the geothermal gradient associated with the post-tectonic magmatism.

It is generally assumed that the Pan-African-related high heat flow decreased during the post-orogenic cooling leading to a subsequent reaccomodation and decompression of isotherms as well as to the establishment of a stable normal geothermal gradient within the crust. For the post-Pan-African tectono-thermal evolution of CDML, this would imply that the basement cooled until ~450-300 Ma by ~350°C, if a palaeotemperature of ~650°C (depth of ~15 km) for 530-500 Ma is assumed (cf. Piazolo and Markl, 1998). By employing a palaeogeotherm of 20-30°C/km (depth of 300°C-isotherm: 10-15 km) for the early to middle Paleozoic, a total amount of denudation of no more than 5 km can be calculated. This corresponds to a denudation rate of ~22-100 m/Ma. The Paleozoic gradient was chosen in order to account for a fluctuating thermal regime after the Pan-African cycle. The lowermost value corresponds to a normal cratonic gradient whilst the maximum value represents a slightly elevated geotherm.

It is diffcult to estimate the rate of denudation more precisely because the scatter in the titanite FTA could have been produced as the result of perturbation of the isotherms during post-orogenic cooling. The amount of denudation could have been substantially higher, because Jacobs et al. (1998) as well as Colombo and Talarico (1999) postulated granulite facies conditions for the last metamorphic overprinting in CDML.

In CDML, the Pan-African event was terminated by an orogenic collapse resulting from continental underthrusting and doubling of the thickness of the crust (Bauer et al., 1999; Colombo and Talarico, 1999). The relief and the topographic elevation expected from a collapsed orogen are likely to be low, and thus promoting low denudation rates. Because of the double thickened crust and the resulting isostatic rebound, the subsequent denudation of the orogen could have been maintained for considerable time.

5.3 Mid-Paleozoic to early Mesozoic steady cooling in CDML

The zircon FTA (~310-240 Ma) record a period of Late Carboniferous to Early Triassic steady cooling and denudation and indicate that the basement of CDML had cooled by ~60°C in not more than 210 Ma. This corresponds to a total denudation of ≤6 km of crustal material at a rate of ~30-600 m/Ma adopting a geothermal gradient of 15-25°C/km. As the zircon FTA correspond well with the topographic elevation and are not as significantly scattered as the titanite FTA, it is assumed that the critical isotherms must have attained a stable position within the upper crust at around 310-240 Ma. Therefore, it is likely that the thermal gradient at this time covered the range usually applied to cratonic values (cf. Chapman, 1986; Brown et al., 1994).

Field evidence recording the post-Pan African geological development of CDML in the Paleozoic has so far not been recognised. However, in western Dronning Maud Land sedimentary rocks of the Permo-Triassic Beacon Supergroup provide valuable information about the cooling history of the basement at this time (e.g. Juckes, 1972). The strata of the Beacon Supergroup unconformably overly the basement and are capped by basaltic lava flows. However, it is not known if CDML was a region either of erosion or deposition during the mid- to late Paleozoic. There is no evidence for thermal overprinting of the fission tracks by burial due to depositional loading in the zircon FTA from CDML. This would require cooling of the samples below the ZPAZ (320-210°C) before reheating. However, no evidence for this is seen in the zircon fission-track data which rather point towards a slow continuous cooling history. Compelling evidence for a thermal overprinting is also not included in the Late Carboniferous to Late Permian apatite FTA of the samples from the southernmost localities of CDML (Drygalskiberge, Bjerkenuten, Gjeruldsenhøgda and Weyprechtberge, see Fig. 4.17) which indicate cooling to ~100°C by this time. The zircon and apatite fission-track data imply that CDML most probably served as a region of progressive cooling and denudation where crustal material was removed and deposited elsewhere.

5.4 East Antarctica in early Paleozoic to early Mesozoic times

The post-Pan-African Paleozoic history of CDML has previously only been poorly constrained from field evidence and other geochronological methods with the latest cooling episode being Pan-African. As outlined in the previous discussion, the middle Paleozoic to early Mesozoic titanite and zircon FTA reflect a continuous thermal evolution rather than a succession of short-lived cooling events.

Due to the lack of good geological evidence, the better studied regions of East Antarctica should be able to provide conclusive ideas about the Paleozoic evolution of CDML. For instance, a wealth of information is available concerning the Paleozoic evolution of the Pacific margin (Transantarctic Mountains including the Thiel, Pensacola and Theron Mountains) of the East Antarctic craton that, on a large scale, potentially could have influenced the tectono-thermal development of CDML (Fig 5.2) (e.g. Laird, 1963, 1981; Clarkson, 1981; Cooper et al., 1983; Pankhurst et al., 1983; Webers and Spörli, 1983).

Since the late Proterozoic the Pacific rim of the East Antarctic craton formed part of the Panthalassan margin of Gondwana that extended from southern South America, southern Africa and East Antarctica into the Australian continent (e.g. Collinson et al., 1994; Powell and Li, 1994). The Panthalassan margin in East Antarctica has subsequently been modified by at least three orogenies, the earliest taking place in the Late Proterozoic (Beardmore Orogeny). The Cambro-Ordovician Ross Orogeny of Pacific East Antarctica, contemporaneous with the Pan-African event in the Atlantic section of East Antarctica, led to widespread folding, metamorphism and granite intrusions (Collinson et al., 1994). The Ross Orogeny was followed by an episode of erosion and tectonic quiescence which lead to subsidence of the passive continental margin along the Transantarctic Mountains margin of East Antarctica and to the subsequent formation of a peneplanation surface termed the Kukri peneplain (Gunn and Warren, 1962). Remnants of peneplanation surfaces are widespread in the Transantarctic Mountains, the Pensacola and the Ellsworth Mountains, but also occur to a lesser extent in western Dronning Maud Land and possibly in the Gjelsvikfjella (Barrett et al., 1972; Näslund, 1998). On this erosional surface the Devonian to Jurassic sedimentary rocks of the Beacon Supergroup were deposited creating a pronounced unconformity with the basement rocks beneath.

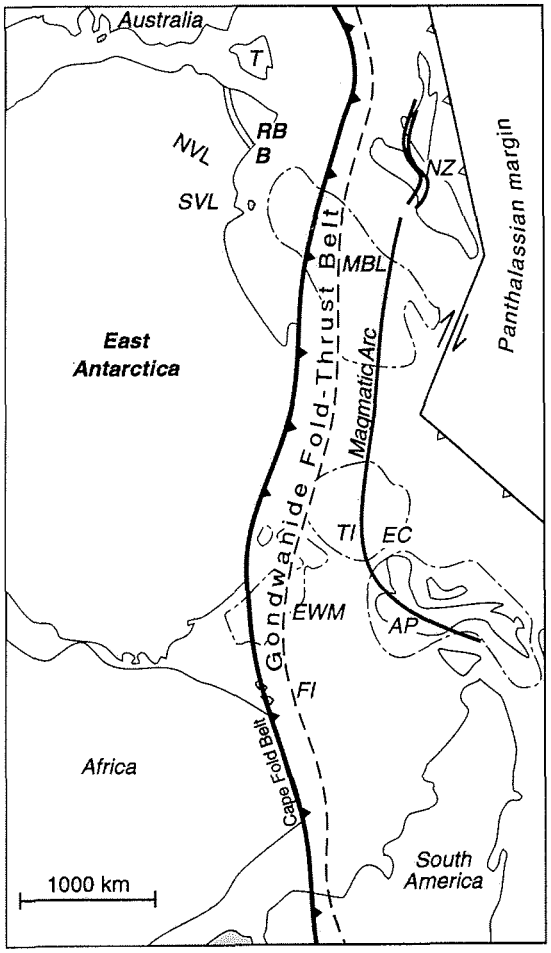

Fig. 5.2 Panthalassan margin of East Antarctica during the final Gondwanide deformation and prior to the fragmentation of Gondwana. The palinspastic reconstruction for the Late Triassic (~230 Ma) is based on Grunow et al. (1991) (see Collinson et al. (1994) for description). Abbreviations: AP - Antarctic Peninsula, B - Bowers terrane, EC - Eights Coast, EWM - Ellsworth-Whitmore Mountains, FI = Falkland Islands, MBL - Marie Byrd Land, NZ – New Zealand, NVL – North Victoria Land, RB - Robertson Bay, SVL – South Victoria Land, T - Tasmania, TI - Thurston Island (from Collinson et al., 1994).

Sequences of the Beacon Supergroup crop out particularly well along the Pacific margin and reach thicknesses ranging from ~2300 m (southern Victoria Land) to ~3500 m in the Pensacola Mountains (Barrett et al., 1972; Collinson et al., 1994; Powell and Li, 1994). It is important to note that similar sedimentary sequences are also found in Australia, Peninsular India, Madagascar, Africa, the Falkland Islands and southern South America (Craddock, 1982).

Although Beacon sedimentary strata have been recognised in the Heimefrontfjella and Kirwanveggen area of western Dronning Maud Land (Juckes, 1972; Groenewald et al.,

1991), no sedimentary record has been identified in the region between the Mühlig-Hofmann-Gebirge (Otha et al., 1990) and the more easterly located Sør Rondane Mountains (Shiraishi et al., 1991). In the Heimefrontfjella, the Beacon sedimentary sequences reach a thickness of no more than 160 m and are capped by a 130 m thick pile of Jurassic basaltic lavas (cf. Jacobs et al., 1992). Juckes (1972) recognised an erosional hiatus between the deposition of the sediments and the eruption of the volcanic rocks.

As was mentioned earlier in this chapter, subsidence along the Pacific margin of the East Antarctic craton resumed in the middle Paleozoic. From the Late Permian a major depositional foreland basin developed, termed the Transantarctic basin. This basin has occupied almost the full length of the East Antarctic Panthalassan margin (e.g. Barrett et al., 1972; Collinson et al., 1994; Powell and Li, 1994; Veevers et al., 1994a). The subsequent deepening of this basin occurred contemporaneously with the Gondwanide Orogeny that affected the Panthalassan margin of Gondwana from the Late Permian to the Triassic. It is known that the deposition of the Gondwana Sequence elsewhere in Gondwana was strongly associated with extension and subsidence parallel to this dominant convergent margin. In southern Africa the subsidence of the Karoo Basin and Zambezi Basin as well as the sedimentation of the Karoo Sequence are intimately related to the formation of the Cape Fold Belt during the Gondwanide Orogeny (Groenewald et al., 1991; Veevers et al., 1994b). In East Antarctica subsidence resumed after the Ross Orogeny, whereas the basin development in southern Africa started somewhat later in the Late Carboniferous spreading northwards as far as to the equatorial region (Veevers et al., 1994b). According to Rust (1975) subsidence across the African continent was triggered by two tectonic processes. The first of these involved warping of basins (Karoo, Kalahari, Congo and Gabon) and the development of intervening swells. In contrast, the Zambezi terrain underwent intense faulting with the creation of graben-type depositional realms. Similarly, in Peninsular India sedimentation in the Gondwana Master Basin started in the latest Carboniferous with the deposition of the glaciogenic Talchir Formation. Further subsidence of this basin in the Late Triassic was enhanced by faulting and rifting (Veevers and Tewari, 1995). The termination of the depositional regime along the East Antarctic and southern African Panthalassan margin and also in Peninsular India is defined by the effusion of basaltic lavas that preceded the breakup of Gondwana in the Early Jurassic and which are locally preserved as resistant cap rocks on top of the pre-Jurassic sedimentary strata.

Plate tectonic and palaeogeographic reconstructions of East Antarctica for the Pan-African and for the pre-Gondwana breakup assembly show that CDML represented a region in the

East Antarctic craton, where the edges of three continental fragments were connected. According to the Pan-African reconstructions, CDML formed part of the East Antarctic mobile belt that trended from the Mozambique Belt (southern Africa) to Dronning Maud Land and propagating eastward into the Kerala Khondalite Belt (southern India) (Stackebrandt, 1990; Jacobs et al., 1998; Piazolo and Markl, 1998). Gilchrist and Summerfield (1994) have demonstrated that the palaeosurface elevations in the central parts of the Gondwana supercontinent were most probably significant for two reasons. They concluded that the distances from source to mouth were much greater than for modern cratonic drainage systems and therefore the mean river gradients would have been low enough not to have promoted enhanced incision and sediment transport. Landscape modification would have been further retarded because of the arid climate that prevailed, for instance, in the Triassic of southern Africa. In CDML a slowly progressing landscape modification seems to be reflected in the relatively low denudation rates (~25-120 m/Ma) after the termination of the Pan-African until the mid-Paleozoic. Titanite and zircon fission-track results and the estimated late Paleozoic denudation rate indicate that CDML was a region of low relief which became successively eroded at that time. This is in good agreement with the presumed smooth morphology of a Pan-African collapsed orogen. The eroded material could be transported from CDML to regions of subsidence and sedimentation which predominated, for instance, along the Panthalassan margin of East Antarctica and southern Africa. Hypothetically, CDML could have been located at the periphery of the Transantarctic basin because it appears that western Dronning Maud Land was still influenced by the depositional regime prevailing along this continental margin at that time. Furthermore, CDML was most probably a continuation of the Pan-African Mozambique Belt and therefore its later involvement, particularly in context with the formation of the Zambezi Basin and the associated faulting, cannot be ruled out.

5.5 Late Paleozoic/early Mesozoic fault control on zircon and apatite fission-track pattern

The oldest apatite FTA from the samples of the Drygalskiberge, Bjerkenuten, Gjeruldsenhøgda and Weyprechtberge indicate cooling to below ~110°C during the Late Carboniferous to Late Permian. It should be stressed that the majority of samples at this time were still at temperatures of ~240°C and cooled to below 110°C in Early Jurassic times. This implies that from at least the Late Carboniferous the central part of the Orvinfjella (Holtedahlfjella, Conradgebirge and Dallmannberge) and the Wohlthatmassiv (A.-v.-Humboldt-Gebirge, Zwieselhöhe, Petermannketten, Schneidegebirge, Oddenskjera, O.-v.-Gruber-Gebirge and Untersee) were subjected to a different thermal evolution than the southernmost areas. Since the titanite FTA of all samples from CDML are believed to share a common cooling path, all samples from CDML should share a common tectono-thermal history from the early until the mid-Paleozoic. It thus needs to be explained how the samples from the southernmost localities with the oldest apatite FTA cooled to temperatures of the APAZ during the Paleozoic, while the other samples remained at temperatures of ~240°C. It appears that the samples with the late Paleozoic/early Mesozoic zircon and the Jurassic apatite FTA could represent the general cooling path of the basement rocks whilst those with the pre-Jurassic apatite FTA were subjected to accelerated cooling probably caused by tectonic denudation.

To suppress a cooling process, a heating mechanism, such as magmatic intrusion, is required whereby samples are kept at temperatures of ~240°C while others cool by ~140°C. However, because of their spatial vicinity (samples having late Paleozoic apatite FTA and those with Jurassic FTA lie side by side), such a mechanism cannot account for the observed distribution of apatite FTA in the south of CDML. It therefore seems likely that after the Pan-African and prior to the Late Carboniferous physical separation of the samples from the southernmost localities from the remaining samples by faulting occurred.

Unfortunately extensive ice coverage means that field evidence for the presence of faults that were either created or reactivated during this time is only sparsely available. In the southern Conradgebirge, at Bjerkenuten, a major sinistral transpressional shear zone (South Orvinfjella Shear Zone) runs through the outcropping basement rocks in an E-W direction and is also apparent in the Kurzegebirge and the Dallmannberge (see Fig. 5.3). According to Jacobs et al. (1998) this shear zone reflects a general sinistral transpressional setting that predominated during the amalgamation of East and West Gondwana in the Pan-African. The lateral offset of the South Orvinfjella Shear Zone in the Dallmannberge most probably is caused by a later N-S trending fault (Bauer et al.,

1999). Further to the east the extension of the shear zone is obscured beneath the ice (Bauer et al., 1999) but potentially it might cut through the basement somewhere north of the Weyprechtberge.

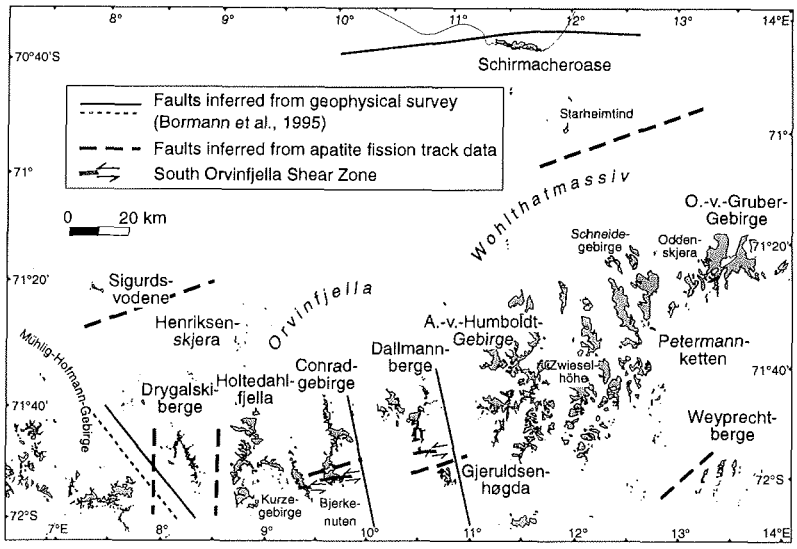

Fig. 5.3 Fault distribution in CDML. Fault locations after Bormann et al. (1995) are given in their approximate positions.

Apparently, all samples belonging to the group of the oldest apatite FTA are located south of the South Orvinfjella Shear Zone while the Jurassic- and younger apatite FTA are situated north of it. This does not include the samples from the Drygalskiberge where the shear zone does not crop out. By inferring a N-S trending fault between the Holtedahlfjella and the Drygalskiberge and possibly between the latter and the eastern Mühlig-Hofmann-Gebirge, and by taking into account that the shear zone experienced a lateral offset along these faults, the shear zone is expected to run somewhere north of the Drygalskiberge. From the apatite FTA it therefore seems likely that the South Orvinfjella Shear Zone was reactivated during the Late Paleozoic, with the samples with older apatite FTA being exhumed to a crustal level corresponding to the APAZ. This also requires that the lateral offset along N-S striking faults must have postdated movement along the shear zone.

Alternatively, differential tectonic denudation could have taken place solely along N-S trending faults without involving the South Orvinfjella Shear Zone. As reported from

photogeological and geophysical investigations in the Schirmacheroase and the Wohlthatmassiv, ice covered N-S trending faults are inferred to occur throughout the eastern part of CDML, separating the mountain chains along a pronounced N-S trend (e.g. Bankwitz and Bankwitz, 1995a; Bormann et al., 1995).
Another possibility for differential cooling of the older samples from CDML is provided by NE-SW trending fault zones that are spread across CDML (Kämpf et al., 1995). In the Schirmacheroase these faults are intruded by lamprophyre dykes which are considered as being older than the Jurassic basaltic dykes from crosscutting relationships, although they have not been dated so far (Wand, 1995). But K-Ar whole rock ages from subalkaline dykes give ages of ~320 Ma pointing towards extensional forces by this time (Wand et al., 1988).
In the late Paleozoic Gondwana supercontinent of the southern hemisphere the deposition of sediments was largely controlled by fault-bounded structures such as in the Zambezi basin (southern Africa) and Peninsular India. Similar extension precursoring the Gondwanide Orogeny may also have peripherally affected CDML and thus led to a N-S or NE-SW directed fault pattern. In addition, it must be considered that CDML probably occupied a critical position within Gondwana being situated at the junction of three continental masses each of which was exposed to different regional subsidence and tension.
The amount of tectonic denudation of the mountain ranges with the pre-Jurassic apatite FTA relative to those with younger, Jurassic ages must have been on the order of ~5.5-9.5 km assuming a palaeogeothermal gradient of 15-25°C/km. The onset of tectonic denudation can only be estimated as having occurred sometime between the early Paleozoic and prior to the Late Carboniferous as constrained by the oldest apatite FTA of the most southerly samples. It cannot be ruled out that the zircon FTA of those samples with Jurassic apatite FTA were also influenced by this tectonic denudation in vicinity to the southernmost samples due to compression of isotherms.

5.6 Early Jurassic basement evolution of CDML - initial breakup of Gondwana

5.6.1 Apatite fission-track evidence for an Early Jurassic pre-rifting cooling

Samples with Jurassic and Cretaceous apatite FTA constitute the majority of the fission-track data and are largely confined to the central mountain chains of the Orvinfjella and

Wohlthatmassiv. The Jurassic ages occur at the highest elevations while the Cretaceous-aged samples are concentrated along the less elevated northern rim of the central mountains. Jurassic FTA have also been obtained for the samples from the nunataks of Sigurdsvodene and Starheimtind further to the north, although they occur at the same elevations as those samples with Cretaceous FTA.

The apatite fission-track data of CDML demonstrate that all samples with Jurassic FTA from elevations between ~1300-3000 m underwent a complex tectono-thermal history and spent considerable time within the APAZ. A maximum value for the geothermal gradient in the Jurassic can be estimated by assuming that all samples from a vertical profile were within the APAZ at the same time. The estimate was derived from the O.-v.-Gruber-Gebirge profile, because this covers the largest range in elevation between Jurassic-aged fission-track samples. The difference of ~1600 m between the upper- and lowermost sample yields a maximum geothermal gradient of 30°C/km during the Jurassic.

For the determination of the amount of denudation in CDML from the late Paleozoic until recent a geotherm of 15-30°C/km is assumed. This spread is to account for potential crustal thermal perturbations which cannot be constrained exactly from the fission-track data alone. By employing a maximum value of 30°C/km, which is a slightly elevated geothermal gradient, a mild thermal influence such as heating of the upper crust due to pervasive magmatism can be ascertained. The lowermost value of 15°C/km represents a gradient found in intracratonic stable crust (cf. Brown et al., 1994).

Through the early Mesozoic until the Jurassic the basement of CDML cooled by ~140°C at an average rate of 1.3-1.8°C/Ma. Consequently, no more than 10 km of crust could have been removed from the late Paleozoic until the Jurassic, implying a mean denudation rate of 90-125 m/Ma.

Compared to the pre-late Paleozoic, the cooling and denudation rate must have increased sometime at the end of the Paleozoic or the early Mesozoic. As has been discussed in the previous chapter (see Fig. 4.18) the apatite FTA-versus-mean track length relationship illustrates an increase in mean track lengths at ~180±20 Ma pointing towards enhanced cooling of the basement during the Early Jurassic. In summary it can be concluded that the basement rocks of CDML cooled steadily from the late Paleozoic until the late Triassic with cooling and denudation increasing significantly at ~180±20 Ma. During this time the samples cooled from <240°C to below ~110°C but still remained at temperatures >60°C until sometime later (Meier et al., 1999).

While the samples with Jurassic apatite FTA cooled to the APAZ, the older samples from the southernmost localities imply cooling to below 60°C during this same episode as indicated by the appearance of apatite single grain ages no younger than Jurassic. Their

post-Early Jurassic cooling history cannot be deduced from the apatite fission-track data. However, the late Mesozoic and Cenozoic tectono-thermal evolution of the basement and the present-day field relationship of old and younger samples suggest that the samples of the southernmost localities and the Orvinfjella/Wohlthatmassiv attained a common crustal level sometime during or after the Early Jurassic, and from then on, have shared the same tectono-thermal evolution. If this was not the case, then cooling of all samples by ~140°C in the Early Jurassic, equivalent to less than 10 km of denudation, could have led to different crustal positions of the older samples and those of the Orvinfjella/Wohlthat-massiv.

The relatively long mean track lengths of the O.-v.-Gruber-Gebirge samples support a fault-control on the distribution of Early Jurassic FTA. In comparison with the Conrad-gebirge profile, for example, the O.-v.-Gruber-Gebirge samples presumably cooled more rapidly through to APAZ temperatures in the Early Jurassic. Due to the moderate differences in the fission-track data it is proposed that any differential movements between the mountain ranges were on the order of no more than a few hundred meters.

5.6.2 Field evidence in CDML for Gondwana breakup

The purpose of the following section is to highlight the field evidence for the Gondwana breakup which have been obtained during numerous studies in the onshore and offshore region of CDML.

5.6.2.1 Onshore record

The initial breakup of East and West Gondwana in CDML is evident from the abundance of mafic dykes crosscutting the basement rocks as well as older dykes. Field evidence for the breakup in CDML is less apparent than in western Dronning Maud Land and southern Africa, where Early Jurassic relics of basaltic lava piles are preserved. K-Ar whole rock datings on unmetamorphosed basaltic dykes and dolerite erratics from the Schirmacher-oase yield a distribution peak at 180-160 Ma that indicates Early Jurassic magmatism prior to the disintegration of Gondwana (Wand et al., 1988). The thermal influence of these intrusions on the host rocks must have been relatively small and only affected the host on a few tens of centimeters scale. From their geochemistry, the basaltic dykes are tholeiites and weakly alkaline intra-plate basalts, while the dolerite erratics are composi-tionally similar to the Kirkpatrick Basalts from North Victoria Land (East Antarctica) (Fig. 5.4) (Wand, 1995).

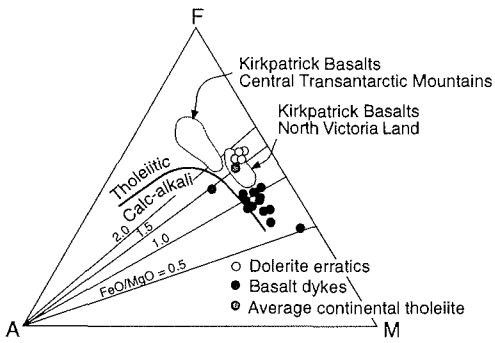

Fig. 5.4 *AFM diagram for basaltic rock samples from the Schirmacheroase in northern CDML.* Dolerite erratics plot in the field of the Kirkpatrick Basalts from North Victoria Land (from Wand et al., 1988).

In the Wohlthatmassiv Bankwitz and Bankwitz (1995a) identified a variety of magmatic dykes spread over the outcropping basement, based on photogeological interpretations. Most are assumed to have a doleritic and lamprophyric composition and generally extend over lengths of 200-5000 m. Apart from the K-Ar data of Wand et al. (1988), no conclusive age information about the various mafic dykes in the interior of CDML are available.

Jurassic magmatism in CDML is thought as having been preceded and/or accompanied by intense fracturing of the basement, particularly in E-W direction with the subsequent intrusion of magma into the fissures now preserved as magmatic dykes (e.g. Bankwitz and Bankwitz, 1995b; Paech et al., 1995). The presence of E-W trending faults and/or fault zones has been confirmed by deep seismic sounding, magnetic, and gravimetric investigations in the onshore area of CDML (cf. Kogan, 1972; Kogan and Stroev, 1972). Furthermore, they postulate a thinning of the crust from ~38-40 km to ~26 km north of the ice shelf edge. Their results were compiled by Bormann et al. (1986, 1995) who inferred from a crustal profile four E-W striking deeply reaching faults that run sublatitudinally between 70-71°S. Bormann et al. (1986) also recognised two major E-W trending fault zones of down-faulting character which are located some 10-20 km and 50-60 km north of the Schirmacheroase. It is proposed that the basement rocks became separated by normal faulting in a staircase-like manner. These faults are interpreted to mark the boundary between continental crust (thickness ~40 km at the Schirmacheroase and south of it) and a transitional crust with a thickness of less than 25 km. The formation of these fault zones was most probably accompanied by mafic intrusions and was closely

related to the breakup of Gondwana. In addition to the formation of E-W striking faults, Bormann et al. (1986) suggest that reactivation of the previously formed N-S trending fractures during Gondwana fragmentation also occurred.

5.2.2.2 Offshore record

Seismic surveys carried out by Hinz and Krause (1982) and Hinz et al. (1998) along the Princess Astrid Coast, offshore CDML, revealed seismic structures that can be traced along the entire coast of Dronning Maud Land. The structures are characterised by a thick wedge of oceanward dipping reflectors which are unconformably overlain by a succession of sedimentary sequences. Most pronounced in the seismic profiles is the marked increase in seismic velocities at an unconformity that has been termed the "Weddell Sea continental margin unconformity" (Hinz and Krause, 1982) which defines the upper boundary of the so-called "WS-4 sequence" or "Explora Wedge" (Hinz, 1981). Although the depth of the lower boundary of the Explora Wedge is unknown, its thickness is estimated to be on the order of a few kilometers. The wedge extends seaward over a length of no more than 120 km (Hinz et al., 1998). West of the Astrid Ridge a second wedge of oceanward dipping reflectors was identified which is somewhat shorter in its seaward extension suggesting it might have been deposited under subaquatic conditions. Furthermore, the existence of a second wedge gives reason to suggest that the creation of this volcanic margin took place in several pulses (Hinz et al., 1998).

Because it is known that similar wedges from other continental margins of different ages have a predominantly volcanic composition, Hinz and Krause (1982) also postulate a volcanogenic origin for the Explora Wedge offshore CDML. For instance, analyses of seaward dipping reflector wedges in drilling cores from the Rockall Plateau in the North Atlantic have revealed the deposition of sub-aerial basalts interlayered with tuffs and sedimentary rocks (Roberts et al., 1979). Along the west coast of South Africa the reflector wedge is mainly composed of mafic and subordinately felsic lavas intercalated with pyroclastics and volcanogenic sediments (DeSwardt and McLachlan, 1981).

Based on age determinations of the Dufek Massiv and Ferrar Group, which range from 179-163 Ma, Hinz and Krause (1982) have deduced a Mid- to Late Jurassic age for the Weddell Sea unconformity. Hence, deposition of the wedge sequence must have occurred before this time. A Jurassic age for the deposition of the Explora Wedge and the Weddell Sea unconformity is in good agreement with the geophysical results of Roeser et al. (1996) and Hinz et al. (1998). They have determined that the onset of seafloor spreading in the western Riiser-Larsen Sea off CDML occurred at 165 Ma and 159 Ma, respectively. Due to the very low relief in the central Riiser-Larsen Sea, Hinz et al. (1998)

have concluded that magmatic activity during the genesis in this region must have been relatively high.

5.6.3 Influence of a mantle plume on apatite fission-track record

The 180-Ma cooling step in CDML took place ~20 Ma before the western Riiser-Larsen Sea, offshore CDML, has opened and thus predates the onset of seafloor spreading (Roeser et al., 1996; Hinz et al., 1998).

A predominantly thermal mechanism to trigger the Early Jurassic cooling in CDML appears not to be realistic, because the apatite fission-track data suggest that the geothermal gradient was only slightly elevated by this time. The surface heat flow and thus the geothermal gradient in rifting settings has been constrained by several authors as being only subordinately influenced by the heat source at the base of the lithosphere (Brown, 1992; Van der Beek, 1995). They infer an increase of 5-10% in the surface heat flow by conduction into the rift flanks and a geothermal gradient of 18-25°C/km. Additionally, the intrusion of the small Jurassic mafic dykes has affected the basement rocks only to a minor extend (cf. Wand, 1995). However, a weak thermal influence due to processes such as igneous activity or heat advection could have contributed to subsequent Jurassic cooling.

It can therefore be concluded that the Early Jurassic cooling in CDML is mainly attributable to exhumation and denudation rather than to the influences of increased heat flow and magmatism. A reasonable explanation to account for exhumation and denudation prior to continental separation could be the generation of a domal bulge due to the development of a thermal anomaly at the base of the continental lithosphere. As discussed in sections 2.1 and 2.2, the impingement of a mantle plume at the base of the lithosphere can lead to broad domal uplifts as a consequence of increased buoyancy, while cool (dense) lithosphere is replaced with hot (less dense) asthenospheric material (e.g. White and McKenzie, 1989; Hill, 1991 and references therein). Such thermal anomalies can extend across a 1000-2000 km diameter region and can be accompanied by dynamic surface uplift of 1000-2000 m (White and McKenzie, 1989). On the other hand, Griffiths and Campbell (1991) report a maximum topographic elevation of 600 m above an evolving mantle plume (diameter of 1300 km) that would become larger if the hot plume is enabled to penetrate the lithosphere and if the plume volume increased as a reaction of additional melting.

If the emplacement of a mantle plume caused the observed Early Jurassic cooling in CDML, then the amount of surface uplift must have been on the order of 600-2000 m,

with any denudation rcorded in the apatite fission-track data having to be somewhat higher because of isostatic reequilibration.

In the Gondwana context, the Karoo Plume beneath the southern African continent and East Antarctica is considered to have played an important role during the separation of East and West Gondwana (Fig. 5.5) (Cox, 1992).

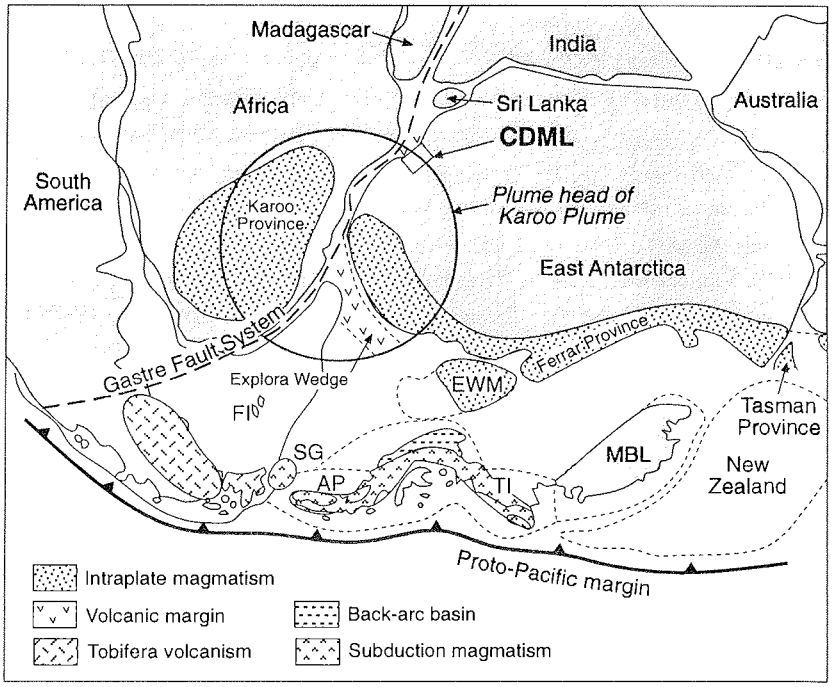

Fig. 5.5 Mid-Jurassic reconstruction of Gondwana. Circular shape of plume head is adopted from White and McKenzie (1989). CDML is located in the periphery of the Karoo Plume. Abbreviations: AP – Antarctic Peninsula, EWM – Ellsworth-Withmore Mountains, FI – Falkland Islands, MBL – Marie Byrd Land, TI – Thurston Island (modified from Storey et al., 1992).

The center of this mantle plume has been suggested as being located either in the Nuanetsi and the Zambezi Valley region (Burke and Dewey, 1972), in the Nuanetsi area (Campbell and Griffiths, 1990) or ~250 km east of Maputo (Mozambique) (White and McKenzie, 1989). This thermal anomaly, which apparently was responsible for widespread magmatic activity across southern Africa and East Antarctica, measured no more than ~2000 km in diameter (White and McKenzie, 1989). This anomaly could have included

the region of the investigated area in CDML, although the plume probably affected CDML rather peripherally. The most prominent indicators for the involvement of the Karoo Plume during the separation of Africa and East Antarctica are the volcanic outpourings of the Karoo Sequence and the basaltic lava pile remnants that crop out in western Dronning Maud Land. The effusion of such basaltic lava flows typically reflects the time when the plume head arrives at the base of lithosphere and considerably predates the onset of seafloor spreading (Hill, 1991). A variety of geochemical studies have revealed that both provinces bear similar geochemical signatures which strongly reflect the contribution of a common source in the asthenospheric upper mantle (e.g. White and McKenzie, 1989; Hill, 1991; Brewer et al., 1992; Cox, 1992). So far, the extent of the Karoo Plume is less well constrained. Encarnacion et al. (1996) have argued against the general assumption that the East Antarctic Ferrar Province is somewhat younger than the Karoo volcanics and that its geochemical signature potentially carries the influence of a subduction zone at the Proto-Pacific margin of East Antarctica (cf. Brewer et al., 1992; Cox, 1992). New zircon and baddelyite U-Pb ages on the Ferrar (183.6±1 Ma) and Karoo (183.7±0.6 Ma) dolerites have been interpreted as resulting from a single mantle thermal anomaly and rifting event (Encarnacion et al., 1996).
However, in spite of the proposed genetic affiliation of the Ferrar Province to the Karoo and Dronning Maud Land volcanic rocks, the southeastern African and East Antarctic continental margins both reveal a thick sequence of oceanward dipping reflectors which are overlain by the distinct Weddell Sea Unconformity (Hinz, 1981; Hinz and Krause, 1982). Their deposition is also attributed to igneous activity resulting from the emplacement of the Karoo mantle plume.

Although evidence for Jurassic magmatism in CDML is less spectacular than in western Dronning Maud Land and southern Africa, the presence of basaltic dykes in CDML as well as the seaward dipping reflector sequences confirm the probable influence of a mantle plume (Karoo Plume) for the continental separation.

The cooling step at ~180 Ma in CDML is also evident in the apatite fission-track data from western Dronning Maud Land. This points towards an active role of this part of the East Antarctic margin during the initial fragmentation of Gondwana. Qualitatively the cooling observed in western Dronning Maud Land is different from that in CDML (cf. Jacobs et al., 1992, 1996). In the analysed sedimentary and basement samples from western Dronning Maud Land, no single grain ages older than ~200 Ma are retained. This was proposed as being indicative of a short-lived thermal event in the Jurassic, when the samples were reheated to temperatures of at least 100-120°C (Jacobs et al., 1992, 1996).

It is most probable that the reheating to APAZ temperatures was caused by compression of isotherms in response to the burial of the Beacon Supergroup deposits and the underlying basement beneath a 1500-2000 m thick pile of poorly heat conductive Jurassic lava flows. After this short-lived event the samples cooled rapidly to ~80°C and remained there until a further period of accelerated cooling during the mid-Cretaceous (Jacobs, unpublished).

Apatite and zircon fission-track studies from the Shackleton Range also imply an Early Jurassic cooling caused by tectonic denudation (Schnellbach, 1992; Schäfer, 1998; Lisker et al., submitted.). Here it is yielded that denudation was triggered by the activation of a major thrust fault in the Read Mountains (southern Shackleton Range) or along other E-W trending faults (Schäfer, 1998; Lisker et al., submitted). For a thermal gradient of 30°C/km it has been estimated that ~6 km of crustal material have been removed in the Shackleton Range during the Jurassic denudation (Lisker et al., submitted).

5.7 Passive margin evolution during the Late Jurassic and Cretaceous

5.7.1 Accelerated cooling at 90 Ma recorded by the apatite fission-track system

The Jurassic and Cretaceous apatite FTA from the central mountain ranges show a positive correlation with the topographic elevation, although in some places this is only moderately developed (see Fig. 4.8 – 4.14). Furthermore, the apatite FTA tend to young not only with decreasing elevation, but also towards the north, i. e. towards the continental margin (see Fig. 4.15 and Fig. 4.16). This trend is, however, interrupted by the samples from Sigurdsvodene and Starheimtind that have Late Triassic to Early Cretaceous apatite FTA.

After Early Jurassic accelerated cooling, most of the samples from the central mountain ranges resided at temperatures within the APAZ. The fission-track data suggest that the Late Jurassic and the Early Cretaceous in CDML was a period of relative tectonic stability when only minor cooling and denudation occurred. This period of stability can be attributed to the isostatic reequilibration of the basement after the Early Jurassic cooling. Assuming that the geothermal gradient did not change during this time, the uppermost samples could have cooled to below 60°C while the lowermost ones underwent cooling to below 110°C.

As illustrated in Fig. 4.18 the mean track lengths show a further increase relative to the apatite FTA at ~90±10 Ma indicating a further episode of enhanced cooling in CDML. This cooling is most obviously reflected in the samples from the Schirmacheroase which are characterised by long mean track lengths as well as by narrow single grain age distributions. In contrast, the samples with similar late Early and early Late Cretaceous apatite FTA from the central mountain ranges have shorter mean track lengths and broader distributions of their single grain ages. The "cooling-age" samples of the Schirmacheroase were collected from near sea level (~50 m), while those with mixed ages were confined to topographic elevations of ~1000-1300 m. Converting the vertical discrepancy between the two into a temperature difference, this would imply that the Schirmacheroase samples were exposed to temperatures ~15-40°C higher (geothermal gradient 15-30°C/km) before accelerated cooling the mid-Cretaceous, than those from the central mountains. This assumption is probably very simplistic because it requires that the basement behaved as an entity and that faulting played only a subordinate role during cooling. Because it is thought that the Schirmacheroase samples were at temperatures of >110°C before the onset of accelerated cooling, then the other samples with similar FTA probably have resided at temperatures between 95-70°C. Furthermore, the Schirmacher-oase fission-track data require cooling of these samples through the whole temperature range of the APAZ to below 60°C during the early Late Cretaceous. Thus, the basement of CDML must have cooled by at least 50°C, corresponding to a minimum denudation of 1.5-3.5 km.

Due to the fact that the apatite fission-track data record tectono-thermal stability and low denudation until the cooling step at ~90±10 Ma, the Early Jurassic passive margin of CDML could not have experienced substantial modifications until the Early to Late Cretaceous boundary. Since this part of the East Antarctic continental margin gradually occupied a more isolated position within the successively dispersing Gondwana fragments, a thermal source for the cooling period at ~90±10 Ma in CDML does not seem to be realistic. It is most likely that the accelerated cooling was either caused by exhumation/tectonic denudation or a purely denudational mechanism without any tectonic component. In order to discriminate between a tectonically controlled and a purely denudational mechanism for the observed cooling, it is crucial to consider the post-rift evolution of a nascent passive margin and the accompanying establishment of a new erosional base level.

5.7.2 Geomorphic constraints on the post-rift evolution of the passive margin

In its present morphological expression the passive margin of CDML conforms to a typical mature high-elevation passive margin as described by Brown et al. (1991) and Gilchrist and Summerfield (1990, 1994). Such a margin is characterised by one or a series of steep escarpments often occurring more than 100 km inland from the original rift hinge. In this context, emphasis has to be stressed on a mechanism which is capable of producing a permanent upwarp, up to >60 Ma after continental rifting was initiated. Such escarpments reflect the inland retreat of a rifting-related marginal upwarp by differential denudation and its flexural isostatic adjustment. This model provides a viable mechanism to maintain such crustal upwarps through time without any associated thermal or tectonic driving forces (Gilchrist and Summerfield, 1990; 1994) (see section 2.4 for detailed description).

In CDML the morphological discontinuity of a low-lying coastal plain and a steep escarpment is strikingly apparent, though the basement throughout is largely ice-covered and strongly dissected by glacial streams (see Fig. 1.2). In the coastal region the outcropping basement has been glacially eroded to near and below sea level, whereby the escarpment is represented by the central mountain ranges of the Orvinfjella and the Wohlthatmassiv, about 150 km inland from the continental margin (~70°S, see Fig. 4.15). This morphological pattern is certainly a simplification because it is not known how far the landscape of CDML has been modified by the erosional forces of the extensive ice sheet, but probably serves as a first order approximation.

As has been described in section 2.4, continental rupture creates significantly lower erosional base levels along the rifted margin. As a consequence two different drainage systems across the margin develop. The two drainage systems are separated by the escarpment crest while draining in opposite direction, perpendicular to the rifted margin. According to Gilchrist and Summerfield (1990, 1994) the differential in denudation rates across the margin will be maintained throughout the future evolution of the passive margin. For the isostatic compensation of the differential denudation a flexural bending of the lithosphere must be invoked to trigger the marginal upwarp parallel to the continental margin. As differential denudation advances, the region of maximum upwarp subsequently migrates inland.

It is proposed here, that the geomorphic development of CDML was basically analogous to the model of Gilchrist and Summerfield (1990, 1994) for the SW African margin. The creation of a new base level along the continental rupture, generated by the separation of East Antarctic and Africa, led to the rapid denudation of the coastal region while flexural isostatic adjustment was responsible for the formation and later conservation of the

upwarp. Rapid denudation in CDML could have been augmented by the warm and humid climate of the mid-Cretaceous, with a mean annual surface temperature of ~7°C for 70°S proposed by Thompson and Barron (1980) and Crowley and North (1991). With progressive denudation the site of maximum isostatic compensation (escarpment crest) retreated further inland. This is in good agreement with the present-day maximum elevations occurring in southern CDML and implies that the bulge of maximum upward movement has retreated as far inland as to the southern parts of the Orvinfjella and the Wohlthatmassiv in about ~90 Ma. This works out at a rate of escarpment retreat from the present-day coastline to the interior during the last 90 Ma of ~1600 m/Ma if the retreating boundary behaved as a single line. The rate of escarpment retreat in CDML does not include denudational mechanisms related to the glacial erosion that was active since the Oligocene when the Antarctic ice sheet has formed (Sagnotti et al., 1998). The rate estimated for CDML is twice the rate of escarpment inland migration seen along the Great Escarpment (667 m/Ma) of the SW-African margin (cf. Gilchrist and Summerfield, 1994). On the basis of the Cretaceous apatite single grain ages it is inferred that the samples confined to localities further inland cooled to below 60°C sometime later in the Cretaceous/early Tertiary when the bulge of maximum elevation had begun migrating inland.

The apatite fission-track data as well as the morphological expression of the passive margin of CDML are good evidence for considering a denudation mechanism for the observed cooling period, driven purely by erosion and isostatic rebound. Due to the increasingly isolated position of CDML in the Cretaceous a major tectonic control for the cooling/denudation appears to be unrealistic. However, it is possible that minor amounts of tectonic movements did accompany the cooling process. Such forces could indeed be responsible for the appearance of the relatively old samples from Starheimtind and Sigurdsvodene between the Cretaceous-aged Schirmacheroase samples and the central mountain ranges (see Fig. 5.3). In addition, the fission-track data from the Untersee oasis suggesting differential track annealing among the samples, could have been related to fault tectonics. According to the observations of Kämpf et al. (1995) two fault zones are flanking the morphologically pronounced Untersee oasis. Thus, the samples possibly were exhumed along these faults at some stage between the Jurassic and the Early Cretaceous. After having cooled to below 60°C, samples J1955 and J1958 were subjected differently to renewed track annealing, for instance by circulating hydrothermal fluids.

From the above discussion it is concluded that the post-rift evolution of the CDML passive margin was initiated at ~90±10 Ma, that is 70-90 Ma later than the initial breakup of Gondwana. In order to determine what caused the delay in the full development of the

passive margin it is crucial to briefly review the dynamic plate reorganisations within Gondwana that culminated in the mid- and Late Cretaceous and which could have affected the development of the CDML continental margin.

5.7.3 Endogenic influence on the passive margin evolution

In the southern hemisphere of the Gondwana assembly in particular, the widespread rifting period that begun in the Jurassic and the Early Cretaceous introduced a fundamental change in the spreading geometry and led to the consequent opening of the major ocean basins of the South Atlantic and the Indian Ocean in the mid- and Late Cretaceous. By this time, all continental margins of the Antarctic continent, except the Proto-Pacific Antarctic margin where subduction prevailed, developed into passive margins in an almost clockwise manner (cf. Fig. 1.8 – 1.12).

The major plate reorganisations during the Cretaceous were generally accompanied by the production of large amounts of ocean floor. According to Summerfield (1991), in the Early Cretaceous this was mainly related to the extension of the world ridge system while from the mid-Cretaceous on, the volume of the spreading ridges as well as the spreading rates increased significantly.

A drastic rearrangement of the plate tectonic pattern occurred in the southern hemisphere in the Early Cretaceous. At ~130 Ma the two-plate configuration of East and West Gondwana was replaced by a three-plate assembly, with a triple junction developing between Antarctica, Africa-India and South America, situated at the southern tip of the Agulhas Plateau (e.g. Martin and Hartnady, 1986; Lawver et al., 1991; Storey, 1995). This was broadly synchronous with the opening of the South Atlantic between Africa and South America as well as with the onset of rifting between India and Sri Lanka at ~130 Ma. By approximately this time (~135-130 Ma) the rift zone between India and Sri Lanka propagated further eastward promoting the continental separation between East Antarctica-Sri Lanka and India (Lawver et al., 1991; Roeser et al., 1996). Strike-slip motions between India and Madagascar were also initiated at ~135 Ma (Roeser et al., 1996). The rifting stage between India and East Antarctica was followed by the subsequent production of seafloor between 124-118 Ma (Lawver et al., 1991). Due to enhanced seafloor spreading from 96 Ma on, India then started its northward drift away from the East Antarctic continent. This was closely related to the large-scale realignment of the spreading ridge between India and Australia-Antarctica and the formation of a new spreading ridge between East-Antarctica and Australia-New Zealand at ~110-90 Ma (Powell et al., 1988; Storey, 1995). At ~100 Ma the Gondwanide subduction beneath

northeastern Australia and New Zealand ceased, but probably continued until ~80 Ma along the Pacific margin of Antarctica (Barker, 1982; Bradshaw, 1991).

Focussing on CDML, the Jurassic and Cretaceous expansion of the Riiser-Larsen Sea was strongly associated with the development of the Mozambique Basin and the separation of India from East Antarctica. In this context, the Astrid Ridge (10-16°E) and the Gunnerus Ridge (32-36°E), which embrace the Riiser-Larsen Sea, are important markers for the reconstruction of the Gondwana assembly due to their tight fit against the Mozambique Ridge and the tip of India, respectively (Powell et al., 1988). Based on GEOSAT gravity anomalies, a fracture zone can be traced connecting the Astrid Ridge to the eastern edge of the Mozambique Ridge (Sandwell, 1992; Roeser et al., 1996).
However, prior to the breakup of South America/Africa and Antarctica-Madagascar-India (>160 Ma), the Riiser-Larsen Sea-Mozambique Basin and the Somali Basin were the major ocean basins whose formation was promoted by strike-slip motions along the Davie Fracture Zone between Africa and Madagascar. The direction of the initial strike-slip movements was dextral with Antarctica moving southward relative to Africa.
Seafloor spreading in the Riiser-Larsen Sea started in the Late Jurassic at ~159 Ma as constrained by the youngest identified magnetic anomaly (M24: 153 Ma) (Hinz et al., 1998). This is about 5 Ma later than the estimated onset of seafloor spreading in the western Riiser-Larsen Sea proposed by Roeser et al. (1996). The production of oceanfloor commenced contemporaneously in the Somali Basin with its spreading axis linked to that of the Riiser-Larsen Sea/Mozambique Basin by the Davie Fracture Zone (Rabinowitz et al., 1983; Cochran, 1988). During the interval between 150-135 Ma (M22-M10) approximately 950 km of oceanic crust were produced in the Somali Basin, whilst in the Riiser-Larsen Sea/Mozambique Basin only 650 km were generated (Rabinowitz et al., 1983).
Between 135-124 Ma (M10-M0) a closed basin evolved between Antarctica, Madagascar, India and Sri Lanka. This assembly was rearranged when India started to separate from Antarctica. The spreading ridge between the two continental masses then propagated westward and cut through the northern tip of the Gunnerus Ridge at ~124 Ma while seafloor spreading was initiated in the eastern part of the Riiser-Larsen Sea. Through further propagation and ridge axis jumps, the continuation of the SE-Indian spreading ridge promoted the separation of Antarctica and Madagascar and, after a further ridge jump, joined into the spreading axis between the western Riiser-Larsen Sea and the Mozambique Basin (Roeser et al., 1996).

5.7.4 Contributions of interacting endogenic and exogenic processes on the development of the continental margin

The apatite fission-track results suggest that the full development of the passive margin of CDML occurred with substantial delay in response to the fundamental plate-tectonic rearrangements in the Cretaceous. Because spreading rates in the Riiser-Larsen Sea were low during the initial stage (~17 mm/a) it is believed that the lithosphere of CDML experienced only minor amounts of subsidence as it moved further away from the heat source (cf. Roeser et al., 1996; Hinz et al., 1998). A persisting magmatic influence is also reflected in the K-Ar whole rock data of alkaline dykes which record magmatic activity in CDML until ~100 Ma (Wand et al., 1988). The Cretaceous geodynamic reorganisation was coeval with the opening of the eastern Riiser-Larsen Sea at 124 Ma and the northward drift of India away from East Antarctica which accelerated substantially at 96 Ma. For comparison, the total spreading rates along the developing SW-Indian Ridge were 100-180 mm/a between 80-50 Ma (Summerfield, 1991).

This leads to the conclusion that the passive margin of CDML fully developed ~90-70 Ma after the onset of rifting between East Antarctica and Africa. Because of the relatively low spreading rates in the western Riiser-Larsen Sea after its opening, the lithospheric thermal contraction and the resulting subsidence probably proceeded sluggish until the mid-Cretaceous. In the mid-Cretaceous when seafloor production increased globally, a new base level could have been established along the continental rupture due to enhanced subsidence of the oceanward region. This could then have promoted differential denudation of the coastal region and the loading of the continental shelf and slope with the removed crustal material. By this time the lithosphere of CDML would have been cool enough to attain a sufficient rigidity to compensate the denudational unloading and coupled sediment loading by flexural isostatic upward and downward motion, respectively. The cooling step at 90±10 Ma deduced from the apatite fission-track data is considered being the result of such an isostatic upward movement of the inland side of the passive margin. Consequently, the early Late Cretaceous in CDML was a time when a redistribution of masses took place, with material being denuded from the rising continental interior and thereafter becoming deposited on the subsiding seaward part of the continental margin. The sedimentary record on the continental shelf and slope should thus provide more information about the temporal and quantitative coupling of isostatic uplift and depression in CDML.

5.7.5 Stratigraphic marine record and chronology of mass redistribution

Information about the age of the marine sedimentary record adjacent to CDML is so far only available from the interpretation of the seismic data that were collected by Hinz and Krause (1982) (see section 5.6.2.2). According to this study the sequence of seaward dipping reflectors (WS-4) is unconformably overlain by a package of sedimentary strata (WS-3a,b, WS-2, WS-1) which are considered being Cenozoic in age, even though the age of the basal unit WS-3a is not constrained (Fig. 5.6).

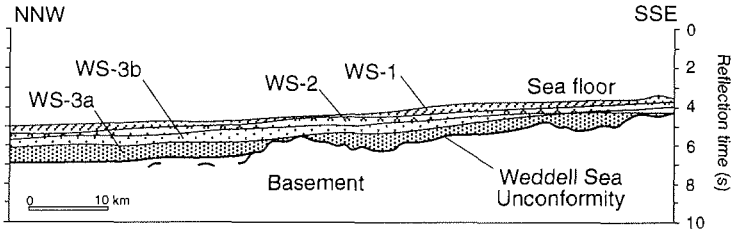

Fig. 5.6 Seismostratigraphic digram of the eastern part of the Astrid Ridge showing the sedimentary sequences WS-3a to WS-1 (line BGR 78-012) (from Hinz and Krause, 1982). The basement surface has a hummocky relief and appears to pierce the Wedell Sea Unconformity. A higher resolution of the basement unit could not be obtained from reflection seismic record due to its high consolidation. Sequence WS-4 was not identified along the Astrid Ridge.

For the unconformity on top of WS-4 a Middle to Late Jurassic age is assumed. The stratigraphic age of the boundary between the subsequences WS-3a and WS-3b, which is marked by an erosional hiatus, is correlated to the opening of the Tasmanian Seaway and the onset of the Antarctic sea ice formation in the Eocene/Oligocene. Hence, deposition of subsequence WS-3a must have occurred sometime between post-Middle Jurassic and pre-Oligocene times. Both subsequences show the characteristic pattern of a deposition during times of sea level lowstand (Hinz and Krause, 1982).

The sediment thickness overlying the sequence WS-4, offshore CDML, was determined on the basis of the refraction seismic results of Hinz and Krause (1982). Between ~6°20'E and 15°25'E the sediment thicknesses range from approximately 1.5 km to 3.3 km with the largest thicknesses obtained for those stations closest to the coastline and at the mouth of glacier discharge, east of the Schirmacheroase.

Despite the lack of detailed information about the sedimentary stratigraphic record along the neighbouring sections of the CDML margin, the sediments further east than 25°E reach an average thickness of more than 2 km (cf. Hayes and LaBreque, 1991). Sediment

thickness estimations for the section between 25°W and 9°E, also based on the study of Hinz and Krause (1982), give values between 0.7-2.9 km. In drill cores from the ODP Leg 113 from the eastern edge of the Weddell Sea (drilling sites 691-693) a depositional sequence from the Late Jurassic onwards was observed. According to Baker et al. (1988), the lowermost unit was deposited in the Late Jurassic and Early Cretaceous in an anoxic environment due to the restricted circulation in small ocean basins shortly after the breakup of East and West Gondwana. In addition, although relatively remote from CDML, a stratigraphic record which postdates the onset of seafloor production, is available from the drilling sites 689 and 690 of the ODP Leg 113, located in vicinity of the Maud Rise (see Fig. 4.1). The oldest sediments drilled in this area show a depositional age of late Campanian to early Maastrichtian (~75-65 Ma) while the underlying basement most probably formed during the Cenomanian (~98-91 Ma) (Baker et al., 1988). In the Maud Rise region the sedimentary cover reaches a total thickness of ≤1 km (cf. Hayes and LaBreque, 1991).

The results of Hinz and Krause (1982) thus provide a first approximation for the sedimentation process in CDML. In the Weddell Sea region where similar structures, i. e. the seaward dipping reflector wedge and the overlying sedimentary strata, along the continental margin were observed, sedimentation most probably was initiated in the Late Jurassic (Baker et al., 1988). Hence, it is possible that the continental rupture at ~180 Ma in CDML was coincident with or followed by hinterland denudation and the subsequent accumulation of sediments on the seaward side of CDML prior or during the Late Jurassic. However, the sediment thicknesses obtained from offshore CDML do not ubiquitously confirm if the cooling step derived from the apatite fission-track data led to increasing sedimentation on the subsiding margin, because the thickness of the oldest sedimentary layer (WS-3a) is unknown and the total thickness of sediments does not represent a suite of continuously progressing deposition since the Late Jurassic. It should be noted that a number of hiatuses are recognised from distinctive reflection horizons within the sedimentary sequences of the profiles of Hinz and Krause (1982) as well as in the drilling cores of ODP Leg 113 from the Maud Rise (Baker et al., 1988). Apart from the loss of sediment charge through erosion, a variety of other parameters can also control the denudation and deposition process, but they are rarely quantifiable (see Summerfield, 1991 for discussion).

Potentially, sedimentation in CDML could have begun after the initial doming at ~180±20 Ma. While the basement of CDML was denuded slowly until the Late Cretaceous only minor amounts of crustal material would have been deposited on the evolving continental shelf and slope. Sedimentation enhanced at ~90±10 Ma when subsidence in the offshore

region increased and coupled flexural isostatic uplift and erosion of the continental interior occurred. The post-Late Cretaceous history of CDML cannot be constrained from the apatite fission-track data, but deposition probably continued until the boundary of the Eocene/Oligocene which is recorded in the sedimentary strata as a major erosional unconformity between the subsequences WS-3a and WS-3b (cf. Hinz and Krause, 1982). Before deposition of the WS-3b layer (Miocene) progressed, an unknown extent of the WS-3a subsequence may have been removed by erosion.

Summarising the above discussion, the retarded evolution of the rifted continental margin of CDML in the early Late Cretaceous is interpreted being the result of an initially slowly cooling oceanic lithosphere, where thermal contraction and subsidence was inhibited by slow spreading rates and by the vicinity to the heat source underneath the spreading axis in the Riiser-Larsen Sea/Mozambique Basin. The continental margin to CDML presumably underwent more rapid subsidence in the Cretaceous, reacting on the globally increasing oceanfloor production, by which CDML was strongly influenced through the opening of the eastern Riiser-Larsen Sea and the beginning of the fast northward drift of India at ~96 Ma. Due to the increasing lithospheric cooling and the subsequent lowering of the erosional base level at ~90±10 Ma, the landward part of CDML then experienced differential denudation and isostatic uplift revealed by an accelerated cooling phase in apatite fission-track data.

Similarly, in the Heimefrontfjella (western Dronning Maud Land) the apatite fission-track results gave reason for a cooling step at ~100 Ma and are interpreted as being related to the flexural uplift of the lithosphere at the transition between normal and stretched continental crust. The flexural bending was accompanied by tilting of the Heimefrontfjella with creation of a topographic relief in excess of ~3500 m. The mass redistribution occurred via some graben-systems, which developed later than ~140 Ma, through which the sediment load was channeled towards the Weddell Sea and the South Atlantic (Jacobs et al., 1992, 1996).

Apatite fission-track analysis on basement rocks from the Shackleton Range show a cooling episode at ~110 Ma that is probably attributable to the suturing of Weddellia and East Antarctica and the establishment of a new isostatic equilibrium in the Weddell Sea embayment. It is likely that differential movements were active during or possible after this cooling episode. This has been inferred from the vertical offsets in the breaks-in-slopes across different crustal blocks of the Shackleton Range (Lisker et al., submitted).

5.8 Post-Early Cretaceous basement cooling

After the Early Cretaceous accelerated cooling episode, the samples from CDML successively cooled to surface temperatures. Whether the post-Early Cretaceous cooling and denudation of the basement was a continuous process or a stepwise cooling, cannot be ascertained from the fission-track data. The cooling and denudation rates are thus reported as mean values.

In the Schirmacheroase region at least 1.5-3.5 km of crust were denuded during the Late Cretaceous. By adopting a present-day mean annual surface temperature of -10°C for this part of East Antarctica, the Schirmacheroase samples must have cooled by further ~70°C in the Cenozoic. This corresponds to a total denudation of 4-8 km of crust at a rate of ~45-90 m/Ma for a gradient of 15-30°C/km since the Early Cretaceous. When the lowermost samples of the Conradgebirge and O.-v.-Gruber-Gebirge with a Cretaceous age are employed as a reference frame, then the samples in the central mountain ranges have cooled by no more than 85-100°C (palaeotemperature of 75-90°C) at a rate of 0.9-1.1°C/Ma since the Early Cretaceous. Since then, the samples from the Orvinfjella and the Wohlthatmassiv have experienced a denudation of ~3-6.5 km at a corresponding rate of ~30-75 m/Ma.

The differential in the amount of denudation of the Orvinfjella/Wohlthatmassiv and the Schirmacheroase indicates that the continental interior of CDML experienced at least one third less of denudation than the marginal part adjacent to the coast. This differential is clearly reflected in the present-day morphology of the continental margin which indicates a greater depth of denudation for the coastal region than for the interior part, i. e. the Orvinfjella and the Wohlthatmassiv. Though not indicated by the fission-track data, it is suggested that the 90±10 Ma-accelerated cooling step initiated the geomorphological shaping of the passive margin of CDML, with the subsequent cooling of the fission-track samples to surface temperatures controlled by exogenic factors.

The relatively high elevations in the Orvinfjella and the Wohlthatmassiv point towards a young alpine relief whereas the Schirmacheroase has experienced far more erosional denudation. This is indicative of a somewhat later exhumation of the central mountain ranges. As has been stated earlier, this corresponds well with the interpretation of the apatite fission-track data. These predict that cooling of the crust follows the N-S retreat of the bulge of maximum elevation with the more aggressive erosional forces seaward of the main escarpment crest causing continued backcutting of the escarpment front. The present day morphology of CDML also indicates that the evolution of the passive margin is still an active process.

5.9 A comparison: western and central Dronning Maud Land

During the Pan-African event both regions have experienced intense magmatism, metamorphism and deformation resetting the conventional isotopic systems (e.g. K-Ar, Ar/Ar) (cf. Jacobs, 1991; Henjes-Kunst and Markl, 1998). In CDML the post-Pan African cooling of the basement is largely constrained by the titanite and zircon fission-track systems, which indicate a slow post-orogenic cooling through the Paleozoic. Although no titantite and zircon fission-track data are available for western Dronning Maud Land, the peneplain underlying the Permo-Triassic Beacon Supergroup sequences proves that the basement there has cooled to surface temperatures in the Paleozoic. It is thus concluded that basement of CDML cropping out at present corresponds to a lower crustal level than that exposed in western Dronning Maud Land.

The apatite fission-track data from CDML and western Dronning Maud Land point towards a similar Mesozoic thermal history, although the mechanisms inducing the observed cooling vary. For both regions the apatite fission-track data indicate a cooling phase in the Early Jurassic related to the impingement of a mantle plume beneath the lithosphere of Gondwana. In western Dronning Maud Land the effusion of basaltic lavas during the initial fragmentation of Gondwana led to the burial of the basement and the overlying sedimentary sequence of the Beacon Supergroup with reheating the basement to 100-120°C (cf. Jacobs et al., 1992, 1996; Jacobs and Lisker, submitted). In CDML the cooling is thought as being caused by mantle plume-related surface uplift and denudation. It is likely that the Early Jurassic cooling in western Dronning Maud Land reflects a stronger thermal influence of the mantle plume on the continental separation than it is the case for CDML. This is in good agreement with the reconstruction of White and McKenzie (1989). CDML probably has occupied a peripheral position in the mantle plume-affected region, whereas western Dronning Maud Land was located closer to its centre. Accelerated cooling at ~100 Ma in western Dronning Maud Land was due to the rapid erosion of the basaltic lava pile that persisted in the continental interior for ~80 Ma. The mechanism that triggered cooling at ~90 Ma in CDML is interpreted as being purely denudational occurring as a reaction to accelerated shelf subsidence and coupled inland isostatic upward movement. The apatite fission-track data as well as the high-elevation-margin morphology of CDML suggest a typical passive margin evolution for this section of East Antarctica (see chapter 2). Western Dronning Maud Land, in contrast, underwent a more complicated evolution that included rifting and shearing of the margin in the Jurassic followed by extension of the continental margin to a width of ~350 km in the Cretaceous (Jacobs and Lisker, submitted). In the Cretaceous western Dronning Maud

Land was still located in a region where major plate-tectonic rearrangements affected East Antarctica such as the opening of the Weddell Sea in the Early Cretaceous (cf. Livermore and Woolett, 1993; DiVenere et al., 1994; DiVenere and Kent, 1995). They have potentially influenced the development of the continental margin of western Dronning Maud Land to a far greater extent than in CDML, which attained a more isolated position within the dispersing Gondwana fragments.

6. References

Adams, C.J., Seward, D., and Weaver, S.D. (1995) Geochronology of Cretaceous granites and metasedimentary basement of Edward VII Peninsula, Marie Byrd Land, West Antarctica. Antarctic Science, 7(3), 265-277.

Arne, D.C., Kelly, P.R., Brown, R.W., and Gleadow, A.J.W. (1993) Reconnaissance apatite fission-track data from the East Antarctic Shield. In R.H. Findlay, R. Unrug, M.R. Banks, and J.J. Veevers, Eds. Gondwana Eight: assembly, evolution and dispersal, 605-611. Balkema, Hobart.

— (1994) Phanerozoic exhumation history of northern Prince Charles Mountains (East Antarctica). Antarctic Science, 6(1), 69-84.

Baker, P.F., Kennett, J.P., and al. (1988) Initial Report (Pt A,B), ODP 113. College Station, TX (Ocean Drilling Program).

Baksi, A.K. (1994) Geochronological studies on whole rock basalts, Deccan Traps, India; evaluation of the timing of volcanism relative to the K/T boundary. Earth and Planetary Science Letters, 121, 43-56.

Balestrieri, M.L., Bigazzi, G., Ghezzo, C., and Lombardo, B. (1993) Fission track dating of apatites from the Granite Harbour Intrusive Suite and uplift-denudation history of the Transantarctic Mountains in the area between the Mariner and David Glaciers (Northern Victoria Land, Antarctica). Terra Antartica, 1, 82-87.

Bankwitz, E., and Bankwitz, P. (1995a) Photogeological structures of the basement of the Wohlthat Massif. In P. Bormann, and D. Fritzsche, Eds. The Schirmacher Oasis, Queen Maud Land, East Antarctica, and its surroundings, 289, 152-169. Justus Perthes Verlag, Gotha.

— and Bankwitz, P. (1995b) Photogeological indications. In P. Bormann, and D. Fritzsche, Eds. The Schirmacher Oasis, Queen Maud Land, East Antarctica, and its surroundings, 289, 112. Justus Perthes Verlag, Gotha.

Barker, B.F., and Burrell, J. (1977) The opening of the Drake Passage. Marine Geology, 25, 15-34.

— (1982) The Cenozoic subduction history of the Pacific margin of the Antarctic Peninsula: ridge crest-trench interaction. Journal of the Geological Society, London, 139, 787-801.

Barrett, P.J., Grindley, G.W., and Webb, P.N. (1972) The Beacon Supergroup of East Antarctica. In R.J. Adie, Ed. Antarctic Geology and Geophysics, B1, 319-332. Universitetsforlaget, Oslo.

Bathmann, U.. Schulz-Bades, M., Fahrbach, E., Smetacek, V., and Hubberten, H.-W. (1992) Die Expeditionen ANT-IX/1-4 des Forschungsschiffes 'Polarstern' 1990/91. Berichte zur Polarforschung.

Bauer, W., Jacobs, J., and Paech, H.-J. (1996) Structural evolution of polyphase metamorphosed basement rocks in Central Dronning Maud Land, East Antarctica. In M. Santosh, and M. Yoshida, Eds. IGCP-368 International Field Workshop on Proterozoic Continental Crust of Southern India, 4, 4-6, India.

—, Jacobs, J., and Paech, H.-J. (1999) Structural Evolution of the Crystalline Basement of Central Dronning Maud Land, East Antarctica. Geologisches Jahrbuch, in press.

Beaumont, C., Keen, C.E., and Boutilier, R. (1982) A comparison of foreland and rift margin sedimentary basins. Philosophical Transactions of the Royal Society London, A305, 295-317.

Bergh, H.W. (1987) Underlying fracture zone nature of Astrid Ridge off Antarctica's Queen Maud Land. Journal of Geophysical Research, 92(B1), 475-484.

Bohannon, R.G., Naeser, C.N., Schmidt, D.L., and Zimmermann, R.A. (1989) The timing and uplift, volcanism, and rifting peripheral to the Red Sea: A case for passive rifting? Journal of Geophysical Research, 94, 1683-1701.

Bormann, P., Bankwitz, P., Bankwitz, E., Damm, V., Hurtig, E., Kämpf, H., Menning, M., Paech, H.J., Schäfer, U., and Stackebrandt, W. (1986) Structure and development of the passive continental margin across the Princess Astrid Coast, East Antarctica. Journal of Geodynamics, 6, 347-373.

—, Schäfer, U., Kopsch, C., and Wagner, S. (1995) Geophysical investigations. In P. Bormann, and D. Fritzsche, Eds. The Schirmacher Oasis, Queen Maud Land, East Antarctica, and its surroundings, 289, 39-58. Justus Perthes Verlag, Gotha.

Bott, M.H.P. (1995) Mechanisms of rifting: Geodynamic modeling of continental rift systems. In K.H. Olsen, Ed. Continental Rifts: Evolution, Structure, Tectonics, 264, 27-43. Elsevier, New York.

Bradshaw, J.D. (1991) Cretaceous dispersion of Gondwana: continental and oceanic spreading in the south-west Pacific-Antarctic sector. In M.R.A. Thomson, J.A. Crame, and J.W. Thomson, Eds. Geological Evolution of Antarctica, 581-585. Cambridge University Press, Cambrigde.

Brewer, T.S., Hergt, J.M., Hawkesworth, C.J., Rex, D., and Storey, B.C. (1992) Coats Land dolerites and the generation of Antarctic continental flood basalts. In B.C. Storey, T. Alabaster, and R.J. Pankhurst, Eds. Magmatism and the Causes of Continental Break-up, 68, 185-208. Geological Society Special Publications, London.

Brown, R.W., Rust, D.J., Summerfield, M.A., Gleadow, A.J.W., and De Wit, M.C.J. (1990) An early Cretaceous phase of accelerated erosion on the south-western margin of Africa: evidence from apatite fission track analysis and the offshore sedimentary record. Nuclear Tracks and Radiation Measurements, 17, 339-350.

— (1991) Backstacking apatite fission-track "stratigraphy": A method for resolving the erosional and isostatic rebound components of tectonic uplift histories. Geology, 19, 74-77.

— (1992) A Fission Track Thermochronology Study of the Tectonic and Geomorphic Development of the Sub-aerial Continental Margins of Southern Africa. PhD Thesis, La Trobe University, Melbourne.

—, Summerfield, M.A., and Gleadow, A.J.W. (1994) Apatite Fission Track Analysis: Its Potential for the Estimation of Denudation Rates and Implications for Models of Long-term Landscape Development. In M.J. Kirkby, Ed. Process models and theoretical geomorphology, 3, 23-54. Wiley & Sons.

Buck, W.R. (1986) Small-scale convection induced by passive rifting: the cause for uplift of rift shoulders. Earth and Planetary Science Letters, 77, 362-372.

—, Martinez, F., Steckler, M.S., and Cochran, F.R. (1988) Thermal consequences of lithospheric extension: pure and simple. Tectonics, 7, 213-234.

Burke, K., and Dewey, J.F. (1972) Plume-generated triple junctions: key indicators in applying plate tectonics to old rocks. Journal of Geology, 81, 406-433.

Campbell, I.H., and Griffiths, R.W. (1990) Implication of mantle plume structure for the evolution of flood basalts. Earth and Planetary Science Letters, 99, 79-93.

Carpena, J., Kienast, J.R., Ouzegane, K., and Jehanno, C. (1988) Evidence of the contrasted fission-track clock behavior of the apatites from In Ouzzal carbonatites (northwest Hoggar): The low-temperature thermal history of an Archean basement. Geological Society of America Bulletin, 100, 1237-1242.

— (1998) Uranium-235 fission track annealing in minerals of the apatite group: an experimental study. In P. Van den haute, and F. De Corte, Eds. Advances in Fission-track Geochronology, 10, 81-92. Kluwer Academic Publishers, Dordrecht.

Chapman, D.S. (1986) Thermal gradients in the continental crust. In J.B. Dawson, D.A. Carswell, J. Hall, and K.H. Wedepohl, Eds. The Nature of the Lower Continental Crust, 24, 63-70. Blackwell Scientific Publications.

Clarkson, P.D. (1981) Geology of the Shackleton Range: II, the Turnpike Bluff Group. Bulletin of the British Antarctic Survey, 52, 109-124.

Cochran, J.R. (1988) Somali Basin, Chain Ridge, and origin of the northern Somali Basin gravity and geoid low. Journal of Geophysical Research, 93(B10), 11985-12008.

Collinson, J.W., Isbell, J.L., Eliott, D.H., Miller, M.F., and Miller, J.M.G. (1994) Permian-Triassic Transantarctic basin. In J.J. Veever, and C.M. Powell, Eds. Permian-Triassic Pangean Basins and Foldbelts Along the Panthalassan Margin of Gondwanaland, 184, 173-222, Boulder, Colorado.

Colombo, F., and Talrico, F. (1999) Regional metamorphism in the high grade basement of central Dronning Maud Land, East Antarctica. Geologisches Jahrbuch, in press.

Cooper, R.A., Jago, J.B., Rowell, A.J., and Braddock, P. (1983) Age and correlation of the Cambrian-Ordovician Bowers Supergroup, northern Victoria Land. In R.L. Oliver, P.R. James, and J.B. Jago, Eds. Antarctic Earth Science, 128-131. Australian Academy of Science, Canberra.

Cox, K.G. (1988) The Karoo Province. In J.D. Macdougall, Ed. Continental Flood Basalts, 239-271. Kluwer, Dordrecht.

— (1992) Karoo igneous activity, and the early stages of the break-up of Gondwanaland. In B.C. Storey, T. Alabaster, and R.J. Pankhurst, Eds. Magmatism and the Causes of Continental Break-up, 68, 137-148. Geological Society Special Publications, London.

Coyle, D.A., and Wagner, G.A. (1998) Positioning the titanite fission-track partial annealing zone. Chemical Geology, 149, 117-125.

Craddock, C. (1982) Antarctica and Gondwanaland. In C. Craddock, Ed. Symposium on Antarctic Geolgy and Geophysics, B4, 3-13. The University of Wisconsin Press, Wisconsin.

Crough, S.T. (1983) Hotspot swells. Annual Review of Earth and Planetary Sciences, 11, 165-193.

Crowley, T.J., and North, G.R. (1991) Paleoclimatology. 339, Oxford University Press.

D'Souza, M.J., Mukerji, S., Beg, M.J., Ravindra, R., Chaturvedi, A., Kaul, M.K., and Bejarniya, B.R. (1994) Some aspects of lamprophyre intrusives of Schirmacher Oasis in central Dronning Maud Land,

Antarctica and their relevance to pre-rift reconstruction. Ninth International Gondwana Symposium, 935-947, Hyderabad, India.

Dalziel, I.W.D. (1997) Neoproterozoic-Paleozoic geography and tectonics: Review, hypothesis, environmental speculation. Geological Society of America Bulletin, 109, 16-42.

Damm, V., and Eisenburger, D. (1999) Ice thicknesses and subice morphology in central Dronning Maud Land deduced by radio echo soundings (RES). Geologisches Jahrbuch, in press.

Dayal, A.M., and Hussain, S.M. (1997) Rb-Sr ages of lamprophyre dykes from Schirmacher Oasis, Queen Maud Land, East Antarctica. Journal of the Geological Society of India, 50, 457-460.

De Swardt, A.M.J., and Bennett, G. (1974) Structural and physiographic development of Natal since the late Jurassic. Transactions of the Geological Society of South Africa, 77, 309-322.

— and McLachlan, I.R. (1981) Petroleum exploration in the South African offshore - The geological framework and hydrocarbon potential, Report Southern Oil Exploration Corp. Ltd. (SOEKOR), Johannesburg.

Dirks, P.H.G.M., and Wilson, C.J.L. (1995) Crustal evolution of the East Antarctic mobile belt in Prydz Bay: Continental collision at 500 Ma? Precambrian Research, 75, 209-230.

DiVenere, V.J., Kent, D.V., and Dalziel, I.W.D. (1994) Mid-Cretaceous paleomagnetic results from Marie Byrd Land, West Antarctica: A test of post-100 Ma relative motion between East and West Antarctica. Journal of Geophysical Research, 99(B8), 15115-15139.

— and Kent, D.V. (1995) Early Cretaceous paleomagnetic results from Marie Byrd Land, West Antarctica: implication for the Weddallia collage of crustal blocks. Journal of Geophysical Research, 100(B5), 8133-8151.

Donelick, R.A. (1991) Crystallographic orientation dependence of mean etchable fission track length in apatite: An empirical model and experimental observations. American Mineralogist, 76, 83-91.

Dumitru, T., Hill, K.C., Coyle, D.A., Duddy, I.R., Foster, D.A., Gleadow, A.J.W., Green, P.F., Kohn, B.P., Laslett, G.M., and O'Sullivan, A.J. (1991) Fission track thermochronology: Application to continental rifting of south-eastern Australia. Australian Petroleum Exploration Association Journal, 31, 131-142.

— (1993a) FT-Stage, Stanford University.

— (1993b) A new computer-automated microscope stage system for fission-track analysis. Nuclear Tracks and Radiation Measurements, 21(4), 575-580.

— (1996) Fission-track geochronology. Quaternary Geochronology, manuscript in prep. (Special Paper 3XX), 15 p.

Duncan, R.A., Hooper, P.R., Rehacek, J., Marsh, J.S., and Duncan, A.R. (1997) The timing and duration of the Karoo igneous event, southern Gondwana. Journal of Geophysical Research, 102(B8), 18127-18138.

Eales, H.V., Marsh, J.S., and Cox, K.G. (1984) The Karoo igneous province: an introduction. In A.J. Erlank, Ed. Petrogenesis of the volcanic rocks of the Karoo province, 13, p. 1-26.

Encarnacion, J., Fleming, T.H., Elliot, D.H., and Eales, H.V. (1996) Synchronous emplacement of Ferrar and Karoo dolerites and the early breakup of Gondwana. Geology, 24(6), 535-538.

England, P., and Molnar, P. (1990) Surface uplift, uplift of rocks, and exhumation of rocks. Geology, 18, 1173-1177.

Fitzgerald, P.G. (1986) Fission-track tectonic studies of the Transantarctic Mountains, Beardmore Glacier area. Antarctic Journal of the United States, 21, 38-41.

— and Gleadow, A.J.W. (1988) Fission-track geochronology, tectonics and structure of the Transantarctic Mountains in northern Victoria Land, Antarctica. Chemical Geology (Isotope Geoscience Section), 73, 169-198.

— and Stump, E. (1991) Early Cretaceous uplift in the Ellsworth Mountains of West Antarctica. Science, 254(5028), 92-94.

— (1992) The Transantarctic Mountains of southern Victoria Land: the application of apatite fission track analysis to a rift shoulder uplift. Tectonics, 11(3), 634-662.

— and Stump, E. (1992) Early Cretaceous uplift of the southern Sentinel Range, Ellsworth Mountains, West Antarctica. In Y. Yoshida, K. Kaminuma, and K. Shiraishi, Eds. Recent Progress in Antarctic Earth Science, 331-340. Terra Scientific Publishing Company, Tokyo.

—, Sorkhabi, R.B., Redfield, T.F., and Stump, E. (1995) Uplift and denudation of the central Alaska Range: a case study in the use of apatite fission track thermochronology to determine absolute uplift parameters. Journal of Geophysical Research, 100(B10), 20175-20191.

— and Stump, E. (1997) Cretaceous and Cenozoic episodic denudation of the Transantarctic Mountains, Antarctica: new constraints from apatite fission track thermochronology in the Scott Glacier region. Journal of Geophysical Research, 102(B4), 7747-7765.

Fleischer, R.L., Price, P.B., and Walker, R.M. (1975) Nuclear Tracks in Solids: Principles and Applications. 605 p., University of California Press, Berkely.

Fleitout, L., Froidevaux, C., and Yuen, D. (1986) Active lithospheric thinning. Tectonophysics, 132, 271-278.

Fritzsche, D. and Bormann, P. (1995) The Schirmacher Oasis as a part of Queen Maud Land. In P. Bormann, and D. Fritzsche, Eds. The Schirmacher Oasis, Queen Maud Land, East Antarctica, and its surroundings, 289, 21-38. Justus Perthes Verlag, Gotha.

Galbraith, R.F. (1981) On Statistical Models for Fission Track Counts. Mathematical Geology, 13(6), 471.

— (1989) The radial plot: graphical assessment of spread in ages. Nuclear Tracks and Radiation Measurements, 17, 207-212.

— and Laslett, G.M. (1993) Statistical models for mixed fission track ages. Nuclear Tracks, 21, 207-214.

Gallagher, K., Hawkesworth, C.J., and Mantovani, M.S.M. (1994) The denudation history of the onshore continental margin of SE Brazil inferred from apatite fission track data. Journal of Geophysical Research, 99(B9), 18117-18145.

— (1995) Evolving temperatures histories from apatite fission-track data. Earth and Planetary Science Letters, 136, 421-435.

— and Brown, R. (1997) The onshore record of passive margin evolution. Journal of the Geological Society, London, 154, 451-457.

Gilchrist, A.R., and Summerfield, M.A. (1990) Differential denudation and flexural isostasy in formation of rifted-margin upwarps. Nature, 346, 739-742.

— and Summerfield, M.A. (1994) Tectonic models of passive margin evolution and their implications for theories of long-term landscape development. In M.J. Kirkby, Ed. Process models and theoretical geomorphology, 3, 55-84. Wiley & Sons.

—, Kooi, H., and Beaumont, C. (1994) Post-Gondwana geomorphic evolution of southwestern Africa: implications for the controls on landscape development from observations and numerical experiments. Journal of Geophysical Research, 99(B6), 12211-12228.

Gleadow, A.J.W., Hurford, A.J., and Quaife, R.D. (1976) Fission track dating of zircon: Improved etching techniques. Earth and Planetary Science Letters, 33, 273-276. (1984) Fission track dating methods II - A manual of principles and techniques. Workshop on fission track analysis, principles and applications, 1-35. J. Cook University, Townsville.

— and Duddy, I.R. (1981) A natural long-term track annealing experiment for apatite. Nuclear Tracks, 5, 169-174.

—, McKelvey, B.C., and Ferguson, K.U. (1984) Uplift history of the Transantarctic Mountains in the Dry Valleys area, southern Victoria Land, Antarctica, from apatite fission track ages. New Zealand Journal of Geology and Geophysics, 27, 457-464.

—, Duddy, I.R., Green, P.F., and Hegarty, K.A. (1986a) Fission track lengths in the apatite annealing zone and the interpretation of mixed ages. Earth and Planetary Science Letters, 78, 245-254.

—, Duddy, I.R., Green, P.F., and Lovering, J.F. (1986b) Confined fission track lengths in apatite: a diagnostic tool for thermal history analysis. Contributions to Mineralogy and Petrology, 94, 405-415.

— and Fitzgerald, P.G. (1987) Uplift history and structure of the Transantarctic Mountains: new evidence from fission track dating of basement apatites in the Dry Valleys area, southern Victoria Land. Earth and Planetary Science Letters, 82, 1-14.

— and Fitzgerald, P.G. (1988) Fission track geochronology, tectonics and structure of the Transantarctic Mountains in northern Victoria Land, Antarctica. Chemical Geology (Isotope Geoscience Section), 73, 169-198.

Green, P.F. and Durrani, S.A. (1977) Annealing studies of tracks in crystals. Nuclear Track Detection, 1, 33-39.

— (1981) A new look at statistics in fission-track dating. Nuclear Tracks, 5, 77-86.

— (1985) Comparison of zeta calibration baselines for fission-track dating of apatite, zircon and sphene. Chemical Geology (Isotope Geoscience Section), 58, 1-22.

—, Duddy, I.R., Gleadow, A.J.W., Tingate, P.R., and Laslett, G.M. (1986) Thermal annealing of fission tracks in apatite 1. A qualitative description. Chemical Geology, 59, 237-253.

—, Duddy, I.R., Laslett, G.M., Hegarty, K.A., Gleadow, A.J.W., and Lovering, J.F. (1989) Thermal annealing of fission tracks in apatite. 4. Quantitative modelling techniques and extension to geological timescales. Chemical Geology (Isotope Geoscience Section), 79, 155-182.

Grikurov, G.E. (1982) Sturcture of Antarctica and outline of its evolution. In C. Craddock, Ed. Antarctic Geoscience, 791-804. University of Wisconsin Press, Wisconsin.

Groenewald, P.B., Grantham, G.H., and Watkeys, M.K. (1991) Geological evidence for a Proterozoic to Mesozoic link between southeastern Africa and Dronning Maud Land, Antarctica. Journal of the Geological Society, London, 148, 1115-1123.

Grunow, A., Hanson, R., and Wilson, T. (1996) Were aspects of Pan-African deformation linked to Iapetus opening? Geology, 24, 1063-1066.

Gunn, B.M., and Warren, G. (1962) Geology of Victoria Land between the Mawson and Mulock Glaciers, Antarctica. Bulletin of the Geological Survey of New Zealand, 71, 157.

Haq, B.U. (1981) Paleogene paleoceanography: Early Cenozoic ocean revisited. Oceanologica Acta, SP, 71-82.

Hayes, D.E., and LaBreque, J.L. (1991) Sediment Isopachs: Circum-Antarctic to 30°S. In D.E. Hayes, Ed. Marine Geological and Geophysical Atlas of the Circum-Antarctic to 30°S, 29-33, Washington.

Henjes-Kunst, F., and Markl, G. (1998) Charnockitic intrusive rocks and related lamprophyres in central Dronning Maud Land, East Antarctica: evidence fro long-lasting igneous activities in Late Pan-African times. Journal of African Earth Sciences, 21(Special Abstract Issue Gondwana 10: Event Stratigraphy of Gondwana), 110.

Hill, R.I. (1991) Starting plumes and continental break-up. Earth and Planetary Science Letters, 104, 398-416.

Hinz, K. (1981) A hypothesis on terrestrial catastrophes. Wedges of very thick oceanward dipping layers beneath passive continental margins. Geologisches Jahrbuch, E22, 3-28.

— and Krause, W. (1982) The Continental Margin of Queen Maud Land/Antarctica: Seismic Sequences, Structural Elements and Geological Development. Geologisches Jahrbuch, E23, 17-41.

—, Gouseva, Y.B., Kudryavtsev, G.A., Neben, S., and Roeser, H.A. (1998) ÖGRILAS: Frühe Öffnungsgeschichte der Lazarev-See und der Riiser-Larsen-See - Kompilation und Interpretation neuer geophysikalischer Datensätze. In H. Miller, Ed. "Koordiniertes Progamm Antarktisforschung" Berichtskolloquium im Rahmen des Koordinierten Programms "Antarktisforschung mit vergleichenden Untersuchungen in arktischen Eisgebieten", 277, 56-57. Alfred-Wegener-Institut, Bremerhaven.

Holden, N.E. (1989) Total and spontaneous fission half-lives for uranium, plutonium, americium and curium nuclides. Pure Applied Chemistry, 61.

Hurford, A.J., and Green, P.F. (1983) The zeta age calibration of fission-track dating. Chemical Geology (Isotope Geoscience Section), 41, 285-317.

— and Hammerschmidt, K. (1985) $^{40}Ar/^{39}Ar$ and K/Ar dating of the Bishop and Fish Canyon tuffs: calibration ages for fission-track dating standards. Chemical Geology, 58, 23-32.

—, Flisch, M., and Jaeger, E. (1989) Unraveling the thermo-tectonic evolution of the Alps: a contribution from fission track analysis and mica dating. In M.P. Coward, D. Dietrich, and R.G. Park, Eds. Alpine Tectonics, 45, 369-398, London.

—, Hammerschnidt, K., Green, P.F., Carter, A., and Lux, D. Age of the Tardree rhyolite, Co. Antrim: evidence for the timing of lower Tertiary magmatism in northern Ireland. unpublished.

Jacobs, J. (1991) Strukturelle Entwicklung und Abkühlungsgeschichte der Heimefrontfjella (Westliches Dronning Maud Land/ Antarktika). Berichte zur Polarforschung, 97, 141 p.

—, Hejl, E., Wagner, G.A., and Weber, K. (1992) Apatite fission track evidence for contrasting thermal and uplift histories of metamorphic basement blocks in western Dronning Maud Land. In Y. Yoshida, K. Kaminuma, and K. Shiraishi, Eds. Recent Progress in Antarctic Earth Science, 323-330. Terrapub, Tokyo.

—, Kaul, N., and Weber, K. (1996) The history of denudation and resedimentation at the continental margin of western Dronning Maud Land, Antarctica, during break-up of Gondwana. In B.C. King, and R.A. Livermore, Eds. Weddell Sea Tectonics and Gondwana Break-up, 108, 191-199. Geological Society Special Publication, London.

—, Fanning, C.M., Henjes-Kunst, F., Olesch, M., and Paech, H.-J. (1998) Continuation of the Mozambique Belt into East Antarctica: Grenville-Age Metamorphism and Polyphase Pan-African High-Grade Events in Central Dronning Maud Land. The Journal of Geology, 106, 385-406.

— and Lisker, F. (submitted) Post Permian tectono-thermal evolution of western Dronning Maud Land, E-Antarctica: an apatite fission-track approach. Antarctic Science.

Juckes, L.M. (1972) The geology of north-eastern Heimefrontfjella, Dronning Maud Land. In B.A. Survey, Ed. British Antarctic Scientific Reports, 65, London.

Kaiser, G., and Wand, U. (1984) K-Ar Dating of Basalt Dykes in the Schirmacher Oasis, Dronning Maud Land, East Antarctica. Mitteilungen des Zentralinstitutes für Isotopen- und Strahlenforschung, 123-132.

— and Wand, U. (1985) K-Ar dating of basalt dykes in the Schirmacher Oasis area, Dronning Maud Land, East Antarctica. Zeitschrift für geologische Wissenschaft, 13, 299-307.

Kamp, P.J., F., G.P., and White, S.H. (1989) Fission track analysis reveals character of collisional tectonics in New Zealand. Tectonics, 8, 169-185.

Kämpf, H., and Stackebrandt, W. (1985) Geologic investigations in the Eliseev Anorthosite Massif, Central Dronning Maud Land, East Antarctica. Zeitschrift der Geologischen Wissenschaft, 13, 321-333.

—, Stackebrandt, W., Hahne, K., Paech, H.-J., and Lepin, V.S. (1995) Wohlthat Massif. In P. Bormann, and D. Fritzsche, Eds. The Schirmacher Oasis, Queen Maud Land, East Antarctica, and its surroundings, 289, 133-145. Justus Perthes Verlag, Gotha.

Keen, C.E. (1985) The dynamics of rifting: deformation of the lithosphere by active and passive driving forces. Geophysical Journal of the Royal Astronomical Society, 80, 95-120.

— and Beaumont, C. (1990) Geodynamics of rifted continental margins. In M.J. Keen, and G.L. Williams, Eds. Geology of the Continental Margin of Eastern Canada, 2, 391-472.

Kennett, J.P. (1980) Paleoceanographic and biogeographic evolution of the southern ocean during the Cenozoic, and Cenozoic microfossil datums. Paleography, Paleoclimatology, Paleoecology, 31, 123-152.

Kogan, A.L. (1972) Results of Deep Seismic Sounding of Earth's Crust in East Antarctica. In R.J. Adie, Ed. Antarctic Geology and Geophysics, B1, 485-489. Universitetsforlaget, Oslo.

— and Stroev, P.A. (1972) Gravimetricheskie issledvaniya v rayone Sovietskikh Antarcticheskikh stantsiy Lazarev i Novolazarevskaya (Gravimetric survey in the region of the Soviet Antarctic station Lazarev and Novolazarevskaya). Trudy gosudarstvennogo astornomicheskogo Instituta im PK Shernberga, XLIII (2), 3-7.

Kohn, B.P., Shagam, R., Banks, P.O., and Burkley, L.A. (1984) Mesozoic-Pleistocene fission track ages on rocks of the Venezuelan Andes and their tectonic implications. Geological Society of America Memoir, 162, 365-384.

Kooi, H., and Beaumont, C. (1994) Escarpment evolution on high-elevation rifted margins: Insights derived from a surface processes model that combines diffusion, advection, and reaction. Journal of Geophysical Research, 99(B6), 12191-12209.

Kristoffersen, Y., and Haugland, K. (1986) Geophysical evidence for the East Antarctic plate boundary in the Weddell Sea. Nature, 322, 538-541.

Kröner, A., Pidgeon, R.J., Sacchi, R., and Windley, B.F. (1997) Single zircon ages from high-grade gneisses of the Mozambique Belt in Malwi, northern Mozambique and Madagascar: Evidence for Pan-African metamorphism and implications for Gondwana assembly. (Abstract EUG9) Terra Nova, 9, 163.

Kuhn, G., Melles, M., Ehrmann, W.U., Hambrey, M.J., and Schmiedl, G. (1993) Character of clasts in glaciomarine sediments as an indicator of transport and depositional processes, Weddell and Lazarev Seas, Antarctica. Journal of Sedimentary Petrology, 63(3), 477-487.

Kutzbach, J.E., and Gallimore, R.G. (1989) Pangaean climates: Megamonsoons of the megacontinent. Journal of Geophysical Research, 94, 3341-3357.

Kyle, P.R., Elliot, D.H., and Sutter, J.F. (1981) Jurassic Ferrar Supergroup tholeiites from the Tranantarctic Mountains, Antarctica, and their relation to the initial fragmentation of Gondwana. In M.M. Cresswell, and P. Vella, Eds. Gondwana Five, Porceedings of the Fifth International Gondwana Symposium, Wellington, New Zealand, p. 283-287. Balkema, Rotterdam.

Laird, M.G. (1963) Geomorphology and stratigraphy of the Nimrod Glacier-Beaumont Bay region, southern Victoria Land, Antarctica. New Zealand Journal of Geology and Geophysics, 6, 465-484.

— (1981) Lower Paleozoic rocks of the Ross Sea area and theri significance in the Gondwana context. Journal of the Royal Society of New Zealand, 11, 425-438.

Laslett, G.M., Green, P.F., Duddy, I.R., and Gleadow, A.J.W. (1987) Thermal annealing of fission tracks in apatite. 2. A quantitative analysis. Chemical Geology (Isotope Geoscience Section, 65, 1-13.

Lawver, L.A., and Scotese, C.R. (1987) A revised reconstruction of Gondwanaland. In G.D. McKenzie, Ed. Gondwana six: Structure, Tectonics, and Geophysics, 40, 17-23. American Geophysical Union Geophysical Monographs.

—, Royer, J.-Y., Sandwell, D.T., and Scotese, C.R. (1991) Evolution of the Antarctic continental margins. In M.R.A. Thomson, J.A. Crame, and J.W. Thomson, Eds. Geological Evolution of Antarctica, 533-540. Cambridge University Press, Cambrigde.

Lisker, F. (1996) Geodynamik des Westantarktischen Riftsystems basierend auf Apatit-Spaltspuranalysen. Berichte zur Polarforschung, 198, 108 pp.

— and Olesch, M. (1997) Cooling and denudation history of the Alexandra Mountains and Rockefeller Mountains, Marie Byrd Land, based on apatite fission tracks. In C.A. Ricci, Ed. The Antarctic region: Geological evolution and processes, 475-480. Terra Antarctica Publication, Siena.

— and Olesch, M. (1998) Cooling and denudation history of western Marie Byrd Land, Antarctica, based on apatite fission-tracks. In P. Van den haute, and F. De Corte, Eds. Advances in fission-track geochronology, p. 225-240. Kluwer Academic Publishers, Dordrecht.

—, Schäfer, T., and Olesch, M. (submitted) The uplift/denudation history of the Shackleton Range (Antarctica) based on fission-track analyses. Terra Antartica.

Lister, G.S., Etheridge, M.A., and Symonds, P.A. (1986) Detachment faulting and the evolution of passive continental margins. Geology, 14, 246-250.

Livermore, R.A., and Woollett, R.W. (1993) Seafloor spreading in the Weddell Sea and southwest Atlantic since the Late Cretaceous. Earth and Planetary Science Letters, 117, 475-495.

Mancktelow, N.S., and Grasemann, B. (1997) Time-dependent effects of heat advection and topography on cooling histories during erosion. Tectonophysics, 270, 167-195.

Martin, A.K., and Hartnady, C.J.H. (1986) Plate tectonic development of the south west Indian Ocean: a revised reconstruction of East Antarctica and Africa. Journal of Geophysical Research, 91(B5), 4767-4786.

McDowell, F.W., and Keizer, R.P. (1977) Timing of mid-Tertiary volcanism in the Sierra Madre Occidental between Durango City and Mazatlan, Mexico. Geological Society of America Bulletin, 88, 1479-1487.

McKenzie, D. (1978) Some remarks on the development of sedimentary basins. Earth and Planetary Science Letters, 40, 25-32.

— (1984) A possible mechanism for epeirogenic uplift. Nature, 307, 616-618.

Meier, S., Jacobs, J., and Olesch, M. (1999) Tectono-thermal evolution of central Dronning Maud Land (East Antarctica) from middle Paleozoic to Cenozoic times: zircon and apatite fission-track evidence from Conrad- and Schneidegebirge. Geologisches Jahrbuch, in press.

Menzies, M.A., Gallagher, K., Hurford, A.J., and Yelland, A. (1997) Denudational histories of the Red Sea volcanic margin and Gulf of Aden non-volcanic margin, Yemen. Geochimica et Cosmochimica Acta, in press.

Mikhalsky, E.V., Beliatsky, B.V., Savva, E.V., Wetzel, H.-U., Fedorov, L.V., Weiser, T., and Hahne, K. (1997) Reconnaissance Geochronologic Data on Polymetamorphic and Igneous Rocks of the Humboldt Mountains, Central Queen Maud Land, East Antarctica. In C.A. Ricci, Ed. VII International Symposium on Antarctic Earth Sciences, 45-54. Terra Antartica, Siena (Italy).

Moore, M.E., Gleadow, A.J.W., and Lovering, J.F. (1986) Thermal evolution of rifted continental margins: new evidence from fission tracks in basement apatites from southeastern Australia. Earth and Planetary Science Letters, 78, 255-270.

Naeser, C.W. and McKee, E.H. (1970) Fission track and K-Ar ages of Tertiary ash flow tuffs, north-central Nevada. Geological Society of America Bulletin, 81, 3375-3384.

— and Forbes, R.B. (1976) Variation of fission track ages with depth in two deep drill holes. Transactions of the American Geophysical Union, 57, 353.

— (1979) Fission-track dating and geological annealing of fission tracks. In E. Jäger, and J.C. Hunziker, Eds. Lectures in isotope geology, 154-169. Springer Verlag, New York.

— (1981) The fading of fission tracks in the geologic environment: Data from deep drill holes. Nuclear Tracks and Radiation Measurements, 5, 248-250.

Näslund, J.O. (1998) Palaeosurfaces, glacial landforms, and landscape development in Dronning Maud Land, East Antarctica. Palaeogeography, Palaeoclimatology, Palaeoecology, submitted.

O'Sullivan, P.B., and Parrish, R.R. (1995) The importance of apatite composition and single-grain ages when interpreting fission track data from plutonic rocks: a case study from the Coast Ranges, British Columbia. Earth and Planetary Science Letters, 132, 213-224.

— and Currie, L.D. (1996) Thermotectonic history of Mt Logan, Yukon Territory, Canada: implications of multiple episodes of middle to late Cenozoic denudation. Earth and Planetary Science Letters, 144, 251-261.

—, Foster, D.A., Kohn, B.P., and Gleadow, A.J.W. (1996) Multiple postorogenic denudation events: an example from the eastern Lachlan fold belt, Australia. Geology, 24(6), 563-566.

Ollier, C.D. (1985) Morphotectonics of Passive Continental Margins. Zeitschrift für Geomorphologie Supplement, 54, 1-9.

— and Marker, M.E. (1985) The Great Escarpment of southern Africa. Zeitschrift für Geomorphologie Supplement, 54, 37-56.

Omar, G.I., Steckler, M.S., Buck, W.R., and Kohn, B.P. (1989) Fission track analysis of basement apatites at the western margin of the Gulf of Suez rift, Egypt: evidence for synchroneity of uplift and subsidence. Earth and Planetary Science Letters, 94(3-4), 316-328.

— and Steckler, M.S. (1995) Fission track evidence on the initial rifting of the Red Sea: two pulses, no propagation. Science, 270(5240), 1341-1344.

Otha, Y., Törudbakken, B.O., and Shiraishi, K. (1990) Geolgoy of Gjelsvikfjella and western Mühlig-Hofmannfjella, Dronning Maud Land, East Antarctica. Polar Research, 8, 99-126.

Paech, H.-J., Stackebrandt, W., and Wetzel, H.-U. (1995) Generalization of the geological history of the Schirmacher Oasis and Nunatak Metamorphic Complexes. In P. Bormann, and D. Fritzsche, Eds. The Schirmacher Oasis, Queen Maud Land, East Antarctica, and its surroundings, 289, 126. Justus Perthes Verlag, Gotha.

Pankhurst, R.J., Marsh, P.D., and Clarkson, P.D. (1983) A geochronlological investigation of the Shackleton Range. In R.L. Oliver, P.R. James, and J.B. Jago, Eds. Antarctic Earth Science, 176-182. Australian Academy of Science, Canberra.

Parrish, R.R. (1983) Cenozoic thermal evolution and tectonics of the Coast Mountains of British Columbia. 1. Fission-track dating, apparent uplift rates, and patterns of uplift. Tectonics, 2, 601-631.

Partridge, T.C., and Maud, R.R. (1987) Geomorphic evolution of southern Africa since the Mesozoic. South African Journal of Geology, 90, 179-208.

— and Maud, R.R. (1988) The geomorphic evolution of southern Africa: A comparative review. In G.F. Dardis, and B.P. Moon, Eds. Geomorphological Studies in Southern Africa, 5-15. Balkema, Rotterdam.

Piazolo, S., and Markl, G. (1998) Humite- and scapolite-bearing assemblages in marbles and calcsilicates of Dronning Maud Land, Antarctica: new data for Gondwana reconstructions. Journal of metamorphic Geology, 16, in press.

Pinna, P., Jourde, G., Calvez, Y., Mroz, J.P., and Marques, J.M. (1993) The Mozambique Belt in northern Mozambique; Neoproterozoic (1100-850 Ma) crustal growth and tectogenesis, and superimposed Pan-African (800-550 Ma) tectonism. Precambrian Research, 62, 1-59.

Porada, H. (1989) Pan-Afrcan rifting and orogenesis in southern to equatorial Africa and eastern Brazil. Precambrian Research, 44, 103-136.

Powell, C.M., Roots, S.R., and Veevers, J.J. (1988) Pre-breakup continental extension in East Gondwanaland and the early opening of the eastern Indian Ocean. Tectonophysics, 155, 261-283.

— and X.Z., Li (1994) Reconstruction of the Panthalassan margin of Gondwanaland. In J.J. Veever, and C.M. Powell, Eds. Permian-Triassic Pangean Basins and Foldbelts Along the Panthalassan Margin of Gondwanaland, 184, 5-9, Boulder, Colorado.

Pradeepkumar, A.P., Krishnanath, R., and Rosen, K. (1996) Humite marbles of the Kerala Khondalite Belt in the Pan-African Zone of South India, 4, 53-54, Trivandrum.

Rabinowitz, P.D., Coffin, M.F., and Falvey, D. (1983) The separation of Madagascar and Africa. Science, 220, 67-69.

Ravich, M.G., and Solov'ev, D.S. (1966) Geologiya i petrologiya central'noj chasti gor zemli Korolevy Mod (Geology and petrology of the central part of the mountains of central Dronning Maud. 290 Trudy Naucno-Isseldovatel'skogo Instiuta Geologii Arktiki, Leningrad (Nedra).

Reeves, C.V., Karanja, F.M., and MacLeod, I.N. (1987) Geophysical evidence for a failed Jurassic rift and triple junction in Kenya. Earth and Planetary Science Letters, 81, 299-311.

Reitmayr, G. (1996) Bericht über gravimetrische Messungen und sie belgietende GPS-Orsbestimmungen im Königin Maud Land, Antarktis, während der Expedition GEOMAUD, 1996. BGR Archiv 114900, Hannover.

Richard, S.M., Smith, C.H., Kimbrough, D.L., Fitzgerald, P.G., Luyendyk, B.P., and McWilliams, M.O. (1994) Cooling history of the northern Ford Ranges, Marie Byrd Land, West Antarctica. Tectonics, 13, 837-857.

Roberts, D.G., Montadert, L., and Searle, R.C. (1979) The Western Rockall Plateau: Stratigraphy and structural evolution. In L. Montadert, D.G. Roberts, and e. al., Eds. Initial Report on the Deep Sea Drilling Project, 48, 1061-1088. U.S. Government Print. Off., Washington.

Roeser, H.A., Fritsch, J., and Hinz, K. (1996) The development of the crust off Dronning Maud Land, East Antarctica. In B.C. Storey, E.C. King, and R.A. Livermore, Eds. Weddell Sea Tectonics and Gondwana Break-up, 108, 243-264. Geological Society Special Publication, London.

Rosen, K., and Raith, M. (1995) Reaction-textures and *P-T*-fluid evolution of clinohumite, humite and chondrodite marbles from the granulite terrain of S-Madagascar. Terra Nova Abstracts, 7, 316.

Royden, L., and Keen, C.E. (1980) Rifting processes and thermal evolution of the continental margin of eastern Canada determined from subsidence curves. Earth and Planetary Science Letters, 51, 343-361.

Rust, D.J., and Summerfield, M.A. (1990) Isopach and borehole data as indicators of rifted margin evolution in southwestern Africa. Marine and Petroleum Geology, 7, 277-287.

Sagnotti, L., Florindo, F., Verosub, K.L., Wilson, G.S., and Roberts, A.P. (1998) Environmental magnetic record of Antarctic palaeoclimate from Eocene/ Oligocene glaciomarine sediments, Victoria Land Basin. Geophysical Journal International, 134(3), 653-662.

Salman, G., and Abdula, I. (1995) Development of the Mozambique and Ruvuma sedimentary basins, offshore Mozambique. Sedimentary Geology, 96, 7-41.

Sandwell, D.T. (1992) Antarctic marine gravity field from high-density satellite altimetry. Geophysical Journal of the Royal Astronomical Society, 109, 27-48.

Schäfer, T. (1998) Thermo-tektonische Entwicklung von Oates Land und der Shackleton Range (Antarktis) basierend auf Spaltspur-Analysen. Berichte zur Polarforschung, 263, 107 pp.

Schnellbach, U. (1992) Neue Erkenntinisse der Hebungsgeschichte des Transantarktischen Gebirges mittels Spaltspurenanalyse. PhD Thesis, Universität Bremen.

Segoufin, J. (1978) Anomalies magnetiques mesozoiques dans le bassin de Mozambique (Mesozoic magnetic anomalies in the Mozambique Basin). Comptes Rendus Hebdomadaires des Seances de l'Academie des Sciences, 287, 109-112.

Sengör, A.M.C., and Burke, K. (1978) Relative timing of rifting and volcanism on earth and its tectonic implications. Geophysical Research Letters, 5, 419-421.

Sengupta, S. (1991) Structural and petrological evolution of basement rocks in the Schirmacher Hills, Queen Maud Land, East Antarctica (Extended abstract). In J.A. Thomson, J.A. Crame, and J.W. Thomson, Eds. Geological evolution of Antarctica, 95-97. Cambridge University Press.

Shackleton, N.J., and Kennett, J.P. (1975) Late Cenozoic oxygen and carbon isotopic changes at DSDP site 284: implication for glacial history of the Northern Hemisphere and Antarctica. In J.P. Kennett, R.E. Houtz, and e. al., Eds. Initial Report on the Deep Sea Drilling Project, 29, 801-807. U.S. Government Print. Off, Washington.

Shackleton, R.M. (1996) The final collision zone between East and West Gondwana: Where is it? Journal of African Earth Sciences, 23, 271-287.

Shiraishi, K., Asami, M., Ishizuka, H., Kojima, H., Kojima, S., Osanai, Y., Sakiyama, T., Takahashi, Y., Yamazaki, M., and Yoshikura, S. (1991) Geology and metamorphism of the Sör Rondane Mountains, East Antarctica. In M.R.A. Thomson, J.A. Crame, and J.W. Thomson, Eds. Geological Evolution of Antarctica, 77-82. Cambridge University Press, Cambridge.

Simpson, E.S.W., Sclater, J.G., Parsons, B., Norton, I., and Meinke, L. (1979) Mesozoic magnetic lineations in the Mozambique Basin. Earth and Planetary Science Letters, 43, 260-264.

Stackebrandt, W. (1990) Geological relations between Queen Maud Land, East Antarctica and South India. Geodätische und Geophysikalische Veröffentlichungen, 15, 49-61.

Steckler, M.S., and Watts, A.B. (1978) Subsidence of the Atlantic-Type continental margin off New York. Earth and Planetary Science Letters, 41, 1-13.

Stephenson, R., and Lambeck, K. (1985) Erosion-iostatic rebound models for uplift: an application to south-eastern Australia. Geophysical Journal of the Royal Astronomical Society, 82, 31-55.

Storey, B.C., Pankhurst, R.J., Evans, I.B., and Carter, A. (1989) Reconnaissance fission track dating within West Antarctica. International Workshop on Antarctic Geochronology, Munich.

—, Alabaster, T., Hole, M.J., Pankhurst, R.J., and Wever, H.E. (1992) Role of subduction-plate boundary forces during the initial stages Gondwana break-up: evidence from the proto-Pacific margin of Antarctica. In B.C. Storey, T. Alabaster, and R.J. Pankhurst, Eds. Magmatism and the Causes of Continental Break-up, 68, 149-164. Cromwell Press.

—(1995) The role of mantle plumes in continental breakup: case histories from Gondwanaland. Nature, 377, 301-308.

—, et-al, (1996) Fission-track evidence for the thermotectonic evolution of a Mesozoic-Cenozoic fore-arc, Antarctica. Journal of the Geological Society, London, 153, 65-82.

Stüwe, K., White, L., and Brown, R. (1994) The influence of eroding topography on steady-state isotherms. Application to fission track analysis. Earth and Planetary Science Letters, 124, 63-74.

Summerfield, M.A. (1985) Plate tectonics and landscape development on the African continent. In M. Morisawa, and T.J. Hack, Eds. Tectonic Geomorphology, 27-51. Unwin Hyman Ltd, Winchester.

— (1991) Sub-aerial denudation of passive margins: regional elevation versus local relief models. Earth and Planetary Science Letters, 102, 460-469.

— and Brown, R.W. (1998) Geomorphic factors in the interpretation of fission-track data. In P. Van den haute, and F. De Corte, Eds. Advances in Fission-track Geochronology, 10, 269-284. Kluwer Academic Publishers, Dordrecht.

Ten Brink, U., and Stern, T. (1992) Rift Flank Uplifts and Hinterland Basins: Comparison of the Transantarctic Mountains With the Great Escarpment of Southern Africa. Journal of Geophysical Research, 97(B1), 569-585.

Thompson, S.L., and Barron, E.J. (1981) Comparison of Cretaceous and present earth albedos: Implications for the causes of paleoclimates. Journal of Geology, 89, 143-167.

Tucker, G.E., and Slingerland, R.L. (1994) Erosional dynamics, flexural isostasy, and long-lived escarpments: A numerical modeling study. Journal of Geophysical Research, 99(B6), 12229-12243.

Unrug, R. (1996) The Assembly of Gondwana Supercontinent: Contrasting Histories of East and West Gondwana. Ninth International Gondwana Symposium, 2, 989-1002. Hyderabad, India.

Van Autenboer, T., and Loy, W. (1972) Recent geological investigations in the Sør Rondane Mountains, Belgicafjella and Sverdrupfjella, DML. In R.D. Adie, Ed. Antarctic Geology and Geophysics, B1, 563-572. Universitetsforlaget, Oslo.

Van Der Beek, P. (1995) Tectonic evolution of continental rifts: inferences from numerical modelling and fission track thermochronology. 232 p., PhD Thesis, Vrije Universiteit te Amsterdam.

Veevers, J.J., Cole, D.I., and Cowan, E.J. (1994a) Southern Africa: Karoo Basin and Cape Fold Belt. In J.J. Veever, and C.M. Powell, Eds. Permian-Triassic Pangean Basins and Foldbelts Along the Panthalassan Margin of Gondwanaland, 184, 223-279, Boulder, Colorado.

—, Powell, C.M., Collinson, J.W., and Lopez-Gamundi, O.R. (1994b) Synthesis. In J.J. Veever, and C.M. Powell, Eds. Permian-Triassic Pangean Basins and Foldbelts Along the Panthalassan Margin of Gondwanaland, 184, 331-350, Boulder, Colorado.

— (1995) Emergent, long-lived Gondwanaland vs. submergent, short-lived Laurasia: Supercontinental and Pan-African heat imparts long-term buoyancy by mafic underplating. Geology, 23(12), 1131-1134.

— and Tewari, R.C. (1995) Gondwana Master Basin of Peninsular India Between Tethys and the Interior of the Gondwanaland Province of Pangea. 72 p.

Wagner, G.A. (1979) Correction and interpretation of fission track ages. In E. Jäger, and J.C. Hunziker, Eds. Lectures in Isotope Geology, 170, 170-177. Springer-Verlag, Berlin Heidelberg.

— (1988) Apatite fission-track geochrono-thermometer to 60°C: projected length studies. Chemical Geology (Isotope Geoscience Section), 72, 145-153.

— and Van den haute, P. (1992) Fission-track dating. 285p., Enke Verlag, Stuttgart.

Wand, U., Becker, S., and Kaiser, G. (1988) Zur Alterstellung und Geochemie der Basaltgänge in der Schirmacheroase, Dronning-Maud-Land, Ostantarktis. Freiberger Forschungshefte, C421, 41-64.

— (1995) Dykes. In P. Bormann, and D. Fritzsche, Eds. The Schirmacher Oasis, Queen Maud Land, East Antarctica, and its surroundings, 289, 109-111. Justus Perthes Verlag, Gotha.

Webers, G.F., and Spörli, K.B. (1983) Palaeontological and stratigraphic investigations in the Ellworth Mountains, West Antarctica. In R.L. Oliver, P.R. James, and J.B. Jago, Eds. Antarctic Earth Science, p. 261-264. Australian Academy of Science, Canberra.

Weissel, J.K., and Karner, G.D. (1989) Flexural uplift of rift flanks due to mechanical unloading of the lithosphere during extension. Journal of Geophysical Research, 94(B10), 13919-13950.

White, N.J., and McKenzie, D.P. (1988) Formation of the "steer's head" geometry of sedimentary basins by differential stretching of the crust and mantle. Geology, 16, 250-253.

White, R., and McKenzie, D. (1989) Magmatism at rift zones: the generation of volcanic continental margins and flood basalts. Journal of Geophysical Research, 94(B6), 7685-7729.

Williams, I.S., Tetley, N.W., Compston, W., and McDougall, I. (1982) A comparison of K-Ar and Rb-Sr ages of rapidly cooled igneous rocks: two points in the Paleozoic time scale re-evaluated. Journal of the Geological Society, London, 139, 557-568.

Wilson, T.J., Grunow, A.M., and Hanson, R.E. (1997) Gondwana assembly: The view from southern Africa and East Gondwana. Journal of Geodynamics, 23(263-286).

Yamada, R., Tagami, T., Nishimura, S., and Ito, H. (1995) Annealing kinetics of fission tracks in zircon: an experimental study. Chemical Geology (Isotope Geoscience Section), 122, 249-258.

— (1998) Comparison of experimental techniques to increase the number of measurable confined fission tracks in zircon. Chemical Geology, 149, 99-107.

Acknowledgement

First of all, I would like to thank Prof. Dr. M. Olesch, University of Bremen, for giving me the opportunity to do this thesis as well as for supervising me. I also thank Prof. Dr. D. Fütterer, Alfred Wegener Institute for Polar and Marine Research, for taking on the second expert report.

Prof. Dr. M. Olesch and Dr. habil. J. Jacobs, University of Bremen, are gratefully acknowledged for the application to the Deutsche Forschungsgemeinschaft (DFG). This study is part of project OL 25/10 and was funded by the DFG.

I would like to thank the Federal Institute for Geosciences and Natural Resources (BGR Hannover) for inviting Prof. Dr. M. Olesch and Dr. habil. J. Jacobs to participate in the Antarctic expedition GeoMaud 1995/96 (expedition leader Prof. Dr. H.-J. Paech, BGR Hannover). The Alfred Wegener Institute for Polar and Marine Research is also thanked for providing polar equipment and logistic support during the GeoMaud 1995/96 expedition.

Thanks to Dr. habil. J. Jacobs who kindly provided me with samples collected during the GeoMaud 1995/96 Antarctic expedition. I also acknowledge his introduction to fission-track analysis as well as critical comments and ideas.

Dr. H. Grobe, Alfred Wegener Institute for Polar and Marine Research, is appreciated for providing the dropstone samples taken during the Polarstern cruise ANT-IX/3. Dr. H. Kämpf from the Geoforschungszentrum, Potsdam, is thanked for supplying additional samples from the Schirmacheroase. Dr. S. N. Thomson, Ruhr University of Bochum, is acknowledged for his thoroughful comments on the language.

For their help and support in practical and bureaucratic matters, I am grateful to P. Witte, B. Schröder and V. Kolb.

A very special thank to my competent and positive colleague Dr. F. Lisker for numberless discussions and his general support throughout the work with my thesis. Additionally, I would especially acknowledge my colleagues Dipl.-Geol. B. Kleinefeld, Prof. Dr. R.

Klemd, Dipl.-Geol. M. Gorke and former colleague Dr. T. Schäfer for inspiration, discussions as well as social events.

Appendix

I. Tables of fission-track sample details and analytical data

Table I.I – I.III The geographic coordinates give the approximate position of the samples, because no GPS determinations were possible during the sample collection. Grains = number of grains counted; N_s, N_i = number of spontaneous and induced tracks, N_d = number of tracks counted in glass dosimeter; ρ_s, ρ_i = density of spontaneous and induced tracks, ρ_d = density of tracks counted in age standard (see Tab. 1.1). U = Uranium content of the sample; FTA ± 1σ = Fission-track age ± 1σ-error, χ^2 = see section 3.5; MTL ± 1σ = Mean track length ± 1σ-error, Std. Dev. = Standard deviation of the mean track length, n = number of track lengths measured. For fission-track dating the ζ-approach by Hurford and Green (1983) was applied (see section 3.5). The ζ-values (weighted mean values) employed for dating of titanites were 177±3 (±1σ) ($\rho_d = 0.38 \times 10^6$ cm^{-2}; CN2 dosimeter) and 132±3 ($\rho_d = 1.87 \times 10^6$ cm^{-2}; CN2). For zircon fission-track dating a ζ-value of 153±3 (CN2) was used. The ζ-values applied to dating of the apatite samples which were determined separately for each irradiation, were 277±8 ($\rho_d = 1.04 \times 10^6$ cm^{-2}; CN5), 383±5 ($\rho_d = 1.08 \times 10^6$ cm^{-2}; CN5), 399±4 ($\rho_d = 1.04 \times 10^6$ cm^{-2}; CN5), 286±4 ($\rho_d = 1.22 \times 10^6$ cm^{-2}; CN5), 398±4 ($\rho_d = 1.03 \times 10^6$ cm^{-2}; CN5), 362±4 ($\rho_d = 1.15 \times 10^6$ cm^{-2}; CN5) and 320±4 ($\rho_d = 1.13 \times 10^6$ cm^{-2}; CN5). A gradient in the neutron fluence was observed in the irradiated samples for which ζ-values of 277±8 and 362±4 were attained. The ρ_d-values of these samples were thus determined individually. The range in ζ-values might be indicative, for instance, of an incoherent thermalisation of the reactor.

Tab. I.I Titanite sample details and fission-track analytical data (for legend see p. I Appendix).

Sample No. (Mineral)	Latitude S/ Longitude E	Locality	Elevation [m]	Rock type	Grains	N_s (ρ_s) [x 10^6 cm^{-2}]	N_i (ρ_i) [x 10^6 cm^{-2}]	N_d (ρ_d) [x 10^6 cm^{-2}]	U [ppm]	FTA ± 1σ [Ma]	χ^2 %
J 1743	71°50/7°00	M.-H.-Gebirge	1690	Syenite	22	1959	146	1419	70	431 ± 39	94
(Titanite)						(9.60)	(0.72)	(0.38)			
GM 699	71°21/7°37	Sigurdsvodene	1100	Gneiss	23	1623	117	1419	48	445 ± 45	100
(Titanite)						(6.79)	(0.49)	(0.38)			
SP 40-1	71°21/7°37	Sigurdsvodene	1100	Gneiss	22	2116	127	1419	61	531 ± 51	99
(Titanite)						(10.46)	(0.63)	(0.38)			
J 1700	71°50/8°10	Drygalskiberge	1745	Syenite	15	838	29	1419	22	894 ± 171	100
(Titanite)						(6.52)	(0.23)	(0.38)			
GM 651	71°51/9°53	Conradgebige	1750	Gneiss	10	870	80	1419	156	351 ± 43	66
(Titanite)						(17.39)	(1.60)	(0.38)			
J 1754	71°48/10°30	Dallmannberge	2080	Orthogneiss	16	898	349	4238	49	316 ± 57	<5
(Titanite)						(6.38)	(2.48)	(1.87)			
J 1797	71°46/10°23	Dallmannberge	1745	Augen-	24	1947	681	4238	36	345 ± 22	<5
(Titanite)				gneiss		(5.24)	(1.83)	(1.87)			
J 1760	71°59/10°50	Gjeruldsenhøgda	2660	Syenite	13	1575	441	4238	46	428 ± 24	45
(Titanite)						(8.38)	(2.35)	(1.87)			
GM 945	71°42/11°45	Humboldt-Gebirge	2110		25	2655	202	1419	27	422 ± 34	65
(Titanite)						(3.57)	(0.27)	(0.38)			
J 1815	71°44/12°09	Zwieselhöhe	2830	Gabbro	20	800	289	4238	42	334 ± 24	18
(Titanite)						(5.86)	(2.12)	(1.87)			
J 1817	71°44/12°07	Zwieselhöhe	2620	Gabbro	18	390	161	4238	28	293 ± 28	73
(Titanite)						(3.44)	(1.42)	(1.87)			
J 1822	71°42/12°10	Zwieselhöhe	1885	Gabbro	11	906	78	1419	64	375 ± 46	26
(Titanite)						(7.58)	(0.65)	(0.38)			
J 1826	71°42/12°10	Zwieselhöhe	1600	Gabbro	13	960	63	1419	36	487 ± 65	46
(Titanite)						(5.63)	(0.37)	(0.38)			
J 1931	71°33/12°14	Petermannketten	1475	Granodiorite-	20	1842	648	4238	43	343 ± 23	<5
(Titanite)				dyke		(6.28)	(2.21)	(1.87)			

Sample No. (Mineral)	Latitude S/ Longitude E	Locality	Elevation [m]	Rock type	Grains	N_s (ρ_s) [x 10^6 cm^{-2}]	N_i (ρ_i) [x 10^6 cm^{-2}]	N_d (ρ_d) [x 10^6 cm^{-2}]	U [ppm]	FTA ± 1σ [Ma]	χ^2 %
J 1940	71°14/12°45	Oddenskjera	1190	Biotite-Fluorite	14	1549	469	4238	53	398 ± 43	<5
(Titanite)				Granite		(8.96)	(2.71)	(1.87)			
J 1958	71°19/13°33	Untersee	745	Anorthosite	15	148	36	4238	3	490 ± 92	99
(Titanite)						(0.72)	(0.18)	(1.87)			
J 1976	71°00/12°01	Starheimtind	1345	Diorite	9	37	10	4238	1	443 ± 158	99
(Titanite)						(0.23)	(0.06)	(1.87)			
GM 1034	70°46/11°14	Schirmacheroase	50	Gneiss	11	1098	78	1419	91	451 ± 55	39
(Titanite)						(13.09)	(0.93)	(0.38)			

Tab. I.II Zircon sample details and fission-track analytical data (for legend see p. I Appendix).

Sample No. (Mineral)	Latitude S/ Longitude E	Locality	Elevation [m]	Rock type	Grains	N_s (ρ_s) [x 10^6 cm^{-2}]	N_i (ρ_i) [x 10^6 cm^{-2}]	N_d (ρ_d) [x 10^6 cm^{-2}]	U [ppm]	FTA ± 1σ [Ma]	χ^2 %
J 1640 (Zircon)	71°47'/9°38'	Conradgebirge	2200	Augen-gneiss	19	1934 (26.08)	176 (2.37)	1425 (0.38)	231	309 ± 26	77
J 1655 (Zircon)	71°51'/9°46'	Conradgebirge	2755	Granitic gneiss	7	884 (37.21)	68 (2.86)	1425 (0.38)	278	364 ± 47	79
J 1717 (Zircon)	71°52'/9°42'	Conradgebirge	3100	Tonalite	9	1229 (33.80)	137 (3.77)	1425 (0.38)	366	253 ± 24	20
J1719 (Zircon)	71°52'/9°42'	Conradgebirge	2980	Tonalite	12	1538 (34.73)	145 (3.28)	1425 (0.38)	318	299 ± 28	66
J 1721 (Zircon)	71°52'/9°42'	Conradgebirge	2860	Tonalite	11	1815 (33.39)	180 (3.31)	1425 (0.38)	322	284 ± 24	39
J 1723 (Zircon)	71°49'/9°40'	Conradgebirge	2280	Augen-gneiss	8	1096 (39.03)	102 (3.63)	1425 (0.38)	353	302 ± 33	99
J 1868 (Zircon)	71°21'/12°35'	Schneidegebirge	1020	Syenite	11	1147 (29.23)	135 (3.44)	1425 (0.38)	335	240 ± 23	75
J 1870 (Zircon)	71°21'/12°35'	Schneidegebirge	1105	Syenite	9	1120 (31.75)	119 (3.37)	1425 (0.38)	328	266 ± 27	35
J 1871 (Zircon)	71°21'/12°35'	Schneidegebirge	1155	Syenite	11	1162 (28.82)	128 (3.18)	1425 (0.38)	309	256 ± 25	21
J 1873 (Zircon)	71°21'/12°35'	Schneidegebirge	1250	Syenite	11	972 (22.88)	102 (2.40)	1425 (0.38)	233	269 ± 37	40
J 1874 (Zircon)	71°21'/12°35'	Schneidegebirge	1325	Syenite	7	571 (22.99)	68 (2.74)	1425 (0.38)	266	237 ± 31	88
J 1877 (Zircon)	71°21'/12°35'	Schneidegebirge	1565	Syenite	12	1215 (26.16)	122 (2.63)	1425 (0.38)	255	281 ± 28	71
J 1879 (Zircon)	71°21'/12°35'	Schneidegebirge	1695	Syenite	9	854 (24.97)	83 (2.43)	1425 (0.38)	236	290 ± 35	39
J 1880 (Zircon)	71°21'/12°35'	Schneidegebirge	1765	Syenite	13	1727 (35.27)	170 (3.47)	1425 (0.38)	338	286 ± 25	51

Tab. I.III Apatite sample data and fission-track analytical data (for legend see p. I Appendix). Abbreviations: M.-H.-Geb. – Mühlig-Hofmann-Gebirge, Sigurdsv. – Sigurdsvodene, Drygalskib. – Drygalskiberge, Holtedahlf. – Holtedahlfjella, Henriksens. – Henriksenskjera, Conradgeb. – Conradgebirge, Dallmannb. – Dallmannberge, Gjeruldsenh. – Gjeruldsenhøgda, Humboldt-Geb. – A.-v.-Humboldt-Gebirge, Zwieselh. – Zwieselhöhe, Weyprechtb. – Weyprechtberge, Petermannk. – Petermannketten, Schneidegeb. – Schneidegebirge, Gruber-Geb. – O.-v.-Gruber-Gebirge, Schirmachero. – Schirmacheroase.

Sample No. (Mineral)	Latitude S/ Longitude E	Locality	Elevation [m]	Rock type	Grains	N_s (ρ_s) [$x10^6 cm^{-2}$]	N_i (ρ_i) [$x10^6 cm^{-2}$]	N_d (ρ_d) [$x10^6 cm^{-2}$]	U [ppm]	FTA ± 1σ [Ma]	χ^2 %	MTL ± 1σ [µm]	Std. Dev. [µm]	n
J 1742 (Apatite)	71°44'/7°06'	M.-H.-Geb.	1410	Granitic gneiss	30	1520 (1.93)	1865 (2.36)	4066 (1.08)	27	169 ± 9	<5	12.7 ± 0.3	1.9	54
J 1743 (Apatite)	71°50'/7°00'	M.-H.-Geb.	1690	Syenite	26	1390 (2.00)	1331 (1.92)	4066 (1.08)	22	210 ± 12	<5	12.4 ± 0.4	1.9	23
J 1730 (Apatite)	71°21'/7°37'	Sigurdsv.	1035	Felsic gneiss	29	1410 (0.96)	1360 (0.93)	2561 (1.13)	10	189 ± 11	<5			
J 1731 (Apatite)	71°21'/7°37'	Sigurdsv.	1155	Hornblende gneiss	27	815 (0.61)	1010 (0.75)	4066 (1.08)	9	166 ± 10	7			
J 1732 (Apatite)	71°21'/7°37'	Sigurdsv.	1105	Amphibolite	30	421 (0.45)	327 (0.35)	2561 (1.13)	4	229 ± 18	14			
SP 40-1 (Apatite)	71°21'/7°37'	Sigurdsv.	1100	Felsic gneiss	13	1097 (2.07)	1397 (2.64)	4201 (1.11)	30	156 ± 7	39			
J 1700 (Apatite)	71°50'/8°10'	Drygalskib.	1745	Syenite	26	1614 (1.50)	1281 (1.19)	4066 (1.08)	14	255 ± 11	7	10.4 ± 0.3	1.6	30
J 1768 (Apatite)	71°58'/8°27'	Drygalskib.	2145	Migmatic metavolcanic	26	1013 (1.49)	733 (1.08)	4066 (1.08)	13	285 ± 18	<5	12.1 ± 0.2	1.1	20
J 1769 (Apatite)	71°58'/8°27'	Drygalskib.	2105	Amphibolite	24	1245 (2.71)	981 (2.14)	4066 (1.08)	25	257 ± 12	70	11.1 ± 0.2	1.1	38
J 1681 (Apatite)	72°02'/8°57'	Holtedahlf.	2765	Migmatic gneiss	20	980 (1.52)	767 (1.19)	3904 (1.04)	14	181 ± 12	<5	13.1 ± 0.2	1.6	101
J 1682	72°02'/8°57'	Holtedahlf.	2680	Migmatic gneiss	28	808 (0.48)	613 (0.36)	3904 (1.04)	4	186 ± 12	49	13.5 ± 0.2	1.3	41
J 1685 (Apatite)	71°55'/8°45'	Holtedahlf.	1710	Syenite	20	700 (1.03)	574 (0.84)	3904 (1.04)	10	173 ± 10	17	12.8 ± 0.2	1.6	52

Sample No. (Mineral)	Latitude S/ Longitude E	Locality	Elevation [m]	Rock type	Grains	N_s (ρ_s) [$x10^6 cm^{-2}$]	N_i (ρ_i) [$x10^6 cm^{-2}$]	N_d (ρ_d) [$x10^6 cm^{-2}$]	U [ppm]	FTA ± 1σ [Ma]	χ^2 %	MTL ± 1σ [µm]	Std. Dev. [µm]	n
J 1673 (Apatite)	71°26'/9°00'	Henriksens.	1200	Leuco-granite	20	756 (0.57)	1024 (0.77)	3904 (1.04)	9	108 ± 13	<5	12.4 ± 0.2	1.6	48
J 1677 (Apatite)	71°37'/8°58'	Henriksens	1315	Gneiss	28	533 (0.38)	863 (0.62)	3904 (1.04)	8	88 ± 7	<5	13 ± 0.2	1.7	79
J 1621 (Apatite)	71°51'/9°53'	Conradgeb.	1785	Granite	26	1675 (1.14)	1558 (1.06)	3887 (1.03)	13	218 ± 9	<5			
J 1634 (Apatite)	71°51'/9°53'	Conradgeb.	1785	Gneiss	20	1183 (1.59)	945 (1.27)	3904 (1.04)	15	177 ± 10	18	13.2 ± 0.1	1.5	101
J 1635 (Apatite)	71°51'/9°53'	Conradgeb.	1785	Amphibolite	15	615 (1.68)	549 (1.50)	3904 (1.04)	18	159 ± 11	26	13.1 ± 0.2	1.8	100
J 1640 (Apatite)	71°47'/9°38'	Conradgeb.	2200	Augen-gneiss	24	939 (0.85)	840 (0.76)	3904 (1.04)	9	158 ± 9	12			
J 1647 (Apatite)	71°45'/9°38'	Conradgeb.	2010	metavolcanic	26	820 (0.61)	759 (0.56)	3904 (1.04)	7	153 ± 9	16	12.5 ± 0.2	1.3	28
J 1651 (Apatite)	71°52'/9°50'	Conradgeb.	2375	Granitic gneiss	24	1123 (1.29)	654 (0.75)	3904 (1.04)	9	242 ± 14	12	12.1 ± 0.2	1.6	50
J 1652 (Apatite)	71°52'/9°50'	Conradgeb.	2485	Granitic gneiss	20	1774 (5.27)	1387 (4.12)	3904 (1.04)	47	201 ± 18	23	12.9 ± 0.1	1.3	101
J 1653 (Apatite)	71°52'/9°49'	Conradgeb.	2650	Granitic gneiss	12	1011 (4.21)	668 (2.78)	3904 (1.04)	34	213 ± 13	49			
J 1655 (Apatite)	71°51'/9°46'	Conradgeb.	2755	Granitic gneiss	20	1289 (2.22)	946 (1.63)	3904 (1.04)	20	192 ± 10	60			
J 1691 (Apatite)	71°51'/9°53'	Conradgeb.	2030	Orthogneiss	28	922 (2.56)	814 (2.26)	3904 (1.04)	26	179 ± 17	75	12.3 ± 0.3	2.3	50
J 1692 (Apatite)	71°51'/9°53'	Conradgeb.	1960	Orthogneiss	24	1231 (1.84)	1019 (1.52)	3904 (1.04)	18	176 ± 12	<5	12.4 ± 0.1	1.5	103
J 1698 (Apatite)	71°51'/9°48'	Conradgeb.	1785	Tonalitic orthogneiss	20	368 (0.30)	313 (0.25)	3917 (1.04)	3	239 ± 19	17			

Sample No. (Mineral)	Latitude S/ Longitude E	Locality	Elevation [m]	Rock type	Grains	N_s (ρ_s) [$x10^6 cm^{-2}$]	N_i (ρ_i) [$x10^6 cm^{-2}$]	N_d (ρ_d) [$x10^6 cm^{-2}$]	U [ppm]	FTA ± 1σ [Ma]	χ^2 %	MTL ± 1σ [µm]	Std. Dev. [µm]	n
J 1699 (Apatite)	71°51'/9°48'	Conradgeb.	1785	Tonalitic orthogneiss	28	1147 (1.06)	1071 (0.99)	3917 (1.04)	12	213 ± 17	<5	12 ± 0.1	1	52
J1719 (Apatite)	71°52'/9°42'	Conradgeb.	2980	Tonalite	20	1164 (1.51)	842 (1.09)	3904 (1.04)	13	195 ± 11	6			
J 1720 (Apatite)	71°52'/9°42'	Conradgeb.	2985	Tonalite	15	911 (3.75)	801 (3.30)	3904 (1.04)	40	153 ± 14	<5	12.4 ± 0.1	1.2	105
J 1721 (Apatite)	71°52'/9°42'	Conradgeb.	2860	Tonalite	22	1578 (1.74)	1237 (1.36)	3904 (1.04)	16	180 ± 9	8	12.6 ± 0.2	1.7	61
J 1723 (Apatite)	71°49'/9°40'	Conradgeb.	2280	Augen-gneiss	30	3074 (2.08)	2821 (1.91)	3917 (1.04)	23	221 ± 7	28	13.4 ± 0.2	1.3	74
J 1736 (Apatite)	71°59'/9°41'	Conradgeb.	2605	Augen-gneiss	23	2861 (3.35)	1964 (2.30)	3887 (1.03)	28	292 ± 10	57	12.7 ± 0.2	1.9	104
J 1745 (Apatite)	71°51'/9°48'	Conradgeb.	1785	Pegmatite	23	1941 (2.59)	2023 (2.70)	3917 (1.04)	33	195 ± 7	22	13.1 ± 0.2	1.7	104
J 1746 (Apatite)	71°51'/9°48'	Conradgeb.	1590	Tonalite	30	1693 (1.27)	1694 (1.27)	3887 (1.03)	15	202 ± 10	<5			
J 1661 (Apatite)	71°44'/10°17'	Dallmannb.	2010	Granite-dyke	24	1816 (1.73)	1754 (1.67)	3887 (1.03)	20	210 ± 9	<5			
J 1671 (Apatite)	71°46'/10°32'	Dallmannb.	1640	metavolcanic	19	1226 (1.45)	1313 (1.56)	3887 (1.03)	19	188 ± 20	<5	12.8 ± 0.3	1.9	43
J 1672 (Apatite)	71°46'/10°32'	Dallmannb.	1640	Tonalitic gneiss	21	607 (0.63)	655 (0.68)	3917 (1.04)	8	177 ± 15	<5			
J 1754 (Apatite)	71°48'/10°30'	Dallmannb.	2080	Orthogneiss	23	691 (1.07)	681 (1.06)	3917 (1.04)	13	199 ± 19	<5	13 ± 0.2	1.5	63
J 1795 (Apatite)	71°44'/10°20'	Dallmannb.	1715	Orthogneiss	30	957 (0.74)	1101 (0.85)	4066 (1.08)	10	177 ± 9	8	12 ± 0.2	1.5	63
J 1796 (Apatite)	71°44'/10°20'	Dallmannb.	1745	Orthogneiss	31	1001 (0.68)	1055 (0.72)	2561 (1.13)	8	169 ± 9	<5			
J 1797 (Apatite)	71°46'/10°23'	Dallmannb.	1745	Augen-gneiss	27	754 (0.76)	811 (0.82)	3917 (1.04)	10	189 ± 10	47	13.4 ± 0.2	1.4	55

Sample No. (Mineral)	Latitude S/ Longitude E	Locality	Elevation [m]	Rock type	Grains	N_s (ρ_s) [$x10^6 cm^{-2}$]	N_i (ρ_i) [$x10^6 cm^{-2}$]	N_d (ρ_d) [$x10^6 cm^{-2}$]	U [ppm]	FTA ± 1σ [Ma]	χ^2 %	MTL ± 1σ [µm]	Std. Dev. [µm]	n
J 1760 (Apatite)	71°59'/10°50'	Gjeruldsenh.	2660	Amphibolite	19	809 (2.17)	646 (1.73)	4066 (1.08)	20	253 ± 14	17			
J 1761 (Apatite)	71°59'/10°50'	Gjeruldsenh.	2630	Syenite	22	1414 (2.19)	1217 (1.88)	4066 (1.08)	22	235 ± 11	35	12.6 ± 0.2	1.6	88
J 1762 (Apatite)	71°59'/10°50'	Gjeruldsenh.	2525	Amphibolite	26	2405 (1.50)	1630 (1.02)	2561 (1.13)	11	263 ± 12	<5	13.1 ± 0.2	1.7	51
J 1763 (Apatite)	71°58'/10°47'	Gjeruldsenh.	2430	Diorite	22	1069 (2.19)	882 (1.80)	4066 (1.08)	21	245 ± 12	6	12.6 ± 0.2	1.7	101
J 1766 (Apatite)	71°58'/10°47'	Gjeruldsenh.	2100	Syenite	22	1904 (1.49)	1596 (1.25)	4066 (1.08)	15	247 ± 16	<5	13.4 ± 0.4	1.7	20
J 1790 (Apatite)	71°40'/11°30'	Humboldt-Geb.	2110	Amphibolite	31	1571 (1.88)	1401 (1.68)	2561 (1.13)	19	200 ± 9	21			
J 1812 (Apatite)	71°44'/12°09'	Zwieselh.	2965	Gabbro	26	1001 (1.42)	1056 (1.50)	3917 (1.04)	18	193 ± 9	92	12 ± 0.2	1.5	78
J 1813 (Apatite)	71°44'/12°09'	Zwieselh.	2935	Gabbro	29	2084 (1.77)	2053 (1.74)	3887 (1.03)	21	205 ± 8	7	12.8 ± 0.2	1.5	84
J 1815 (Apatite)	71°44'/12°09'	Zwieselh.	2830	Gabbro	20	1583 (3.35)	1743 (3.69)	3917 (1.04)	44	187 ± 12	<5	12.4 ± 0.2	1.6	55
J 1816 (Apatite)	71°44'/12°09'	Zwieselh.	2755	Gabbro	29	856 (1.49)	608 (0.95)	3917 (1.04)	11	330 ± 25	<5			
J 1817 (Apatite)	71°44'/12°07'	Zwieselh.	2620	Gabbro	26	1729 (1.68)	1926 (1.77)	3887 (1.03)	22	193 ± 10	<5			
J 1818 (Apatite)	71°44'/12°06'	Zwieselh.	2335	Gabbro	24	1532 (3.05)	1616 (3.21)	4066 (1.08)	37	193 ± 8	72	13.2 ± 0.2	1.6	60
J 1819 (Apatite)	71°42'/12°10'	Zwieselh.	2070	Gabbro	31	2284 (1.40)	2712 (1.67)	3887 (1.03)	20	170 ± 6	58	12.7 ± 0.2	1.6	104
J 1821 (Apatite)	71°42'/12°10'	Zwieselh.	1980	Charnockite	25	597 (1.22)	485 (0.99)	4066 (1.08)	12	251 ± 18	<5			
J 1822 (Apatite)	71°42'/12°10'	Zwieselh.	1885	Gabbro	23	523 (1.33)	327 (0.83)	3917 (1.04)	10	344 ± 20	<5			

Sample No. (Mineral)	Latitude S/ Longitude E	Locality	Elevation [m]	Rock type	Grains	N_s (ρ_s) [$x10^6 cm^{-2}$]	N_i (ρ_i) [$x10^6 cm^{-2}$]	N_d (ρ_d) [$x10^6 cm^{-2}$]	U [ppm]	FTA ± 1σ [Ma]	χ^2 %	MTL ± 1σ [µm]	Std. Dev. [µm]	n
J 1823 (Apatite)	71°42'/12°10'	Zwieselh.	1820	Augen-gneiss	14	1027 (3.62)	1195 (4.21)	3917 (1.04)	51	186 ± 16	<5			
J 1923 (Apatite)	71°58'/13°27'	Weyprechtb.	2365	Gneiss	18	893 (1.82)	570 (1.16)	4066 (1.08)	14	315 ± 18	58	14 ± 0.2	1.4	52
J 1924 (Apatite)	72°03'/13°13'	Weyprechtb.	2685	Gneiss	22	1084 (1.99)	800 (1.47)	4066 (1.08)	17	274 ± 14	15	13 ± 0.3	1.8	50
J 1867 (Apatite)	71°27'/11°57'	Petermannk.	1410	Granitic gneiss	20	1726 (2.60)	2179 (3.29)	2561 (1.13)	36	142 ± 6	32			
J 1886 (Apatite)	71°26'/12°43'	Petermannk.	1125	Augen-gneiss	28	725 (1.03)	1323 (1.87)	3917 (1.04)	23	113 ± 7	<5	13.6 ± 0.5	1.9	13
J 1887 (Apatite)	71°26'/12°43'	Petermannk.	1125	Granite-dyke	24	2111 (3.34)	2845 (4.50)	3887 (1.03)	55	150 ± 6	<5	13 ± 0.3	1.9	40
J 1838 (Apatite)	71°35'/12°30'	Petermannk.	1260	Gneiss	19	280 (0.35)	534 (0.66)	3887 (1.03)	8	108 ± 12	<5			
J 1851 (Apatite)	71°34'/12°09'	Petermannk.	1600	Augen-gneiss	28	1439 (0.80)	1780 (0.99)	2561 (1.13)	11	145 ± 6	20			
J 1930 (Apatite)	71°31'/12°12'	Petermannk.	1475	Leucosome	30	965 (0.48)	1264 (0.63)	4066 (1.08)	7	156 ± 7	11	12.4 ± 0.2	0.9	15
J 1931 (Apatite)	71°33'/12°14'	Petermannk.	1475	Granodiorite-dyke	30	1001 (0.42)	1084 (0.45)	4066 (1.08)	5	103 ± 4	<5	13.2 ± 0.6	2.5	15
J 1868 (Apatite)	71°21'/12°35'	Schneidegeb.	1020	Syenite	26	2459 (3.70)	4506 (6.78)	3917 (1.04)	82	109 ± 5	<5			
J 1869 (Apatite)	71°21'/12°35'	Schneidegeb.	1060	Syenite	13	816 (2.65)	1171 (3.80)	3887 (1.03)	46	140 ± 7	8			
J 1872 (Apatite)	71°21'/12°35'	Schneidegeb.	1190	Syenite	23	1537 (2.43)	2012 (3.18)	3887 (1.03)	39	158 ± 10	<5	13.3 ± 0.3	1.6	28
J 1874 (Apatite)	71°21'/12°35'	Schneidegeb.	1325	Syenite	29	2699 (2.66)	3856 (3.79)	3917 (1.04)	46	141 ± 8	<5			
J 1875 (Apatite)	71°21'/12°35'	Schneidegeb.	1400	Syenite	30	498 (0.53)	568 (0.61)	4341 (1.15)	7	180 ± 12	74			

Sample No. (Mineral)	Latitude S/ Longitude E	Locality	Elevation [m]	Rock type	Grains	N_s (ρ_s) [$x10^6 cm^{-2}$]	N_i (ρ_i) [$x10^6 cm^{-2}$]	N_d (ρ_d) [$x10^6 cm^{-2}$]	U [ppm]	FTA ± 1σ [Ma]	χ^2 %	MTL ± 1σ [µm]	Std. Dev. [µm]	n
J 1876 (Apatite)	71°21'/12°35'	Schneidegeb.	1475	Syenite	21	1806 (3.16)	2501 (4.38)	3887 (1.03)	53	148 ± 7	<5	13.3 ± 0.3	1.7	43
J 1877 (Apatite)	71°21'/12°35'	Schneidegeb.	1565	Syenite	17	1686 (3.84)	2664 (6.06)	3917 (1.04)	73	128 ± 12	<5			
J 1878 (Apatite)	71°21'/12°35'	Schneidegeb.	1620	Syenite	10	922 (4.43)	1504 (7.22)	4066 (1.08)	84	135 ± 17	<5			
J 1879 (Apatite)	71°21'/12°35'	Schneidegeb.	1695	Syenite	18	2019 (3.22)	3325 (5.31)	3917 (1.04)	64	124 ± 4	<5			
J 1942 (Apatite)	71°21'/12°37'	Schneidegeb.	1980	Amphibolite	31	629 (0.40)	736 (0.47)	3917 (1.04)	6	174 ± 10	86			
J 1940 (Apatite)	71°14'/12°45'	Oddenskjera	1190	Biotite-Fluorite Granite	19	1208 (1.57)	2361 (3.07)	3917 (1.04)	37	105 ± 6	<5	13.7 ± 0.2	1.3	40
J 1889 (Apatite)	71°24'/13°21'	Gruber-Geb.	2840	Anorthosite	24	2309 (2.45)	2428 (2.58)	3917 (1.04)	31	193 ± 9	<5	13.2 ± 0.2	1.7	101
J 1890 (Apatite)	71°24'/13°21'	Gruber-Geb.	2800	Anorthosite	20	1762 (2.57)	1477 (2.15)	3887 (1.03)	26	246 ± 13	<5	13.3 ± 0.3	1.3	17
J 1891 (Apatite)	71°24'/13°21'	Gruber-Geb.	2715	Anorthosite	20	1544 (5.11)	1400 (4.64)	4066 (1.08)	54	224 ± 14	<5	13.3 ± 0.1	0.7	31
J 1893 (Apatite)	71°24'/13°19'	Gruber-Geb.	2440	Anorthosite	23	1883 (2.45)	2131 (2.77)	3917 (1.04)	33	180 ± 8	<5	14 ± 0.2	1.2	56
J 1894 (Apatite)	71°24'/13°19'	Gruber-Geb.	2365	Anorthosite	22	1684 (1.44)	1625 (1.39)	3887 (1.03)	17	211 ± 11	<5	13.7 ± 0.2	1.6	78
J 1895 (Apatite)	71°24'/13°19'	Gruber-Geb.	2335	Anorthosite	31	2223 (1.38)	2447 (1.52)	3887 (1.03)	18	184 ± 6	24	13.3 ± 0.1	1.5	103
J 1896 (Apatite)	71°24'/13°17'	Gruber-Geb.	2270	Anorthosite	20	849 (0.95)	732 (0.82)	4066 (1.08)	10	235 ± 13	22			
J 1897 (Apatite)	71°24'/13°17'	Gruber-Geb.	2175	Anorthosite	30	2192 (1.87)	2702 (2.30)	3917 (1.04)	28	166 ± 6	7			
J 1898 (Apatite)	71°24'/13°20'	Gruber-Geb.	2590	Anorthosite	21	1272 (1.29)	1208 (1.23)	3917 (1.04)	15	217 ± 13	<5	13.5 ± 0.1	1.4	105

Sample No. (Mineral)	Latitude S/ Longitude E	Locality	Elevation [m]	Rock type	Grains	N_s (ρ_s) [$x10^6 cm^{-2}$]	N_i (ρ_i) [$x10^6 cm^{-2}$]	N_d (ρ_d) [$x10^6 cm^{-2}$]	U [ppm]	FTA ± 1σ [Ma]	χ^2 %	MTL ± 1σ [µm]	Std. Dev. [µm]	n
J 1900 (Apatite)	71°24'/13°17'	Gruber-Geb.	2080	Anorthosite	20	1085 (1.66)	1211 (1.86)	3917 (1.04)	22	183 ± 8	67	13.6 ± 0.3	1.8	40
J 1901 (Apatite)	71°24'/13°17'	Gruber-Geb.	2000	Anorthosite	26	2837 (2.66)	2906 (2.73)	3887 (1.03)	33	197 ± 9	<5	13.1 ± 0.2	1.7	103
J 1902 (Apatite)	71°24'/13°17'	Gruber-Geb.	1915	Gabbronorite	32	748 (0.52)	797 (0.56)	4066 (1.08)	6	191 ± 11	69			
J 1903 (Apatite)	71°24'/13°17'	Gruber-Geb.	1860	Anorthosite	25	2255 (2.89)	2794 (3.58)	3917 (1.04)	43	165 ± 6	19	13.5 ± 0.3	1.7	24
J 1904 (Apatite)	71°23'/13°16'	Gruber-Geb.	1765	Anorthosite	23	746 (0.85)	928 (1.06)	4066 (1.08)	12	164 ± 9	45	12.5 ± 0.1	0.8	53
J 1905 (Apatite)	71°23'/13°16'	Gruber-Geb.	1705	Anorthosite	26	2220 (2.56)	2382 (2.74)	3887 (1.03)	33	188 ± 9	<5	13.9 ± 0.2	1.8	69
J 1906 (Apatite)	71°23'/13°16'	Gruber-Geb.	1610	Anorthosite	26	2862 (2.12)	3489 (2.59)	3887 (1.03)	31	167 ± 6	<5	13.2 ± 0.2	1.8	105
J 1907 (Apatite)	71°23'/13°15'	Gruber-Geb.	1570	Gabbronorite	16	606 (0.72)	588 (0.70)	4066 (1.08)	8	209 ± 13	12			
J 1909 (Apatite)	71°23'/13°15'	Gruber-Geb.	1450	Anorthosite	20	1275 (2.99)	1612 (3.79)	3917 (1.04)	46	163 ± 8	<5	12.9 ± 0.3	2	54
J 1910 (Apatite)	71°23'/13°15'	Gruber-Geb.	1370	Anorthosite	26	1615 (1.84)	2001 (2.29)	4066 (1.08)	27	164 ± 7	70	10.8 ± 0.2	1.2	58
J 1911 (Apatite)	71°23'/13°15'	Gruber-Geb.	1285	Anorthosite	23	1169 (1.80)	1499 (2.30)	3917 (1.04)	28	159 ± 7	38	13.5 ± 0.2	1.4	65
J 1955 (Apatite)	71°21'/13°27'	Untersee	745	Anorthosite	20	369 (0.25)	545 (0.36)	3917 (1.04)	4	138 ± 10	84			
J 1956 (Apatite)	71°21'/13°27'	Untersee	745	Anorthosite	20	2159 (2.44)	2616 (2.96)	3887 (1.03)	36	168 ± 7	60	13.7 ± 0.2	1.6	108
J 1958 (Apatite)	71°19'/13°33'	Untersee	745	Anorthosite	20	1070 (0.87)	2323 (1.90)	3917 (1.04)	23	95 ± 3	82	13.3 ± 0.1	0.9	102
J 1973b (Apatite)	71°00'/12°01'	Starheimtind	1155	Diorite	26	180 (0.07)	265 (0.11)	4066 (1.08)	1	139 ± 14	14			

Sample No. (Mineral)	Latitude S/ Longitude E	Locality	Elevation [m]	Rock type	Grains	N_s (ρ_s) [$x10^6 cm^{-2}$]	N_i (ρ_i) [$x10^6 cm^{-2}$]	N_d (ρ_d) [$x10^6 cm^{-2}$]	U [ppm]	FTA ± 1σ [Ma]	χ^2 %	MTL ± 1σ [µm]	Std. Dev. [µm]	n
J 1974	71°00'/12°01'	Starheimtind	1075	Granodiorite	30	585	646	3887	6	183 ± 11	83			
(Apatite)						(0.46)	(0.50)	(1.03)						
J 1975	71°00'/12°01'	Starheimtind	1240	Diorite	21	502	630	3887	8	161 ± 10	30			
(Apatite)						(0.55)	(0.69)	(1.03)						
J 1976	71°00'/12°01'	Starheimtind	1345	Diorite	20	423	509	4066	7	169 ± 12	72			
(Apatite)						(0.52)	(0.62)	(1.08)						
J 1984	70°46'/11°14'	Schirmacher o.	50	Augen-	23	1270	2118	3887	19	117 ± 5	50	13.8 ± 0.2	1.3	44
(Apatite)				gneiss		(0.96)	(1.60)	(1.03)						
HK2/1	70°46'/11°14'	Schirmacher o.	50	Gneiss	26	1086	2283	4630	21	83 ± 3	43			
(Apatite)						(0.97)	(2.05)	(1.23)						
HK3/1	70°46'/11°14'	Schirmacher o.	50	Gneiss	31	1861	3787	4618	25	85 ± 3	48	13.9 ± 0.2	1.3	56
(Apatite)						(1.20)	(2.44)	(1.22)						
HK4/1	70°46'/11°14'	Schirmacher o.	50	Gneiss	30	1557	3095	4605	24	87 ± 3	19			
(Apatite)						(1.17)	(2.32)	(1.22)						
HK7/1	70°46'/11°14'	Schirmacher o.	50	Gneiss	22	1653	3330	4612	49	86 ± 3	86	14.1 ± 0.1	1.1	104
(Apatite)						(2.36)	(4.75)	(1.22)						
2031-1 GKG	69°59'/8°58'	Dropstone	-450	Monzonite	26	555	815	4276	6	138 ± 8	68			
(Apatite)						(0.40)	(0.58)	(1.13)						
2057/1 GKG	69°57'/11°48'	Dropstone	-210	Basalt	27	1613	2226	4239	26	146 ± 9	<5			
(Apatite)						(1.68)	(2.32)	(1.12)						
2057/2 GKG	69°57'/11°48'	Dropstone	-210	Anorthosite	17	814	959	4229	35	170 ± 9	62			
(Apatite)						(2.67)	(3.14)	(1.12)						
2034-3 GKG	69°57'/6°15'	Dropstone	-734	Gabbro	19	290	428	4322	5	139 ± 11	<5			
(Apatite)						(0.31)	(0.46)	(1.15)						

Sample No. (Mineral)	Latitude S/ Longitude E	Locality	Elevation [m]	Rock type	Grains	N_s (ρ_s) [$x10^6 cm^{-2}$]	N_i (ρ_i) [$x10^6 cm^{-2}$]	N_d (ρ_d) [$x10^6 cm^{-2}$]	U [ppm]	FTA ± 1σ [Ma]	χ^2 %	MTL ± 1σ [µm]	Std. Dev. [µm]	n
2033-2 AGT (Apatite)	69°58'/6°06'	Dropstone	-311	Gneiss	20	1871 (1.52)	5001 (4.07)	4257 (1.13)	45	78 ± 4	<5			
2058-1 GKG (Apatite)	69°58'/12°11'	Dropstone	-155	Granite	25	1907 (1.68)	2312 (2.03)	4192 (1.11)	23	167 ± 10	<5			

II. Radialplots, FTA and track length histograms

Fig. I Fission-track data of **(A)** titanite, **(B)** zircon and **(C)** apatite samples. The single grain age distributions are shown as radialplots and histograms, the mean track length distributions for the apatite samples are also depicted as frequency distributions. The radialplot (cf. Galbraith, 1989) allows to illustrate single grain age distributions with respect to their individual precision which is represented by the x-axis (here: error in age). The 2σ-error on the FTA is reported by y- axis and the FTA can be read off from the circular scale by extrapolating a line through (x,y) and the zero-value of the y-axis.
Together with the histograms, the FTA $\pm$ 1σ and the χ^2-result of the sample as well as the mean track length $\pm$ standard deviation are shown.

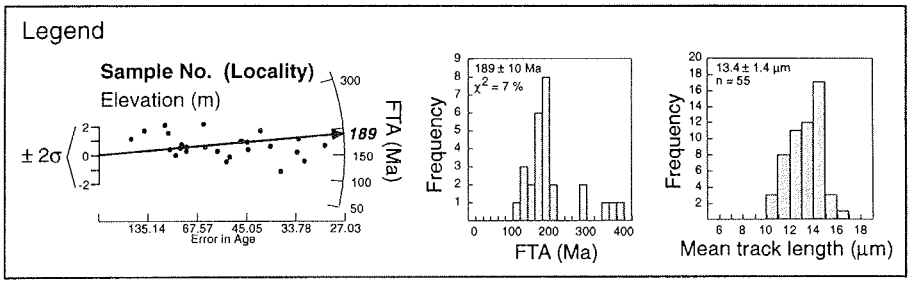

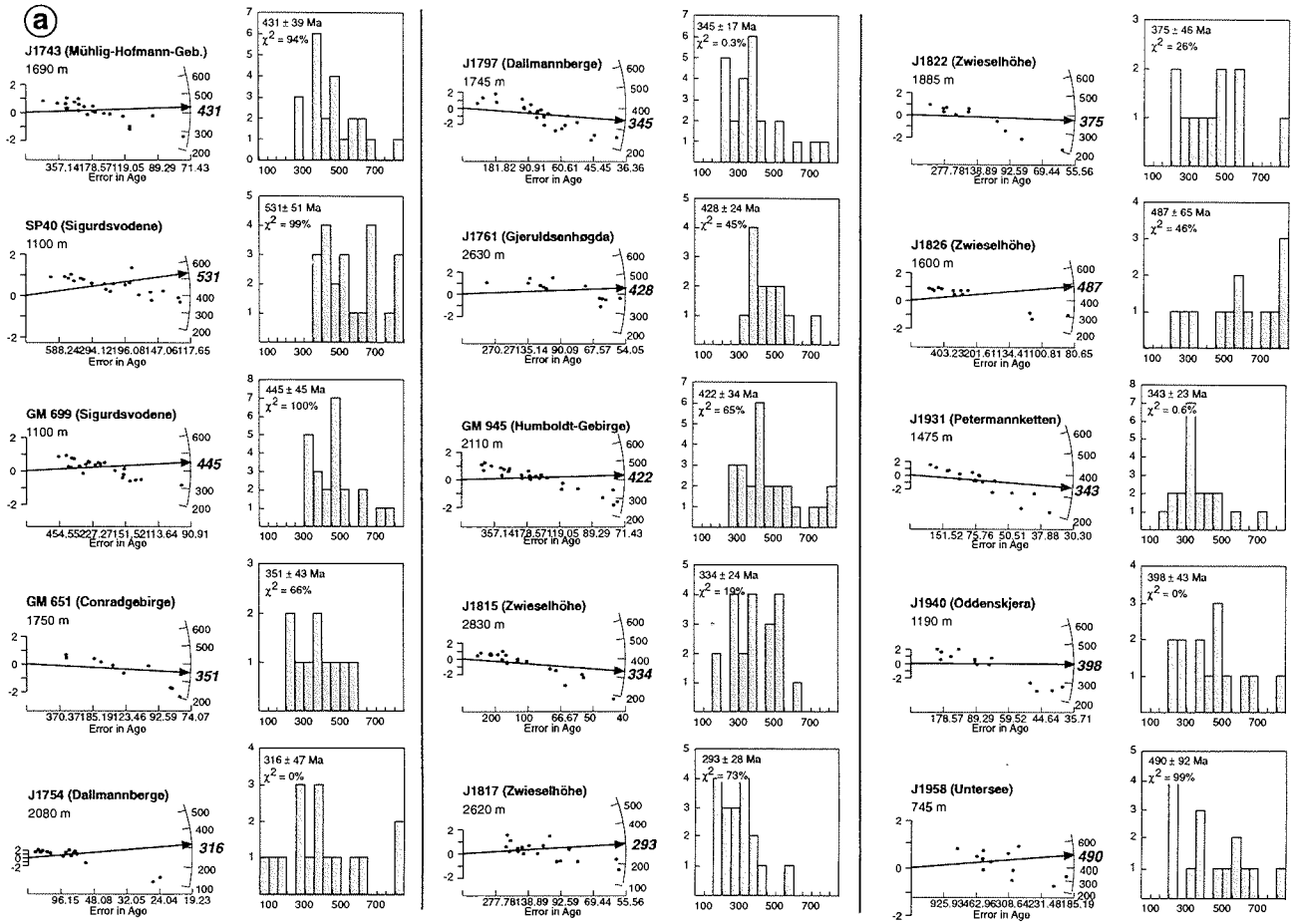
a
J1743 (Mühlig-Hofmann-Geb.)
1690 m
431
357.14178.57119.05 89.29 71.43
Error in Age
431 ± 39 Ma
χ² = 94%
SP40 (Sigurdsvodene)
1100 m
531
588.24294.12196.08147.06117.65
Error in Age
531 ± 51 Ma
χ² = 99%
GM 699 (Sigurdsvodene)
1100 m
445
454.55227.27151.52113.64 90.91
Error in Age
445 ± 45 Ma
χ² = 100%
GM 651 (Conradgebirge)
1750 m
351
370.37185.19123.46 92.59 74.07
Error in Age
351 ± 43 Ma
χ² = 66%
J1754 (Dallmannberge)
2080 m
316
96.15 48.08 32.05 24.04 19.23
Error in Age
316 ± 47 Ma
χ² = 0%
J1797 (Dallmannberge)
1745 m
345
181.82 90.91 60.61 45.45 36.36
Error in Age
345 ± 17 Ma
χ² = 0.3%
J1761 (Gjeruldsenhøgda)
2630 m
428
270.27135.14 90.09 67.57 54.05
Error in Age
428 ± 24 Ma
χ² = 45%
GM 945 (Humboldt-Gebirge)
2110 m
422
357.14178.57119.05 89.29 71.43
Error in Age
422 ± 34 Ma
χ² = 65%
J1815 (Zwieselhöhe)
2830 m
334
200 100 66.67 50 40
Error in Age
334 ± 24 Ma
χ² = 19%
J1817 (Zwieselhöhe)
2620 m
293
277.78138.89 92.59 69.44 55.56
Error in Age
293 ± 28 Ma
χ² = 73%
J1822 (Zwieselhöhe)
1885 m
375
277.78138.89 92.59 69.44 55.56
Error in Age
375 ± 46 Ma
χ² = 26%
J1826 (Zwieselhöhe)
1600 m
487
403.23201.61134.41100.81 80.65
Error in Age
487 ± 65 Ma
χ² = 46%
J1931 (Petermannketten)
1475 m
343
151.52 75.76 50.51 37.88 30.30
Error in Age
343 ± 23 Ma
χ² = 0.6%
J1940 (Oddenskjera)
1190 m
398
178.57 89.29 59.52 44.64 35.71
Error in Age
398 ± 43 Ma
χ² = 0%
J1958 (Untersee)
745 m
490
925.93462.96308.64231.48185.19
Error in Age
490 ± 92 Ma
χ² = 99%

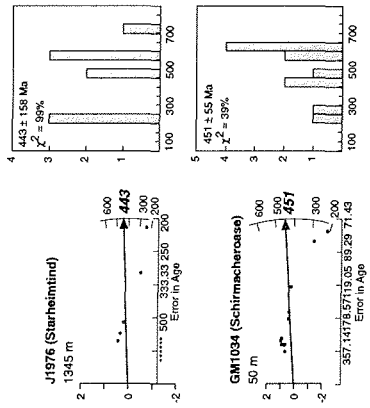
443 ± 158 Ma
χ^2 = 99%
451 ± 55 Ma
χ^2 = 39%
J1976 (Starheimtind)
1345 m
443
Error in Age
GM1034 (Schirmacheroase)
50 m
451
Error in Age
357.14178,57119.05 89.29 71.43

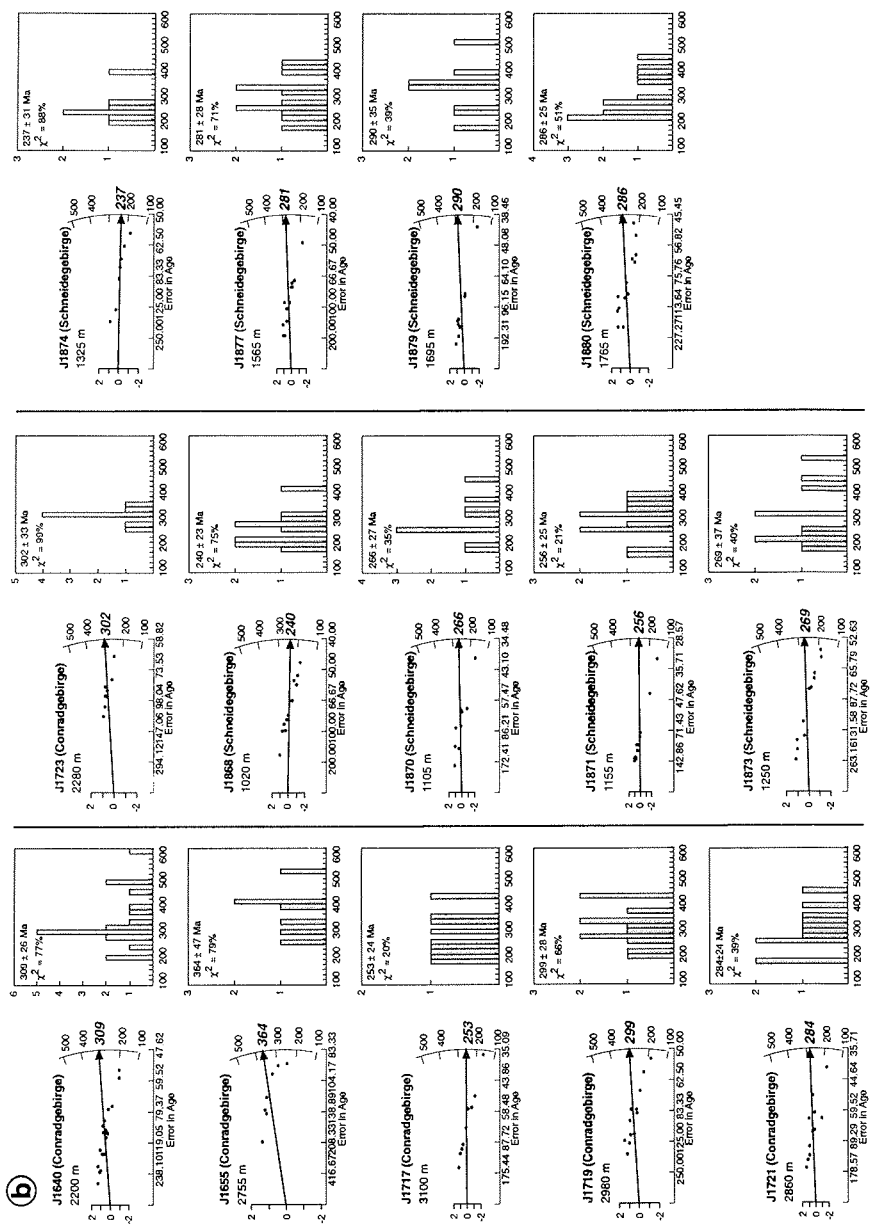
b
J1640 (Conradgebirge)
2200 m
309
Error in Age
J1655 (Conradgebirge)
2755 m
364
Error in Age
J1717 (Conradgebirge)
3100 m
253
Error in Age
J1719 (Conradgebirge)
2980 m
299
Error in Age
J1721 (Conradgebirge)
2860 m
284
Error in Age
J1723 (Conradgebirge)
2280 m
302
Error in Age
J1868 (Schneidegebirge)
1020 m
240
Error in Age
J1870 (Schneidegebirge)
1105 m
266
Error in Age
J1871 (Schneidegebirge)
1155 m
256
Error in Age
J1873 (Schneidegebirge)
1250 m
269
Error in Age
J1874 (Schneidegebirge)
1325 m
237
Error in Age
J1877 (Schneidegebirge)
1565 m
281
Error in Age
J1879 (Schneidegebirge)
1695 m
290
Error in Age
J1880 (Schneidegebirge)
1765 m
286
Error in Age

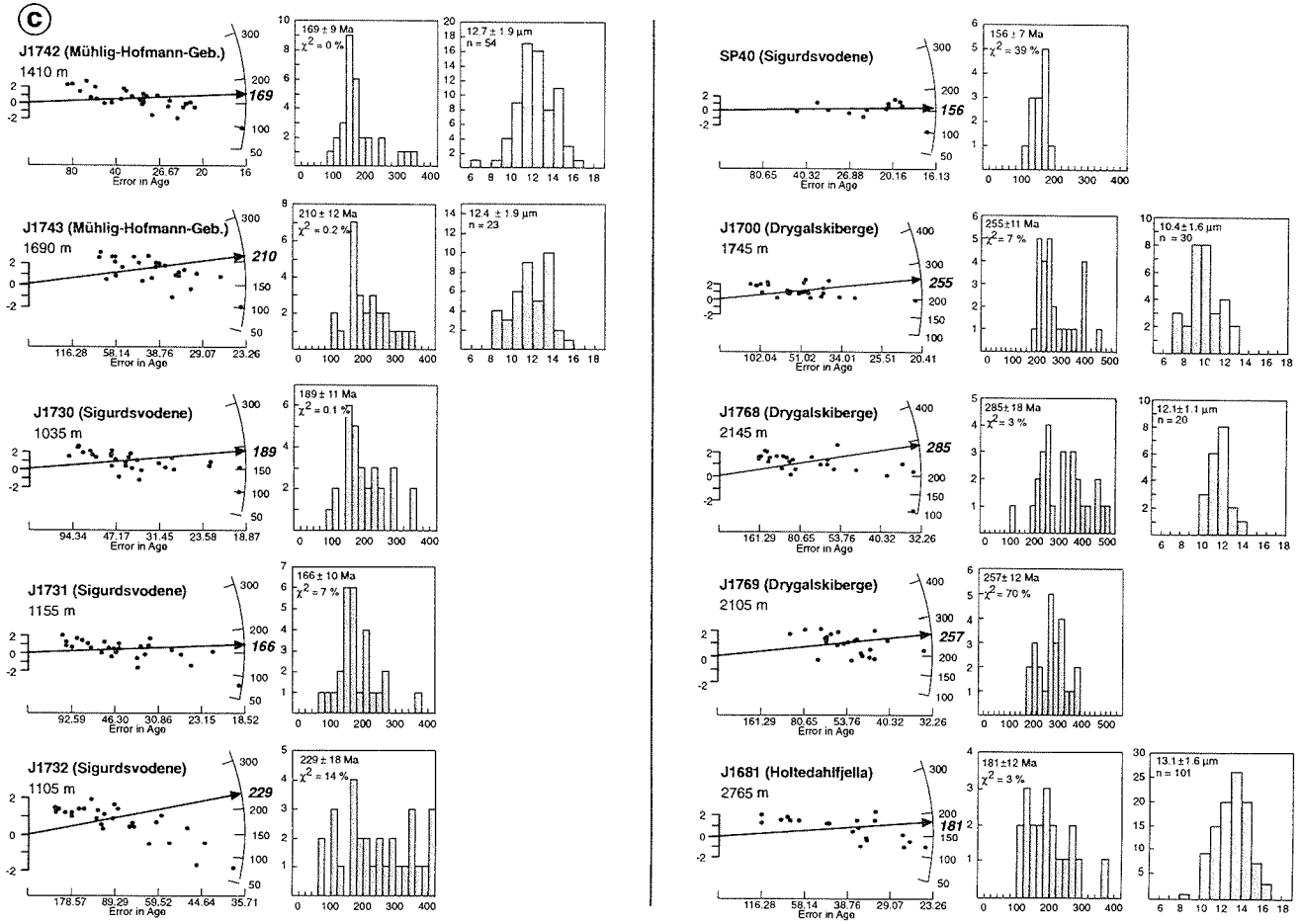
C
J1742 (Mühlig-Hofmann-Geb.)
1410 m
169
Error in Age
169 ± 9 Ma
χ² = 0 %
12.7 ± 1.9 µm
n = 54
J1743 (Mühlig-Hofmann-Geb.)
1690 m
210
Error in Age
210 ± 12 Ma
χ² = 0.2 %
12.4 ± 1.9 µm
n = 23
J1730 (Sigurdsvodene)
1035 m
189
Error in Age
189 ± 11 Ma
χ² = 0.1 %
J1731 (Sigurdsvodene)
1155 m
166
Error in Age
166 ± 10 Ma
χ² = 7 %
J1732 (Sigurdsvodene)
1105 m
229
Error in Age
229 ± 18 Ma
χ² = 14 %
SP40 (Sigurdsvodene)
156
Error in Age
156 ± 7 Ma
χ² = 39 %
J1700 (Drygalskiberge)
1745 m
255
Error in Age
255±11 Ma
χ² = 7 %
10.4±1.6 µm
n = 30
J1768 (Drygalskiberge)
2145 m
285
Error in Age
285±18 Ma
χ² = 3 %
12.1±1.1 µm
n = 20
J1769 (Drygalskiberge)
2105 m
257
Error in Age
257±12 Ma
χ² = 70 %
J1681 (Holtedahlfjella)
2765 m
181
Error in Age
181±12 Ma
χ² = 3 %
13.1±1.6 µm
n = 101

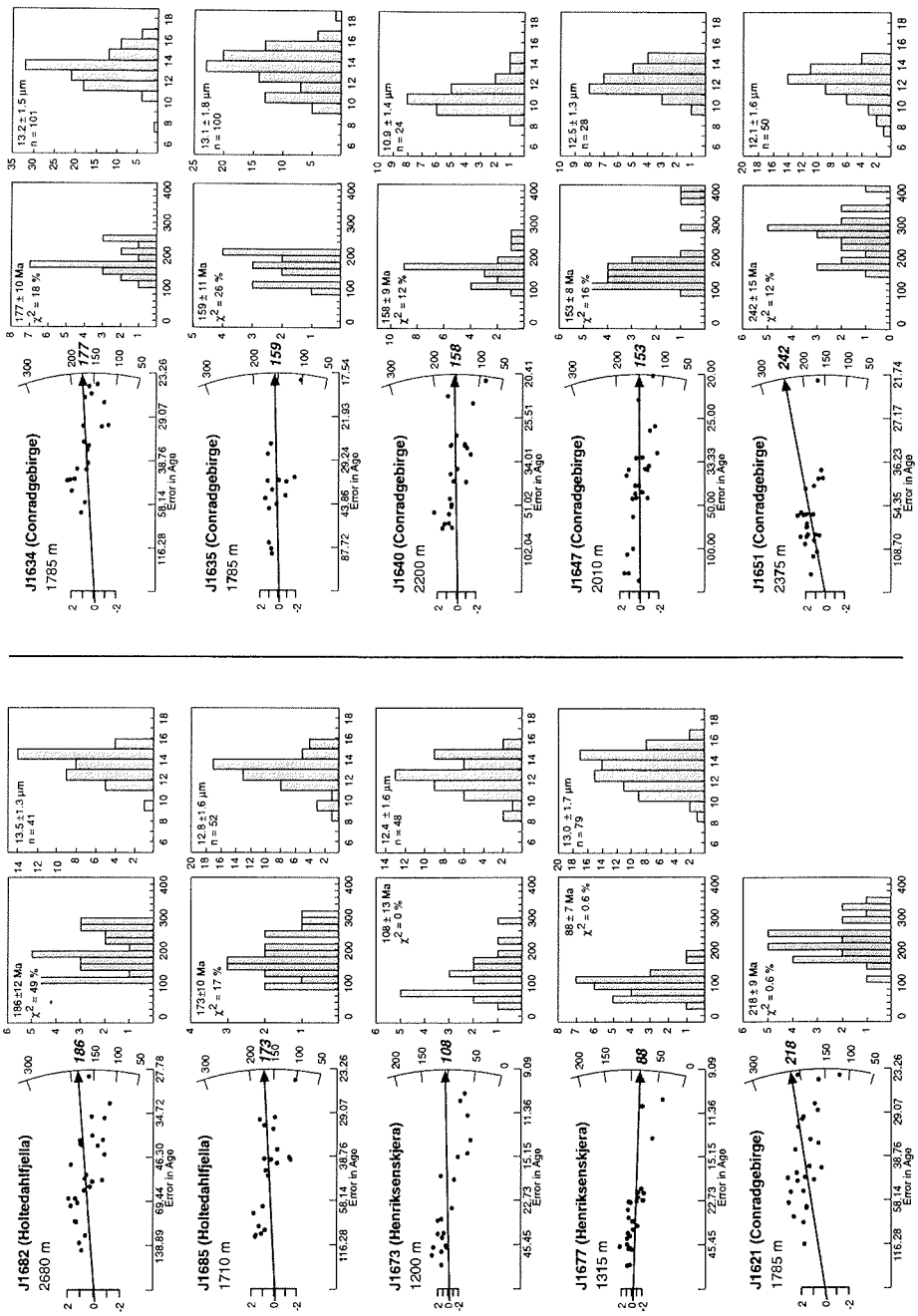
J1682 (Holtedahlfjella)
2680 m
J1685 (Holtedahlfjella)
1710 m
J1673 (Henriksenskjera)
1200 m
J1677 (Henriksenskjera)
1315 m
J1621 (Conradgebirge)
1785 m
J1634 (Conradgebirge)
1785 m
J1635 (Conradgebirge)
1785 m
J1640 (Conradgebirge)
2200 m
J1647 (Conradgebirge)
2010 m
J1651 (Conradgebirge)
2375 m
Error in Age

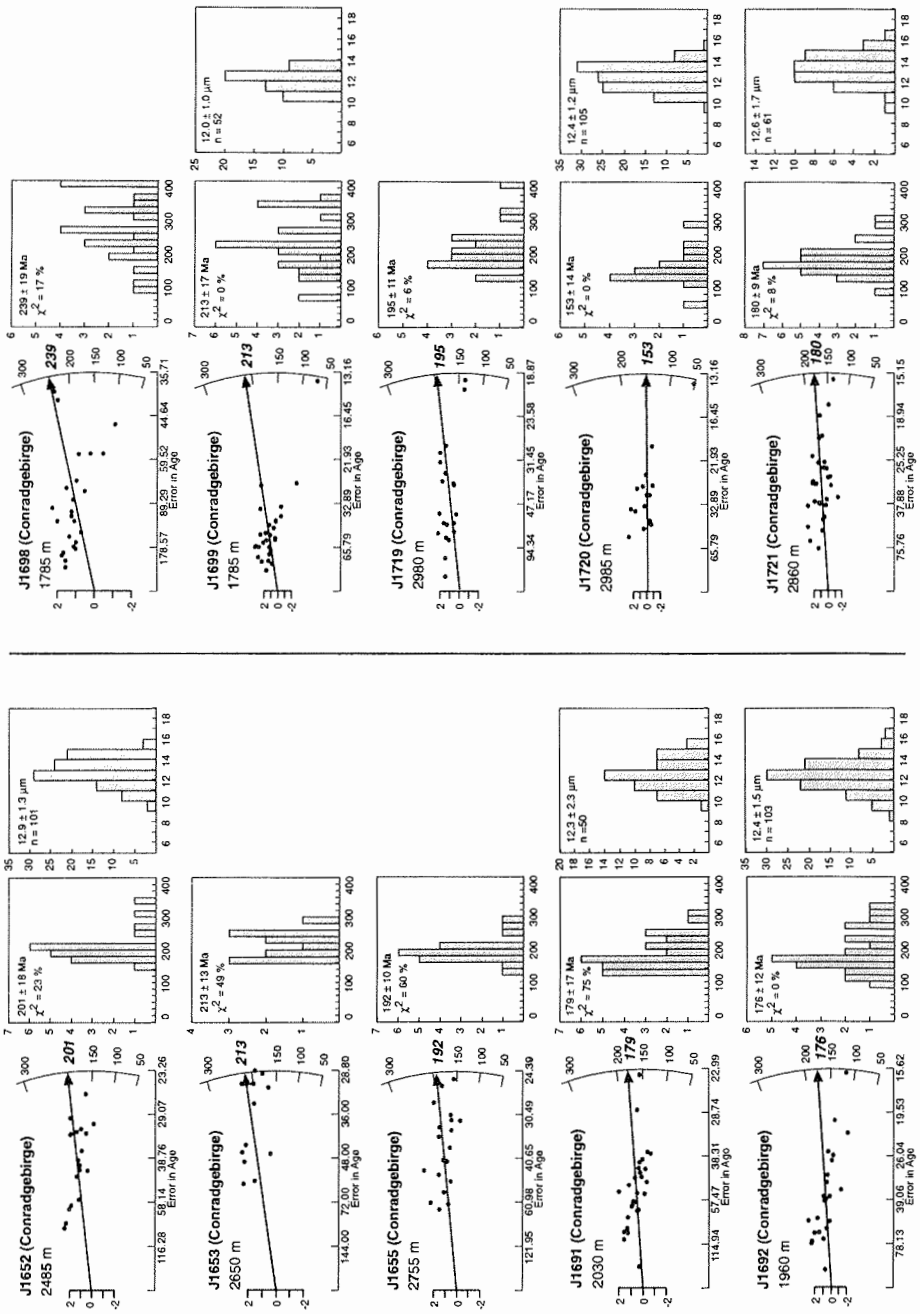
J1652 (Conradgebirge)
2485 m
201 ± 18 Ma
χ² = 23 %
12.9 ± 1.3 µm
n = 101
201
116.28 58.14 38.76 29.07 23.26
Error in Age
J1653 (Conradgebirge)
2650 m
213 ± 13 Ma
χ² = 49 %
213
144.00 72.00 48.00 36.00 28.80
Error in Age
J1655 (Conradgebirge)
2755 m
192 ± 10 Ma
χ² = 60 %
192
121.95 60.98 40.65 30.49 24.39
Error in Age
J1691 (Conradgebirge)
2030 m
179 ± 17 Ma
χ² = 75 %
12.3 ± 2.3 µm
n =50
179
114.94 57.47 38.31 28.74 22.99
Error in Age
J1692 (Conradgebirge)
1960 m
176 ± 12 Ma
χ² = 0 %
12.4 ± 1.5 µm
n = 103
176
78.13 39.06 26.04 19.53 15.62
Error in Age
J1698 (Conradgebirge)
1785 m
239 ± 19 Ma
χ² = 17 %
12.0 ± 1.0 µm
n = 52
239
178.57 89.29 59.52 44.64 35.71
Error in Age
J1699 (Conradgebirge)
1785 m
213 ± 17 Ma
χ² = 0 %
213
65.79 32.89 21.93 16.45 13.16
Error in Age
J1719 (Conradgebirge)
2980 m
195 ± 11 Ma
χ² = 6 %
195
94.34 47.17 31.45 23.58 18.87
Error in Age
J1720 (Conradgebirge)
2985 m
153 ± 14 Ma
χ² = 0 %
12.4 ± 1.2 µm
n = 105
153
65.79 32.89 21.93 16.45 13.16
Error in Age
J1721 (Conradgebirge)
2860 m
180 ± 9 Ma
χ² = 8 %
12.6 ± 1.7 µm
n = 61
180
75.76 37.88 25.25 18.94 15.15
Error in Age

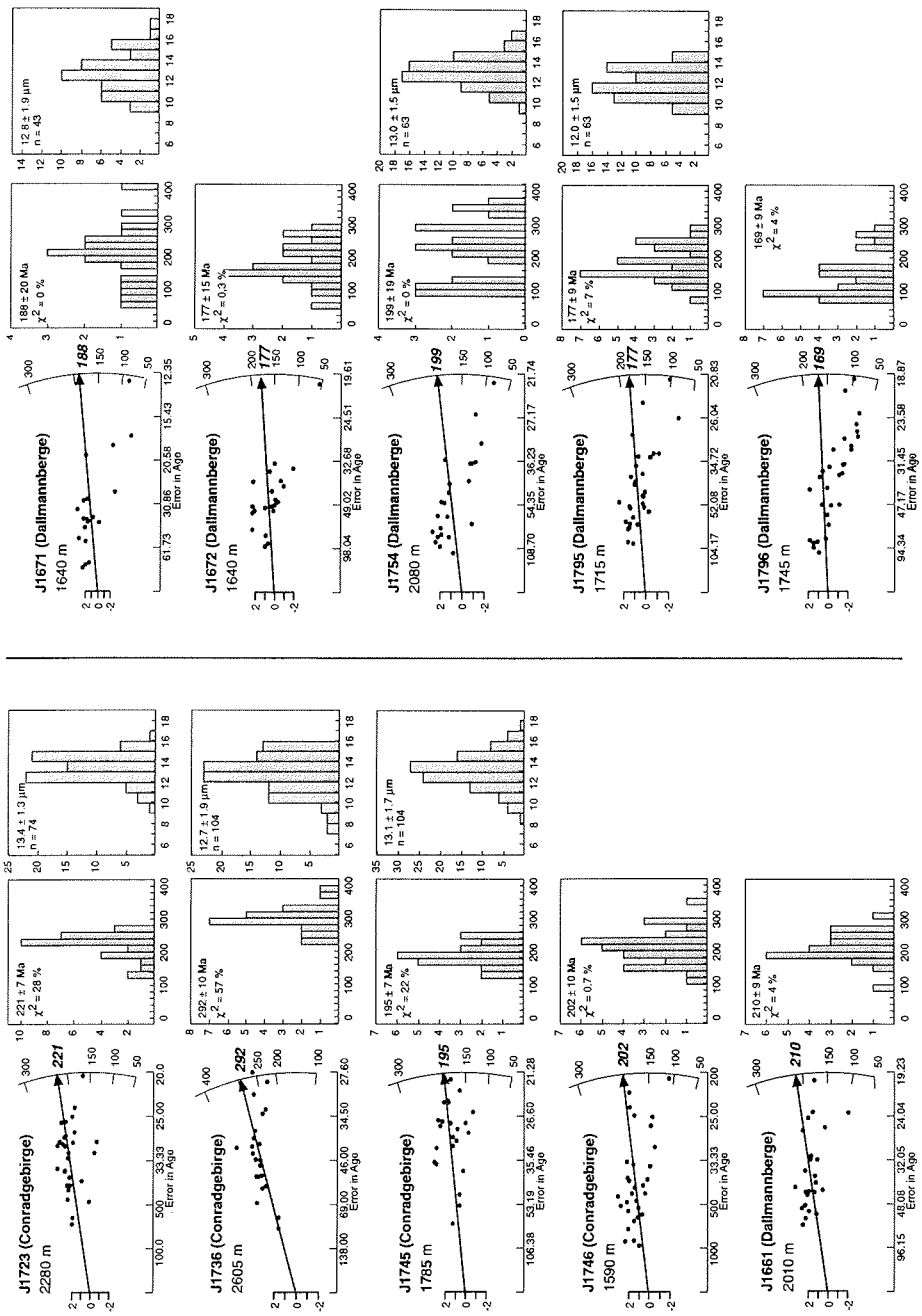
J1723 (Conradgebirge)
2280 m
221 ± 7 Ma
χ² = 28 %
13.4 ± 1.3 µm
n = 74
J1736 (Conradgebirge)
2605 m
292 ± 10 Ma
χ² = 57 %
12.7 ± 1.9 µm
n = 104
J1745 (Conradgebirge)
1785 m
195 ± 7 Ma
χ² = 22 %
13.1 ± 1.7 µm
n = 104
J1746 (Conradgebirge)
1590 m
202 ± 10 Ma
χ² = 0.7 %
J1661 (Dallmannberge)
2010 m
210 ± 9 Ma
χ² = 4 %
J1671 (Dallmannberge)
1640 m
188 ± 20 Ma
χ² = 0 %
12.8 ± 1.9 µm
n = 43
J1672 (Dallmannberge)
1640 m
177 ± 15 Ma
χ² = 0.3 %
J1754 (Dallmannberge)
2080 m
199 ± 19 Ma
χ² = 0 %
13.0 ± 1.5 µm
n = 63
J1795 (Dallmannberge)
1715 m
177 ± 9 Ma
χ² = 7 %
12.0 ± 1.5 µm
n = 63
J1796 (Dallmannberge)
1745 m
169 ± 9 Ma
χ² = 4 %
Error in Age

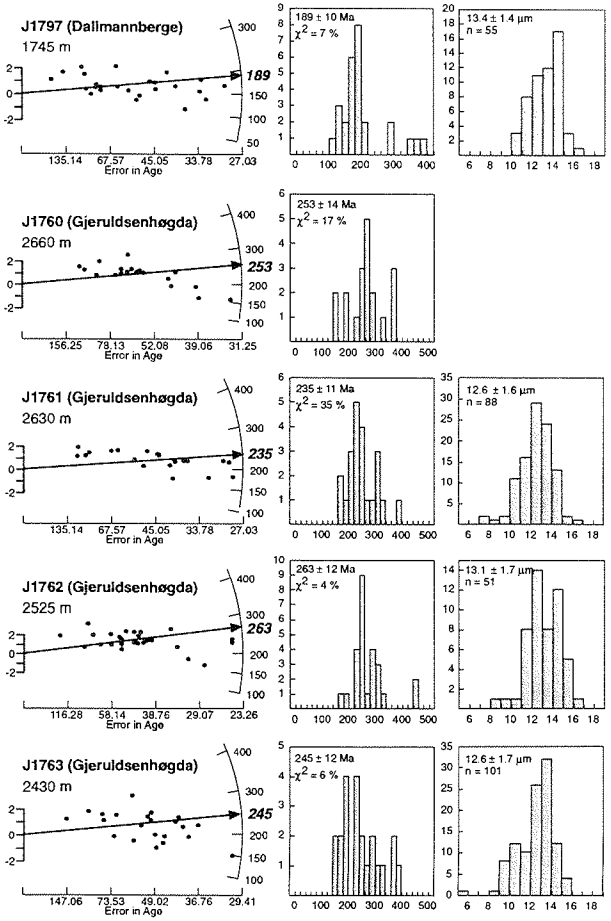
J1797 (Dallmannberge)
1745 m
189
189 ± 10 Ma
χ² = 7 %
13.4 ± 1.4 µm
n = 55
Error in Age
J1760 (Gjeruldsenhøgda)
2660 m
253
253 ± 14 Ma
χ² = 17 %
Error in Age
J1761 (Gjeruldsenhøgda)
2630 m
235
235 ± 11 Ma
χ² = 35 %
12.6 ± 1.6 µm
n = 88
Error in Age
J1762 (Gjeruldsenhøgda)
2525 m
263
263 ± 12 Ma
χ² = 4 %
13.1 ± 1.7 µm
n = 51
Error in Age
J1763 (Gjeruldsenhøgda)
2430 m
245
245 ± 12 Ma
χ² = 6 %
12.6 ± 1.7 µm
n = 101
Error in Age

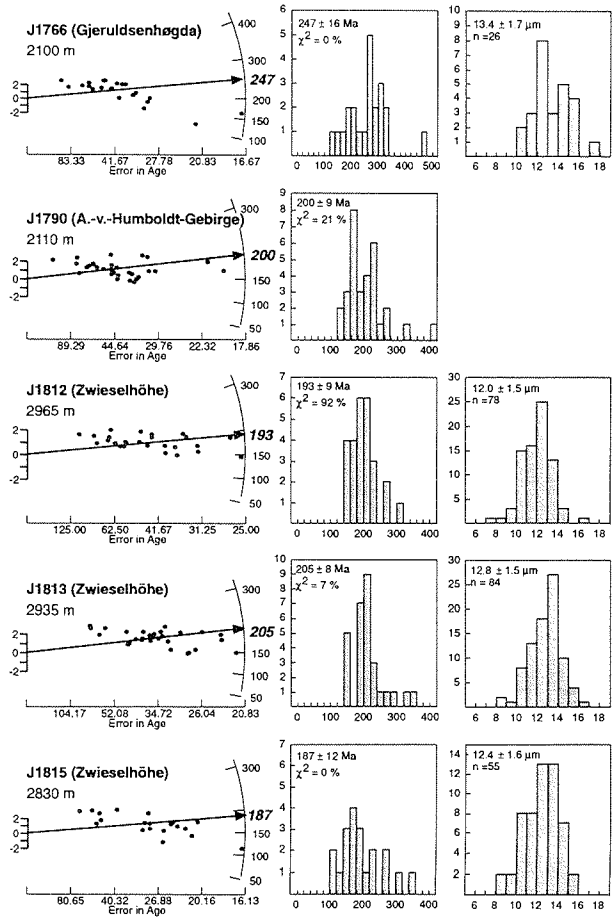
J1766 (Gjeruldsenhøgda)
2100 m
247
247 ± 16 Ma
χ² = 0 %
13.4 ± 1.7 µm
n =26
Error in Age
J1790 (A.-v.-Humboldt-Gebirge)
2110 m
200
200 ± 9 Ma
χ² = 21 %
Error in Age
J1812 (Zwieselhöhe)
2965 m
193
193 ± 9 Ma
χ² = 92 %
12.0 ± 1.5 µm
n =78
Error in Age
J1813 (Zwieselhöhe)
2935 m
205
205 ± 8 Ma
χ² = 7 %
12.8 ± 1.5 µm
n = 84
Error in Age
J1815 (Zwieselhöhe)
2830 m
187
187 ± 12 Ma
χ² = 0 %
12.4 ± 1.6 µm
n =55
Error in Age

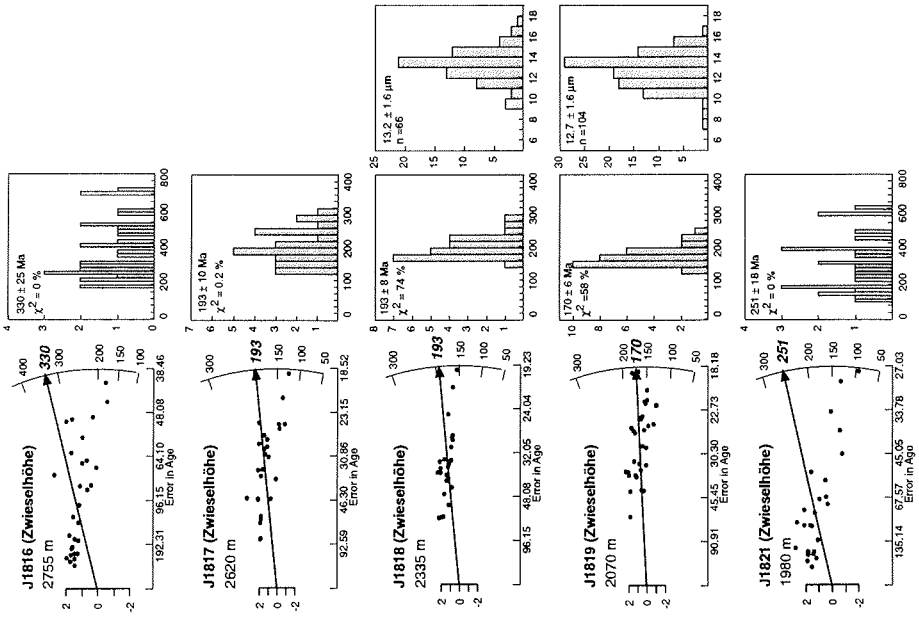
J1816 (Zwieselhöhe)
2755 m
330 ± 25 Ma
χ² = 0 %
330
J1817 (Zwieselhöhe)
2620 m
193 ± 10 Ma
χ² = 0.2 %
193
J1818 (Zwieselhöhe)
2335 m
193 ± 8 Ma
χ² = 74 %
193
13.2 ± 1.6 µm
n =86
J1819 (Zwieselhöhe)
2070 m
170 ± 6 Ma
χ² =58 %
170
12.7 ± 1.6 µm
n =104
J1821 (Zwieselhöhe)
1980 m
251 ± 18 Ma
χ² = 0 %
251
J1822 (Zwieselhöhe)
1885 m
344 ± 20 Ma
χ² =0.1 %
344
J1823 (Zwieselhöhe)
1820 m
186 ± 16 Ma
χ² = 0 %
186
14.0 ± 1.6 µm
n = 52
J1923 (Weyprechtberge)
2365 m
315 ± 18 Ma
χ² = 58 %
315
13.0 ± 1.8 µm
n = 50
J1924 (Weyprechtberge)
2685 m
274 ± 14 Ma
χ² = 15 %
274
J1838 (Petermannketten)
1260 m
108 ± 12 Ma
χ² = 1 %
108
Error in Age

J1851 (Petermannketten)
1600 m
145 ± 6 Ma
χ² = 20 %
145
Error in Age
J1867 (Petermannketten)
1410 m
142 ± 6 Ma
χ² = 32 %
142
Error in Age
J1886 (Petermannketten)
1125 m
113 ± 7 Ma
χ² = 0.3 %
113
13.6 ± 1.9 µm
n = 13
Error in Age
J1887 (Petermannketten)
1125 m
150 ± 6 Ma
χ² = 1 %
150
13.0 ± 1.9 µm
n = 40
Error in Age
J1930 (Petermannketten)
1475 m
156 ± 7 Ma
χ² = 11 %
156
12.4 ± 0.9 µm
n = 15
Error in Age
J1931 (Petermannketten)
1475 m
103 ± 4 Ma
χ² = 0.1 %
103
13.2 ± 2.5 µm
n = 15
Error in Age
J1868 (Schneidegebirge)
1020 m
109 ± 5 Ma
χ² = 0 %
109
Error in Age
J1869 (Schneidegebirge)
1060 m
140 ± 7 Ma
χ² = 8 %
140
Error in Age
J1872 (Schneidegebirge)
1190 m
158 ± 10 Ma
χ² = 0 %
158
13.3 ± 1.6 µm
n = 28
Error in Age
J1874 (Schneidegebirge)
1325 m
141 ± 8 Ma
χ² = 0 %
141
13.1 ± 1.5 µm
n = 40
Error in Age

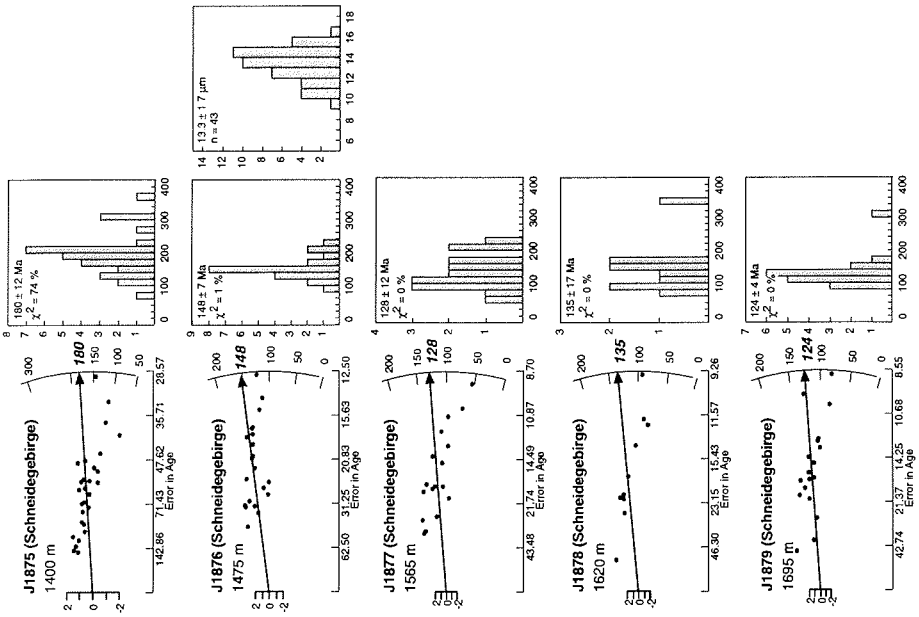
J1875 (Schneidegebirge)
1400 m
180 ± 12 Ma
χ² = 74 %
180
142.86 71.43 47.62 35.71 28.57
Error in Age
J1876 (Schneidegebirge)
1475 m
148 ± 7 Ma
χ² = 1 %
148
62.50 31.25 20.83 15.63 12.50
Error in Age
13.3 ± 1.7 µm
n = 43
J1877 (Schneidegebirge)
1565 m
128 ± 12 Ma
χ² = 0 %
128
43.48 21.74 14.49 10.87 8.70
Error in Age
J1878 (Schneidegebirge)
1620 m
135 ± 17 Ma
χ² = 0 %
135
46.30 23.15 15.43 11.57 9.26
Error in Age
J1879 (Schneidegebirge)
1695 m
124 ± 4 Ma
χ² = 0 %
124
42.74 21.37 14.25 10.68 8.55
Error in Age
J1942 (Schneidegebirge)
1980 m
174 ± 10 Ma
χ² = 86 %
174
125.00 62.50 41.67 31.25 25.00
Error in Age
J1940 (Oddenskjera)
1190 m
105 ± 6 Ma
χ² = 0.1 %
105
47.17 23.58 15.72 11.79 9.43
Error in Age
13.7 ± 1.3 µm
n = 40
J1889 (O.-v.-Grubergebirge)
2840 m
193 ± 9 Ma
χ² = 0.2 %
193
81.97 40.98 27.32 20.49 16.39
Error in Age
13.2 ± 1.7 µm
n = 101
J1890 (O.-v.-Grubergebirge)
2800 m
246 ± 13 Ma
χ² = 0.6 %
246
89.29 44.64 29.76 22.32 17.86
Error in Age
13.3 ± 1.3 µm
n = 17
J1891 (O.-v.-Grubergebirge)
2715 m
224 ± 14 Ma
χ² = 0 %
224
116.28 58.14 38.76 29.07 23.26
Error in Age
13.3 ± 0.7 µm
n = 31

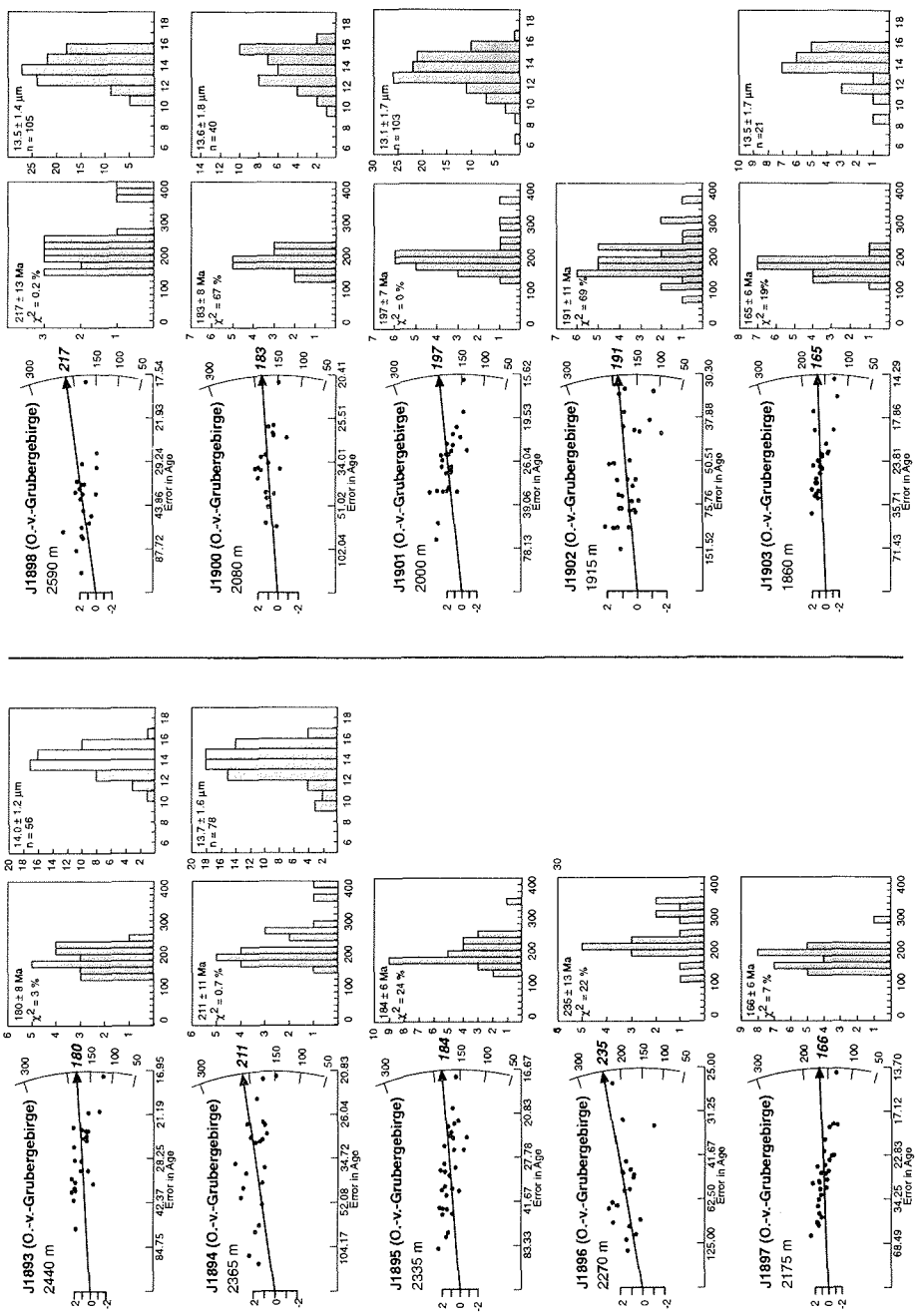
J1893 (O.-v.-Grubergebirge)
2440 m
180 ± 8 Ma
χ² = 3 %
14.0 ± 1.2 µm
n = 96
J1894 (O.-v.-Grubergebirge)
2365 m
211 ± 11 Ma
χ² = 0.7 %
13.7 ± 1.6 µm
n = 78
J1895 (O.-v.-Grubergebirge)
2335 m
184 ± 6 Ma
χ² = 24 %
J1896 (O.-v.-Grubergebirge)
2270 m
235 ± 13 Ma
χ² = 22 %
J1897 (O.-v.-Grubergebirge)
2175 m
166 ± 6 Ma
χ² = 7 %
J1898 (O.-v.-Grubergebirge)
2590 m
217 ± 13 Ma
χ² = 0.2 %
13.5 ± 1.4 µm
n = 105
J1900 (O.-v.-Grubergebirge)
2080 m
183 ± 8 Ma
χ² = 67 %
13.6 ± 1.8 µm
n = 40
J1901 (O.-v.-Grubergebirge)
2000 m
197 ± 7 Ma
χ² = 0 %
13.1 ± 1.7 µm
n = 103
J1902 (O.-v.-Grubergebirge)
1915 m
191 ± 11 Ma
χ² = 69 %
J1903 (O.-v.-Grubergebirge)
1860 m
165 ± 6 Ma
χ² = 19 %
13.5 ± 1.7 µm
n = 21
Error in Age

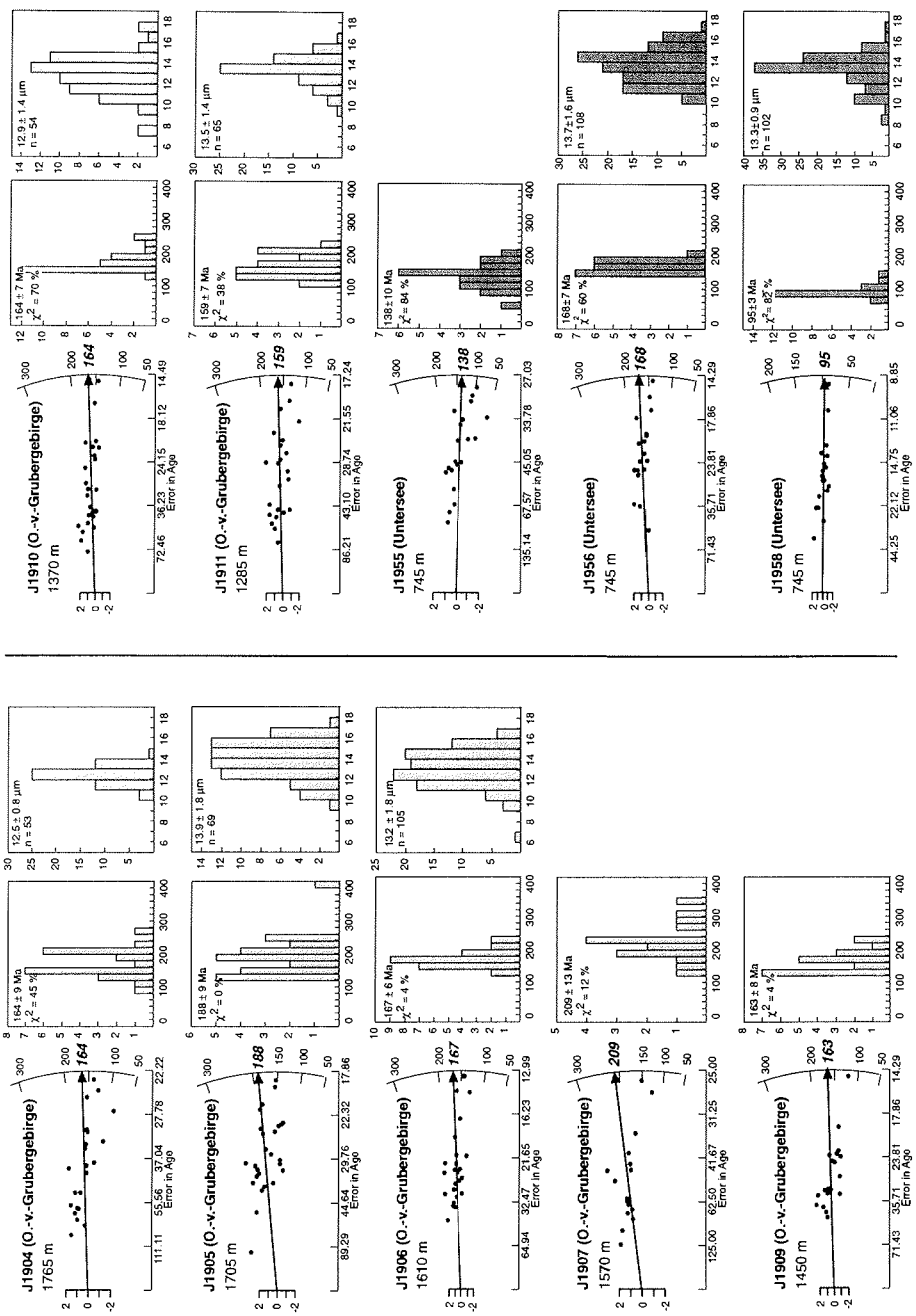
J1904 (O.-v.-Grubergebirge)
1765 m
164 ± 9 Ma
χ² = 45 %
164
12.5 ± 0.8 µm
n = 53
J1905 (O.-v.-Grubergebirge)
1705 m
188 ± 9 Ma
χ² = 0 %
188
13.9 ± 1.8 µm
n = 69
J1906 (O.-v.-Grubergebirge)
1610 m
167 ± 6 Ma
χ² = 4 %
167
132 ± 1.8 µm
n = 105
J1907 (O.-v.-Grubergebirge)
1570 m
209 ± 13 Ma
χ² = 12 %
209
J1909 (O.-v.-Grubergebirge)
1450 m
163 ± 8 Ma
χ² = 4 %
163
J1910 (O.-v.-Grubergebirge)
1370 m
164 ± 7 Ma
χ² = 70 %
164
12.9 ± 1.4 µm
n = 54
J1911 (O.-v.-Grubergebirge)
1285 m
159 ± 7 Ma
χ² = 38 %
159
13.5 ± 1.4 µm
n = 65
J1955 (Untersee)
745 m
138 ± 10 Ma
χ² = 84 %
138
J1956 (Untersee)
745 m
168 ± 7 Ma
χ² = 60 %
168
13.7 ± 1.6 µm
n = 108
J1958 (Untersee)
745 m
95 ± 3 Ma
χ² = 82 %
95
13.3 ± 0.9 µm
n = 102
Error in Age

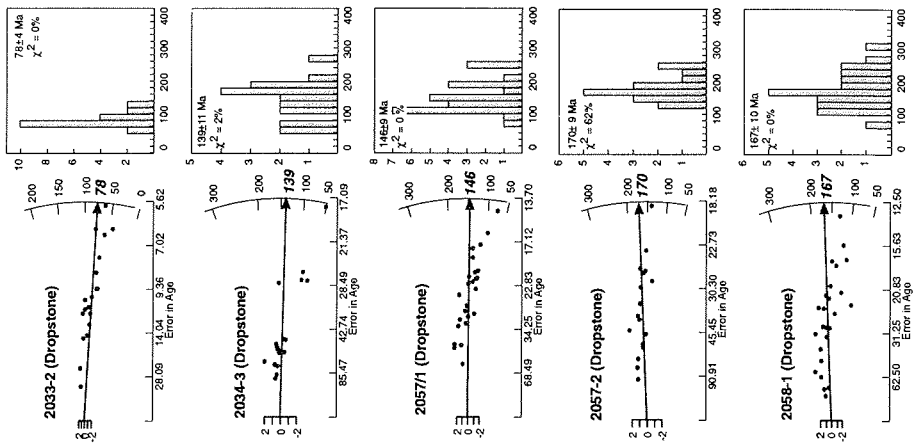
2033-2 (Dropstone)
78±4 Ma
χ² = 0%
78
Error in Age
2034-3 (Dropstone)
139±11 Ma
χ² = 2%
139
Error in Age
2057/1 (Dropstone)
146±9 Ma
χ² = 0%
146
Error in Age
2057-2 (Dropstone)
170± 9 Ma
χ² = 62%
170
Error in Age
2058-1 (Dropstone)
167± 10 Ma
χ² = 0%
167
Error in Age

Folgende Hefte der Reihe „Berichte zur Polarforschung“ sind bisher erschienen:

* **Sonderheft Nr. 1/1981** – „Die Antarktis und ihr Lebensraum“
Eine Einführung für Besucher – Herausgegeben im Auftrag von SCAR

Heft Nr. 1/1982 – „Die Filchner-Schelfeis-Expedition 1980/81“
zusammengestellt von Heinz Kohnen

* **Heft Nr. 2/1982** – „Deutsche Antarktis-Expedition 1980/81 mit FS „Meteor“
First International BIOMASS Experiment (FIBEX) – Liste der Zooplankton- und Mikronektonnetzfänge
zusammengestellt von Norbert Klages

Heft Nr. 3/1982 – „Digitale und analoge Krill-Echolot-Rohdatenerfassung an Bord des Forschungsschiffes ‚Meteor‘“ (im Rahmen von FIBEX 1980/81, Fahrtabschnitt ANT III), von Bodo Morgenstern

Heft Nr. 4/1982 – „Filchner-Schelfeis-Expedition 1980/81“
Liste der Planktonfänge und Lichtstärkemessungen
zusammengestellt von Gerd Hubold und H. Eberhard Drescher

* **Heft Nr. 5/1982** – “Joint Biological Expedition on RRS ‘John Biscoe’, February 1982“
by G. Hempel and R. B. Heywood

* **Heft Nr. 6/1982** – „Antarktis-Expedition 1981/82 (Unternehmen ‚Eiswarte‘)“
zusammengestellt von Gode Gravenhorst

Heft Nr. 7/1982 – „Marin-Biologisches Begleitprogramm zur Standorterkundung 1979/80 mit MS ‚Polarsirkel‘ (Pre-Site Survey)“ – Stationslisten der Mikronekton- und Zooplanktonfänge sowie der Bodenfischerei
zusammengestellt von R. Schneppenheim

Heft Nr. 8/1983 – “The Post-Fibex Data Interpretation Workshop“
by D. L. Cram and J.-C. Freytag with the collaboration of J. W. Schmidt, M. Mall, R. Kresse, T. Schwinghammer

* **Heft Nr. 9/1983** – “Distribution of some groups of zooplankton in the inner Weddell Sea in summer 1979/80“
by I. Hempel, G. Hubold, B. Kaczmaruk, R. Keller, R. Weigmann-Haass

Heft Nr. 10/1983 – „Fluor im antarktischen Ökosystem“ – DFG-Symposium November 1982
zusammengestellt von Dieter Adelung

Heft Nr. 11/1983 – “Joint Biological Expedition on RRS ‘John Biscoe’, February 1982 (II)“
Data of micronecton and zooplankton hauls, by Uwe Piatkowski

Heft Nr. 12/1983 – „Das biologische Programm der ANTARKTIS-I-Expedition 1983 mit FS ‚Polarstern‘“
Stationslisten der Plankton-, Benthos- und Grundschleppnetzfänge und Liste der Probennahme an Robben und Vögeln, von H. E. Drescher, G. Hubold, U. Piatkowski, J. Plötz und J. Voß

* **Heft Nr. 13/1983** – „Die Antarktis-Expedition von MS ‚Polarbjörn‘ 1982/83“ (Sommerkampagne zur Atka-Bucht und zu den Kraul-Bergen), zusammengestellt von Heinz Kohnen

* **Sonderheft Nr. 2/1983** – „Die erste Antarktis-Expedition von FS ‚Polarstern‘ (Kapstadt, 20. Januar 1983 – Rio de Janeiro, 25. März 1983)“, Bericht des Fahrtleiters Prof. Dr. Gotthilf Hempel

Sonderheft Nr. 3/1983 – „Sicherheit und Überleben bei Polarexpeditionen“
zusammengestellt von Heinz Kohnen

* **Heft Nr. 14/1983** – „Die erste Antarktis-Expedition (ANTARKTIS I) von FS ‚Polarstern‘ 1982/83“
herausgegeben von Gotthilf Hempel

Sonderheft Nr. 4/1983 – “On the Biology of Krill *Euphausia superba*“ – Proceedings of the Seminar and Report of the Krill Ecology Group, Bremerhaven 12. - 16. May 1983, edited by S. B. Schnack

Heft Nr. 15/1983 – “German Antarctic Expedition 1980/81 with FRV ‘Walther Herwig’ and RV ‘Meteor’“ – First International BIOMASS Experiment (FIBEX) – Data of micronekton and zooplankton hauls
by Uwe Piatkowski and Norbert Klages

Sonderheft Nr. 5/1984 – “The observatories of the Georg von Neumayer Station“, by Ernst Augstein

Heft Nr. 16/1984 – “FIBEX cruise zooplankton data“
by U. Piatkowski, I. Hempel and S. Rakusa-Suszczewski

Heft Nr. 17/1984 – Fahrtbericht (cruise report) der ‚Polarstern‘-Reise ARKTIS I, 1983“
von E. Augstein, G. Hempel und J. Thiede

Heft Nr. 18/1984 – „Die Expedition ANTARKTIS II mit FS ‚Polarstern‘ 1983/84“,
Bericht von den Fahrtabschnitten 1, 2 und 3, herausgegeben von D. Fütterer

Heft Nr. 19/1984 – „Die Expedition ANTARKTIS II mit FS ‚Polarstern‘ 1983/84“,
Bericht vom Fahrtabschnitt 4, Punta Arenas-Kapstadt (Ant-II/4), herausgegeben von H. Kohnen

Heft Nr. 20/1984 – „Die Expedition ARKTIS II des FS ‚Polarstern‘ 1984, mit Beiträgen des FS ‚Valdivia‘ und des Forschungsflugzeuges ‚Falcon 20‘ zum Marginal Ice Zone Experiment 1984 (MIZEX)“
von E. Augstein, G. Hempel, J. Schwarz, J. Thiede und W. Weigel

Heft Nr. 21/1985 – “Euphausiid larvae in plankton from the vicinity of the Antarctic Penisula, February 1982“ by Sigrid Marschall and Elke Mizdalski

Heft Nr. 22/1985 – “Maps of the geographical distribution of macrozooplankton in the Atlantic sector of the Southern Ocean“ by Uwe Piatkowski

Heft Nr. 23/1985 – „Untersuchungen zur Funktionsmorphologie und Nahrungsaufnahme der Larven des Antarktischen Krills *Euphausia superba* Dana“ von Hans-Peter Marschall

Heft Nr. 24/1985 – „Untersuchungen zum Periglazial auf der König-Georg-Insel Südshetlandinseln/ Antarktika. Deutsche physiogeographische Forschungen in der Antarktis. – Bericht über die Kampagne 1983/84" von Dietrich Barsch, Wolf-Dieter Blümel, Wolfgang Flügel, Roland Mäusbacher, Gerhard Stäblein, Wolfgang Zick

- **Heft Nr. 25/1985** – „Die Expedition ANTARKTIS III mit FS ‚Polarstern' 1984/1985" herausgegeben von Gotthilf Hempel.
- **Heft Nr. 26/1985** – "The Southern Ocean"; A survey of oceanographic and marine meteorological research work by Hellmer et al.

Heft Nr. 27/1986 – „Spätpleistozäne Sedimentationsprozesse am antarktischen Kontinentalhang vor Kapp Norvegia, östliche Weddell-See" von Hannes Grobe

Heft Nr. 28/1986 – „Die Expedition ARKTIS III mit ‚Polarstern' 1985 mit Beiträgen der Fahrtteilnehmer, herausgegeben von Rainer Gersonde

- **Heft Nr. 29/1986** – „5 Jahre Schwerpunktprogramm ‚Antarktisforschung' der Deutschen Forschungsgemeisnchaft." Rückblick und Ausblick. Zusammengestellt von Gotthilf Hempel, Sprecher des Schwerpunktprogramms

Heft Nr. 30/1986 – "The Meteorological Data of the Georg-von-Neumayer-Station for 1981 and 1982" by Marianne Gube and Friedrich Obleitner

Heft Nr. 31/1986 – „Zur Biologie der Jugendstadien der Notothenioidei (Pisces) an der Antarktischen Halbinsel" von A. Kellermann

Heft Nr. 32/1986 – „Die Expedition ANTARKTIS IV mit FS ‚Polarstern' 1985/86" mit Beiträgen der Fahrtteilnehmer, herausgegeben von Dieter Fütterer

Heft Nr. 33/1987 – „Die Expedition ANTARKTIS-IV mit FS ‚Polarstern' 1985/86 – Bericht zu den Fahrtabschnitten ANT-IV/3-4" von Dieter Karl Fütterer

Heft Nr. 34/1987 – „Zoogeographische Untersuchungen und Gemeinschaftsanalysen an antarktischen Makroplankton" von U. Piatkowski

Heft Nr. 35/1987 – „Zur Verbreitung des Meso- und Makrozooplanktons in Oberflächenwasser der Weddell See (Antarktis)" von E. Boysen-Ennen

Heft Nr. 36/1987 – „Zur Nahrungs- und Bewegungsphysiologie von *Salpa thompsoni* und *Salpa fusiformis*" von M. Reinke

Heft Nr. 37/1987 – "The Eastern Weddell Sea Drifting Buoy Data Set of the Winter Weddell Sea Project (WWSP)" 1986 by Heinrich Hoeber und Marianne Gube-Lehnhardt

Heft Nr. 38/1987 – "The Meteorological Data of the Georg von Neumayer Station for 1983 and 1984" by M. Gube-Lenhardt

Heft Nr. 39/1987 – „Die Winter-Expedition mit FS ‚Polarstern' in die Antarktis (ANT V/1-3)" herausgegeben von Sigrid Schnack-Schiel

Heft Nr. 40/1987 – "Weather and Synoptic Situation during Winter Weddell Sea Project 1986 (ANT V/2) July 16 - September 10, 1986" by Werner Rabe

Heft Nr. 41/1988 – „Zur Verbreitung und Ökologie der Seegurken im Weddellmeer (Antarktis)" von Julian Gutt

Heft Nr. 42/1988 – "The zooplankton community in the deep bathyal and abyssal zones of the eastern North Atlantic" by Werner Beckmann

Heft Nr. 43/1988 – "Scientific cruise report of Arctic Expedition ARK IV/3" Wissenschaftlicher Fahrtbericht der Arktis-Expedition ARK IV/3, compiled by Jörn Thiede

Heft Nr. 44/1988 – "Data Report for FV 'Polarstern' Cruise ARK IV/1, 1987 to the Arctic and Polar Fronts" by Hans-Jürgen Hirche

Heft Nr. 45/1988 – „Zoogeographie und Gemeinschaftsanalyse des Makrozoobenthos des Weddellmeeres (Antarktis)" von Joachim Voß

Heft Nr. 46/1988 – "Meteorological and Oceanographic Data of the Winter-Weddell-Sea Project 1986 (ANT V/3)" by Eberhard Fahrbach

Heft Nr. 47/1988 – „Verteilung und Herkunft glazial-mariner Gerölle am Antarktischen Kontinentalrand des östlichen Weddellmeeres" von Wolfgang Oskierski

Heft Nr. 48/1988 – „Variationen des Erdmagnetfeldes an der GvN-Station" von Arnold Brodscholl

- **Heft Nr. 49/1988** – „Zur Bedeutung der Lipide im antarktischen Zooplankton" von Wilhelm Hagen

Heft Nr. 50/1988 – „Die gezeitenbedingte Dynamik des Ekström-Schelfeises, Antarktis" von Wolfgang Kobarg

Heft Nr. 51/1988 – „Ökomorphologie notothenüder Fische aus dem Weddellmeer, Antarktis" von Werner Ekau

Heft Nr. 52/1988 – „Zusammensetzung der Bodenfauna in der westlichen Fram-Straße" von Dieter Piepenburg

- **Heft Nr. 53/1988** – „Untersuchungen zur Ökologie des Phytoplanktons im südöstlichen Weddellmeer (Antarktis) im Jan./Febr. 1985" von Eva-Maria Nöthig

Heft Nr. 54/1988 – „Die Fischfauna des östlichen und südlichen Weddellmeeres: geographische Verbreitung, Nahrung und trophische Stellung der Fischarten" von Wiebke Schwarzbach

Heft Nr. 55/1988 – "Weight and length data of zooplankton in the Weddell Sea in austral spring 1986 (Ant. V/3)" by Elke Mizdalski

Heft Nr. 56/1989 – "Scientific cruise report of Arctic expeditions ARK IV/1, 2 & 3" by G. Krause, J. Meinke und J. Thiede

Heft Nr. 57/1989 – „Die Expedition ANTARKTIS V mit FS ‚Polarstern' 1986/87"
Bericht von den Fahrtabschnitten ANT V/4-5 von H. Miller und H. Oerter

• **Heft Nr. 58/1989** – „Die Expedition ANTARKTIS VI mit FS ‚Polarstern' 1987/88"
von D. K. Fütterer

Heft Nr. 59/1989 – „Die Expedition ARKTIS V/1a, 1b und 2 mit FS ‚Polarstern' 1988"
von M. Spindler

Heft Nr. 60/1989 – „Ein zweidimensionales Modell zur thermohalinen Zirkulation unter dem Schelfeis"
von H. H. Hellmer

Heft Nr. 61/1989 – "Die Vulkanite im westlichen und mittleren Neuschwabenland,
Vestfjella und Ahlmannryggen, Antarktika" von M. Peters

• **Heft Nr. 62/1989** – "The Expedition ANTARKTIS VII/1 and 2 (EPOS I) of RV 'Polarstern'
in 1988/89", by I. Hempel

Heft Nr. 63/1989 – „Die Eisalgenflora des Weddellmeeres (Antarktis): Artenzusammensetzung und Biomasse
sowie Ökophysiologie ausgewählter Arten" von Annette Bartsch

Heft Nr. 64/1989 – "Meteorological Data of the G.-v.-Neumayer-Station (Antarctica)" by L. Helmes

Heft Nr. 65/1989 – "Expedition Antarktis VII/3 in 1988/89" by I. Hempel, P. H. Schalk, V. Smetacek

Heft Nr. 66/1989 – „Geomorphologisch-glaziologische Detailkartierung
des arid-hochpolaren Borgmassivet, Neuschwabenland, Antarktika" von Karsten Brunk

Heft Nr. 67/1990 – "Identification key and catalogue of larval Antarctic fishes",
edited by Adolf Kellermann

Heft Nr. 68/1990 – "The Expedition Antarktis VII/4 (Epos leg 3) and VII/5 of RV 'Polarstern' in 1989",
edited by W. Arntz, W. Ernst, I. Hempel

Heft Nr. 69/1990 – „Abhängigkeiten elastischer und rheologischer Eigenschaften des Meereises vom
Eisgefüge", von Harald Hellmann

Heft Nr. 70/1990 – „Die beschalten benthischen Mollusken (Gastropoda und Bivalvia) des
Weddellmeeres, Antarktis", von Stefan Hain

Heft Nr. 71/1990 – „Sedimentologie und Paläomagnetik an Sedimenten der Maudkuppe (Nordöstliches
Weddellmeer)", von Dieter Cordes

Heft Nr. 72/1990 – "Distribution and abundance of planktonic copepods (Crustacea) in the Weddell Sea
in summer 1980/81", by F. Kurbjeweit and S. Ali-Khan

Heft Nr. 73/1990 – „Zur Frühdiagenese von organischem Kohlenstoff und Opal in Sedimenten des südlichen
und östlichen Weddellmeeres", von M. Schlüter

Heft Nr. 74/1990 – „Expeditionen ANTARKTIS-VIII/3 und VIII/4 mit FS ‚Polarstern' 1989"
von Rainer Gersonde und Gotthilf Hempel

Heft Nr. 75/1991 – „Quartäre Sedimentationsprozesse am Kontinentalhang des Süd-Orkey-Plateaus im
nordwestlichen Weddellmeer (Antarktis)", von Sigrun Grünig

Heft Nr. 76/1990 – „Ergebnisse der faunistischen Arbeiten im Benthal von King George Island
(Südshetlandinseln, Antarktis)", von Martin Rauschert

Heft Nr. 77/1990 – „Verteilung von Mikroplankton-Organismen nordwestlich der Antarktischen Halbinsel
unter dem Einfluß sich ändernder Umweltbedingungen im Herbst", von Heinz Klöser

Heft Nr. 78/1991 – „Hochauflösende Magnetostratigraphie spätquartärer Sedimente arktischer
Meeresgebiete", von Norbert R. Nowaczyk

Heft Nr. 79/1991 – „Ökophysiologische Untersuchungen zur Salinitäts- und Temperaturtoleranz
antarktischer Grünalgen unter besonderer Berücksichtigung des β-Dimethylsulfoniumpropionat
(DMSP) - Stoffwechsels", von Ulf Karsten

Heft Nr. 80/1991 – „Die Expedition ARKTIS VII/1 mit FS ‚Polarstern' 1990",
herausgegeben von Jörn Thiede und Gotthilf Hempel

Heft Nr. 81/1991 – „Paläoglaziologie und Paläozeanographie im Spätquartär am Kontinentalrand des
südlichen Weddelmeeres, Antarktis", von Martin Melles

Heft Nr. 82/1991 – „Quantifizierung von Meereseigenschaften: Automatische Bildanalyse von
Dünnschnitten und Parametisierung von Chlorophyll- und Salzgehaltsverteilungen", von Hajo Eicken

Heft Nr. 83/1991 – „Das Fließen von Schelfeisen - numerische Simulationen
mit der Metholde der finiten Differenzen", von Jürgen Determann

Heft Nr. 84/1991 – „Die Expedition ANTARKTIS-VIII/1-2, 1989 mit der Winter Weddell Gyre Study
der Forschungsschiffe ‚Polarstern' und ‚Akademik Fedorov'", von Ernst Augstein,
Nikolai Bagriantsev und Hans Werner Schenke

Heft Nr. 85/1991 – „Zur Entstehung von Unterwassereis und das Wachstum und die Energiebilanz
des Meereises in der Atka Bucht, Antarktis", von Josef Kipfstuhl

Heft Nr. 86/1991 – „Die Expedition ANTARKTIS-VIII mit FS ‚Polarstern' 1989/90. Bericht vom
Fahrtabschnitt ANT-VIII/5", von Heinz Miller und Hans Oerter

Heft Nr. 87/1991 – "Scientific cruise reports of Arctic expeditions ARK VI/1-4 of RV 'Polarstern'
in 1989", edited by G. Krause, J. Meincke & H. J. Schwarz

Heft Nr. 88/1991 – „Zur Lebensgeschichte dominanter Copepodenarten (*Calanus finmarchicus,
C. glacialis, C. hyperboreus, Metridia longa*) in der Framstraße", von Sabine Diel

Heft Nr. 89/1991 – „Detaillierte seismische Untersuchungen am östlichen Kontinentalrand des Weddell-Meeres vor Kapp Norvegia, Antarktis", von Norbert E. Kaul

Heft Nr. 90/1991 – „Die Expedition ANTARKTIS-VIII mit FS ‚Polarstern' 1989/90. Bericht von den Fahrtabschnitten ANT-VIII/6-7", herausgegeben von Dieter Karl Fütterer und Otto Schrems

Heft Nr. 91/1991 – "Blood physiology and ecological consequences in Weddell Sea fishes (Antarctica)", by Andreas Kunzmann

Heft Nr. 92/1991 – „Zur sommerlichen Verteilung des Mesozooplanktons im Nansen-Becken, Nordpolarmeer", von Nicolai Mumm

Heft Nr. 93/1991 – „Die Expedition ARKTIS VII mit FS ‚Polarstern', 1990. Bericht vom Fahrtabschnitt ARK VII/2", herausgegeben von Gunther Krause

Heft Nr. 94/1991 – „Die Entwicklung des Phytoplanktons im östlichen Weddellmeer (Antarktis) beim Übergang vom Spätwinter zum Frühjahr", von Renate Scharek

Heft Nr. 95/1991 – „Radioisotopenstratigraphie, Sedimentologie und Geochemie jungquartärer Sedimente des östlichen Arktischen Ozeans", von Horst Bohrmann

Heft Nr. 96/1991 – „Holozäne Sedimentationsentwicklung im Scoresby Sund, Ost-Grönland", von Peter Marienfeld

Heft Nr. 97/1991 – „Strukturelle Entwicklung und Abkühlungsgeschichte von Heimefrontfjella (Westliches Dronning Maud Land/Antarktika)", von Joachim Jacobs

Heft Nr. 98/1991 – „Zur Besiedlungsgeschichte des antarktischen Schelfes am Beispiel der Isopoda (Crustacea, Malacostraca)", von Angelika Brandt

Heft Nr. 99/1992 – "The Antarctic ice sheet and environmental change: a three-dimensional modelling study", by Philippe Huybrechts

* **Heft Nr. 100/1992** – „Die Expeditionen ANTARKTIS IX/1-4 des Forschungsschiffes ‚Polarstern' 1990/91" herausgegeben von Ulrich Bathmann, Meinhard Schulz-Baldes, Eberhard Fahrbach, Victor Smetacek und Hans-Wolfgang Hubberten

Heft Nr. 101/1992 – „Wechselbeziehungen zwischen Schwermetallkonzentrationen (Cd, Cu, Pb, Zn) im Meerwasser und in Zooplanktonorganismen (Copepoda) der Arktis und des Atlantiks", von Christa Pohl

Heft Nr. 102/1992 – „Physiologie und Ultrastruktur der antarktischen Grünalge *Prasiola crispa ssp. antarctica* unter osmotischem Streß und Austrocknung", von Andreas Jacob

Heft Nr. 103/1992 – „Zur Ökologie der Fische im Weddellmeer", von Gerd Hubold

Heft Nr. 104/1992 – „Mehrkanalige adaptive Filter für die Unterdrückung von multiplen Reflexionen in Verbindung mit der freien Oberfläche in marinen Seismogrammen", von Andreas Rosenberger

Heft Nr. 105/1992 – "Radiation and Eddy Flux Experiment 1991 *(REFLEX I)*", von Jörg Hartmann, Christoph Kottmeier und Christian Wamser

Heft Nr. 106/1992 – „Ostracoden im Epipelagial vor der Antarktischen Halbinsel - ein Beitrag zur Systematik sowie zur Verbreitung und Populationsstruktur unter Berücksichtigung der Saisonalität", von Rüdiger Kock

Heft Nr. 107/1992 – „ARCTIC '91: Die Expedition ARK-VIII/3 mit FS ‚Polarstern' 1991", von Dieter K. Fütterer

Heft Nr. 108/1992 – „Dehnungsbeben an einer Störungszone im Ekström-Schelfeis nördlich der Georg-von-Neumayer-Station, Antarktis. – Eine Untersuchung mit seismologischen und geodätischen Methoden", von Uwe Nixdorf.

Heft Nr. 109/1992 – „Spätquartäre Sedimentation am Kontinentalrand des südöstlichen Weddellmeeres, Antarktis", von Michael Weber.

Heft Nr. 110/1992 – „Sedimentfazies und Bodenwasserstrom am Kontinentalhang des nordwestlichen Weddellmeeres", von Isa Brehme.

Heft Nr. 111/1992 – „Die Lebensbedingungen in den Solekanälchen des antarktischen Meereises", von Jürgen Weissenberger.

Heft Nr. 112/1992 – „Zur Taxonomie von rezenten benthischen Foraminiferen aus dem Nansen Becken, Arktischer Ozean", von Jutta Wollenburg.

Heft Nr. 113/1992 – „Die Expedition ARKTIS VIII/1 mit FS ‚Polarstern' 1991", herausgegeben von Gerhard Kattner.

* **Heft Nr. 114/1992** – „Die Gründungsphase deutscher Polarforschung, 1865 - 1875", von Reinhard A. Krause.

Heft Nr. 115/1992 – "Scientific Cruise Report of the 1991 Arctic Expedition ARK VIII/2 of RV 'Polarstern' (EPOS II)", by Eike Rachor.

Heft Nr. 116/1992 – "The Meteorological Data of the Georg-von-Neumayer-Station (Antarctica) for 1988, 1989, 1990 and 1991", by Gert König-Langlo.

Heft Nr. 117/1992 – „Petrogenese des metamorphen Grundgebirges der zentralen Heimefrontfjella (westliches Dronning Maud Land / Antarktis)", von Peter Schulze.

Heft Nr. 118/1993 – „Die mafischen Gänge der Shackleton Range / Antarktika: Petrographie, Geochemie, Isotopengeochemie und Paläomagnetik", von Rüdiger Hotten.

* **Heft Nr. 119/1993** – „Gefrierschutz bei Fischen der Polarmeere", von Andreas P. A. Wöhrmann.

* **Heft Nr. 120/1993** – "East Siberian Arctic Region Expedition '92: The Laptev Sea - its Significance for Arctic Sea-Ice Formation and Transpolar Sediment Flux", by D. Dethleff, D. Nürnberg, E. Reimnitz, M. Saarso and Y. P. Sacchenko. – "Expedition to Novaja Zemlja and Franz Josef Land with RV. 'Dalnie Zelentsy'", by D. Nürnberg and E. Groth.

* **Heft Nr. 121/1993** – „Die Expedition ANTARKTIS X/3 mit FS ‚Polarstern' 1992", herausgegeben von Michael Spindler, Gerhard Dieckmann und David Thomas

Heft Nr. 122/1993 – „Die Beschreibung der Korngestalt mit Hilfe der Fourier-Analyse: Parametrisierung der morphologischen Eigenschaften von Sedimentpartikeln", von Michael Diepenbroek.

* **Heft Nr. 123/1993** – „Zerstörungsfreie hochauflösende Dichteuntersuchungen mariner Sedimente", von Sebastian Gerland.

Heft Nr. 124/1993 – „Umsatz und Verteilung von Lipiden in arktischen marinen Organismen unter besonderer Berücksichtigung unterer trophischer Stufen", von Martin Graeve.

Heft Nr. 125/1993 – „Ökologie und Respiration ausgewählter arktischer Bodenfischarten", von Christian F. von Dorrien.

Heft Nr. 126/1993 – „Quantitative Bestimmung von Paläoumweltparametern des Antarktischen Oberflächenwassers im Spätquartier anhand von Transferfunktionen mit Diatomeen", von Ulrich Zielinski

Heft Nr. 127/1993 – „Sedimenttransport durch das arktische Meereis: Die rezente lithogene und biogene Materialfracht", von Ingo Wollenburg.

Heft Nr. 128/1993 – "Cruise ANTARKTIS X/3 of RV 'Polarstern': CTD-Report", von Marek Zwierz.

Heft Nr. 129/1993 – „Reproduktion und Lebenszyklen dominanter Copepodenarten aus dem Weddellmeer, Antarktis", von Frank Kurbjeweit

Heft Nr. 130/1993 – „Untersuchungen zu Temperaturregime und Massenhaushalt des Filchner-Ronne-Schelfeises, Antarktis, unter besonderer Berücksichtigung von Anfrier- und Abschmelzprozessen", von Klaus Grosfeld

Heft Nr. 131/1993 – „Die Expedition ANTARKTIS X/5 mit FS ‚Polarstern' 1992", herausgegeben von Rainer Gersonde

Heft Nr. 132/1993 – „Bildung und Abgabe kurzkettiger halogenierter Kohlenwasserstoffe durch Makroalgen der Polarregionen", von Frank Laturnus

Heft Nr. 133/1994 – "Radiation and Eddy Flux Experiment 1993 *(REFLEX II)*", by Christoph Kottmeier, Jörg Hartmann, Christian Wamser, Axel Bochert, Christof Lüpkes, Dietmar Freese and Wolfgang Cohrs

* **Heft Nr. 134/1994** – "The Expedition ARKTIS-IX/1", edited by Hajo Eicken and Jens Meincke

Heft Nr. 135/1994 – „Die Expeditionen ANTARKTIS X/6-8", herausgegeben von Ulrich Bathmann, Victor Smetacek, Hein de Baar, Eberhard Fahrbach und Gunter Krause

Heft Nr. 136/1994 – „Untersuchungen zur Ernährungsökologie von Kaiserpinguinen *(Aptenodytes forsteri)* und Königspinguinen *(Aptenodytes patagonicus)*", von Klemens Pütz

* **Heft Nr. 137/1994** – „Die känozoische Vereisungsgeschichte der Antarktis", von Werner U. Ehrmann

Heft Nr. 138/1994 – „Untersuchungen stratosphärischer Aerosole vulkanischen Ursprungs und polarer stratosphärischer Wolken mit einem Mehrwellenlängen-Lidar auf Spitzbergen *(79° N, 12° E)*", von Georg Beyerle

Heft Nr. 139/1994 – „Charakterisierung der Isopodenfauna (Crustacea, Malacostraca) des Scotia-Bogens aus biogeographischer Sicht: Ein multivariater Ansatz", von Holger Winkler.

Heft Nr. 140/1994 – „Die Expedition ANTARKTIS X/4 mit FS ‚Polarstern' 1992", herausgegeben von Peter Lemke

Heft Nr. 141/1994 – „Satellitenaltimetrie über Eis – Anwendung des GEOSAT-Altimeters über dem Ekströmisen, Antarktis", von Clemens Heidland

Heft Nr. 142/1994 – "The 1993 Northeast Water Expedition. Scientific cruise report of RV 'Polartstern' Arctic cruises ARK IX/2 and 3, USCG 'Polar Bear' cruise NEWP and the NEWLand expedition", edited by Hans-Jürgen Hirche and Gerhard Kattner

Heft Nr. 143/1994 – „Detaillierte refraktionsseismische Untersuchungen im inneren Scoresby Sund Ost-Grönland", von Notker Fechner

Heft Nr. 144/1994 – "Russian-German Cooperation in the Siberian Shelf Seas: Geo-System Laptev Sea", edited by Heidemarie Kassens, Hans-Wolfgang Hubberten, Sergey M. Pryamikov and Rüdiger Stein

* **Heft Nr. 145/1994** – "The 1993 Northeast Water Expedition. Data Report of RV ‚Polarstern' Arctic Cruises IX/2 and 3", edited by Gerhard Kattner and Hans-Jürgen Hirche.

Heft Nr. 146/1994 – "Radiation Measurements at the German Antarctic Station Neumayer 1982 - 1992", by Torsten Schmidt and Gerd König-Langlo.

Heft Nr. 147/1994 – „Krustenstrukturen und Verlauf des Kontinentalrandes im Weddell-Meer / Antarktis", von Christian Hübscher.

Heft Nr. 148/1994 – "The expeditions NORILSK/TAYMYR 1993 and BUNGER OASIS 1993/94 of the AWI Research Unit Potsdam", edited by Martin Melles.

** **Heft Nr. 149/1994** – „Die Expedition ARCTIC '93. Der Fahrtabschnitt ARK-IX/4 mit FS ‚Polarstern' 1993", herausgegeben von Dieter K. Fütterer.

Heft Nr. 150/1994 – „Der Energiebedarf der Pygoscelis-Pinguine: eine Synopse", von Boris M. Culik.

Heft Nr. 151/1994 – "Russian-German Cooperation: The Transdrift I Expedition to the Laptev Sea", edited by Heidemarie Kassens and Valeriy Y. Karpiy.

Heft Nr. 152/1994 – „Die Expedition ANTARKTIS-X mit FS ‚Polarstern' 1992. Bericht von den Fahrtabschnitten / ANT-X / 1a und 2", herausgegeben von Heinz Miller.

Heft Nr. 153/1994 – „Aminosäuren und Huminstoffe im Stickstoffkreislauf polarer Meere", von Ulrike Hubberten.

Heft Nr. 154/1994 – "Regional and seasonal variability in the vertical distribution of mesozooplankton in the Greenland Sea", by Claudio Richter.

Heft Nr. 155/1995 – „Benthos in polaren Gewässern", herausgegeben von Christian Wiencke und Wolf Arntz.
Heft Nr. 156/1995 – "An adjoint model for the determination of the mean oceanic circulation, air-sea fluxes and mixing coefficients", by Reiner Schlitzer.
Heft Nr. 157/1995 – „Biochemische Untersuchungen zum Lipidstoffwechsel antarktischer Copepoden", von Kirsten Fahl.
Heft Nr. 158/1995 – „Die Deutsche Polarforschung seit der Jahrhundertwende und der Einfluß Erich von Drygalskis", von Cornelia Lüdecke.
Heft Nr. 159/1995 – "The distribution of $\partial^{18}O$ in the Arctic Ocean: Implications for the freshwater balance of the halocline and the sources of deep and bottom waters", by Dorothea Bauch.
Heft Nr. 160/1995 – „Rekonstruktion der spätquartären Tiefenwasserzirkulation und Produktivität im östlichen Südatlantik anhand von benthischen Foraminiferenvergesellschaftungen", von Gerhard Schmiedl.
Heft Nr. 161/1995 – „Der Einfluß von Salinität und Lichtintensität auf die Osmolytkonzentrationen, die Zellvolumina und die Wachstumsraten der antarktischen Eisdiatomeen *Chaetoceros sp.* und *Navicula sp.* unter besonderer Berücksichtigung der Aminosäure Prolin", von Jürgen Nothnagel.
Heft Nr. 162/1995 – „Meereistransportiertes lithogenes Feinmaterial in spätquartären Tiefseesedimenten des zentralen östlichen Arktischen Ozeans und der Framstraße", von Thomas Letzig.
Heft Nr. 163/1995 – „Die Expedition ANTARKTIS-XI/2 mit FS ‚Polarstern' 1993/94", herausgegeben von Rainer Gersonde.
Heft Nr. 164/1995 – „Regionale und altersabhängige Variation gesteinsmagnetischer Parameter in marinen Sedimenten der Arktis", von Thomas Frederichs.
Heft Nr. 165/1995 – „Vorkommen, Verteilung und Umsatz biogener organischer Spurenstoffe: Sterole in antarktischen Gewässern", von Georg Hanke.
Heft Nr. 166/1995 – „Vergleichende Untersuchungen eines optimierten dynamisch-thermodynamischen Meereismodells mit Beobachtungen im Weddellmeer", von Holger Fischer.
Heft Nr. 167/1995 – „Rekonstruktionen von Paläo-Umweltparametern anhand von stabilen Isotopen und Faunen-Vergesellschaftungen planktischer Foraminiferen im Südatlantik", von Hans-Stefan Niebler
Heft Nr. 168/1995 – „Die Expedition ANTARKTIS XII mit FS ‚Polarstern' 1993/94. Bericht von den Fahrtabschnitten ANT XII/1 und 2", herausgegeben von Gerhard Kattner und Dieter Karl Fütterer
Heft Nr. 169/1995 – „Medizinische Untersuchung zur Circadianrhythmik und zum Verhalten bei Überwinterern auf einer antarktischen Forschungsstation", von Hans Wortmann
Heft-Nr. 170/1995 – DFG-Kolloquium: Terrestrische Geowissenschaften -- Geologie und Geophysik der Antarktis.
Heft Nr. 171/1995 – „Strukturentwicklung und Petrogenese des metamorphen Grundgebirges der nördlichen Heimfrontfjella (westliches Dronning Maud Land/Antarktika)", von Wilfried Bauer.
Heft Nr. 172/1995 – „Die Struktur der Erdkruste im Bereich des Scoresby Sund, Ostgrönland: Ergebnisse refraktionsseismischer und gravimetrischer Untersuchungen", von Holger Mandler.
Heft Nr. 173/1995 – „Paläozoische Akkretion am paläopazifischen Kontinentalrand der Antarktis in Nordvictorialand – P-T-D-Geschichte und Deformationsmechanismen im Bowers Terrane", von Stefan Matzer.
Heft Nr. 174/1995 – "The Expedition ARKTIS-X/2 of RV 'Polarstern' in 1994", edited by Hans-W. Hubberten
Heft Nr. 175/1995 – "Russian-German Cooperation: The Expedition TAYMYR 1994", edited by Christine Siegert and Gmitry Bolshiyanov.
Heft Nr. 176/1995 – "Russian-German Cooperation: Laptev Sea System", edited by Heidemarie Kassens, Dieter Piepenburg, Jörn Thiede, Leonid Timokhov, Hans-Wolfgang Hubberten and Sergey M. Priamikov.
Heft Nr. 177/1995 – „Organischer Kohlenstoff in spätquartären Sedimenten des Arktischen Ozeans: Terrigener Eintrag und marine Produktivität", von Carsten J. Schubert
Heft Nr. 178/1995 – "Cruise ANTARKTIS XII/4 of RV 'Polarstern' in 1995: CTD-Report", by Jüri Sildam.
Heft Nr. 179/1995 – „Benthische Foraminiferenfaunen als Wassermassen-, Produktions- und Eisdriftanzeiger im Arktischen Ozean", von Jutta Wollenburg.
Heft Nr. 180/1995 – „Biogenopal und biogenes Barium als Indikatoren für spätquartäre Produktivitätsänderungen am antarktischen Kontinentalhang, atlantischer Sektor", von Wolfgang J. Bonn.
Heft Nr. 181/1995 – „Die Expedition ARKTIS X/1 des Forschungsschiffes ‚Polarstern' 1994", herausgegeben von Eberhard Fahrbach.
Heft Nr. 182/1995 – "Laptev Sea System: Expeditions in 1994", edited by Heidemarie Kassens.
Heft Nr. 183/1996 – „Interpretation digitaler Parasound Echolotaufzeichnungen im östlichen Arktischen Ozean auf der Grundlage physikalischer Sedimenteigenschaften", von Uwe Bergmann.
Heft Nr. 184/1996 – "Distribution and dynamics of inorganic nitrogen compounds in the troposphere of continental, coastal, marine and Arctic areas", by Maria Dolores Andrés Hernández.
Heft Nr. 185/1996 – „Verbreitung und Lebensweise der Aphroditen und Polynoiden (Polychaeta) im östlichen Weddellmeer und im Lazarevmeer (Antarktis)", von Michael Stiller.
Heft Nr. 186/1996 – "Reconstruction of Late Quaternary environmental conditions applying the natural radionuclides ^{230}Th, ^{10}Be, ^{231}Pa and ^{233}U: A study of deep-sea sediments from the eastern sector of the Antarctic Circumpolar Current System", by Martin Frank.
Heft Nr. 187/1996 – "The Meteorological Data of the Neumayer Station (Antarctica) for 1992, 1993 and 1994", by Gert König-Langlo and Andreas Herber.
Heft Nr. 188/1996 – „Die Expedition ANTARKTIS-XI/3 mit FS ‚Polarstern' 1994", herausgegeben von Heinz Miller und Hannes Grobe.
Heft Nr. 189/1996 – „Die Expedition ARKTIS-VII/3 mit FS ‚Polarstern' 1990", herausgegeben von Heinz Miller und Hannes Grobe

Heft Nr. 190/1996 – "Cruise report of the Joint Chilean-German-Italian Magellan ‚Victor Hensen' Campaign in 1994", edited by Wolf Arntz and Matthias Gorny.

Heft Nr. 191/1996 – „Leitfähigkeits- und Dichtemessung an Eisbohrkernen", von Frank Wilhelms.

Heft Nr. 192/1996 – „Photosynthese-Charakteristika und Lebensstrategie antarktischer Makroalgen", von Gabriele Weykam.

Heft Nr. 193/1996 – „Heterogene Reaktionen von N_2O_5 und Hbr und ihr Einfluß auf den Ozonabbau in der polaren Stratosphäre", von Sabine Seisel.

Heft Nr. 194/1996 – „Ökologie und Populationsdynamik antarktischer Ophiuroiden (Echinodermata)", von Corinna Dahm.

Heft Nr. 195/1996 – „Die planktische Foraminifere *Neogloboquadrina pachyderma* (Ehrenberg) im Weddellmeer, Antarktis", von Doris Berberich.

Heft Nr. 196/1996 – „Untersuchungen zum Beitrag chemischer und dynamischer Prozesse zur Variabilität des stratosphärischen Ozons über der Arktis", von Birgit Heese

Heft Nr. 197/1996 – "The Expedition ARKTIS-XI/2 of 'Polarstern' in 1995", edited by Gunther Krause.

Heft Nr. 198/1996 – „Geodynamik des Westantarktischen Riftsystems basierend auf Apatit-Spaltspuranalysen", von Frank Lisker.

Heft Nr. 199/1996 – "The 1993 Northeast Water Expedition. Data Report on CTD Measurements of RV 'Polarstern' Cruises ARKTIS IX/2 and 3", by Gerion Budéus and Wolfgang Schneider.

Heft Nr. 200/1996 – "Stability of the Thermohaline Circulation in analytical and numerical models", by Gerrit Lohmann.

Heft Nr. 201/1996 – „Trophische Beziehungen zwischen Makroalgen und Herbivoren in der Potter Cove (King George-Insel, Antarktis)", von Katrin Iken.

Heft Nr. 202/1996 – „Zur Verbreitung und Respiration ökologisch wichtiger Bodentiere in den Gewässern um Svalbard (Arktis)", von Michael K. Schmid.

Heft Nr. 203/1996 – „Dynamik, Rauhigkeit und Alter des Meereises in der Arktis – Numerische Untersuchungen mit einem großskaligen Modell", von Markus Harder.

Heft Nr. 204/1996 – „Zur Parametrisierung der stabilen atmosphärischen Grenzschicht über einem antarktischen Schelfeis", von Dörthe Handorf.

Heft Nr. 205/1996 – "Textures and fabrics in the GRIP ice core, in relation to climate history and ice deformation", by Thorsteinn Thorsteinsson.

Heft Nr. 206/1996 – „Der Ozean als Teil des gekoppelten Klimasystems: Versuch der Rekonstruktion der glazialen Zirkulation mit verschieden komplexen Atmosphärenkomponenten", von Kerstin Fieg.

Heft Nr. 207/1996 – „Lebensstrategien dominanter antarktischer Oithonidae (Cyclopoida, Copepoda) und Oncaeidae (Poecilostomatoida, Copepoda) im Bellingshausenmeer", von Cornelia Metz.

Heft Nr. 208/1996 – „Atmosphäreneinfluß bei der Fernerkundung von Meereis mit passiven Mikrowellenradiometern", von Christoph Oelke.

Heft Nr. 209/1996 – „Klassifikation von Radarsatellitendaten zur Meereiserkennung mit Hilfe von LIne-Scanner-Messungen", von Axel Bochert.

Heft Nr. 210/1996 – „Die mit ausgewählten Schwämmen (Hexactinellida und Demospongiae) aus dem Weddellmeer, Antarktis, vergesellschaftete Fauna", von Kathrin Kunzmann.

Heft Nr. 211/1996 – "Russian-German Cooperation: The Expedition TAYMYR 1995 and the Expedition KOLYMA 1995", by Dima Yu. Bolshiyanov and Hans-W. Hubberten.

Heft Nr. 212/1996 – "Surface-sediment composition and sedimentary processes in the central Arctic Ocean and along the Eurasian Continental Margin", by Ruediger Stein, Gennadij I. Ivanov, Michael A. Levitan, and Kirsten Fahl.

Heft Nr. 213/1996 – „Gonadenentwicklung und Eiproduktion dreier *Calanus*-Arten (Copepoda): Freilandbeobachtungen, Histologie und Experimente", von Barbara Niehoff

Heft Nr. 214/1996 – „Numerische Modellierung der Übergangszone zwischen Eisschild und Eisschelf", von Christoph Mayer.

Heft Nr. 215/1996 – „Arbeiten der AWI-Forschungsstelle Potsdam in Antarktika, 1994/95", herausgegeben von Ulrich Wand.

Heft Nr. 216/1996 – „Rekonstruktion quartärer Klimaänderungen im atlantischen Sektor des Südpolarmeeres anhand von Radiolarien", von Uta Brathauer.

Heft Nr. 217/1996 – „Adaptive Semi-Lagrange-Finite-Elemente-Methode zur Lösung der Flachwassergleichungen: Implementierung und Parallelisierung", von Jörn Behrens.

Heft Nr. 218/1997 – "Radiation and Eddy Flux Experiment 1995 (REFLEX III)", by Jörg Hartmann, Axel Bochert, Dietmar Freese, Christoph Kottmeier, Dagmar Nagel and Andreas Reuter.

Heft Nr. 219/1997 – „Die Expedition ANTARKTIS-XII mit FS ‚Polarstern' 1995. Bericht vom Fahrtabschnitt ANT-XII/3, herausgegeben von Wilfried Jokat und Hans Oerter.

Heft Nr. 220/1997 – „Ein Beitrag zum Schwerefeld im Bereich des Weddellmeeres, Antarktis. Nutzung von Altimetermessungen des GEOSAT und ERS-1", von Tilo Schöne.

Heft Nr. 221/1997 – „Die Expeditionen ANTARKTIS-XIII/1-2 des Forschungsschiffes ‚Polarstern' 1995/96", herausgegeben von Ulrich Bathmann, Mike Lukas und Victor Smetacek.

Heft Nr. 222/1997 – "Tectonic Structures and Glaciomarine Sedimentation in the South-Eastern Weddell Sea from Seismic Reflection Data", by László Oszkó.

Heft Nr. 223/1997 – „Bestimmung der Meereisdicke mit seismischen und elektromagnetisch-induktiven Verfahren", von Christian Haas.

Heft Nr. 224/1997 – „Troposphärische Ozonvariationen in Polarregionen", von Silke Wessel.

Heft Nr. 225/1997 – „Biologische und ökologische Untersuchungen zur kryopelagischen Amphipodenfauna des arktischen Meereises", von Michael Poltermann.

Heft Nr. 226/1997 – "Scientific Cruise Report of the Arctic Expedition ARK-XI/1 of RV 'Polarstern' in 1995", edited by Eike Rachor.

Heft Nr. 227/1997 – „Der Einfluß kompatibler Substanzen und Kryoprotektoren auf die Enzyme Malatdehydrogenase (MDH) und Glucose-6-phosphat-Dehydrogenase (G6P-DH) aus *Acrosiphonia arcta* (Chlorophyta) der Arktis", von Katharina Kück.

Heft Nr. 228/1997 – „Die Verbreitung epibenthischer Mollusken im chilenischen Beagle-Kanal", von Katrin Linse.

Heft Nr. 229/1997 – „Das Mesozooplankton im Laptevmeer und östlichen Nansen-Becken - Verteilung und Gemeinschaftsstrukturen im Spätsommer", von Hinrich Hanssen.

Heft Nr. 230/1997 – „Modell eines adaptierbaren, rechnergestützten, wissenschaftlichen Arbeitsplatzes am Alfred-Wegener-Institut für Polar- und Meeresforschung", von Lutz-Peter Kurdelski

Heft Nr. 231/1997 – „Zur Ökologie arktischer und antarktischer Fische: Aktivität, Sinnesleistungen und Verhalten", von Christopher Zimmermann

Heft Nr. 232/1997 – „Persistente chlororganische Verbindungen in hochantarktischen Fischen", von Stephan Zimmermann

Heft Nr. 233/1997 – „Zur Ökologie des Dimethylsulfoniumpropionat (DMSP)-Gehaltes temperierter und polarer Phytoplanktongemeinschaften im Vergleich mit Laborkulturen der Coccolithophoride *Emiliania huxleyi* und der antarktischen Diatomee *Nitzschia lecointei*", von Doris Meyerdierks.

Heft Nr. 234/1997 – „Die Expedition ARCTIC '96 des FS ‚Polarstern' (ARK XIII) mit der Arctic Climate System Study (ACSYS)", von Ernst Augstein und den Fahrtteilnehmern.

Heft Nr. 235/1997 – „Polonium-210 und Blei-219 im Südpolarmeer: Natürliche Tracer für biologische und hydrographische Prozesse im Oberflächenwasser des Antarktischen Zirkumpolarstroms und des Weddellmeeres", von Jana Friedrich

Heft Nr. 236/1997 – "Determination of atmospheric trace gas amounts and corresponding natural isotopic ratios by means of ground-based FTIR spectroscopy in the high Arctic", by Arndt Meier.

Heft Nr. 237/1997 – "Russian-German Cooperation: The Expedition TAYMYR/SEVERNAYA ZEMLYA 1996", edited by Martin Melles, Birgit Hagedorn and Dmitri Yu. Bolshiyanov

Heft Nr. 238/1997 – "Life strategy and ecophysiology of Antarctic macroalgae", by Iván M. Gómez.

Heft Nr. 239/1997 – „Die Expedition ANTARKTIS XIII/4-5 des Forschungsschiffes ‚Polarstern' 1996", herausgegeben von Eberhard Fahrbach und Dieter Gerdes.

Heft Nr. 240/1997 – „Untersuchungen zur Chrom-Speziation in Meerwasser, Meereis und Schnee aus ausgewählten Gebieten der Arktis", von Heide Giese.

Heft Nr. 241/1997 – "Late Quaternary glacial history and paleoceanographic reconstructions along the East Greenland continental margin: Evidence from high-resolution records of stable isotopes and ice-rafted debris", by Seung-Il Nam.

Heft Nr. 242/1997 – "Thermal, hydrological and geochemical dynamics of the active layer at a continuous permafrost site, Taymyr Peninsula, Siberia", by Julia Boike.

Heft Nr. 243/1997 – „Zur Paläoozeanographie hoher Breiten: Stellvertreterdaten aus Foraminiferen", von Andreas Mackensen.

Heft Nr. 244/1997 – "The Geophysical Observatory at Neumayer Station, Antarctica, Geomagnetic and seismological observations in 1995 and 1996", by Alfons Eckstaller, Thomas Schmidt, Viola Graw, Christian Müller and Johannes Rogenhagen.

Heft Nr. 245/1997 – „Temperaturbedarf und Biogeographie mariner Makroalgen - Anpassung mariner Makroalgen an tiefe Temperaturen, von Bettina Bischoff-Bäsmann.

Heft Nr. 246/1997 – „Ökologische Untersuchungen zur Fauna des arktischen Meereises", von Christine Friedrich.

Heft Nr. 247/1997 – „Entstehung und Modifizierung von marinen gelösten organischen Substanzen", von Berit Kirchhoff.

Heft Nr. 248/1997 – "Laptev Sea System: Expeditions in 1995", edited by Heidemarie Kassens.

Heft Nr. 249/1997 – "The Expedition ANTARKTIS XIII/3 (EASIZ I) of RV 'Polarstern' to the eastern Weddell Sea in 1996", edited by Wolf Arntz and Julian Gutt.

Heft Nr. 250/1997 – „Vergleichende Untersuchungen zur Ökologie und Biodiversität des Mega-Epibenthos der Arktis und Antarktis", von Adreas Starmans.

Heft Nr. 251/1997 – „Zeitliche und räumliche Verteilung von Mineralvergesellschaftungen in spätquartären Sedimenten des Arktischen Ozeans und ihre Nützlichkeit als Klimaindikatoren während der Glazial/Interglazial-Wechsel", von Christoph Vogt.

Heft Nr. 252/1997 – „Solitäre Ascidien in der Potter Cove (King George Island, Antarktis). Ihre ökologische Bedeutung und Populationsdynamik", von Stephan Kühne.

Heft Nr. 253/1997 – "Distribution and role of microprotozoa in the Southern Ocean", by Christine Klaas.

Heft Nr. 254/1997 – „Die spätquartäre Klima- und Umweltgeschichte der Bunger-Oase, Ostantarktis", von Thomas Kulbe

Heft Nr. 255/1997 – "Scientific Cruise Report of the Arctic Expedition ARK-XIII/2 of RV 'Polarstern' in 1997", edited by Ruediger Stein and Kirsten Fahl.

Heft Nr. 256/1998 – „Das Radionuklid Tritium im Ozean: Meßverfahren und Verteilung von Tritium im Südatlantik und im Weddellmeer", von Jürgen Sültenfuß.

Heft Nr. 257/1998 – „Untersuchungen der Saisonalität von atmosphärischem Dimethylsulfid in der Arktis und Antarktis", von Christoph Kleefeld.

Heft Nr. 258/1998 – „Bellingshausen- und Amundsenmeer: Entwicklung eines Sedimentationsmodells", von Frank-Oliver Nitsche.

Heft Nr. 259/1998 – "The Expedition ANTARKTIS-XIV/4 of RV 'Polarstern' in 1997", by Dieter K. Fütterer.

Heft Nr. 260/1998 – „Die Diatomeen der Laptevsee (Arktischer Ozean): Taxonomie und biogeographische Verbreitung", von Holger Cremer

Heft Nr. 261/1998 – „Die Krustenstruktur und Sedimentdecke des Eurasischen Beckens, Arktischer Ozean: Resultate aus seismischen und gravimetrischen Untersuchungen", von Estella Weigelt.

Heft Nr. 262/1998 – "The Expedition ARKTIS-XIII/3 of RV 'Polarstern' in 1997", by Gunther Krause.

Heft Nr. 263/1998 – „Thermo-tektonische Entwicklung von Oates Land und der Shackleton Range (Antarktis) basierend auf Spaltspuranalysen", von Thorsten Schäfer.

Heft Nr. 264/1998 – „Messungen der stratosphärischen Spurengase ClO, HCl, O_3, N_2O, H_2O und OH mittels flugzeuggetragener Submillimeterwellen-Radiometrie", von Joachim Urban.

Heft Nr. 265/1998 – „Untersuchungen zu Massenhaushalt und Dynamik des Ronne Ice Shelfs, Antarktis", von Astrid Lambrecht.

Heft Nr. 266/1998 – "Scientific Cruise Report of the Kara Sea Expedition of RV 'Akademic Boris Petrov' in 1997", edited by Jens Matthiessen and Oleg Stepanets.

Heft Nr. 267/1998 – „Die Expedition ANTARKTIS-XIV mit FS ‚Polarstern' 1997. Bericht vom Fahrtabschnitt ANT-XIV/3", herausgegeben von Wilfried Jokat und Hans Oerter.

Heft Nr. 268/1998 – „Numerische Modellierung der Wechselwirkung zwischen Atmosphäre und Meereis in der arktischen Eisrandzone", von Gerit Birnbaum.

Heft Nr. 269/1998 – "Katabatic wind and Boundary Layer Front Experiment around Greenland (KABEG '97)", by Günther Heinemann.

Heft Nr. 270/1998 – "Architecture and evolution of the continental crust of East Greenland from integrated geophysical studies", by Vera Schlindwein.

Heft Nr. 271/1998 – "Winter Expedition to the Southwestern Kara Sea - Investigations on Formation and Transport of Turbid Sea-Ice", by Dirk Dethleff, Per Loewe, Dominik Weiel, Hartmut Nies, Gesa Kuhlmann, Christian Bahe and Gennady Tarasov.

Heft Nr. 272/1998 – „FTIR-Emissionsspektroskopische Untersuchungen der arktischen Atmosphäre", von Edo Becker.

Heft Nr. 273/1998 – „Sedimentation und Tektonik im Gebiet des Agulhas Rückens und des Agulhas Plateaus (‚SETA-RAP')", von Gabriele Uenzelmann-Neben.

Heft Nr. 274/1998 – "The Expedition ANTARKTIS XIV/2", by Gerhard Kattner.

Heft Nr. 275/1998 – „Die Auswirkung der 'NorthEastWater'-Polynya auf die Sedimentation von NO-Grönland und Untersuchungen zur Paläo-Ozeanographie seit dem Mittelweichsel", von Hanne Notholt.

Heft Nr. 276/1998 – „Interpretation und Analyse von Potentialfelddaten im Weddellmeer, Antarktis: der Zerfall des Superkontinents Gondwana", von Michael Studinger.

Heft Nr. 277/1998 – „Koordiniertes Programm Antarktisforschung". Berichtskolloquium im Rahmen des Koordinierten Programms „Antarktisforschung mit vergleichenden Untersuchungen in arktischen Eisgebieten", herausgegeben von Hubert Miller.

Heft Nr. 278/1998 – „Messung stratosphärischer Spurengase über Ny-Ålesund, Spitzbergen, mit Hilfe eines bodengebundenen Mikrowellen-Radiometers", von Uwe Raffalski.

Heft Nr. 279/1998 – "Arctic Paleo-River Discharge (APARD). A New Research Programme of the Arctic Ocean Science Board (AOSB)", edited by Ruediger Stein.

Heft Nr. 280/1998 – „Fernerkundungs- und GIS-Studien in Nordostgrönland" von Friedrich Jung-Rothenhäusler.

Heft Nr. 281/1998 – „Rekonstruktion der Oberflächenwassermassen der östlichen Laptevsee im Holozän anhand von aquatischen Palynomorphen", von Martina Kunz-Pirrung.

Heft Nr. 282/1998 – "Scavenging of ^{231}Pa and ^{230}Th in the South Atlantic: Implications for the use of the $^{231}Pa/^{230}Th$ ratio as a paleoproductivity proxy", by Hans-Jürgen Walter.

Heft Nr. 283/1998 – „Sedimente im arktischen Meereis - Eintrag, Charakterisierung und Quantifizierung", von Frank Lindemann.

Heft Nr. 284/1998 – „Langzeitanalyse der antarktischen Meereisbedeckung aus passiven Mikrowellendaten", von Christian H. Thomas.

Heft Nr. 285/1998 – „Mechanismen und Grenzen der Temperaturanpassung beim Pierwurm *Arenicola marina* (L.)", von Angela Sommer.

Heft Nr. 286/1998 – „Energieumsätze benthischer Filtrierer der Potter Cove (King George Island, Antarktis)", von Jens Kowalke.

Heft Nr. 287/1998 – "Scientific Cooperation in the Russian Arctic: Research from the Barents Sea up to the Laptev Sea", edited by Eike Rachor.

Heft Nr. 288/1998 – „Alfred Wegener. Kommentiertes Verzeichnis der schriftlichen Dokumente seines Lebens und Wirkens", von Ulrich Wutzke.

Heft Nr. 289/1998 – "Retrieval of Atmospheric Water Vapor Content in Polar Regions Using Spaceborne Microwave Radiometry", by Jungang Miao.

Heft Nr. 290/1998 – „Strukturelle Entwicklung und Petrogenese des nördlichen Kristallingürtels der Shackleton Range, Antarktis: Proterozoische und Ross-orogene Krustendynamik am Rand des Ostantarktischen Kratons", von Axel Brommer.

Heft Nr. 291/1998 – „Dynamik des arktischen Meereises - Validierung verschiedener Rheologieansätze für die Anwendung in Klimamodellen", von Martin Kreyscher.

Heft Nr. 292/1998 – „Anthropogene organische Spurenstoffe im Arktischen Ozean, Untersuchungen chlorierter Biphenyle und Pestizide in der Laptevsee, technische und methodische Entwicklungen zur Probenahme in der Arktis und zur Spurenstoffanalyse", von Sven Utschakowski.

Heft Nr. 293/1998 – „Rekonstruktion der spätquartären Klima- und Umweltgeschichte der Schirmacher Oase und des Wohlthat Massivs (Ostantarktika)", von Markus Julius Schwab.

Heft Nr. 294/1998 – „Besiedlungsmuster der benthischen Makrofauna auf dem ostgrönländischen Kontinentalhang", von Klaus Schnack.

Heft Nr. 295/1998 – „Gehäuseuntersuchungen an planktischen Foraminiferen hoher Breiten: Hinweise auf Umweltveränderungen während der letzten 140.000 Jahre", von Harald Hommers.

Heft Nr. 296/1998 – "Scientific Cruise Report of the Arctic Expedition ARK-XIII/1 of RV 'Polarstern' in 1997", edited by Michael Spindler, Wilhelm Hagen and Dorothea Stübing.

Heft Nr. 297/1998 – „Radiometrische Messungen im arktischen Ozean - Vergleich von Theorie und Experiment", von Klaus-Peter Johnsen.

Heft Nr. 298//1998 – "Patterns and Controls of CO_2 Fluxes in Wet Tundra Types of the Taimyr Peninsula, Siberia - the Contribution of Soils and Mosses", by Martin Sommerkorn.

Heft Nr. 299/1998 – "The Potter Cove coastal ecosystem, Antarctica. Synopsis of research performed within the frame of the Argentinean-German Cooperation at the Dallmann Laboratory and Jubany Station (Kind George Island, Antarctica, 1991 - 1997)", by Christian Wiencke, Gustavo Ferreyra, Wolf Arntz & Carlos Rinaldi.

Heft Nr. 300/1999 – "The Kara Sea Expedition of RV 'Akademik Boris Petrov' 1997: First Results of a Joint Russian-German Pilot Study", edited by Jens Matthiessen, Oleg V. Stepanets, Ruediger Stein, Dieter K. Fütterer, and Eric M. Galimov.

Heft Nr. 301/1999 – "The Expedition ANTARKTIS XV/3 (EASIZ II)", edited by Wolf E. Arntz and Julian Gutt.

Heft Nr. 302/1999 – „Sterole im herbstlichen Weddellmeer (Antarktis): Großräumige Verteilung, Vorkommen und Umsatz", von Anneke Mühlebach.

Heft Nr. 303/1999 – „Polare stratosphärische Wolken: Lidar-Beobachtungen, Charakterisierung von Entstehung und Entwicklung", von Jens Biele.

Heft Nr. 304/1999 – „Spätquartäre Paläoumweltbedingungen am nördlichen Kontinentalrand der Barents- und Kara-See. Eine Multi-Parameter-Analyse", von Jochen Knies.

Heft Nr. 305/1999 – "Arctic Radiation and Turbulence Interaction Study (ARTIST)", by Jörg Hartmann, Frank Albers, Stefania Argentini, Axel Bochert, Ubaldo Bonafé, Wolfgang Cohrs, Alessandro Conidi, Dietmar Freese, Teodoro Georgiadis, Alessandro Ippoliti, Lars Kaleschke, Christof Lüpkes, Uwe Maixner, Giangiuseppe Mastrantonio, Fabrizio Ravegnani, Andreas Reuter, Giuliano Trivellone and Angelo Viola.

Heft Nr. 306/1999 – "German-Russian Cooperation: Biogeographic and biostratigraphic investigations on selected sediment cores from the Eurasian continental margin and marginal seas to analyze the Late Quaternary climatic variability", edited by Robert R. Spielhagen, Max S. Barash, Gennady I. Ivanov, and Jörn Thiede.

Heft Nr. 307/1999 – „Struktur und Kohlenstoffbedarf des Makrobenthos am Kontinentalhang Ostgrönlands", von Dan Seiler.

Heft Nr. 308/1999 – "ARCTIC '98: The Expedition ARK-XIV/1a of RV 'Polarstern' in 1998", edited by Wilfried Jokat.

Heft Nr. 309/1999 – „Variabilität der arktischen Ozonschicht: Analyse und Interpretation bodengebundener Millimeterwellenmessungen", von Björn-Martin Sinnhuber.

Heft Nr. 310/1999 – „Rekonstruktion von Meereisdrift und terrigenem Sedimenteintrag im Spätquartär: Schwermineralassoziationen in Sedimenten des Laptev-See-Kontinentalrandes und des zentralen Arktischen Ozeans", von Marion Behrends.

Heft Nr. 311/1999 – „Parameterisierung atmosphärischer Grenzschichtprozesse in einem regionalen Klimamodell der Arktis", von Christoph Abegg.

Heft Nr. 312/1999 – „Solare und terrestrische Strahlungswechselwirkung zwischen arktischen Eisflächen und Wolken", von Dietmar Freese.

Heft Nr. 313/1999 – "Snow accumulation on Ekströmisen, Antarctica", by Elisabeth Schlosser, Hans Oerter and Wolfgang Graf.

Heft Nr. 314/1999 – „Die Expedition ANTARKTIS XV/4 des Forschungsschiffes ‚Polarstern' 1998", herausgegeben von Eberhard Fahrbach.

Heft Nr. 315/1999 – "Expeditions in Siberia in 1998", edited by Volker Rachold.

Heft Nr. 316/1999 – „Die postglaziale Sedimentationsgeschichte der Laptewsee: schwermineralogische und sedimentpetrographische Untersuchungen", von Bernhard Peregovich.

Heft-Nr. 317/1999 – „Adaption an niedrige Temperaturen: Lipide in Eisdiatomeen", von Heidi Lehmal.

Heft-Nr. 318/1999 – „Effiziente parallele Lösungsverfahren für elliptische partielle Differentialgleichungen in der numerischen Ozeanmodellierung", von Natalja Rakowsky.

Heft-Nr. 319/1999 – „The Ecology of Arctic Deep-Sea Copepods (Euchaetidae and Aetideidae). Aspects of their Distribution, Trophodynamics and Effect on the Carbon Flux", by Holger Auel.

Heft-Nr. 320/1999 – „Modellstudien zur arktischen stratosphärischen Chemie im Vergleich mit Meßdaten", von Veronika Eyring.

Heft-Nr. 321/1999 – „Analyse der optischen Eigenschaften des arktischen Aerosols", von Dagmar Nagel.

Heft-Nr. 322/1999 – „Messungen des arktischen stratosphärischen Ozons: Vergleich der Ozonmessungen in Ny-Ålesund, Spitzbergen, 1997 und 1998", von Jens Langer

Heft-Nr. 323/1999 – „Untersuchung struktureller Elemente des südöstlichen Weddellmeeres / Antarktis auf der Basis mariner Potentialfelddaten", von Uwe F. Meyer.

Heft-Nr. 324/1999 – „Geochemische Verwitterungstrends eines basaltischen Ausgangsgesteins nach dem spätpleistozänen Gletscherrückzug auf der Taimyrhalbinsel (Zentralsibirien) - Rekonstruktion an einer sedimentären Abfolge des Lama Sees", von Stefanie K. Harwart.

Heft-Nr. 325/1999 – „Untersuchungen zur Hydrologie des arktischen Meereises - Konsequenzen für den kleinskaligen Stofftransport", von Johannes Freitag.

Heft-Nr. 326/1999 – „Die Expedition ANTARKTIS XIV/2 des Forschungsschiffes 'Polarstern' 1998", herausgegeben von Eberhard Fahrbach.

Heft-Nr. 327/1999 – „Gemeinschaftsanalytische Untersuchungen der Harpacticoidenfauna der Magellanregion, sowie erste similaritätsanalytische Vergleiche mit Assoziationen aus der Antarktis", von Kai Horst George.

Heft-Nr. 328/1999 – „Rekonstruktion der Paläo-Umweltbedingungen am Laptev-See-Kontinentalrand während der beiden letzten Glazial/Interglazial-Zyklen anhand sedimentologischer und mineralogischer Untersuchungen", von Claudia Müller.

Heft-Nr. 329/1999 – „Räumliche und zeitliche Variationen atmosphärischer Spurengase aus bodengebundenen Messungen mit Hilfe eines Michelson Interferometers", von Justus Notholt.

Heft-Nr. 330/1999 – „The 1998 Danish-German Excursion to Disko Island, West Greenland", edited by Angelika Brandt, Helge A. Thomsen, Henning Heide-Jørgensen, Reinhardt M. Kristensen and Hilke Ruhberg.

Heft-Nr. 331/1999 – „Poseidon" Cruise No. 243 (Reykjavik - Greenland - Reykjavik, 24 August - 11 September 1998): Climate change and the Viking-age fjord enviroment of the Eastern Settlement, sw Greenland", by Gerd Hoffmann, Antoon Kuijpers, and Jörn Thiede.

Heft-Nr. 332/1999 – „Modeling of marine biogeochemical cycles with an emphasis on vertical particle fluxes", by Regina Usbeck.

Heft-Nr. 333/1999 – „Die Tanaidaceenfauna des Beagle-Kanals und ihre Beziehungen zur Fauna des antarktischen Festlandsockels", von Anja Schmidt.

Heft-Nr. 334/1999 – „D-Aminosäuren als Tracer für biogeochemische Prozesse im Fluß-Schelf-Ozean-System der Arktis", von Hans Peter Fitznar.

Heft-Nr. 335/1999 – „Ökophysiologische Ursachen der limitierten Verbreitung reptanter decapoder Krebse in der Antarktis", von Markus Frederich.

Heft-Nr. 336/1999 – „Ergebnisse der Untersuchung des grönländischen Inlandeises mit dem elektromagnetischen Reflexionsverfahren in der Umgebung von NGRIP", von Fidan Göktas.

Heft-Nr. 337/1999 – „Paleozoic and mesozoic tectono-thermal history of central Dronning Maud Land, East Antarctica, – evidence from fission-track thermochronology", by Stefanie Meier.

* vergriffen/out of print
** nur noch beim Autor/only from the author.